A STUDY ON RISER GAS AND RISER GAS UNLOADING IN OFFSHORE WELLS

A Dissertation

by

OMER KALDIRIM

Submitted to the Graduate and Professional School of
Texas A&M University
in partial fulfillment of the requirements for the degree of

DOCTOR OF PHILOSOPHY

Chair of Committee,	Jerome J. Schubert
Co-Chair of Committee,	Mahmoud El-Halwagi
Committee Members,	Berna Hascakir
	Samuel Noynaert
Head of Department,	Timothy Jacobs

December 2021

Major Subject: Interdisciplinary Engineering

ABSTRACT

The primary purpose of this study was to investigate riser gas behavior, unloading, and the possibility of using back pressure to control and prevent riser gas unloading. Gas entering a well may be challenging to detect in deep-water wells with the large column of mud located in the riser and the lengthy annulus extending beneath the seabed. If undetected and left alone, the gas kick can migrate into the riser and lead to loss of well control, riser unloading, and blowout. This dissertation investigates gas migration, expansion, riser gas unloading, and how to safely circulate gas influxes in deep-water conditions through experimentation and simulation.

Conventional well control operations include shutting in the well, applying well control methods, and circulating the gas out of the well using the subsea choke and kill lines. However, in some cases where the gas kick goes undetected, shutting in the well using the subsea Blowout Preventers (BOP) may be too late as the gas influx may have entered the riser. Conventional offshore drilling utilizes an open-top riser with a flow line returning the mud from the top of the riser. Gas entering the riser in water-base muds expand and travel up the riser. The primary driver of the gas movement in non-circulating situations is initially be migration dominated then expansion dominated. In oil-base muds, gas remains in solution until the bubble point is reached and then begins bubbling out of the solution. Then, the gas bubble that is liberated from the mud begin expanding. In both cases, if left uncontrolled, the rapid gas expansion can discharge fluid from the top of the

riser onto the rig floor at very high rates leading to a blowout, injuries, fatalities, and loss of well and rig.

The first step of this study is to review the expansion rate of a gas kick using flow loops in the Dual Gradient Drilling (DGD) and Tower Labs located at Texas A&M University and run CFD simulations to verify and scale up the results. The second step is to use the CFD simulations to observe the effects of applying surface back pressure on the impact of gas expansion and riser unloading to study Dynamic Influx Management methods produced through Managed Pressure Drilling (MPD) systems.

The results of this study provide information on the physics behind the sudden gas expansion and unloading of risers during offshore operations and opportunities created with MPD systems to manage riser gas, reduce NPT and improve operational safety and reliability.

DEDICATION

To my mother and father, Esther, and Osman Kaldirim, for their unwavering support and motivation throughout my life.

ACKNOWLEDGEMENTS

I would like to thank my committee chair, Dr. Jerome J. Schubert, for his continuous support and guidance throughout my graduate studies and career. I genuinely appreciate his unending patience and advice and his strong encouragement. I would also like to thank my committee members Dr. El-Halwagi, Dr. Hascakir, and Dr. Noynaert, for their support and advice on my research and career goals. I would also like to thank Dr. Abu Rashid Hasan for his support and encouragement and for granting permission to work and conduct part of my research in his lab. And I am also thankful to the National Academies of Sciences, Engineering, and Medicine for providing funding for this research through the Gulf Research Program.

I want to thank my mother and father, Esther and Osman Kaldirim, for their unending support, encouragement throughout my life, and push to pursue a Ph.D. I would also like to thank my uncle, Lorenzo Marquez, for his encouragement and support. Finally, I want to thank my siblings, Mehmet, Osman, Yasemin, Ali, Nur, Ebubekir Kaldirim, Keila Rivera, Hasan Armutcuoglu, for being supportive and patient with me throughout my life. I would also like to Idris Kirdemir for his support throughout my life.

I would also like to thank John Maldonado from the Petroleum Engineering Department at Texas A&M University for his friendship and the countless hours he spent helping me rebuild the Dual Gradient Drilling and Tower Labs work through my time at Texas A&M University.

I would like to thank Andy Johns, Vincent Doczy, Matthew Bell for their continuous friendship, motivation, and support in the lab. I would also like to thank Pedro Sousa and Dinara Dussenova for their friendship and assistance in the lab. I would like to thank Kaushik Manikonda for all his patience and assistance with rebuilding the Tower Lab and his friendship. I would like to thank Samantha Beevers for her support and help with editing my dissertation.

I would like to thank Ms. Violetta Cook for her continuous encouragement and guidance throughout my graduate studies and always being available for a phone call to seek advice.

I would also like to thank Cameron Geresti, Paul Ofoche, and Tyrell Cunningham for their friendship and discussions in our office space, Room 1007. I would also like to thank Mohamed Khaled, Chinemerem Edmond Obi, and Foster Dawson for their friendship and help in the Tower Lab. Finally, I also want to thank all student workers that have helped me while working at the Dual Gradient Drilling and the Tower Labs, especially Shaun Stephen and Saleh Hussein.

I would like to thank Stan Christman for his friendship and his willingness to help me learn, share his advice and experiences. I truly appreciate and look forward to our long phone calls or lunches to discuss anything from technical subjects to career advice. I would also like to thank Sixto Romero for the opportunity to learn from him about well modeling for drilling applications, instrumentation, and general business skills.

I would like to thank Paul Sonnemann, Oscar Gabaldon, Hari Hariharan, Akram Nabiyev, Sagar Nauduri, Martin Parker, Gavin Humphreys, Brian Piccolo, Tom Proehl,

Dennis Moore, and other members of the IADC Managed Pressure Drilling and Underbalanced Drilling committee and Riser Gas subcommittee members for welcoming me and patiently answering my questions related to my research and drilling operations.

I would like to thank Dr. Charles Taylor with Louisiana State University and Dr. Wesley Williams with Oak Ridge National Laboratory for their assistance in setting up the Tower Lab electronics. I would also like to thank Dr. Namik Ciblak, Dr. Hojin Ahn, and Dr. Fethi Okyar from Yeditepe University for their support and encouragement.

Finally, I would like to thank the faculty and staff of the Petroleum Engineering Department, the Interdisciplinary Engineering Department, and the Richardson Building.

Portions of this research were conducted with the advanced computing resources provided by Texas A&M High Performance Research Computing.

Thank you to all those who have helped, supported, encouraged, and inspired me in any way!

CONTRIBUTORS AND FUNDING SOURCES

Contributors

This work was supported by a dissertation committee consisting of Professor Jerome J. Schubert of the Petroleum Engineering Department, Professor Mahmoud El-Halwagi of the Chemical Engineering Department, Professors Berna Hascakir, and Samuel Noynaert of the Petroleum Engineering Department.

All work conducted for this dissertation was completed independently by the student.

Funding Sources

The graduate study was supported by the Gulf Research Program from the National Academies of Science, Engineering, and Medicine and the Ocean Energy Safety Institute.

NOMENCLATURE

API	American Petroleum Institute
BHP	Bottom Hole Pressure
BOP	Blowout Preventers
CBHP	Constant Bottom Hole Pressure
CFD	Computational Fluid Dynamics
CML	Controlled Mud Level
CO_2	Carbon Dioxide
CSB	Chemical Safety Board
CDAQ	Compact Data Acquisition
DAQ	Data Acquisition
DGD	Dual Gradient Drilling
e	Internal Energy
Gal	Gallons
Gf	Fracture Gradient
Gp	Pore Gradient
GPM	Gallons Per Minute
H_2S	Hydrogen Sulfide
IADC	International Association of Drilling Contractors
ICP	Initial Circulating Pressure
lbs	Pounds

LMRP	Lower Marine Riser Package
LSU	Louisiana State University
MGS	Mud Gas Separator
mL	Milliliters
MMS	Minerals Management Services
MPD	Managed Pressure Drilling
NI	National Instruments
NPT	Non-Productive Time
OBM	Oil Base Mud
Pf	Fracture Pressure
P&ID	Piping and Instrumentation Diagram
Pp	Pore Pressure
PPG	Pound Per Gallon
PRV	Pressure Relief Valve
Psi	Pound per square inch
Q	Heat Source
r	Radius
RCD	Rotating Control Device
Rich	Richardson Building
RP	Recommended Practice
SBM	Synthetic Base Mud
SBP	Surface Back Pressure

SCRC	Schlumberger Cambridge Research Center
SICP	Shut-In Casing Pressure
SITP	Shut-In Tubing Pressure
SPE	Society of Petroleum Engineers
SPP	StandPipe Pressure
t	Time
TAMU	Texas A&M University
Temp	Temperature
TVD	True Vertical Depth
TD	Total Depth
TIW	Texas Iron Works
USB	University Services Building (Old-TI Building)
V	Velocity Vector
VBR	Variable Bore Ram
VFD	Variable Frequency Drive
VOF	Volume of Fluid
WBM	Water Base Mud
ρ	Density
υ	Velocity
$\bar{\bar{\tau}}$	Stress tensor

TABLE OF CONTENTS

Page

LIST OF FIGURES

Page

LIST OF TABLES

Page

1. INTRODUCTION

There are eight sections in this dissertation. The first section describes the problem, provides background and the justification for this research, introduces the methodology, and provides brief descriptions of the concepts.

The second section describes and discusses experimental work performed at the Dual Gradient Drilling Lab. This section provides the challenges faced while modifying the lab and the limitations of the experiments. This section also presents a proof of concept and discusses the results

The third section describes the upgrades performed at the Tower Lab, the challenges, and the limitations. This section also provides final updates and procedures for running experiments.

The fourth section provides the results and discussion of the experiments conducted at the Tower Lab.

The fifth section describes the computational fluid dynamics (CFD) methods and provides results from various simulations. This section also includes the assumptions and limitations of each simulation.

The sixth section presents results from computational fluid dynamics analyses performed on various pipe diameters and sizes.

The seventh section provides conclusions and final observations.

The eighth section proposes a list of future work at the Tower Lab, Dual Gradient Drilling Labs. This section also proposes additional computational fluid dynamics analyses to conduct to understand riser gas behavior and unloading.

1.1. INVESTIGATION OF RISER GAS AND RISER UNLOADING IN OFFSHORE WELLS

Increased demand for hydrocarbons and the limited reservoir remaining under shallow water depths has pushed operators to seek oil and gas in deep waters. With the advancements in offshore drilling vessels, equipment, training, and procedures, deep-water drilling has become safer. However, with the increase in water and reservoir depths, the pressure and volumes have also increased, leading to higher risks associated with drilling these wells. Therefore, procedures, training, and risk assessment have to be improved to drill and complete these wells. Additional research is needed to understand the greater depth, temperature, and pressure effects on the drilling fluid (primary barrier), well control procedures, kick detection and circulation, gas solubility, and migration to improve procedures and training.

Drilling fluids serve many purposes in drilling, such as hole cleaning, cooling the drill bit, building a filter cake, transmitting data from downhole measurement devices, balancing Pore Pressure (P_P) and Fracture Pressure (P_F), and diagnosing downhole problems. Drilling fluids play an essential role in maintaining a safe operational window while drilling offshore wells. Drilling fluids constitute the primary barrier in maintaining a well under control and preventing influxes from entering the wellbore. Whether Oil Based Mud (OBM), Water Based Mud (WBM), or Synthetic Based Mud (SBM),

maintaining primary barrier for well control must be considered while designing drilling mud, preparing the mud program, and testing the mud during operation. It is essential to understand the proper measurement and design procedures for the drilling fluid. It must be supported by the correct Pore Gradient (G_P) and Fracture Gradient (G_F) prediction and measurement.

Using an incorrect mud weight, or the formation properties are incorrectly predicted, the well may become underbalanced to the formation, permitting formation fluids to enter the wellbore. If formation fluids enter the wellbore, the primary barrier is compromised, and the driller must proceed to secondary well control (Blowout Preventers (BOP), Diverter). Well control procedures (flow test, shutting in the well, circulating the kick, and killing the well) must be conducted to bring the well under control. Further ignoring the necessary mud design can lead to a significant well control incident, unloading, blowout, and loss of life and well.

This dissertation presents a study on gas migration and expansion and unloading of the marine riser during drilling operations and the possible opportunities to prevent riser unloading through MPD applications. Lab-scale experiments and Computational Fluid Dynamics (CFD) simulations were conducted for this research. The lab results were used to verify the results of the CFD analyses and scale up to provide Riser Unloading velocity, flow rate, pressure, and temperature of the drilling fluid and gas. CFD analyses were used to study the application of back-pressure to limit the impact of gas migration and expansion and investigate the possibility of preventing or minimizing the effects of riser unloading.

1.1.1. Purpose

The purpose of this research was to study riser gas and riser unloading through lab-scale experiments and CFD analyses and investigate the impact of surface back-pressure on limiting riser gas expansion and unloading. This study improves the understanding of gas migration and expansion in marine risers while drilling and mitigation or preventing riser gas from turning into riser unloading.

1.1.2. Objectives

The objectives of this study are as follows:

1- Update the Dual Gradient Drilling (DGD) Laboratory to conduct gas in riser studies.
   a. Perform these studies in atmospheric conditions with and without liquid circulation.
   b. Perform experiments in a vacuum with a static liquid column.
2- Update the Tower Lab to conduct gas in riser experiments in extended lengths and investigate gas expansion rate.
   a. Perform these studies in atmospheric conditions with and without liquid circulation.
   b. Perform experiments in a vacuum with a static liquid column
3- Perform CFD analyses on the DGD and Tower lab experiments and compare the experimental and simulation results.
4- Scale up the CFD analyses performed on the DGD and Tower lab experiments.

5- Perform CFD analyses on large diameter risers for pipe and annular flow and compare results with existing literature.
6- Perform CFD analyses on actual riser dimensions used in deep-water drilling and verify results with existing literature.
7- Run CFD simulations on riser gas with back pressure to simulate MPD operations in deep-water and the benefits of holding surface back pressure to circulate a gas kick using the riser.

1.2. Literature Review

Well control is achieved through a set of physical barriers, categorized as the Primary Barrier (Drilling Fluid or Mud) and the Secondary Barrier (BOP, Diverter, wellhead, etc.). When the primary barrier is compromised, the secondary barrier is relied upon to secure the well. The primary barrier may become compromised through the influx of formation fluids entering the wellbore. There are multiple causes for an influx to enter the wellbore; however, the leading situation is that the kicking formation has a pore pressure greater than the pressure exerted by the wellbore fluids and a permeability high enough to allow flow. This situation occurs if any of the following conditions are true, the drilling fluid level in the well decreases, low density, swabbing, loss of circulation, drilling through gas zones, or shallow hazards. If these conditions exist, gas, water, oil, or a combination of these fluids may enter the well from the kicking formation (API 2006). If these influxes are not controlled and eliminated in a timely and safe manner, the result could be loss of well control, gas entering the riser, riser unloading, blowout, loss of life, equipment, and well.

1.2.1. Well Control

Procedures to maintain safe drilling operations were provided in the API Recommended Practice 59 (API 2006) and the IADC Deepwater Well Control Guidelines (IADC 2015). International Association of Drilling Contractors (IADC) issues well control certification following the training provided by an accredited training center. These documents provide methods to detect an influx, methods to shut in and secure the well using the secondary barrier equipment, and methods to circulate the influx and kill the well (API 2006).

The API RP 59 document is supported by;

- API Standard 53 "*Well Control Equipment Systems for Drilling Wells*", which provides the standards for design, selection, specification and testing for the Blowout Preventers (BOP) (API 2018),
- API Specifications 16C "*Choke and Kill Equipment*" which provide specifications, description and testing guidelines for the Choke and Kill lines used for well control operations to circulate and kill the well (API 2015),
- API Standard 64 "*Diverter Equipment Systems*" which provide specifications for design, installation, and testing for diverter systems (API 2017a),
- API Specification 16D "*Specification for Control Systems for Drilling Well Control Equipment and Control Systems for Diverter Equipment*", which provide design, sizing, and testing specifications for the BOP and diverter control system (API 2017c),
- API Specification 16F "*Specification for Marine Drilling Riser Equipment*" provides specifications for Riser system components, design, and testing (API 2017c).

For drilling fluid design and testing, API has published recommended practices for design of rheology and hydraulics for drilling muds and the testing procedures - Recommended Practices for Rheology and Hydraulics for Drilling Fluids “API RP 13D” (API 2017b) and testing procedures for OBM “API RP 13B-2” (API 2014) and WBM “API RP 13B-1” (API 2019). These recommended practices serve as a guideline to design and test the mud.

1.2.1.1. Well Control Background

Studies have been conducted on the effects of loss of well control, unloading following significant blowouts. The industry must maintain safe and economically effective operations. The New regulations and restrictions were created following the Santa Barbara Blowout in 1969 (Stracke 1970). Further, the regulations which have improved operational safety in the North Sea were a result of the Pipe Alpha (1988) and the Ekofisk Bravo Blowout (1977), where 1,700 tons of oil per day were discharged from the well (Haegh and Rossemyr 1980). These disasters have led the UK and Norway to adopt a performance-based regulation. Recently, the Macondo (2010) blowout has led to additional regulations by the US government and damaged the positive perception of the public (Visser (2011), Madsen et al. (2014)). Therefore, understanding the physics that led to these disasters is crucial for the industry to implement changes to the procedures. For this process, the IADC Deepwater Well Control Guidelines were developed (Christman et al. 1999).

1.2.1.2. Well Control Research

While drilling in deep-water and ultra-deep waters, the impact of greater pressures, volumes, and significant temperature variations must be considered. For example, the engineer must consider the pressure effect on gas migration and solubility in OBM and the narrow drilling windows. In addition, the engineer must assess volume availability in mud tanks, the volume of mud in the riser, wellbore, and drill pipe. And when considering significant temperature variations, the high temperature in deep wells and the low temperatures surrounding the long risers, and the effects on heat transfer and mud rheology must be considered. These parameters affect well control and influx management.

Researchers have studied the impacts of pressure, temperature, volume, mud rheology, and mud type on well control and gas migration in various labs and wells (Pertt Lab at Louisiana State University (LSU), Schlumberger Cambridge Research Center (SCRC), Dual Gradient Drilling Lab & Tower Lab at Texas A&M University (TAMU), Ullrigg Drilling and Well Centre at IRIS AS., and other facilities) in a lab and full scale, field experiments. In addition, computer-based simulators were built as a result of the need to simulate kick behavior in wells while drilling for planning and operational purposes.

1.2.1.2.1. Lab Scale Experiments

The lab-scale and well experiments and simulations performed at the PERTT Lab at LSU are described in (Rader et al. 1975, Holden and Bourgoyne 1982, Langlinais et al. 1983, Matthews and Bourgoyne 1983, Bourgoyne and Holden 1985, Bryan and Bourgoyne 1990, Casariego and Bourgoyne 1988, Bryan et al. 1988, Bryan and Bourgoyne 1989). In Rader et al. (1975), the authors investigated various factors affecting

bubble rise velocity in pipe annulus using both small lab-scale and full-scale experiments. They investigated the effects of bubble length, liquid density and viscosity, surface tension, liquid velocity, and pipe deviation.

The effects of surface back-pressure on gas migration and expansion were researched in Rader et al. (1975). The authors evaluated expansion and compression by increasing and reducing surface back pressure. When the surface back pressure was reduced, the gas bubble expanded, resulting in a significant increase in bubble rise at the front and a moderate increase in the tail. And when surface pressure was suddenly applied on a rising bubble, the bubble front velocity changed from 0.095 ft/sec to a reversed velocity of -0.115 ft/sec. The upward velocity of the bubble tail was reduced from 0.095 ft/sec to 0.065 ft/sec. The expansion rate for the first case was 0.09 ft/sec, while the compression rate when surface pressure was 0.180 ft/sec. (Rader et al. 1975)

Holden and Bourgoyne (1982) studied the effects of well control in deep-water drilling operations where the authors performed experiments and simulations in a 6000 ft. well. They simulated a deep-water drilling operation with the BOP at 3000-ft by adding a packer at 3000-ft with two tubings for the choke and kill lines to simulate a deep-water drilling operation with the BOP at 3000-ft. These studies were performed to investigate the impact of the greater pressures involved in deep-water drilling on choke and kill line friction pressure and the conventional well control methods. The main conclusion of this study was that the impact of the extended lengths of choke and kill lines did not create as significant an impact as previously simulated. However, extensive training is required for choke management during kick circulation.

Gas rise velocities in lab-scale experiments in WBM and OBM in vertical and inclined flow loops were studied at the SCR in Johnson and White (1991) and Johnson and Cooper (1993). The studies were performed in a 12-m long, 200mm pipe, which was inclinable. Air was used as the gaseous phase, while water and water-xanthan gum solution were used to simulate the liquid (WBM) phase. The study also investigated the effects of viscosity and concluded that gas bubbles rise faster in drilling muds when compared with the rise in water. The reasoning for their conclusion was that gas bubbles tend to form larger slugs in the lower section of the pipe when viscous mud was used (Johnson and White 1991). In Johnson and Cooper (1993), the authors studied the effects of well deviation on gas bubble rise by running inclined pipe experiments with the inclination angles between vertical and 60°. The authors used water-xanthan gum solution, analogous to bentonite mud as the liquid phase and air as the gaseous phase. The authors also performed tests using 6% bentonite mud with the pipe vertically to demonstrate the near-identical results of using water-xanthan gum solution. The authors found that the gas slip velocity increases to the maximum velocity for pipe flow at 15°, then slowly reduced until the inclination reached 45°, and rapidly slowed down after. However, for annular flow, the authors concluded that gas slip velocity does not change with inclination up to 45° then decreases (Johnson and Cooper 1993).

Recently, bubble rise experiments were run at the Dual Gradient Drilling (DGD) laboratory at Texas A&M University. The studies involved air and water on a 27 ft inclinable pipe and annular flow experiments. The initial set of experiments involved testing the migration rate of bubbles while circulating water through the flow loop. The

flow loop for the initial test was built to simulate the Pumped Riser type DGD method, also known as Controlled Mud Level (CML) drilling. The purpose of these experiments was to observe how much gas could be extracted from the flow loop using methods, 1-dispersing bubbles, 2-high pump rates at the inlet and discharge ports. The authors also collected pressure and flow data from the system; however, the experiments provided inconclusive results because additional upgrades were needed. The short length of the flow loop did not provide enough hydrostatic pressure and resulted in a low expansion ratio due to the atmospheric pressure (Kaldirim 2015, Kaldirim and Schubert 2017). The authors then ran the second set of experiments to test the system under vacuum to minimize atmospheric pressure and observed a greater expansion ratio. Their study proved that the short flow loop could provide low-pressure expansion results with greater expansion under vacuum (Kaldirim and Schubert 2018).

1.2.1.2.2. Field Experiments

Rommetveit and Olsen (1989) performed full-scale gas kick simulations in OBM in an inclined well at the Rogaland Research Institute's Ullrigg research well. The total depth (TD) of the well was 2020 meters with a 63° deviation with multiple pressure sensors located along the well and surface sensors to collect pump strokes, mud return rate, pit level, choke position, pressure, liquid density, and StandPipe Pressure (SPP). Gas injection rate and pressure were also controlled and measured using surface sensors. The well design consisted of a 9-5/8-in casing with the casing shoe at 1510 meters, with a 7-in casing extension to 2020 meters. The drill string consisted of; 5-in drill pipe and 100 meters of 6-1/2-in drill collars, and an 8-1/2-in drill bit. After injecting gas into the well,

the total pit gain reached 1 cubic meter. The authors monitored SPP, which reduced as the influx rate increased. The authors controlled the well by using the driller's method and concluded that the mud return flow was the most sensitive measurement and could be significant in kick detection, but it was challenging to maintain Constant Bottomhole Pressure (CBHP) due to high gas concentration influx (Rommetveit and Olsen 1989)

Hovland and Rommetveit (1992) also studied annular gas migration at Ullrigg using WBM and OBM. They varied the circulation rate between 0 and 1200 l/min and injected nitrogen or argon through a coil tubing. They found that in high concentration kicks, the gas mostly migrates as free gas. For WBM experiments, they observed that almost all gas was in free gas form; however, for OBM, the amount of free gas was reduced due to solubility. They found that in medium to low concentration kick experiments, less free gas was observed. For OBM, almost all gas dissolved into the mud, and the amount of dissolved gas depended on the gas concentration, circulation rate, pressure, and the duration that the gas was left in the well. They also tested various gas and mud densities and found that the gas migration rate was independent of density. The authors also observed that gas void fraction, inclination angle, surface tension, mud rheology, and viscosity had no significant effect on gas migration (Hovland and Rommetveit 1992). However, it is challenging to apply these studies in greater water and well depths without additional research. These studies must be included in the well design, procedures, and training programs for well and operational plans. With the great depths, increased volumes, and pressures, it may be challenging to detect gas influxes for both OBM and WBM cases.

1.2.2. Riser Gas and Riser Unloading

The uncontrolled gas movement to the surface, either by circulation or migration and expansion, can lead to severe well control and blowout cases. The secondary barrier (BOP) is located at the surface right below the rig on land operations. However, the BOP is located at the seabed for offshore wells, sometimes thousands of feet below the rig, and could provide gas influxes enough length and time to move into the riser. Considering that the riser top is maintained at atmospheric pressure in conventional drilling operations, this provides a gas influx the opportunity to migrate and expand freely at a rapid rate. This rapid expansion can lead to a situation where the mud is discharged from the riser annulus (Riser Unloading) onto the rig floor.

If gas is detected in the riser, the standard procedure is to close the BOP and divert the flow from the riser using the diverter system (IADC 2015). However, this procedure has faults as the mud is diverted into a mud gas separator (MGS) depending on the MGS capacity or overboard into the sea. This method can result in environmental damage, loss of mud and hydrostatic overbalance to the formation, and fines. More severe consequences of diverter use can occur if the diverter becomes plugged or if the diverter is activated late, leading to riser unloading and, ultimately, a blowout.

Riser gas and riser unloading events have been a topic that has been encountered throughout the history of offshore drilling. For example, Zapata Lexington (1984) and the Macondo (2010) blowouts encountered riser gas. The gas migrated and expanded freely and uncontrolled, leading to mud being discharged from the riser at high rates, driven by

the explosive force of gas expansion. These examples are detailed in the following subsection of this study.

Simulation attempts at understanding gas circulation out of the riser using the diverter lines were presented in Santos et al. (1991). The authors presented results from a simulator they built using the material balance equations and the momentum balance equation. The authors simulated a 3000-ft riser using various gas influx volumes and concentrations. They presented the case for circulation and non-circulation conditions and concluded that the diverter lines could handle the removal of the gas. However, special consideration must be given to riser integrity during the non-circulation case.

Hauge et al. (2015) presented riser gas experiments performed in a well drilled using the CML method with reduced mud level in the riser and five tests completed using nitrogen injection into the well. When they injected 250-kg of nitrogen, the riser unloaded onto the rig floor.

Velmurugan et al. (2016) present their results for gas migration simulations using analytical and iterative schemes for WBM and OBM for various void fractions. The authors were able to demonstrate the effectiveness of their iterative scheme for solubility and non-solubility cases. They also observed that the booster pump plays a role in gas concentration and concluded that the unloading process was slower if the booster pump was turned off earlier.

Further simulation attempts of gas kicks were presented in Manikonda et al. (2019), Manikonda (2020), Manikonda et al. (2020a), Manikonda et al. (2020b), and Manikonda et al. (2021), where the authors performed analytical and iterative simulations

by combining equation of state, thermodynamics, mass balance, and momentum balance equations. The simulations were performed using various gas influx cases for circulation and non-circulation in the annulus. The authors validated their results for cases with solubility using Aspen HYSYS.

Kiran et al. (2020b) present their results on sonic conditions during worst-case discharge using a 5.5-meter-tall flow loop. The authors also presented Computational Fluid Dynamics (CFD) Analyses and experiments in Kiran et al. (2020a), matching CFD results with experimental data.

Worst case discharge, riser gas and riser unloading simulations, and laboratory experiments conducted at the Pertt Lab in Louisiana State University (LSU) were presented in Nahri et al. (2019a), Nahri et al. (2019b), Williams et al. (2020), Waltrich et al. (2019), Sharma et al. (2020), Feo et al. (2020a), and Feo et al. (2020b). In addition, Nwaka et al. (2020) presented simulations on gas influxes both with and without time-dependent desorption. The authors concluded that neglecting desorption for riser gas unloading could lead to underestimations. And assuming instantaneous desorption rather than time-dependent desorption could lead to overestimations. Finally, Santos et al. (2021), Sharma et al. (2020), Feo et al. (2020b), Feo et al. (2020a), Feo et al. (2019) also demonstrate the use of distributed fiber optics sensing technology for real-time kick detection and monitoring in the riser.

The uses of such technologies and sensors are also presented in Zhou et al. (2021). The authors demonstrate the use of the pressure difference method in detecting and tracking gas bubbles in a 12-ft tall lab-scale flow loop at the University of Houston. They

illustrated this by placing closely spaced pressure transmitters along the flow loop and studying the real-time behavior as gas influxes travel by the pressure ports.

Additional studies for kick detection in risers were presented in Wang et al. (2018) and Yin et al. (2020), where the authors present methods of gas detection by using an external acoustic sensor on the riser to detect riser gas.

Gu et al. (2021) reported the simulation results for using the booster pump to dilute the influx in the riser. They demonstrated that the dilution of the gas bubble using the booster reduces the surface back pressure required for riser gas elimination.

1.3. Motivation

The motivation for this research was created as a result of a significant gap in deep-water drilling well control operations, referred to as the riser gas and riser unloading incident, that occurs when a gas influx from a kick migrates or travels into the riser above the BOP. This situation has been investigated in the past, however, it has not been resolved or understood. Therefore, this issue was noted, and solutions were developed by diverting flow from the riser overboard (IADC 2015). Riser unloading events have occurred since offshore drilling began and have led to blowouts, such as the Zapata Lexington (1984) blowout and the Macondo Blowout (2010).

Riser Unloading occurs when a gas influx enters the riser and begins to migrate and expand freely without restriction or additional pressure. The expansion of gas becomes dominant near the surface and releases energy by discharging fluid from the pipe. Similarly, this type of incident has been recently seen on land drilling on the Pryor Trust well, where 100+bbls of gas influx entered the well and flowed freely to the surface. As

the gas migrated to the surface, the well discharged mud from the wellhead, and the well blew out (CSB 2019).

1.3.1. OCS Incident Reports and Investigations

When presenting motivations to research any well control subject, an additional item to research is the blowout incident and investigation reports published by the Gulf Region, Outer Continental Shelf (OCS), Minerals Management Services (MMS), Department of Interior. Similar incidents to unloading the marine riser, gas entering the riser, blowouts, and well control events are used to justify researching riser unloading and riser gas. The following are a few examples of information found in the MMS reports:

1- William Martin (1984), "*Investigation of July 20, 1983, Blowout Matagorda Island Block 657, Lease OCS-G-4139 Gulf of Mexico*"; an offshore well was being drilled using the Penrod 52 Jack Up Rig. When drilling to 3748 ft, a loss of returns incident occurred. After mitigation procedures began, the well began flowing through the annulus with a closed annular. The flow was diverted overboard, but gas, water, and sand discharged from the annulus to a height of 40 ft. After the discharge subsided, the well was attempted to be brought under control by activating the diverters again. However, no flow was observed from the diverters due to the system becoming plugged. As a result, the rig was abandoned, and the continuous flow onto the rotary table sank the rig.

2- Maurice Stewart (1985) "*Investigation of October 20-27, 1983 Blowout, Eugene Island Block 10, Lease OCS-G 289.2, Gulf of Mexico*" reports a blowout in 1982 on the Portal 40 semi-submersible rig. The blowout occurred while running in the

3-1/2" production tubing and displacing the 17.4-ppg mud with spacer pills and 9-ppg $CaCl_2$ packer fluid. The displacement pressure increased to 6,600-psi and reduced to 3,900-psi by pumping the lighter packer fluid. While pumping in the packer fluid, the operations were stopped, and the well was shut in by closing the annular BOP and the choke. The recorded values for shut-in tubing Pressure (SITP) and Shut-in Casing Pressure (SICP) were 5,500-psi and 8,000-psi, respectively. A gain of 5-bbls was observed, which was calculated from the 306-bbls of $CaCl_2$ pumped in and 311-bbls of 17.4-ppg mud return. After shutting in and performing pressure tests on equipment, the decision was made to displace the 9.0-ppg $CaCl_2$ with 17.4-ppg mud through the annulus. A leak occurred between the crossover sub and the Texas Iron Works (TIW) safety valve. After the leak stopped, an attempt was made at closing the TIW valve, which only closed a quarter turn. Gas flowed through the actuator stem on the TIW valve, and after evacuating the rig, the gas ignited.

3- J. L. Guidry (1986), "*Investigation of the December 1985 Blowout and Fire, Lease OCS-G 4268, West Cameron Block 648, Gulf of Mexico, Off the Louisiana Coast*" reports a blowout on Sun Rig No. 14 Platform rig while performing workover. While pumping down a work string, the gas flow was observed coming from the work string. After failing to stab the safety valve, the annular preventers and pipe rams were closed, and the rig was abandoned. The gas was ignited three days later when the traveling block fell onto the drill floor.

4- K. W. Blake (1986), "*Investigation of September 1984 Blowout and Fire Lease OCS-G 5893, Green Canyon Block 69, Gulf of Mexico, Off the Louisiana Coast*" reports the well-known Zapata Lexington Blowout. The blowout occurred on the Zapata Lexington semi-submersible rig while drilling in 1,465 ft of water at 9535 ft MD when the well kicked and the No. 1 annular preventer was closed. The recorded shut-in drill pipe pressure and shut-in casing pressure values were 200 psi and 1000 psi, respectively. The mud was weighted up, and the well was killed. The crew began the procedure to remove trapped gas from the BOP by pumping in the kill line and drill pipe and removing mud from the choke. After the procedure was completed, the No. 3 Variable Bore Rams (VBR) were closed, and the No. 1 annular preventer was opened to allow mud to circulate up the kill line. Mud was then circulated from the kill line, up the riser, and sent to the shale shaker. During the procedure, the riser discharged gas and mud, and the rig caught fire, and as a result, the rig was abandoned. This event was an example of riser gas and riser unloading.

5- F. T. Bryan (1994) "*Investigation of Loss of Well Control, Well No. 24, South Pass Block 60, Lease OCS-G 1608, December 26, 1992*" reported a loss of well control that involved H_2S gas on the Cecil Forbes Jack-Up Rig. After tripping out of the well to run a core barre, the blind rams were opened, and the well flowed. H_2S sensors reported 99 PPM. The flow was diverted by closing the blind rams again and opening the diverters. As a result of this event, 100- to 500-bbls of oil/water was discharged into the sea.

Additional blowouts can be found in other OCS reports and SPE papers.

These incidents prove that there is a need to study riser gas behavior and riser unloading. With improved kick detection methods, riser gas unloading incidents are scarce. However, the existing procedure, diverting flow from the riser overboard using the diverter systems, has remained. The overboard method, when used, comes at a high environmental and financial cost. This study provides analysis on riser gas behavior and unloading through experimentation and simulation. In addition, Managed Pressure Drilling (MPD) methods were simulated to mitigate or limit riser gas unloading. These methods have proven to be a strong candidate for proactively handling gas kicks and riser gas.

1.4. Methodology

This research was performed assuming the worst-case situation for a riser gas incident and utilized water-based muds with negligible gas solubility. Due to the minimal solubility of air in water, expansion occurs as the gas migrates. However, for OBM, gas expansion occurs as the gas comes out of the solution when the bubble point pressure is reached. Thus, gas liberation from OBM is a slow process that may aid in limiting riser unloading.

The following labs and simulation software was used to investigate riser gas migration, expansion, and riser unloading:

1- Dual Gradient Drilling Lab - 27 ft. long 6” diameter clear pipe flow loop.

2- Tower Lab – 142 ft. long 5-1/2” x 2-3/8” diameter clear pipe flow loop.

3- Computational Fluid Dynamics simulation using multiphase flow models in Ansys Fluent software and the Texas A&M University High Performance Research Computing Center.

2. DUAL GRADIENT DRILLING LAB[1]

The Dual Gradient Drilling (DGD) laboratory at the University Services Building (USB) at Texas A&M University was used to conduct flow and static experiments to study gas migration and expansion. The initial design was explained in Kaldirim (2015) and Kaldirim and Schubert (2017).

The DGD Lab contains a 27 ft. long 6-inch diameter clear PVC pipe. The pipe is supported by a rack and hoist to lift the flow loop from horizontal to vertical, allowing for vertical and inclined flow experiments. Flow is provided through two centrifugal pumps with rotary flow meters and gas injection through a compressor and air storage tank. In addition, two differential pressure transmitters are located on the flow loop to monitor and record the pressure change (Kaldirim 2015) and (Kaldirim and Schubert 2017).

[1] Reprinted with permission from "Experimental Study on Riser Gas Expansion and Unloading" by Kaldirim, Omer; Schubert, J. Jerome, 2018. Society of Petroleum Engineers/International Association of Drilling Contractors, Managed Pressure Drilling & Underbalanced Operations Conference and Exhibition, 1-6, Copyright 2018 SPE.

Figure 2-1—DGD Lab Riser Model at 0° from Vertical Reprinted from (Kaldirim 2015)

Figure 2-1 displays the DGD Lab Riser Model in the vertical position while in use. The flow modes in the initial phase of these experiments were achieved through injection at the base using annular flow. These experiments were done using a discharge line at 7ft to simulate the pumped riser system and described in Kaldirim (2015) and Kaldirim and Schubert (2017).

The lab was continuously modified and upgraded throughout this research to run various experiments. The following are the upgrades in the DGD Lab:

1- A vacuum pump was installed to eliminate the ambient pressure during static experiments.

2- A mud gas separator was installed to degas the liquid.

3- A 200-gallon cone-bottom tank was installed to provide increased liquid volume for experiments.

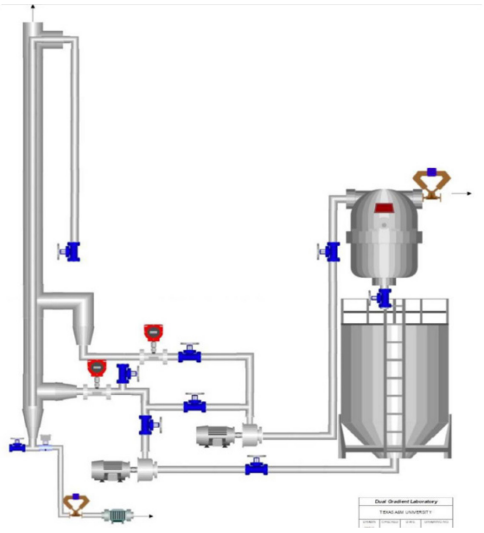

Figure 2-2—DGD Riser Simulator Design after initial upgrades Reprinted from (Kaldirim and Schubert 2017)

Figure 2-2 displays the lab schematic for the DGD lab following the initial modifications listed above. A data acquisition system was used to monitor and collect data from the sensors and flow meters. The system was controlled using a LabView control program.

The experiments consisted of two modes: mud circulation and static conditions. Water was used as the liquid phase and air as the gaseous phase for the mud circulation methods. Water and air were injected at various gas and mud rates.

For the static conditions, water was not circulated, and gas was injected at various rates. In addition, a portion of the static experiments was conducted under vacuum conditions to observe higher expansion rates of the gas.

The Dual Gradient Drilling lab modifications were performed; however, the height limitation validated the limitation of obtaining usable data for a riser gas expansion study.

Therefore, the remainder of this section was reprinted with modifications from SPE-190004-MS.

2.1. Experimental Study on Riser Gas Expansion and Unloading

2.1.1. Abstract

Gas influxes are common during drilling operations. If not handled properly, gas can expand and unload the riser in an open-loop system; in closed-loop systems, unless gas is depressurized, the top section of the riser would become over pressured. Riser unloading has not been accurately modeled due to uncertainties in gas expansion. This paper presents studies on gas expansion and unloading in a lab-scale model at Texas A&M University.

Experiments were performed in a scaled riser at the Dual Gradient Drilling Laboratory and were run using water and air as the gas phase. The change in volume as the gas expands and liquid height was logged. The disproportion of the atmospheric pressure and the scale of the model was mitigated using a vacuum pump. Final gas volume was recorded by measuring the liquid level.

The experiments provide information on the gas expansion and riser unloading. During the expansion process, the top of the bubble travels rapidly, building momentum, which carries a large volume of mud to the top of the riser model. And this occurs through the rapid change in gas volume and the energy released as the pressure decreases. By allowing gas to expand in a controlled environment, the impact of gas expansion was monitored.

This paper provides information on the controlled and uncontrolled gas expansion, impact on riser unloading, and benefits of a closed system.

2.1.2. Introduction

Gas migration is a subject that has been observed and studied to a great extent in industry and research centers. The effect of gas migration through kicks can create unwanted situations if left uncontrolled in wells. And this is especially important in offshore wells where the Blowout Preventers (BOP) are located at a depth away from the rig floor. This space contained by the marine riser is where gas may come out of solution and rapidly migrate and go through volumetric expansion as the hydrostatic pressure is reduced. This issue has been studied in various papers through field experiments.

One such study was described in Hall et al. (1986). The authors proposed methods of handling gas in the riser by closing the BOP, the riser diverter, opening the choke line, and filling the riser with the mud from the riser boost line to control the riser kick.

There are also small-scale lab studies performed on gas migration to determine the migration velocities. For example, in Johnson and Cooper (1993), the authors studied gas migration velocity using air and aqueous Xanthan gum solution and ran tests in a deviated flow loop. They compared their results for migration velocity to the rule of thumb and field experiences.

Various models have been created throughout the years, and procedures have been proposed in technical papers and committees within IADC to establish safe mitigation of gas in the riser. More recent modeling of a field trial and safe mitigation procedure can be

found in Yuan et al. (2017), where the authors modeled a riser gas field trial described in Hauge et al. (2015). In Hauge et al. (2015), the authors describe riser gas influx tests performed using nitrogen injection, and the expansion and rise velocity of the gas was studied as the gas migrated. In addition, Yuan et al. (2017) described a simulation model created and successfully matched using Hauge et al. (2015). The authors also provide procedures for mitigating gas in the riser.

This paper presents an update on the study performed in a lab-scale model at the Dual Gradient Drilling Laboratory at Texas A&M University. This study was performed following the papers Kaldirim and Schubert (2017) and Kaldirim (2015). The scaled riser setup used in these papers was designed with a limited height. The height limitation of the flow loop made it impossible to observe a gas expansion in the system. Although minimal pressure changes were recorded, the hydrostatic pressure created by the flow loop was lower than the atmospheric pressure, resulting in very little gas expansion, this can be explained with the Real Gas Law.

$$Z = \frac{P * V}{nRT}, \ldots\ldots\ldots\ldots\ldots\ldots\ldots (1)$$

The Real Gas Law relates pressure, volume, temperature, and gas compressibility. Starting at this point, the 26 ft height of the flow loop could only create a pressure of about 12 psi using water. The combination of the atmospheric pressure and the hydrostatic can only create a pressure of 26-27 psi. When gas bubbles migrate to the top of the flow loop, the volume can only increase by about 90%.

To better observe expansion, a vacuum pump was installed, allowing the pre-existing pressure in the system to be reduced. With the reduction of atmospheric pressure,

the ratio in the Real Gas Law increases, allowing for a more significant increase in bubble size. For example, assuming the atmospheric pressure is reduced to 5 psia, the new pressure exerted to the bottom of the flow would become approximately 17 psi, and as the bubble migrates to the top, and the pressure above the bubble would decline, causing the bubble volume to increase by 3.5 times. Further reducing the existing pressure in the flow loop would allow this expansion ratio to increase, operating under the assumption that the temperature and properties of the gas did not change and neglecting the Z factor.

2.1.3. Lab Setup

Following the previous setup explained in Kaldirim and Schubert (2017) and Kaldirim (2015), the experimental setup at the Dual Gradient Drilling Laboratory at Texas A&M University was further modified to run experiments in a vacuum to observe gas expansion.

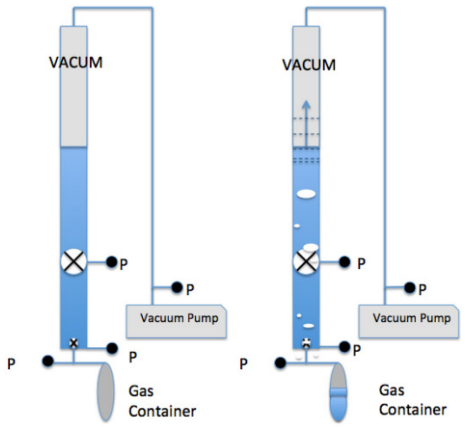

Figure 2-3—Experimental setup with Vacuum Pump. Reprinted from (Kaldirim and Schubert 2018)

As seen in **Figure 2-3**, the flow loop design remained constant except for the vacuum pump, isolation valves, and 300 mL gas container located at the system's

bottom. **Figure 2-4** displays the vacuum pump and vacuum pressure gauge used to monitor pressure at the top of the flow loop.

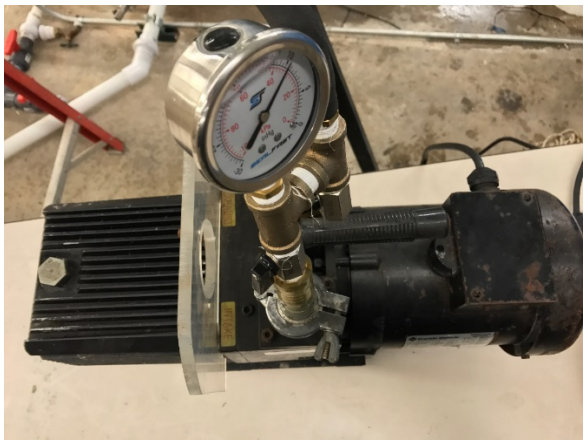

Figure 2-4—Vacuum pump used in experiments. Reprinted from (Kaldirim and Schubert 2018)

Figure 2-5 displays the setup of the base of the flow loop with the 300 mL gas container on the left and the positive and vacuum pressure gauge on the right. This pressure gauge displayed the total pressure applied at the base of the flow loop.

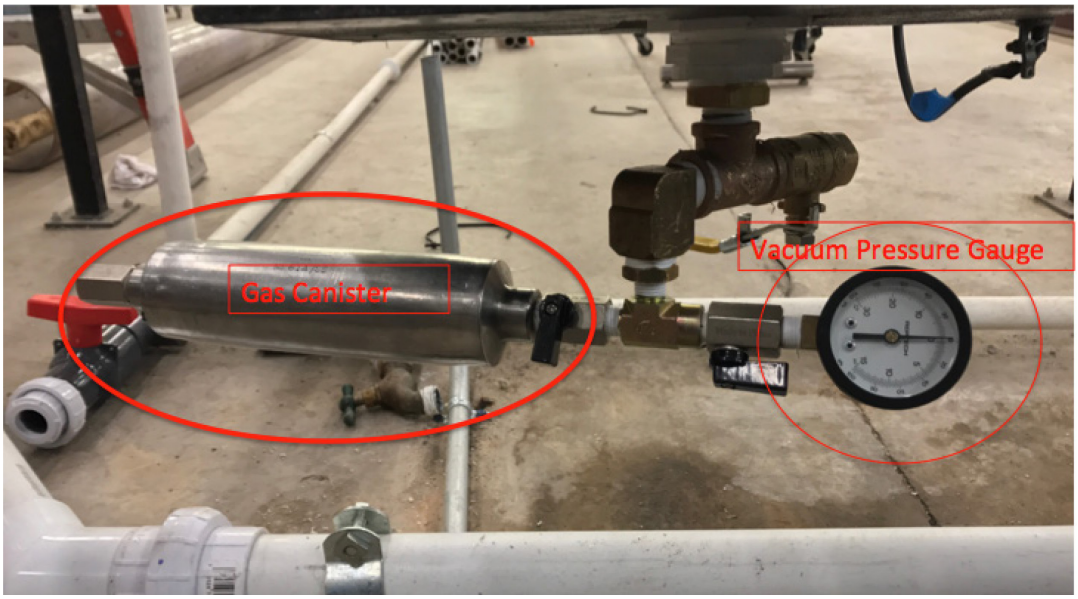

Figure 2-5—Base setup for flow loop with gas canister on the left and vacuum pressure gauge on the right. Reprinted from (Kaldirim and Schubert 2018)

The vacuum pressure gauges were used to record the vacuum pressure. The vacuum pump was switched on before experiments to remove the air and reduce the pressure.

2.1.4. Procedure

The following lists the procedure for the experiments:

1- Before each experiment, the column was filled with water to the desired height.

2- The vacuum pump was switched on. The pressure reduction was closely observed to confirm that the flow loop is holding the vacuum.

3- Once the pressure was lowered to the desired level, the vacuum pump was switched off, and pressure was logged at three locations, 1) the base of the flow loop, 2)the entrance of the flow loop, and 3)7-feet from the base.

4- The video recorders were turned on and set up to record gas bubble migration at 7 feet and 13 feet height from the base of the flow loop.

5- Finally, the gas container isolation valve was opened to pull air into the flow loop.

6- Once the air in the system was removed, the gas container was isolated and drained.

Once draining was complete, the test was repeated.

2.1.5. Experimental Setup

1- The experiments were run at atmospheric pressure, then under vacuum at 10 psia, 5 psia, and 1.95 psia. These values were selected to observe gas expansion.

2- The height of the water column was set at 13 feet, which corresponds to a hydrostatic pressure of 5.85 psi. This height was optimal for visualizing and recording the change in water height.
3- The atmospheric pressure was recorded as 14.59 psi (29.7 in-Hg) when the experiments were performed at College Station, TX.
4- The amount of liquid in the gas canister was measured. This measurement was used to calculate the amount of air pulled into the flow loop.

2.1.6. Results and Discussion

Each test was run until no air migration could be observed. The initial tests were run at atmospheric pressure and a vacuum pressure of 10 psi. These tests yielded no observable expansion. Water level increase was not measurable either.

An observable expansion occurred when the pressure was reduced to 5-psi. The volume of the bubbles almost doubled in size as they migrated to the top of the flow loop. It was also noticed that no water had flowed from the water column into the gas canister.

When the pressure in the system was reduced to 1.95-psi (-26 in-Hg) vacuum pressure, gas expansion began as soon as the gas canister valve was opened. The increased ratio allowed for gas expansion to be observed as the gas bubbles moved up. Also, a change in liquid level of 7-inches was recorded when the bubble reached the top of the column. This level increase corresponds to a volume of 3243.3-mL. Considering the initial volume of the gas injected into the system was about 300 ml at atmospheric conditions, the gas bubble had expanded more than 10 times.

Figure 2-6—Gas bubble expansion experiments under vacuum conditions. Reprinted from (Kaldirim and Schubert 2018)

Figure 2-6 displays images from the slow-motion videos recorded during experiments.

2.1.7. Conclusions

This study continued the work presented in Kaldirim and Schubert (2017) and Kaldirim (2015), where gas migration was studied in circulation.

- In this study, the experiments were conducted under vacuum conditions with no circulation.

- Gas was injected out of a 300 mL canister at atmospheric pressure; expansion was not observed in the first few experiments until the pressure was reduced to 5 psi.
- The lower the vacuum pressure, the more observable the gas expansion was. A volume increase of more than 10 times was achieved through these experiments.
- Gas bubbles changed shape under vacuum; the bubbles were no longer spherical and were more prone to connect and form larger bubbles.
- There was no noticeable change in riser gas migration rates compared to standard tests in atmospheric pressure conditions.

These tests made it evident that applying pressure to the fluid column reduced the gas expansion and kept migration under controllable conditions.

3. TOWER LAB

The Tower Lab contains a flow loop is located at the Richardson building and spans all 10 floors plus the basement, creating a vertical height of 43 meters. The flow loop consists of a 5.5-inch clear pipe with a 2-3/8-inch drill pipe located at the center for annular flow experiments. The system also contains multiple flow meters, control valves, and pressure transmitters. In addition, a 100-gallon separator is located on the 10th floor at the discharge line to separate gas and liquid. The Tower Lab space is displayed in **Figure 3-1**.

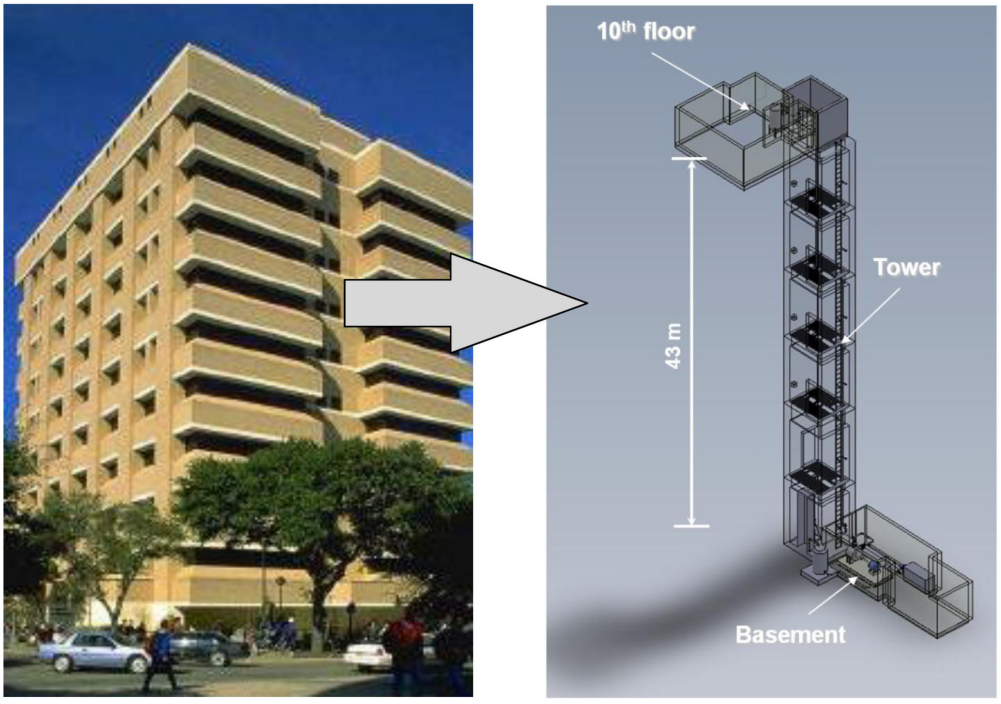

Figure 3-1—Tower Lab Schematic View Reprinted from (Tower Lab Design and Operations Manual, 2012)

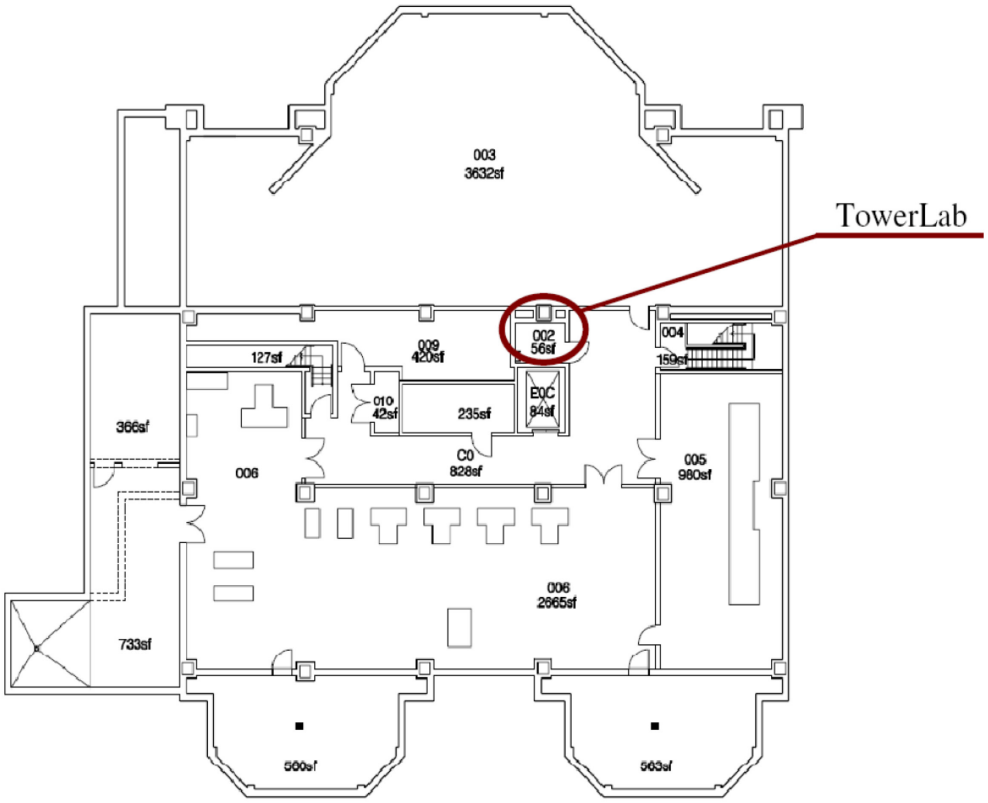

Figure 3-2—First floor level plan showing the location of the Tower Lab inside the Joe C. Richardson building. Reprinted from (Fernandez Alvarez 2009).

Figure 3-2 displays the first level floor plan with the Tower Lab Room indicated. Before modifications, the lab contained a 200-gallon water tank located in the crawl space in the basement and a boost pump to supply water to the lab.

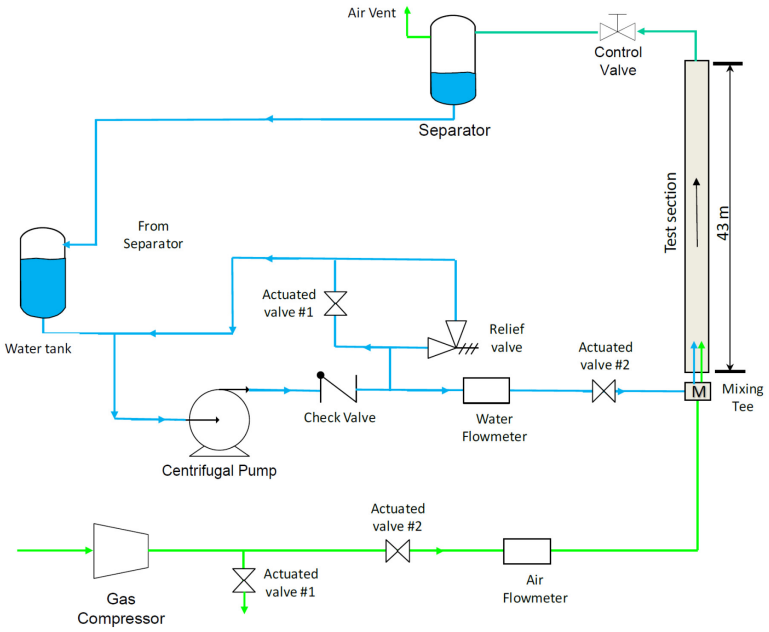

Figure 3-3—Pre-Modification Schematic Diagram of the Tower Lab Flow Loop. Reprinted from (Waltrich et al. 2011)

Figure 3-3 displays the Tower Lab schematic before modifications were performed for this research.

3.1. Challenges

The tower lab modifications required an extensive evaluation of the lab, supply lines, pump, tanks, flow meters, pressure transmitters, wiring and cables, and data acquisition system.

The modifications began with removing the pump and supply lines. The pump was undersized and damaged (**Figure 3-4).**

Figure 3-4—Damaged Boost Pump

Once the pump was removed, the 1-inch steel pipes were visually evaluated and removed due to extensive corrosion and rust **Figure 3-5.**

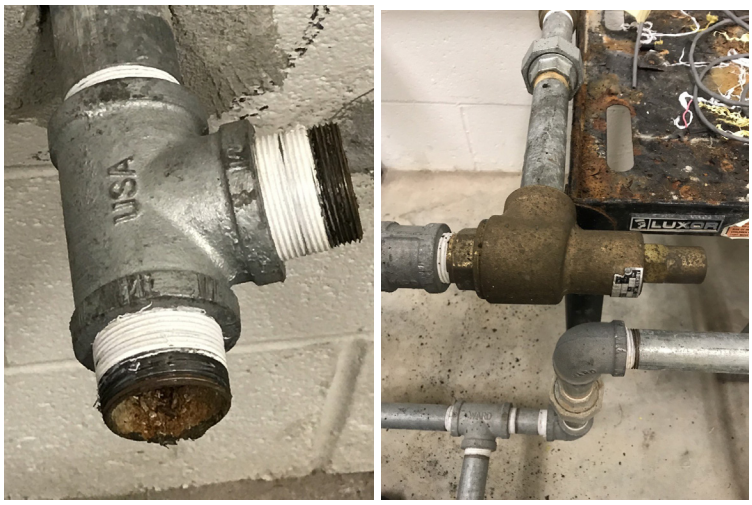

Figure 3-5—Rust and Corrosion on Water Supply Lines

The tower lab pump room also contained a multiphase twin-screw Bornemann pump which was wired to a VFD. Maintenance was performed on the pump, and the pump was tested. After successfully testing the pump, the lab design was changed again to pipe the Bornemann pump into the flow loop, starting with the water line from the water tank. The existing 200-gal flatbottom water tank located in the basement's crawl space was at a level lower than the pump room, and the limited ceiling clearance made the location of the tank inefficient. Moving this tank to another floor was also tricky as the diameter of the tank was too large to slide through the tower lab doors. A new 200-gal cone-bottom tank was installed on the 2nd floor access room to provide additional pressure on the suction side of the pump. Since the supply line to and from the original tank was from the crawl space to the pump room, new 2-inch PVC pipe supply lines were installed. The pipe ran from the flow loop return to the 2nd floor water tank and from the water tank to the Bornemann pump in the basement. After the water supply lines to the pump were installed, the discharge line from the pump to the tower lab flow loop was designed and installed.

The Bornemann pump has a 4-in outlet flange. A steel 4-in pipe was installed, then reduced to 2-in, connecting to a series of ball valves, 1-1/2-in MicroMotion mass flow meter (**Figure 3-6**), and two pneumatic control valves.

Figure 3-6—1-1/2-in MicroMotion Mass Flow Meter (Bottom) and Flow Transmitters (Top)

The manual ball valves were placed on pipe tees to allow water to be diverted to a drain line to drain the flow loop and water tank. The drain lines were also built after building the supply line from the pump to the tower lab flow loop. **Figure 3-7** displays the Bornemann Pump and supply lines to the tower lab flow loop.

Figure 3-7—Multiphase Twin Screw Bornemann Pump and Supply Pipes

Upon completion of all supply lines, the 10th floor discharge and return lines were removed due to rust and corrosion. Next, 2-in steel pipe was installed, and the tower lab flow loop was reconnected to the mud gas separator. Finally, the second 2-in MicroMotion mass flow meter was placed between the flow loop and the separator to measure the discharge rate from the tower lab.

The next step in the modifications was to redesign the air supply line. Due to corrosion, the old air supply line was removed, replaced with a new ¾-in steel line, and reconnected to the tower lab flow loop at the mixing tree. The old flow meter was replaced with a newer ¾-in mass flow meter.

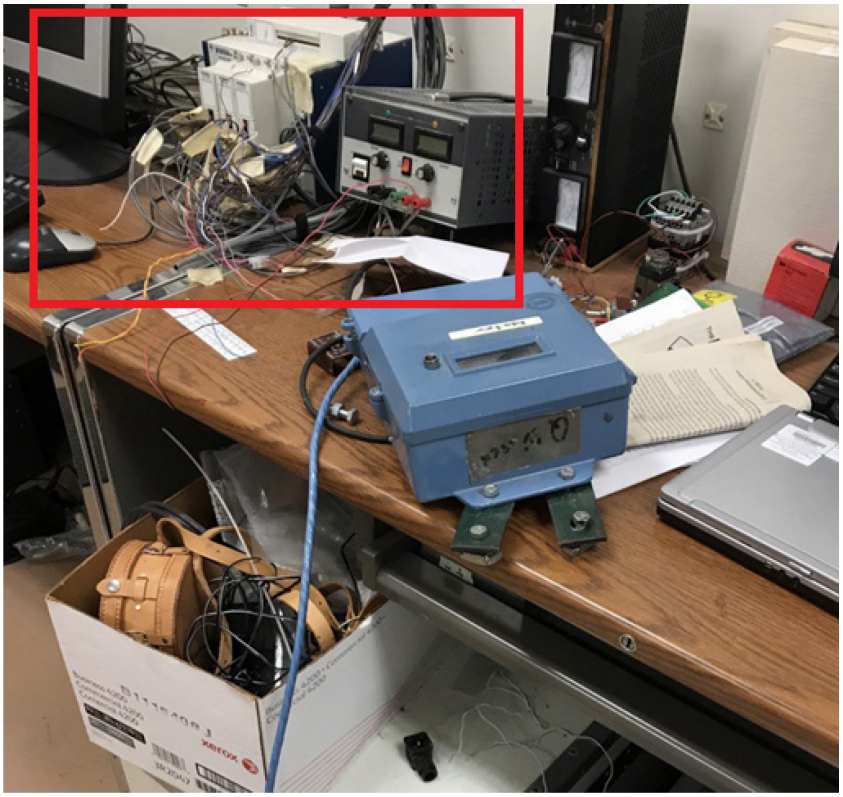

Figure 3-8—Original Data Acquisition System

The original data acquisition system displayed in **Figure 3-8** was also disconnected and removed. All sensor wiring was disconnected, and the cables were removed from the tower lab. After removing all the wiring, 170-ft of 1-1/2-in PVC pipe was installed through the tower lab and the pump room to pull cable. A sensor database was created to log the location of each sensor to prepare cables. Each wire was tagged and wired to the sensors. The new Data Acquisition System was placed inside the enclosure, and the enclosure was mounted in the pump room. The pump room provides easy access to the Data Acquisition System, prevents unauthorized tampering, and eliminates the need for a large bundle of cables entering the 6th floor control room.

All pressure transmitters were cleaned, flushed, and new fittings and tubing were installed. The pressure transmitters were calibrated, tagged, and reinstalled onto the flow loop. The flow meters, control valves, and VFD were wired to the Data Acquisition System. The sensor database was updated with wire tag and data acquisition system port. The new Data Acquisition System and Enclosure is displayed in **Figure 3-9.**

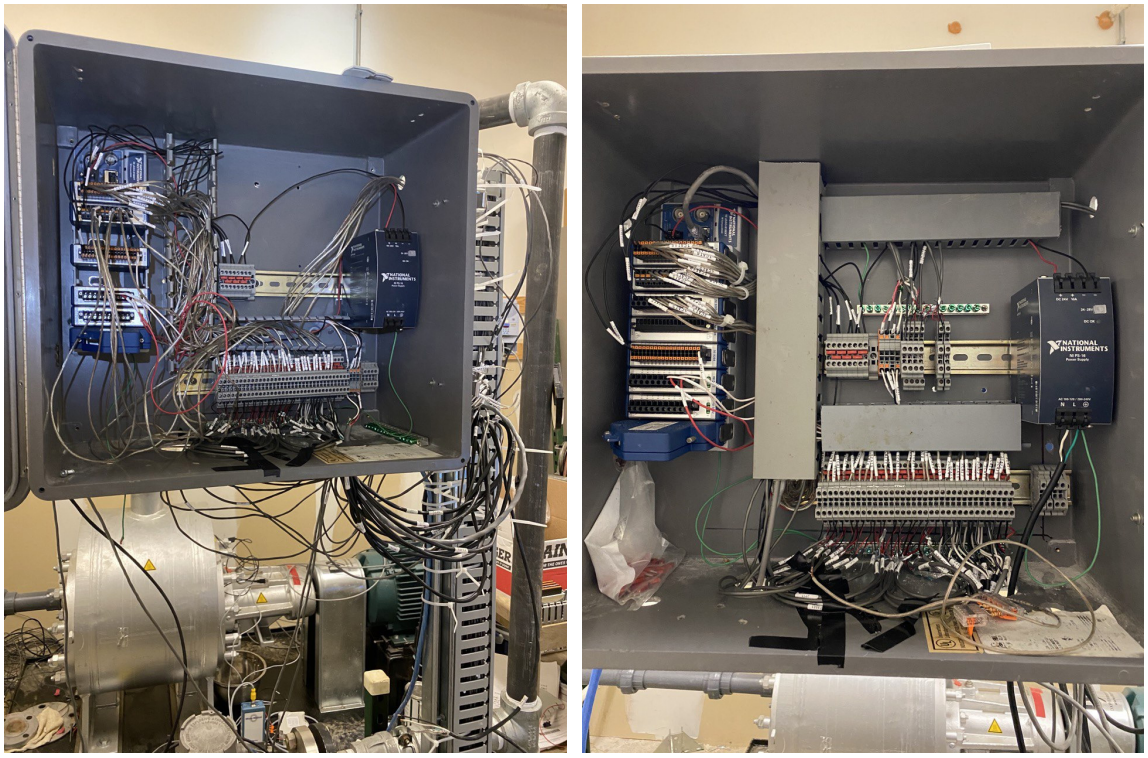

Figure 3-9—New Data Acquisition System

The LabVIEW vi was built with calibration data for the pressure transmitters. A leak test and pressure test were conducted. The valves were also tested, and it was noticed that the Pressure Relief Valve (PRV) on the 1st floor was not holding pressure. The PRV with steel pipes and valves were replaced with new PRV, ball valves, and steel pipe. A new drain line was built using 2-in PVC pipe to eliminate the need for large hoses.

The test also demonstrated that the control valve on the gas injection line was a slow-responding valve, so a solenoid valve was added to start and stop gas injection rapidly. In addition to adding a solenoid valve, a pressure regulator to control the gas injection pressure and a PRV to prevent over-pressuring were installed on the gas line.

To run experiments with solubility, a carbon dioxide (CO_2) tank, a two-stage CO_2 pressure regulator, and 10-ft of ¼-in high-pressure steel tubing were connected to the gas injection line.

3.2. Tower Lab Modifications

For this research project, the Tower Lab was extensively evaluated, upgraded, and modified. As a result, the following upgrades were applied:

1- A 200-gallon cone-bottom tank was installed on the 2nd floor to provide additional suction pressure to the pump inlet to reduce the load on the pump. This modification required 40 ft of 2-in PVC pipe to supply water to the pump at the basement and divert water from the return line to the new water tank.

2- The boost pump and 20-ft of 1-in steel lines were removed. During evaluation and modification, it was noticed that the pump motor had been damaged. Upon removing the pump, the 1-in steel lines were examined and replaced due to extensive corrosion and rust.

3- A multiphase, twin-screw Bornemann pump was connected to the flow loop. The Bornemann pump outputs a flow rate of 200 GPM and 200 psi pressure. Maintenance was performed on the pump, and the Variable Frequency Drive was programmed to limit the pump from damaging the tower lab. After maintenance,

20-ft of 2-in steel pipes were installed to supply water from the pump outlet to the Tower Base. The reason for the steel pipe was to reduce the risk of a pipe burst. A 1-1/2-in Micromotion Mass Flowmeter was also installed on the steel line to collect water injection data.

4- At the 10th floor return line, the 2-in steel lines were replaced with 10-ft of new 2-in steel pipe, and a 2-in MicroMotion Mass Flow Meter was installed at the outlet. The valves were also replaced, and the pressure ports were rearranged.

5- For gas injection, the existing ¾" gas supply line from the compressor to the base of the Tower Lab was replaced with 15-ft of new ¾-in steel pipe, and valves were installed, along with a Pressure Relief Valve (PRV) to prevent over-pressuring of the air supply lines. A pressure regulator was also installed on the gas line to control the injection pressure. The existing Control Valve was reinstalled to be able to start and stop gas injection remotely. However, due to the slow actuation of this valve, a Solenoid valve was installed downstream of the control valve closer to the mixing tree. The existing ¾-in MicroMotion mass flow meter was replaced with a newer ¾" MicroMotion mass flow meter. The flow meter was then moved from the pump room to the tower lab to obtain a more accurate measurement of the volume of gas injected.

6- A carbon dioxide (CO_2) tank was installed in the Pump Room. A two-stage CO_2 Pressure Regulator, ¼" High-Pressure Stainless-Steel pipe, was installed and connected to the air line. A hose was attached from the air supply line PRV

discharge port to the tower to prevent gas from being discharged into the pump room.

7- The PRV and 2-in steel drain lines were removed due to corrosion. New 2-in steel drain lines and a new 2" PRV were installed at the 1st Floor Tower Lab access room. The hose connecting the PRV drain to the drain line was removed and replaced with 20-ft of 2-in PVC pipe to improve safety and make space in the basement tower room.

8- The old data acquisition system (obsolete) was replaced with a new NI CDAQ-9188XT, which comprises three analog current inputs, one analog current output, one analog voltage input, one analog voltage output, and one relay module. The new system was installed in a waterproof enclosure in the basement. First, all old cables were removed from the lab. Next, 170-ft of PVC pipe was installed to use as a conduit for all cables. A total of 3,000-ft of 18 AWG, 400-ft of Cat5, and 2000-ft of 22 AWG paired wire cables were pulled through the conduit, with one end extending into the DAQ Enclosure in the basement. The other end of the cables extends to the flow meters, control valves, and pressure transmitters installed in the tower lab.

9- The 23 Rosemount Pressure Transmitters were removed from the tower, flushed, cleaned, and recalibrated using a deadweight tester, then reinstalled and wired.

10- The three MicroMotion Mass Flow Meters were reprogrammed and wired.

11- The solenoid and control valves on the gas line were wired.

12- The two pneumatic control valves on the water supply line were wired and cleaned.

13- 100-ft ½-in air hose was installed from the 201 Lab access to the air line to provide continuous air supply for experiments.

14- Three 25-ft water hoses were connected from the 201 Lab to the water tank to supply water for experiments.

15- The VFD for the Bornemann pump was wired to the DAQ.

16- A LabVIEW vi was programmed to control and log data from the Tower Lab. In addition, a professional version of MicroMotion Prolink software was used for logging data from the MicroMotion mass flow meters.

17- The four obsolete cameras were removed from the lab, and three GoPro Hero 8 cameras were purchased and placed in the Tower Lab on the 2^{nd}, $5^{th,}$ and 8^{th} floors. The videos from the cameras were used for information on flow patterns and gas migration rates.

Figure 3-10 displays the updated P&ID schematic of the Tower Lab.

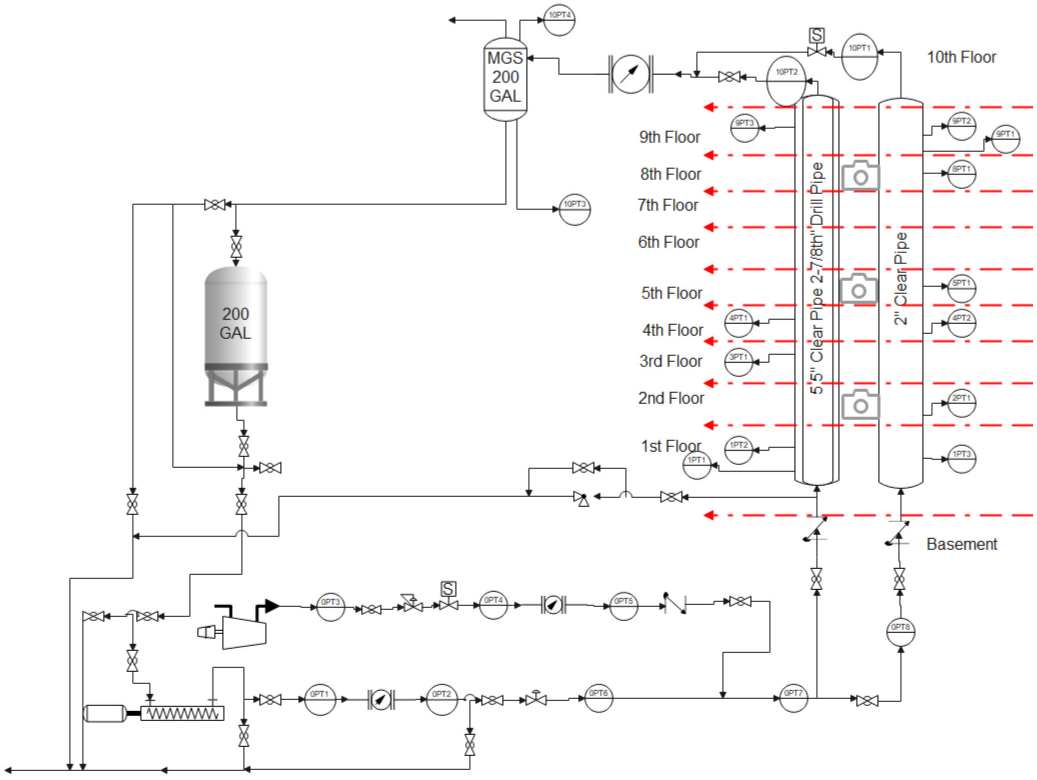

Figure 3-10—Tower Lab P&ID schematic with access floor indicators (Updated as of December 2020)

Following the initial experiments and analyzing data, it was observed that the total volume of gas injected was not correct due to the location of the flow meter on the gas supply line. To improve the accuracy of total injected gas volume, the flow meter, and the solenoid valve were moved closer to the injection port on the mixing tree. These changes minimized the error in the total volume measurement of gas injected.

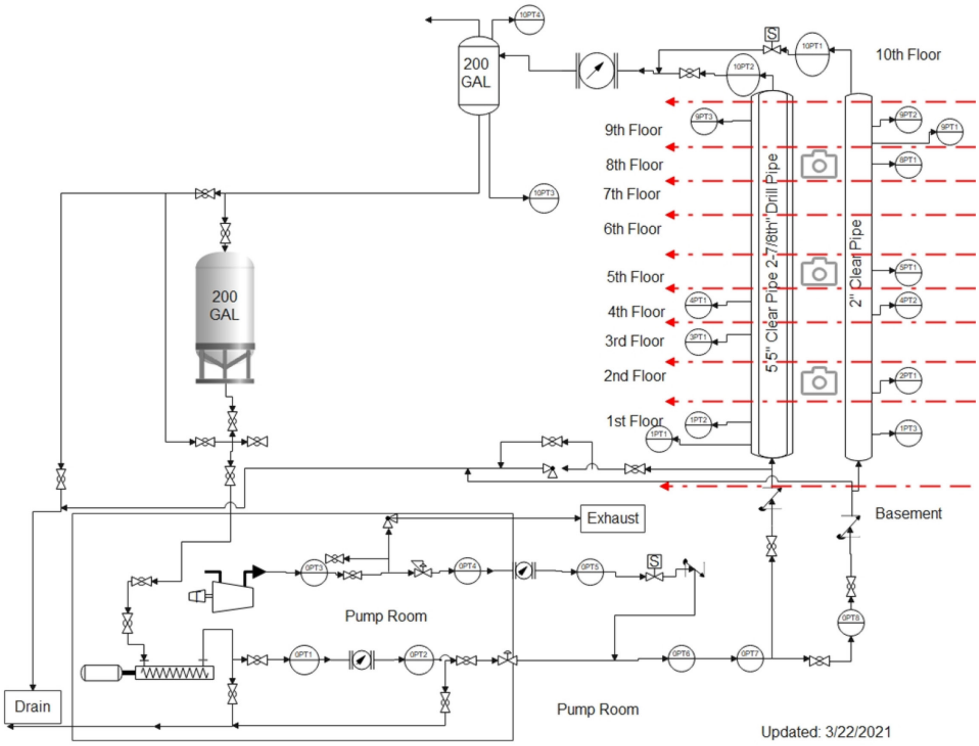

Figure 3-11—Tower Lab P&ID Schematic with access floor indicators (Updated as of March 2021)

Figure 3-11 displays the P&ID schematic of the Tower Lab as of December 2020 and March 2021. The pressure transmitters are indicated on the supply, discharge, and 2" and 5.5" flow loops. The pressure transmitters are tagged, starting with "0PT1" at the basement, immediately downstream of the pump, to "10PT4" ending at the 10th floor at the vent line of the mud gas separator. The pressure transmitter tags are 4-to-5-digit style, with the first digit indicating the floor the transmitter is installed in, while the last digit indicates the series on which the pressure transmitter is installed.

3.3. Test Procedures

3.3.1. Preparation Phase

The preparation phase to run tests at the Tower Lab takes an hour. These steps are listed as follows:

1- Room 1001b

   a. Open the discharge valve inside the Tower room.
   b. Open the valve at the bottom of the mud gas separator, which leads mud from the separator to the return line.
   c. Open the vent valve on the top of the mud gas separator.
   d. Power the MicroMotion flow transmitter to power the Discharge Flow Meter.

2- Basement Pump Room:

   a. Open the PVC Ball Valve located on the supply line of the pump.
   b. Open all steel ball valves downstream of the pump along the flow line.
   c. Close steel ball valves that connect to the PVC drain lines.
   d. Power up the Data Acquisition System, flow transmitter, and compressor drain valve.
   e. Either open the air injection valve or the CO_2 injection valve. Next, the lines need to be flooded with test gas before filling the tower with water by following these steps:
      i. For CO_2: Open the regulator and set the injection pressure on the CO_2 bottles. Next, open the ¼" ball valve on the injection line.

Close the air injection line. Set the injection pressure on the secondary pressure regulator. On LabView, set 0Valve1 to 10 and set the duration for the solenoid valve to 20 seconds. These settings allow for CO2 injection into the flow loop for 20 seconds.

ii. For Air: Plug the black air line in Room 201 into the air supply. Open the air supply valve. In the Basement Tower, open the ¼" ball valve for the air line. Set the secondary regulator pressure to injection pressure. On LabView, set 0Valve1 to 10 and set the duration for the solenoid valve to 20 seconds. These settings allow for air injection into the flow loop for 20 seconds.

3- Basement Tower:

a. Open the vertical ball valve on the PVC line to allow water to flow to the pump.

b. Open the steel ball valves on the flow loop. These manual ball valves isolate the upper section (test section) from the basement.

c. Power the flow transmitter to power the Coriolis meter to monitor and log the gas injection rate.

4- In Lab 201 Access Room:

a. Connect all water hoses to the water supply in room 201. Next, open the water valves to begin filling the water tank.

b. Connect the two air supply lines to the air supply and open the valves on the air supply to allow airflow. The red air supply line provides air to open

the pneumatic valves that isolate the tower from the pump room. These pneumatic valves are in the basement tower, can be controlled using LabVIEW, and are labeled in LabView as 0Valve2 and 0Valve3.

c. Once the water tank is filled, close all water supply valves.

d. Open the manual PVC ball valves #1 and #4, located downstream of the water tank (at the bottom of the water tank). These steps allow water to fill the pump and u-tube into the flow loop.

5- In Basement Pump Room:

a. Switch on the VFD by turning the power switch on inside the panel. Then, on the VFD, set control mode to automatic.

6- In Lab 601 Control Room:

a. Open the LabView control program.

b. Plugin the RS-485 converter into the computer.

c. Turn on Prolink Software.

d. On Labview, set 0Valve3 to 4 to open the pneumatic valve.

e. Click the Enable Pump button.

f. Click the Direction Button.

g. Set VFD Speed to 2.2 V.

h. Water should be flowing into the flow loop.

i. At all times, monitor pressure transmitters 0PT1 (Mud Pump) and 1PT1(1st floor). These pressure transmitters indicate if there is a problem.

j. Once the flow loop is filled, the desired flow rate can be selected by increasing the Pump Rate Voltage.

k. For static tests, set the pump rate to 2.2 volts, set 0Valve3 to 20 mA, and immediately disable the pump by unchecking the enable pump and the direction buttons.

l. The pump should not be run dry.

m. The pump should not be run if 0valve3 is not set to 4 volts.

n. If pump pressure (0PT1) or 1PT1 display a sudden spike exceeding 70 psi, immediately terminate and check the valves. This surge in pressure indicates that a valve is closed on the flow path. Do not over-pressure the supply lines or the flow loop. If a sudden sharp decrease in flow rate or pressure is observed, terminate the test, and inspect the pump. Check for leaks, temperature, and oil level.

3.3.2. Data Logging

3.3.2.1. Flow Rates

One of the goals of this section is to study the effects of kick intensity, kick volume, and circulation rate on the unloading rate and volume. First, a Coriolis meter (MicroMotion R200S series) was placed on the discharge line to obtain an exact outflow measurement. Next, a second Coriolis meter (MicroMotion F100S series) and a solenoid valve were installed on the gas injection line at 10 inches from the injection port. Finally, a third Coriolis meter (MicroMotion DS150S series) was placed downstream of the multiphase flow pump to measure the circulation rate.

The flow meters at the discharge and gas injection were wired to output digital signal through RS-485 connection and linked to the Prolink Software provided by the OEM. These flow meters output, flow rates, and flow totals for volume and mass, density, and temperature data. The flow meter downstream of the pump was older and was wired to output only flow rate on an analog current signal which LabView logged.

3.3.2.2. Pressure Measurements

The pressure was measured along the flow loop at various points using twenty-two Emerson Rosemount 1151HP series differential pressure transmitters, a Rosemount 2088-gauge pressure transmitter, and a Rosemount 3051C differential pressure transmitter. The differential pressure transmitters were connected on a single side to measure single-point pressure. A list of transmitter labels and the location and connection point are listed in **Table 3-1.** Certain pressure transmitters listed as “not used” were attached to the 2” flow loop. The experiments presented in this dissertation were conducted using the 5.5”x2-3/8” annular flow loop. The Transmitters 1PT1, 1PT2, 3PT1, 4PT1, 9PT3, and 10PT2 (Discharge Pressure) are attached to the test section of the flow loop.

Label	Location	Port Connected
0PT1	Basement - Pump Room	Downstream of pump
0PT2	Basement - Pump Room	Downstream of pump
0PT3	Basement - Pump Room	Gas Line
0PT4	Basement - Pump Room	Gas Line downstream of pressure regulator #2
0PT5	Basement - Tower	Gas line downstream of solenoid valve
0PT6	Basement - Tower	Base of Tower
0PT7	Basement - Tower	Injection Port
0PT8	Basement - Tower	Base of 2" Tower (not used)
1PT1	1st Floor	5.5" Tower
1PT2	2nd Floor	5.5"Tower
1PT3	3rd Floor	2" Tower (not used)
2PT1	2nd Floor	2" Tower (not used)
3PT1	3rd Floor	5.5"Tower
4PT1	4th Floor	5.5"Tower
4PT2	4th Floor	2" Tower (not used)
5PT1	5th Floor	2" Tower (not used)
8PT1	8th Floor	2" Tower (not used)
9PT1	9th Floor	2" Tower (not used)
9PT2	9th Floor	2" Tower (not used)
9PT3	9th Floor	5.5"Tower
10PT1	10th Floor - Tower	2" Tower (not used)
10PT2 (Discharge Pressure)	10th Floor - Tower	Discharge Pressure
10PT3	10th Floor - MGS	Base of MGS
10PT4	10th Floor - MGS	Top of MGS

Table 3-1—Tower Lab Pressure Transmitter Labels and Locations

4. TOWER LAB EXPERIMENTS

The Tower Lab provides a unique opportunity to perform various studies on annular flow in a controlled environment with access on multiple levels 14-ft apart. The clear piping allows for visual observation of flow patterns, gas location, and migration rate, which can aid in fingerprint pressure and flow data.

The purpose of the extensive modifications in the Tower Lab was to allow for studying gas migration and expansion using flow rate, pressure, and video footage. Installing a flow meter at the outlet allows for real-time discharge rate logging to study the change in discharge rate as a result of gas expansion and migration. In addition, video footage captured from the experiments provides the ability to measure migration rate between cameras visually. The video footage also verifies pressure changes as the top of the bubble reaches pressure ports along the flow loop.

For this study, static and dynamic mud experiments were run to observe the effects of circulation on gas migration rate, expansion rate, pressure changes, and overall unloading rate (discharge rate). These experiments were also run with gas at 90- and 80-psi injection pressures, controlled using two pressure regulators. Two circulation rates (15- and 30-GPM) were selected for the dynamic cases. Air and carbon dioxide (CO_2) were used for the tests presented in this section to study free gas and solubility.

The main focus was on the worst-case condition, where a high kick intensity insoluble gas influx enters the well and is allowed to migrate with no circulation. Once the static tests were completed, two circulation rates, 15- and 30-GPM, were selected with the

same gas injection pressures and durations for comparison. The final subsection in this chapter presents results from four tests where CO_2 is injected to simulate solubility.

4.1. Air Injection

Tests run in this section were all run using air as the gaseous phase. The objectives of this phase were to understand:

1- Unloading when solubility can be neglected.

2- Effects of Initial Injection Pressure.

3- Effects of circulation rate.

This section is split into three sections, 1- Static, 2- Circulation Rate: 15-GPM, and 3- Circulation Rate: 30-GPM.

4.1.1. Static Mud

All tests presented under this subsection were run with the mud pump off. During the test, all flow rate and pressure data were logged. The tests conducted under this subsection were performed using 90 and 80 Psi initial injection pressures and 60- and 30-seconds injection duration.

Pump Rate (GPM)	0		0	
Initial Injection Pressure (PSI)	90.93	90.7	80.04	74.07
Gas Injection Duration (seconds)	60	30	60	30
Kick Intensity (lbs./gal)	3.9	3.86	2.4	1.65
Maximum Injection Rate (GPM)	9.02	7.34	8.92	7.63
Average Injection Rate (GPM)	6.72	5.99	6.64	5.66
Total Gas Injected (gal)	8.04	3.72	7.83	3.62
Maximum Discharge Rate (GPM)	108.50	83.94	91.01	41.09
Max Rate at Unloading (GPM)	108.50	83.94	40.40	28.69
Total Discharged Volume (gal)	44.27	24.15	42.01	23.77
Total Discharged During Unloading (gal)	43.20	22.37	42.01	18.78

Table 4-1—Summary of results for Static Tests using Air as the gaseous phase

Table 4-1 summarizes the results for tests run at static conditions using air as the injection phase. 60 and 30 seconds were selected as injection duration with approximately 90-psi for high pressure and 80.04- and 74.07-psi for the initial injection pressures. The table displays the maximum and average injection rates, the total volume of gas injected maximum discharge rate, maximum discharge rate at unloading, total discharged volume, and total discharge up to unloading. As seen in the data, higher pressure and duration allowed for greater maximum and average injection rates. These rates were due to pressure drop created overall in the flow loop with gas entering. The maximum discharge rates also displayed the same behavior as larger gas enters the flow loop. However, the discrepancy was observed in the total volume of mud discharged with the longer duration and greater pressure demonstrating a smaller volume logged at discharge. This discrepancy was due to the slug flow reaching the flow meter. When a gas slug arrived at the flow meter, the flow rate was either logged as 0 or dropped to negative. The flow meter also displays an error message that is also logged "drive gain over range". Therefore, the readings obtained during the slug flow were unreliable and were encountered during the larger gas slugs.

The following sections provide data collected during these experiments.

4.1.1.1. 90-Psi Initial Injection Pressure

During these tests, 90-psi was selected as the initial air injection pressure, and the air was injected for 60- and 30-seconds.

Table 4-1 summarizes the results for static tests run with air injection for 60- and 30-seconds with an initial injection pressure of 90 psi. During these tests, the only control parameter that was changed was the duration of injection. The difference in injection duration led to a lower maximum unloading rate and total discharged mud volume up to unloading.

The longer injection time led to a greater average injection rate, maximum injection rate, and total gas volume injected into the flow loop. Greater injection rate and volume yield greater the maximum discharge rate during unloading and total discharged mud volume following unloading.

During the experiments, two behaviors were observed from the flow rate data collected by the discharge Coriolis meter. 1- When a gas-liquid slug reaches the flow meter, the meter either displays unreliable data or reads 0. This limitation also causes difficulties obtaining an accurate instantaneous discharge rate when the gas bubble top reaches the flow meter. 2- When erratic behavior is observed by the flow meter instead of dropping to 0 GPM, the erratic behavior stabilizes at a positive flow rate while no liquid is flowing through the system. This measurement can also indicate gas traveling through the flow meter. However, when 0 GPM is registered due to the gas-liquid slug, no flow measurement is recorded.

4.1.1.1.1. A09060 60 Seconds Air Injection at 90-Psi

This test was run under static condition, with 90-psi initial air injection pressure. Air was injected for 60-seconds and allowed to freely migrate through the annular space in the Tower Lab flow loop.

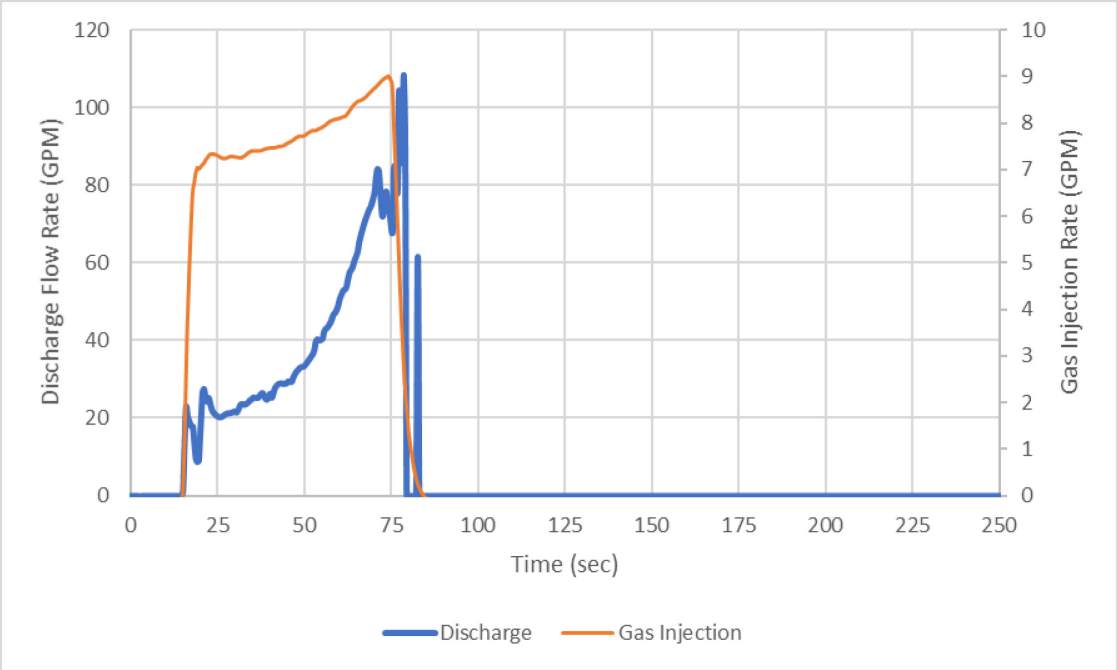

Figure 4-1—Mud Discharge and Gas Injection Rates

Figure 4-1 displays the mud discharge rate and the gas injection rates. Air was injected at an average rate of 6.72 GPM and was terminated at approximately 75 seconds. The mud discharge began as soon as gas injection commenced, and the discharge rate increased and unloaded the flow loop at a rate of 108.5 GPM. Due to the limitations of the flow meter, when the gas and water slug reached the flow meter, the measured flow rate immediately dropped to 0. Figure 4-1 also demonstrates an increasing rate for gas injection with a maximum injection rate of 9.02-GPM right before the solenoid valve closes. This increase was due to the decrease in hydrostatic pressure with water being discharged from the flow loop.

Figure 4-2 displays the cumulative discharge volume and injected gas volume. The total amount of air injected into the flow loop was 8.04-gal. The total mud discharged was logged as 43.20-gal.

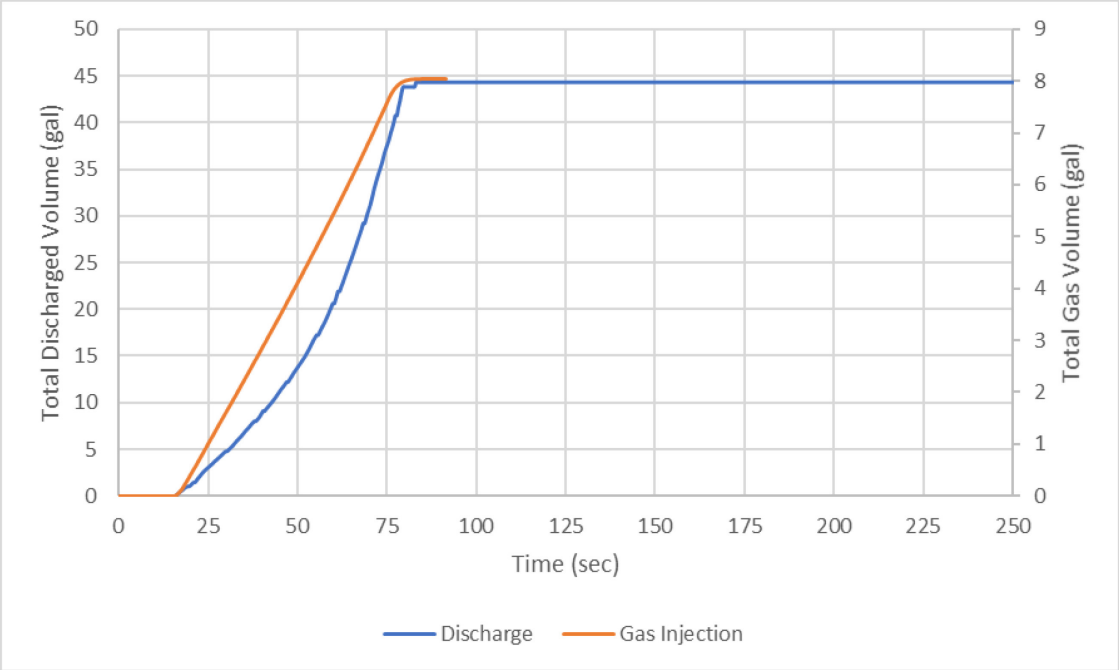

Figure 4-2—Cumulative Discharged Water and Total Gas Volume Injected

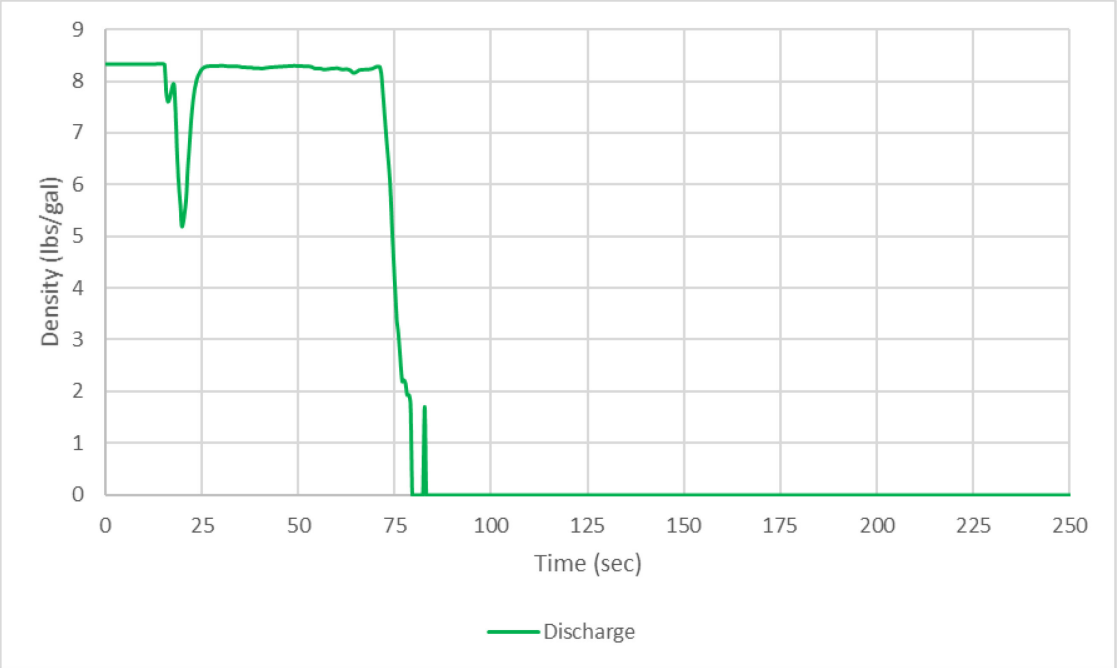

Figure 4-3—Discharge Density

Figure 4-3 displays the density of the fluid logged by the flow meter at discharge. Immediately after unloading, the density dropped to zero as the flow meter stopped

logging data. **Figure 4-4** contains the temperature logged by the flow meters at the injection port and the discharge line. No significant change in temperature was observed.

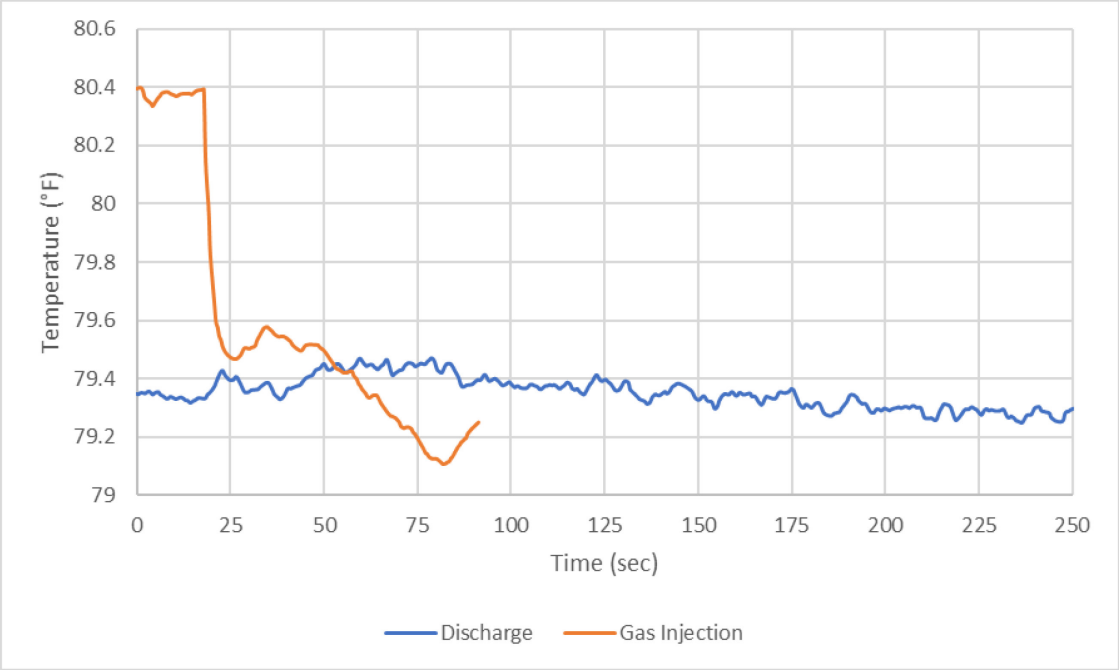

Figure 4-4—Discharge and Gas Injection Temperatures

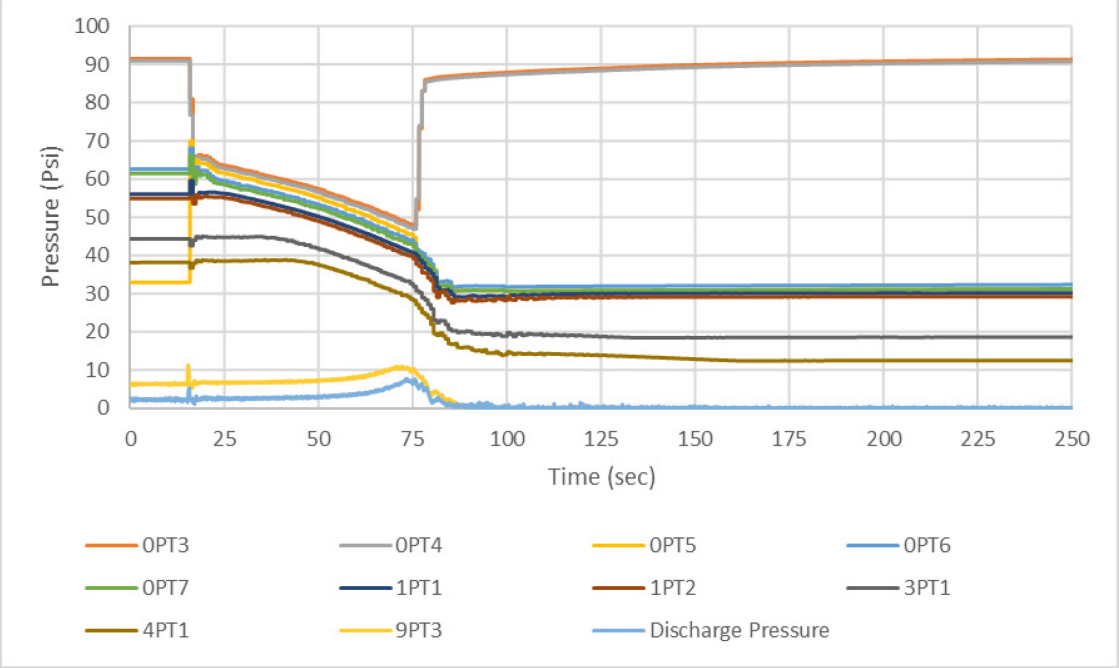

Figure 4-5—All Pressures

Figure 4-5 displays the pressure logged by all the pressure transmitters along the flow loop. The transmitters 0PT3 and 0PT4 track a similar trend. The transmitters on the vertical section near the bottom display a decreasing trend as the gas enters and moves through the flow loop, indicating the pressure drop with water being pushed out of the top and replaced with air. The pressure transmitters at the top, 9PT3, and Discharge Pressure display an increasing pressure as the gas bubble arrives at these points.

Figure 4-6 displays 9PT3 and Discharge Pressure along with Discharge Rate. The initial spike in pressure at approximately 15 seconds is due to the solenoid valve opening and air injection beginning. 9PT3 is located 9 ft below the outlet of the vertical section, with the spike occurring before the Discharge Pressure Transmitter. The large spikes coincide with the unloading event, and the 5 psi increase in the Discharge Pressure is due to the rapid unloading rate creating additional friction and gas bubble arriving at the pressure port. Therefore, these spikes in pressure data also overlap with the unloading event recorded by the discharge flow meter.

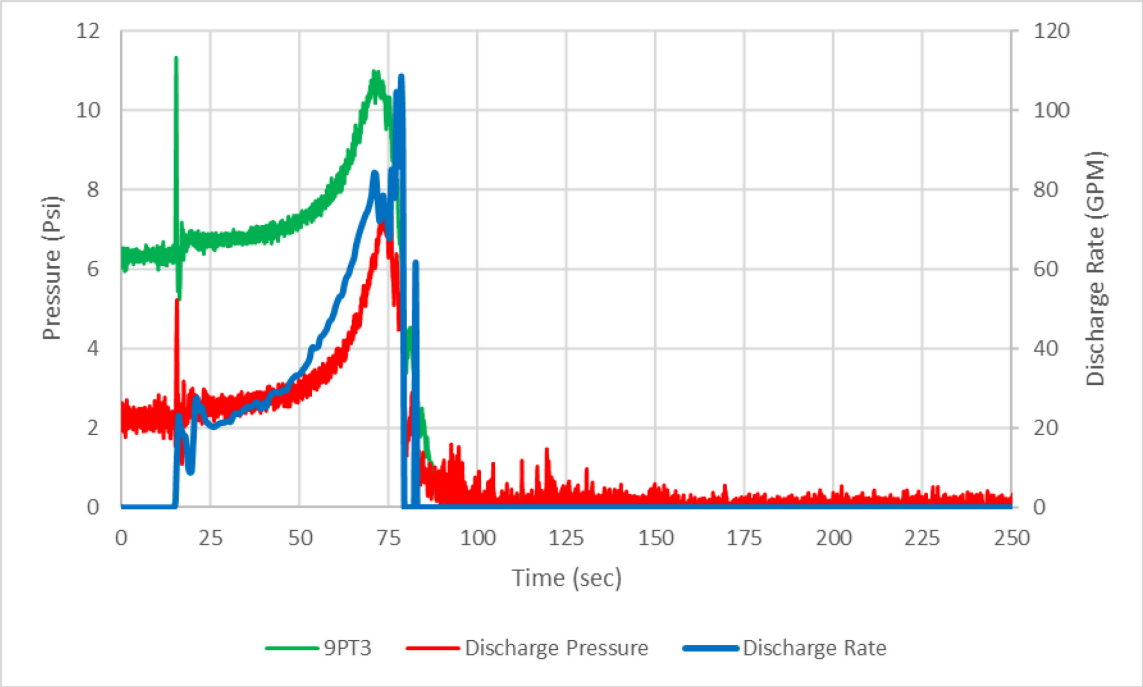

Figure 4-6—Discharge and 9PT3 (15 ft below outlet) pressure and discharge rate

Figure 4-7 displays the difference between 1st floor pressure and the pressure at the 3rd, 4th, 9th floors, and the discharge line. With gas entering and migrating up the flow loop, the drop in pressure measured at the 1st floor can be seen rapidly. The pressure on each floor rapidly decreases as the pressure at the 9th floor and discharge slightly increases with bubbles reaching these pressure ports. The discharge rate increases, creating additional friction. At approximately 80 seconds, after unloading, the water level dropped to the top of the 6th floor. As a result, 9PT3 and Discharge Pressure transmitters logged 0 psi. The lines "1PT1-3PT1 and 1PT1-4PT1" demonstrate a slight decrease until the solenoid valve closes, at which point the lines begin rising, indicating the gas leaving the section between 1PT1-3PT1 and 1PT1-4PT1. The later section also includes the effect of rising friction pressure due to increasing discharge rate.

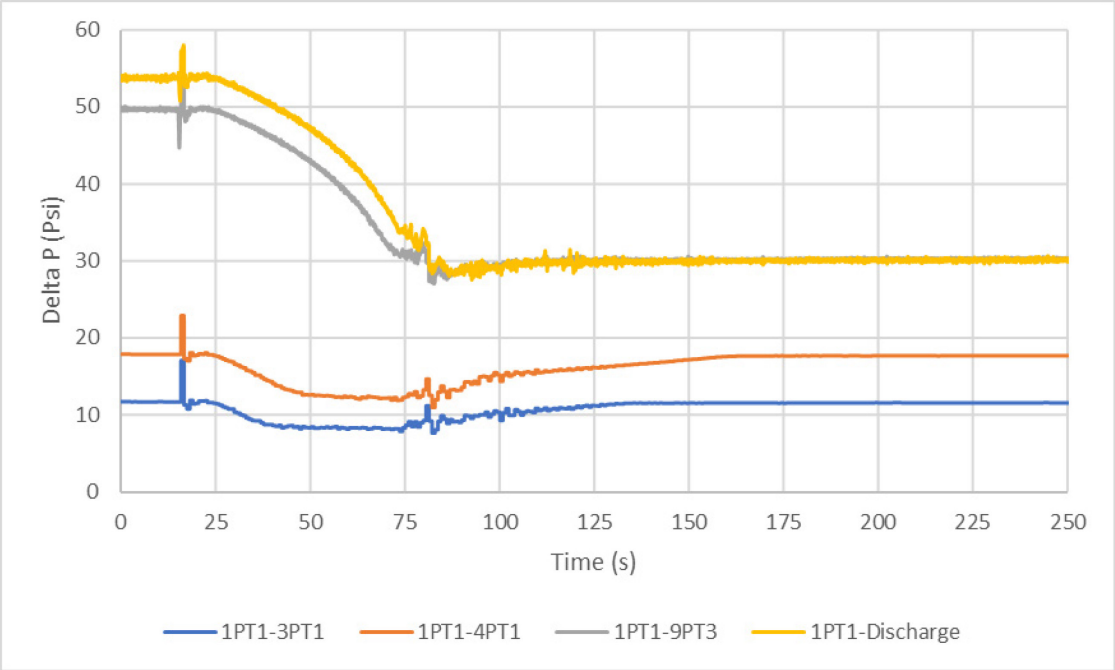

Figure 4-7—Pressure difference between 1st floor and 3rd, 4th, 9th floors, and discharge line

The pressure data was further used to study the maximum pressure per transmitter and the gas front travel time between transmitters. The depth between the transmitter is known and used to calculate the migration rate. **Table 4-2** presents the travel rate of the bubble front between each transmitter.

The bubble front average travel rate was 2.3753 ft/sec or 0.4210 sec/ft; however, the maximum travel rate was calculated as 4.4206-ft/sec or 0.2262 sec/ft. These were calculated based on the transmitter locations and the time of peak pressure logged following the start of gas injection. The 4.4206 ft/sec rate is essential as this is the travel rate of the bubble front from 9pt3 to the discharge line, indicating the unloading velocity through the test section.

	Migration Rate	
	sec/ft	ft/sec
1PT1 to 4PT1	0.4910	2.0365
1PT1 to 9PT3	0.4385	2.2807
1PT1 to Discharge	0.4210	2.3753
4PT1 to 9PT3	0.4090	2.4452
4PT1 to Discharge	0.3865	2.5871
9PT3 to Discharge	0.2262	4.4206

Table 4-2—Bubble front travel rate based on maximum pressure measurements following the initial injection

4.1.1.1.2. A09030 30 Seconds Air Injection at 90-Psi

This test was run under static condition, with 90-psi initial air injection pressure. Air was injected for 30-seconds and allowed to freely migrate through the annular space in the Tower Lab flow loop.

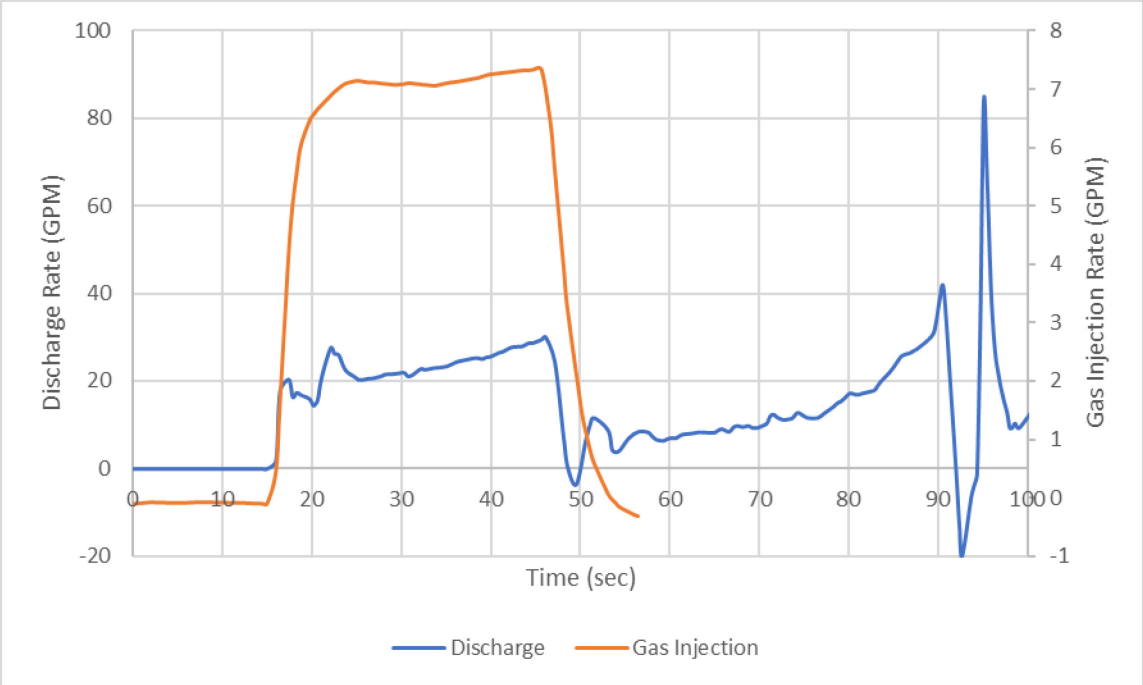

Figure 4-8—Mud Discharge and Gas Injection Rates

Figure 4-8 presents the mud discharge rate and the gas injection rates. Air was injected at an average rate of 5.99-GPM and was terminated at approximately 46 seconds. The mud discharge began as soon as gas injection commenced, and the discharge rate

increased and unloaded the flow loop at a rate of 83.94-GPM. At 47-seconds, the discharge rate also drops when the solenoid valve closes. Then discharge rate continues rising until the flow loop entirely unloads. Figure 4-8 also demonstrates an increasing rate for gas injection with a maximum injection rate of 7.34-GPM right before the solenoid valve closes. This increase was due to the decrease in hydrostatic pressure with water being discharged from the flow loop. However, this test demonstrates a lower average and maximum injection rate due to less water leaving the system.

Figure 4-9 displays the cumulative discharge volume and injected gas volume. The total amount of air injected into the flow loop was 3.72-gal. The total mud discharged during unloading was logged as 22.37-gal. The total discharged volume logged by the flow meter was 24.15-gal.

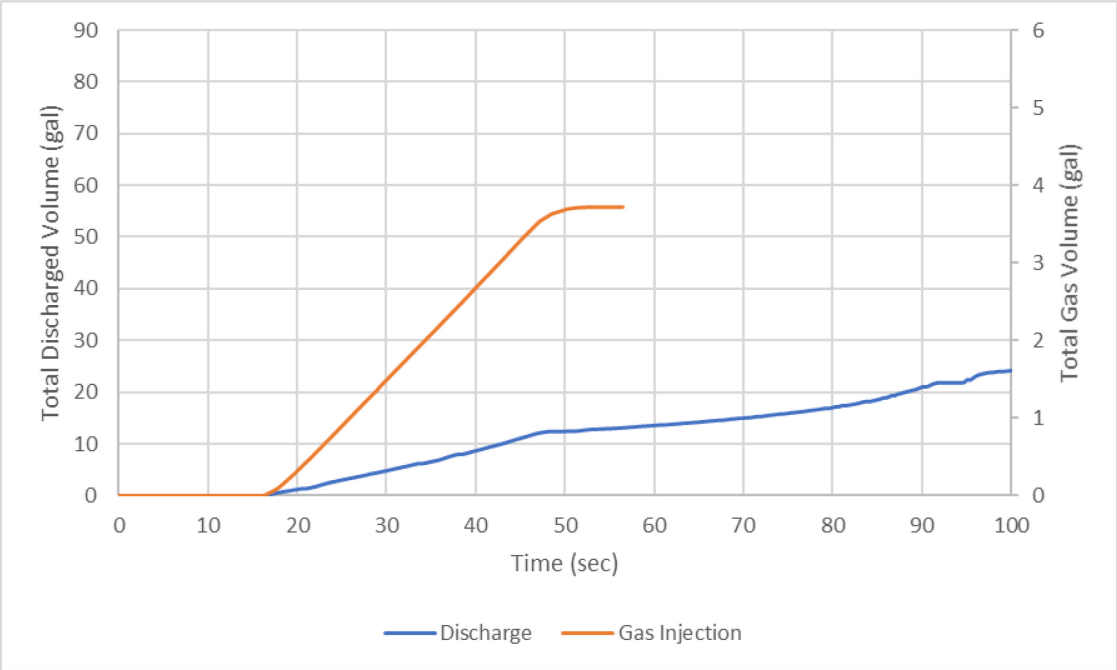

Figure 4-9— Cumulative Discharged Water and Total Gas Volume Injected

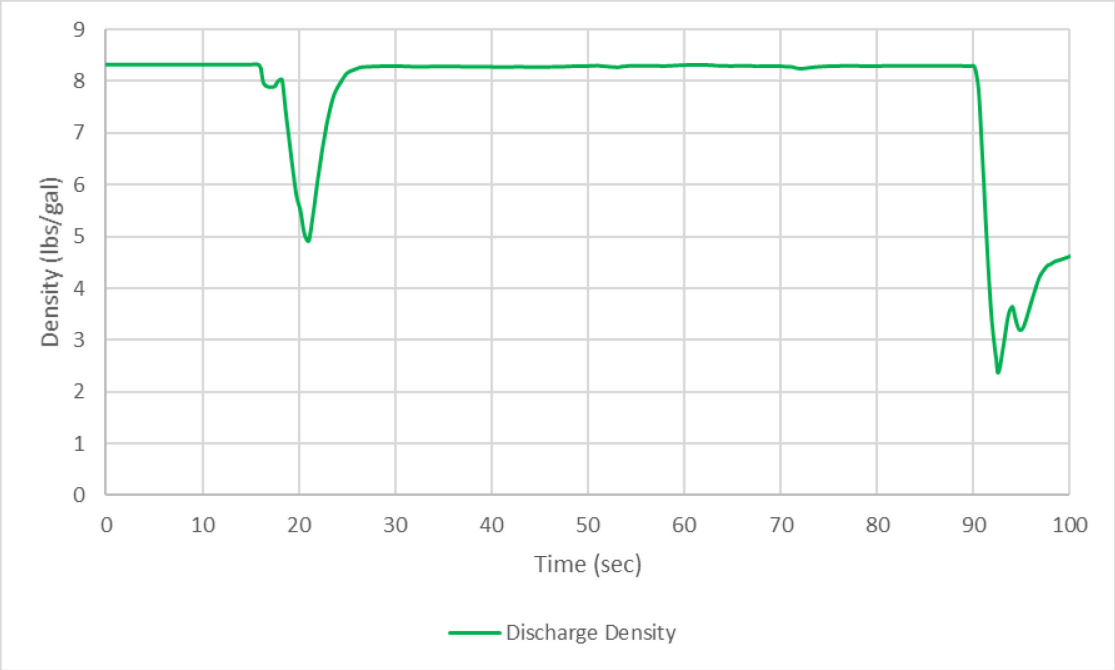

Figure 4-10—Discharge Density

Figure 4-10 displays the density of the fluid logged by the flow meter at discharge. Immediately following the unloading, the density drops to 2.4-lbs/gal, indicating gas slugs moving through the flow meter. **Figure 4-11** displays the temperature logged by the flow meters with no significant change.

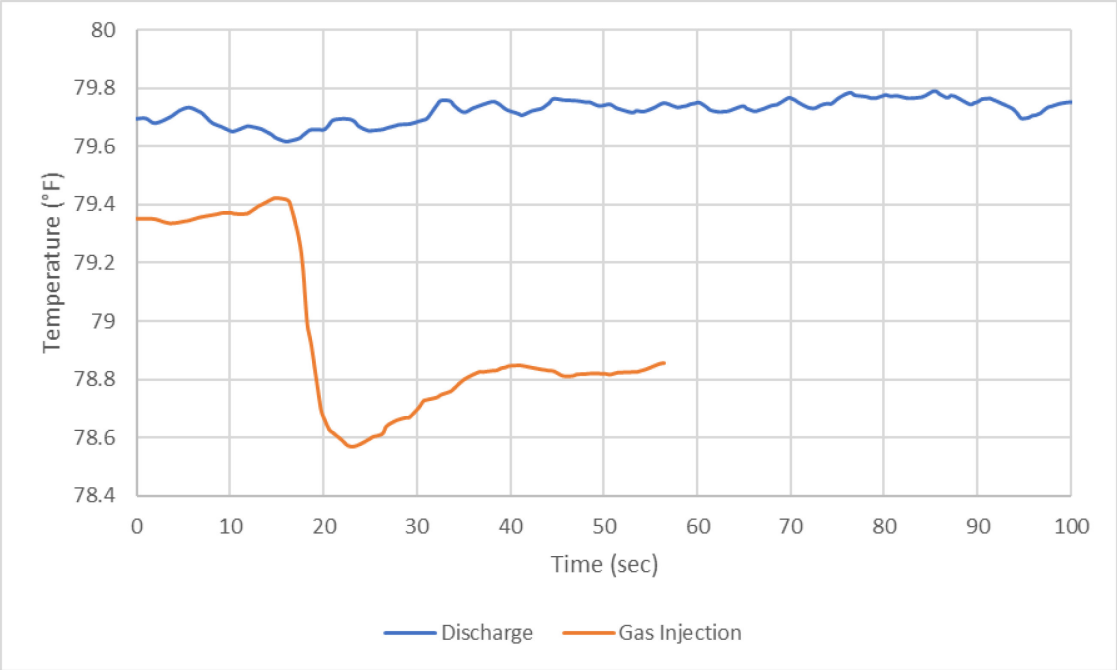

Figure 4-11—Discharge and Gas Injection Temperatures

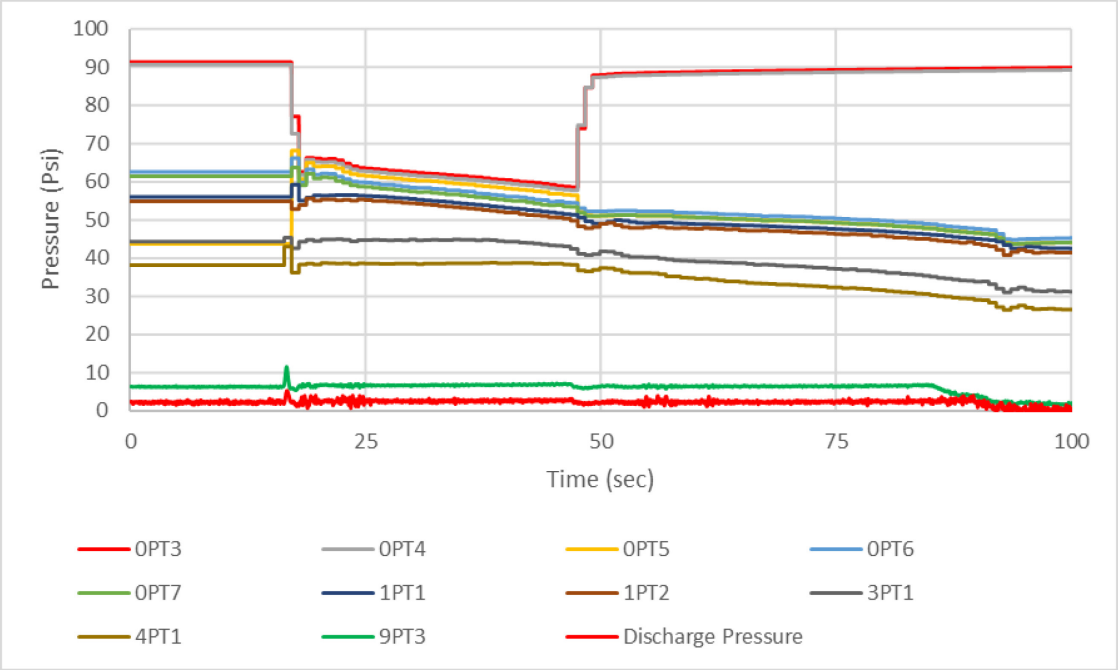

Figure 4-12—All Pressures

Figure 4-12 displays the pressure logged by all the pressure transmitters along the flow loop. All pressure transmitters display a decreasing trend. The point where gas

injection commences and ends and unloading can be easily spotted in the pressure data. The solenoid valve opening for gas injection can be observed earlier in the graph, as the pressure transmitters (1PT1, 1PT2, 3PT1, 4PT1, 9PT3, and Discharge Pressure) on the test section display a sudden upward spike, then a sudden slight decrease with the solenoid valve closing. Following the solenoid valve closing, pressure decreases with the gas traveling by and up the test section. When unloading occurs at the end, pressures all spike downward.

Figure 4-13 displays 9PT3 and Discharge Pressure along with discharge rate. The initial spike in pressure at approximately 17-seconds is due to the solenoid valve opening and air injection beginning. The two pressure transmitters display a slight increase until the solenoid valve closes and stops injection at 47-seconds. This increased pressure also overlaps with the decrease in discharge rate. The pressure data in 9PT3 and Discharge Pressure increase until the gas bubble arrives at these pressure ports and discharges from the system. At this point, pressures logged by these two pressure transmitters drop to 0-psi with the water level at the top of the 7^{th} floor.

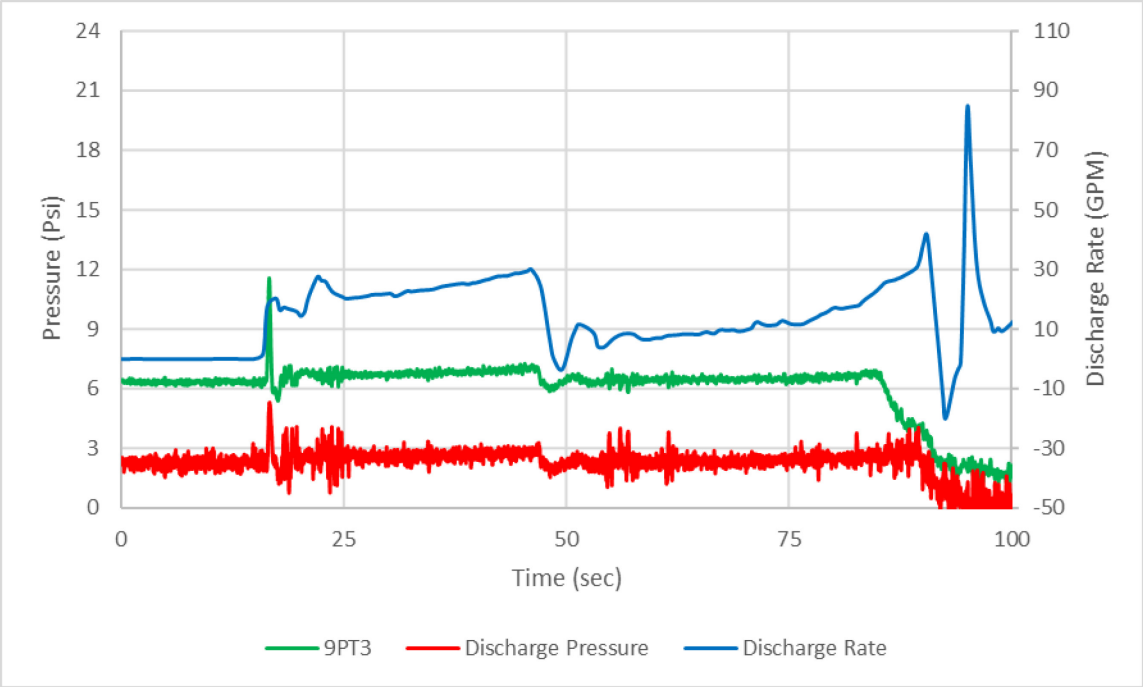

Figure 4-13— Discharge and 9PT3 (15 ft below outlet) pressure and discharge rate

The points where gas injection began, ended, and unloading occurred can be easily observed with the differential pressure method by taking the difference between two pressure transmitters or using a differential pressure transmitter. These points are demonstrated in **Figure 4-14** by subtracting the pressures logged by the 3rd, 4th, 9th, and discharge pressure from the 1st floor pressure transmitter. The lines "1PT1-3PT1 and 1PT1-4PT1" demonstrate a slight decrease until the solenoid valve closes, at which point the lines begin rising, indicating the gas leaving the section between 1PT1-3PT1 and 1PT1-4PT1. The later section also includes the effect of rising friction pressure due to increasing discharge rate.

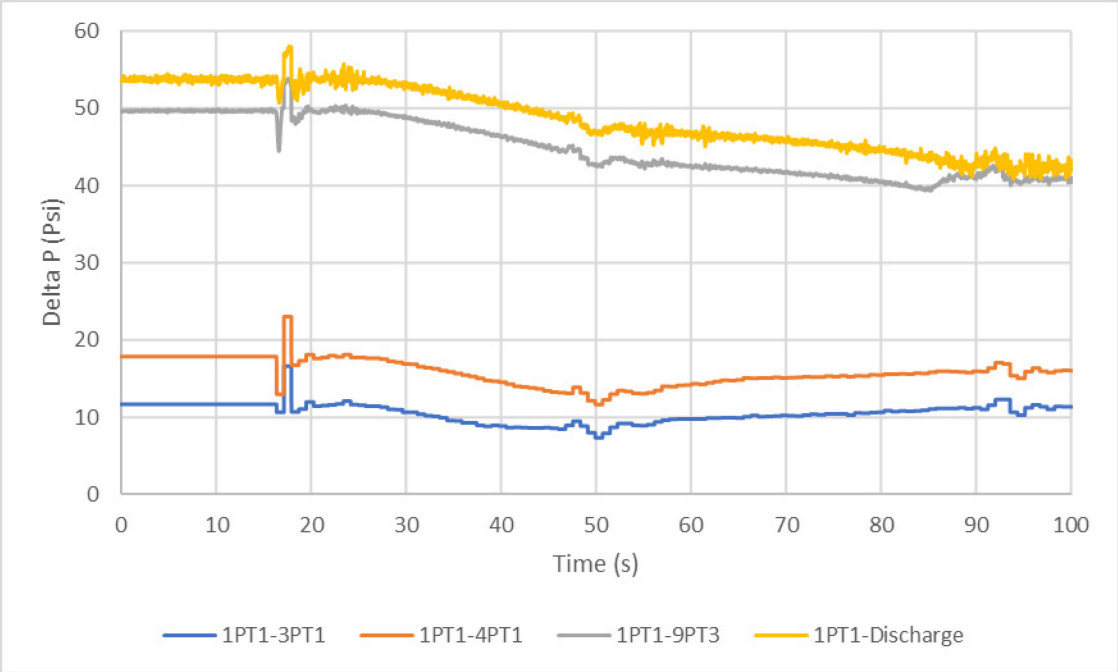

Figure 4-14—Pressure difference between 1st floor and 3rd, 4th, 9th floors, and discharge line

The pressure data was used to analyze the maximum pressure per transmitter to study the gas front travel time between transmitters. The depth between the transmitter is known and used to calculate the migration rate. **Table 4-3** presents the travel rate of the bubble front between each transmitter.

The bubble front average travel rate was 1.8480-ft/sec or 0.5411-sec/ft; however, the maximum travel rate was calculated as 2.5214-ft/sec or 0.3966-sec/ft. These were calculated based on the transmitter locations and the time of peak pressure logged following the start of gas injection. The 2.0600-ft/sec rate is essential as this is the travel rate of the bubble front from 9pt3 to the discharge line, indicating the unloading velocity through the test section.

	Migration Rate	
	sec/ft	ft/sec
1PT1 to 4PT1	0.3966	2.5214
1PT1 to 9PT3	0.5461	1.8311
1PT1 to Discharge	0.5411	1.8480
4PT1 to 9PT3	0.6300	1.5872
4PT1 to Discharge	0.6123	1.6332
9PT3 to Discharge	0.4854	2.0600

Table 4-3—Bubble front travel rate based on maximum pressure measurements following the initial injection

4.1.1.2. 80-Psi and 74-Psi Initial Injection Pressure

Pump Rate (GPM)	0	
Initial Injection Pressure (PSI)	80.04	74.07
Gas Injection Duration (seconds)	60	30
Kick Intensity (lbs./gal)	2.4	1.65
Maximum Injection Rate (GPM)	8.92	7.63
Average Injection Rate (GPM)	6.64	5.66
Total Gas Injected (gal)	7.83	3.62
Maximum Discharge Rate (GPM)	91.01	41.09
Max Rate at Unloading (GPM)	40.40	28.69
Total Discharged Volume (gal)	42.01	23.77
Total Discharged During Unloading (gal)	42.01	18.78

Table 4-4—Summary Results for Static Tests with Air Injected at 80 Psi for 60 and 30 Seconds

4.1.1.2.1. A08060 60 Seconds Air Injection at 80.04 Psi

This test was run under static conditions, with 80.04 psi initial air injection pressure. Air was injected for 60 seconds and allowed to freely migrate through the annular space in the Tower Lab flow loop.

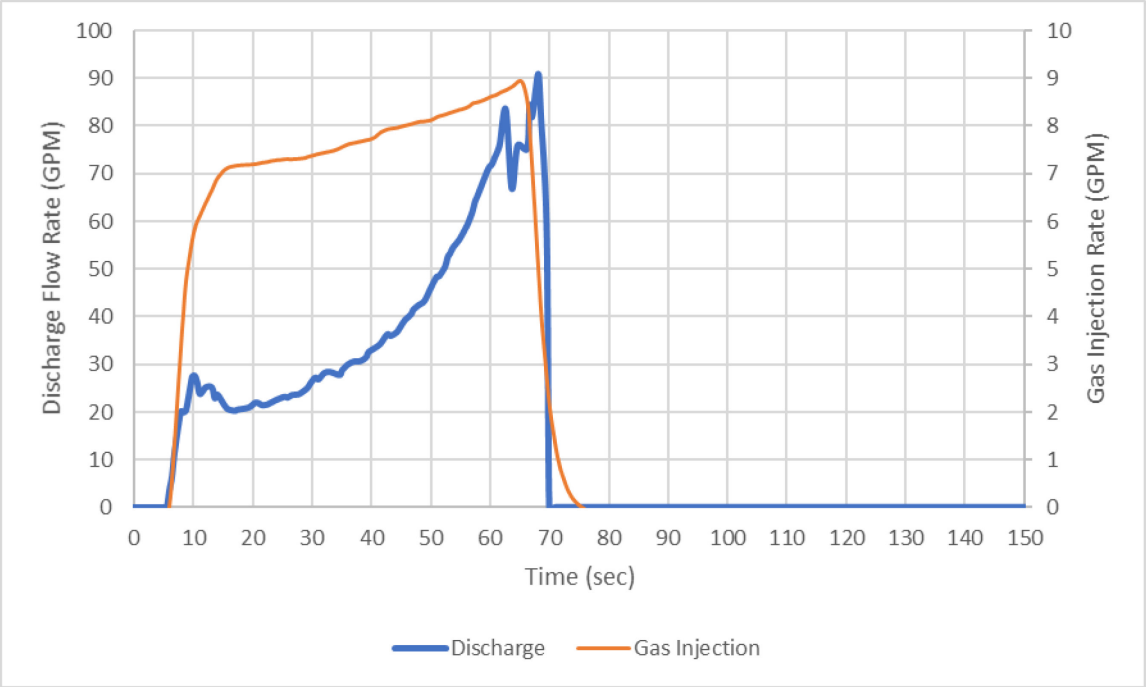

Figure 4-15—Mud Discharge and Gas Injection Rates

Figure 4-15 displays the mud discharge rate and the gas injection rates. Air was injected at an average rate of 6.64-GPM and was terminated at approximately 66-seconds. The mud discharge began as soon as gas injection commenced, and the discharge rate increased until the flow loop was unloaded at a rate of 91.01-GPM. As observed in the test in section 4.2.1.1.1, with the slug of gas arriving at the flow meter, the discharge rate dropped to 0 GPM. Figure 4-15 also demonstrates an increasing rate for gas injection with a maximum injection rate of 8.92-GPM right before the solenoid valve closes.

Figure 4-16 displays the cumulative discharge volume and injected gas volume. The total amount of air injected into the flow loop was 7.83-gal. The total mud discharged during unloading was logged as 42.01-gal.

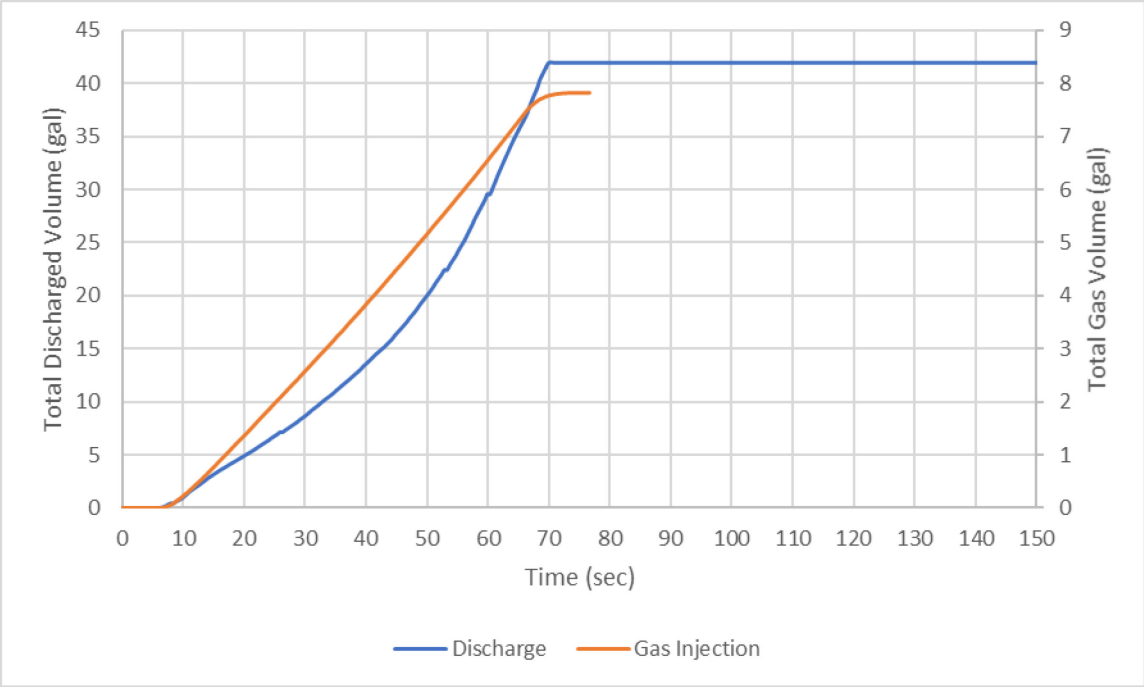

Figure 4-16— Cumulative Discharged Water and Total Gas Volume Injected

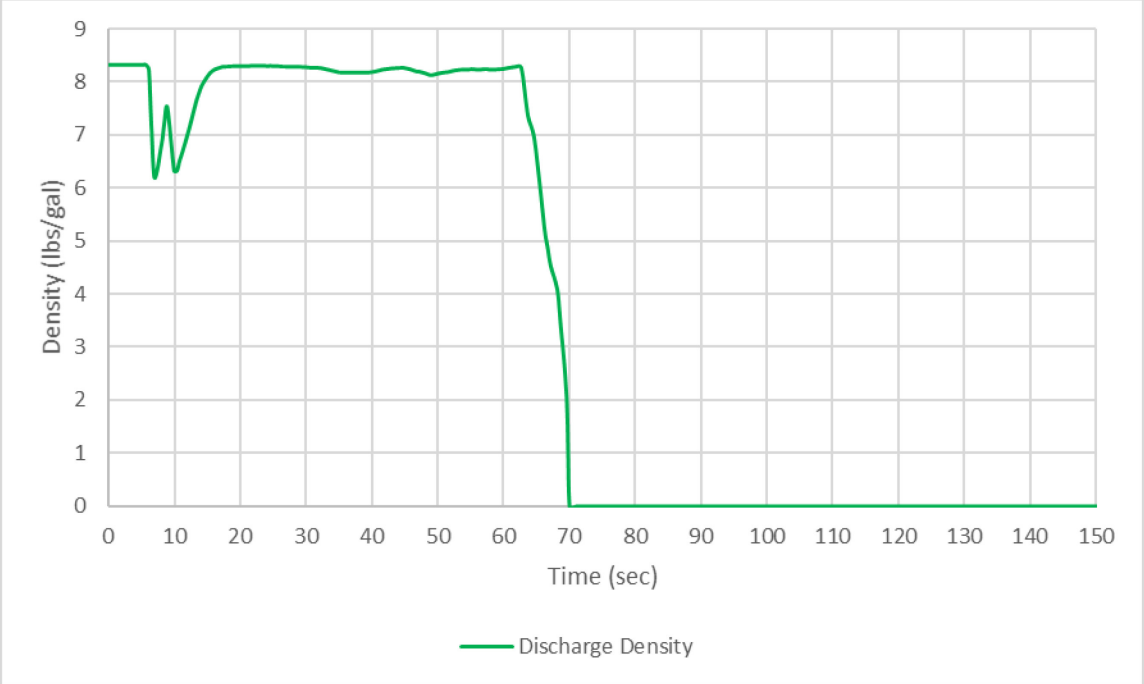

Figure 4-17—Discharge Density

Figure 4-17 displays the density of the fluid logged by the flow meter at discharge. Immediately following unloading, the density drops to zero as the flow meter stopped logging data. This figure confirms the behavior observed in the discharge rate. **Figure 4-18** contains the temperature logged by the flow meters at the injection port and the discharge line. Again, no significant change in temperature was observed.

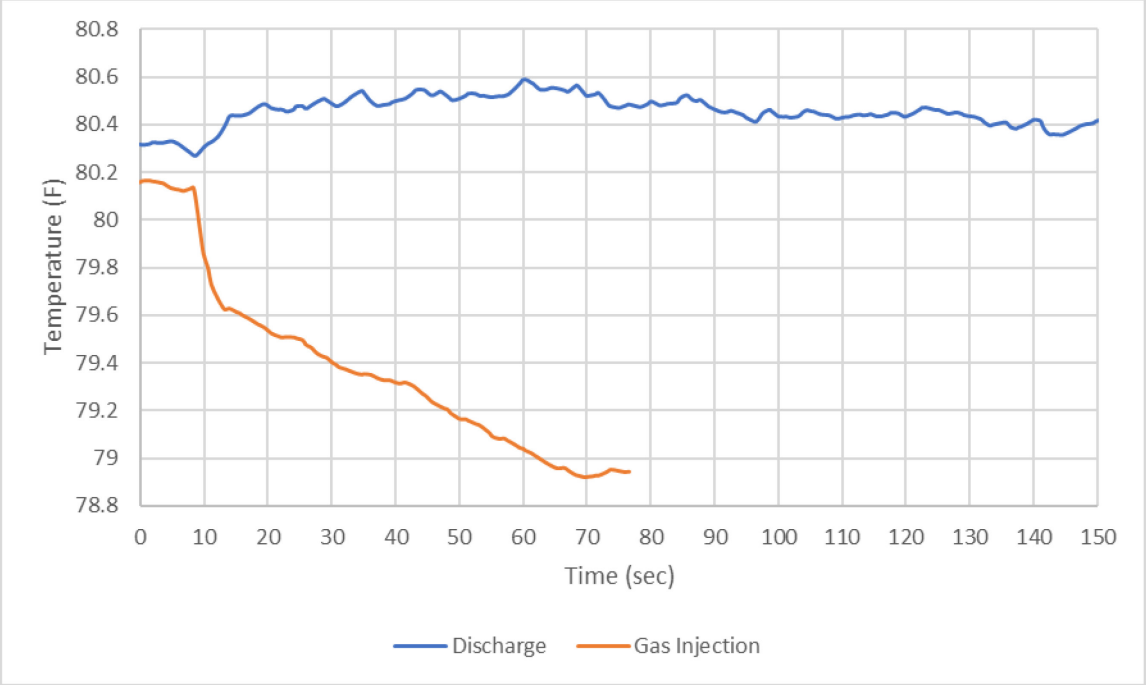

Figure 4-18—Discharge and Gas Injection Temperatures

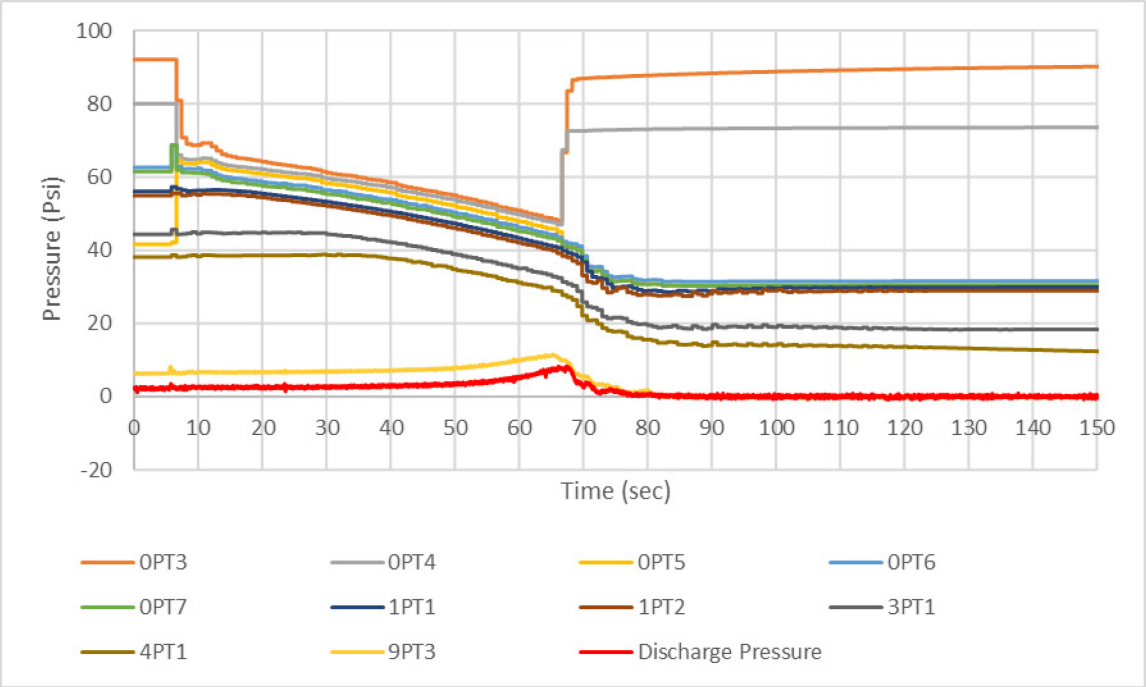

Figure 4-19—All Pressures

Figure 4-19 displays the pressure logged by all the pressure transmitters along the flow loop. All pressure transmitters display a decreasing trend except for 9PT3 and Discharge Pressure. Gas injection beginning and ending points can be easily observed. However, due to the rate at which unloading occurs, it is difficult to observe exactly when the bubble front reaches the discharge line. At 66-seconds, the solenoid valve closes, and the bubble front reaches discharge at approximately 68-seconds. The opening of the solenoid valve for gas injection can be observed at the earlier part, as the pressure transmitters (1PT1, 1PT2, 3PT1, 4PT1, 9PT3, and Discharge Pressure) on the test section display a sudden small upward spike, then a sudden slight decrease with the solenoid valve closing. 9PT3 and Discharge pressure reach peak pressure when the gas bubble front arrives at these pressure ports.

Figure 4-20 displays 9PT3 and Discharge Pressure along with discharge rate. The initial spike in pressure at approximately 6-seconds is due to the solenoid valve opening and air injection beginning. The two pressure transmitters display a slight increase until the solenoid valve closes and stops injection at 66-seconds which overlaps with the slight decrease in discharge rate. The pressure in 9PT3 and Discharge Pressure continue increasing until the gas bubble arrives at these pressure ports and discharges from the system. The pressure logged by these two pressure transmitters drop to 0 psi with the water level on the 7th floor.

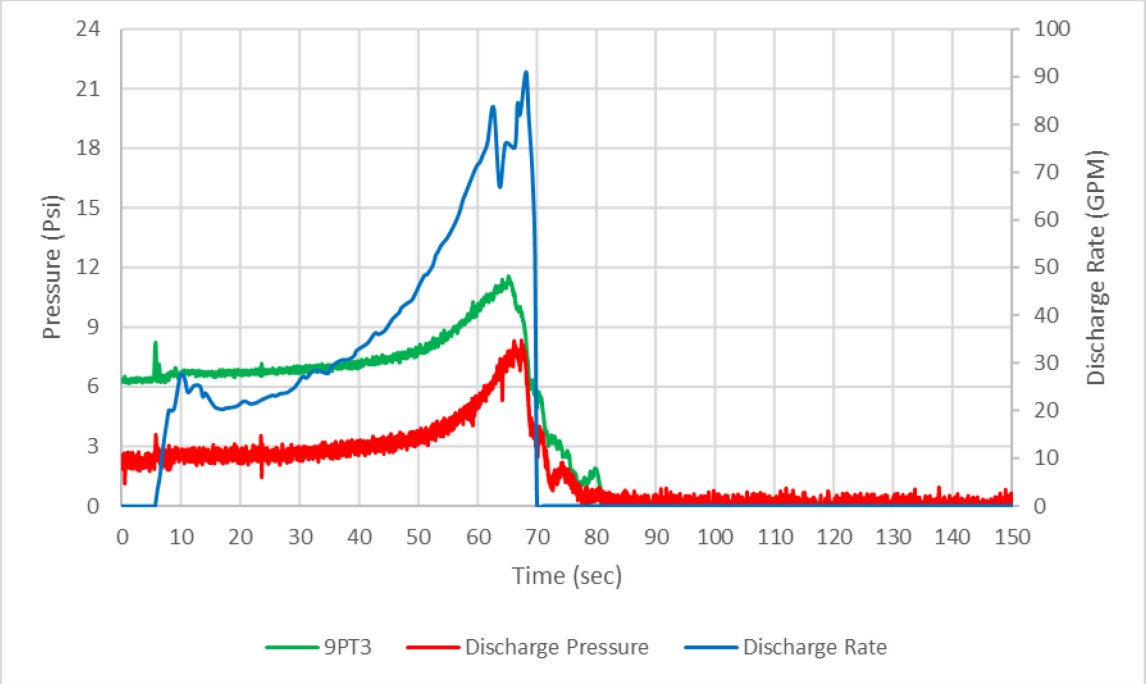

Figure 4-20— Discharge and 9PT3 (15 ft below outlet) pressure and discharge rate

The points where gas injection begins, ends, and the pipe unloads can be easily observed with the differential pressure method by taking the difference between two pressure transmitters or using a differential pressure transmitter. **Figure 4-21** displays the differential pressures by subtracting the pressures logged by the 3rd, 4th, 9th, and discharge

pressure from the 1st floor pressure transmitter. The lines "1PT1-3PT1 and 1PT1-4PT1" demonstrate a slight decrease until the solenoid valve closes, at which point the lines begin rising, indicating the gas leaving the section between 1PT1-3PT1 and 1PT1-4PT1. The later section also includes the effect of rising friction pressure due to increasing discharge rate. Since the pressure transmitters, 9PT3 and Discharge Pressure read 0-Psi following unloading, "1PT1-9PT3 and 1PT1-Discharge Pressure" lines overlap.

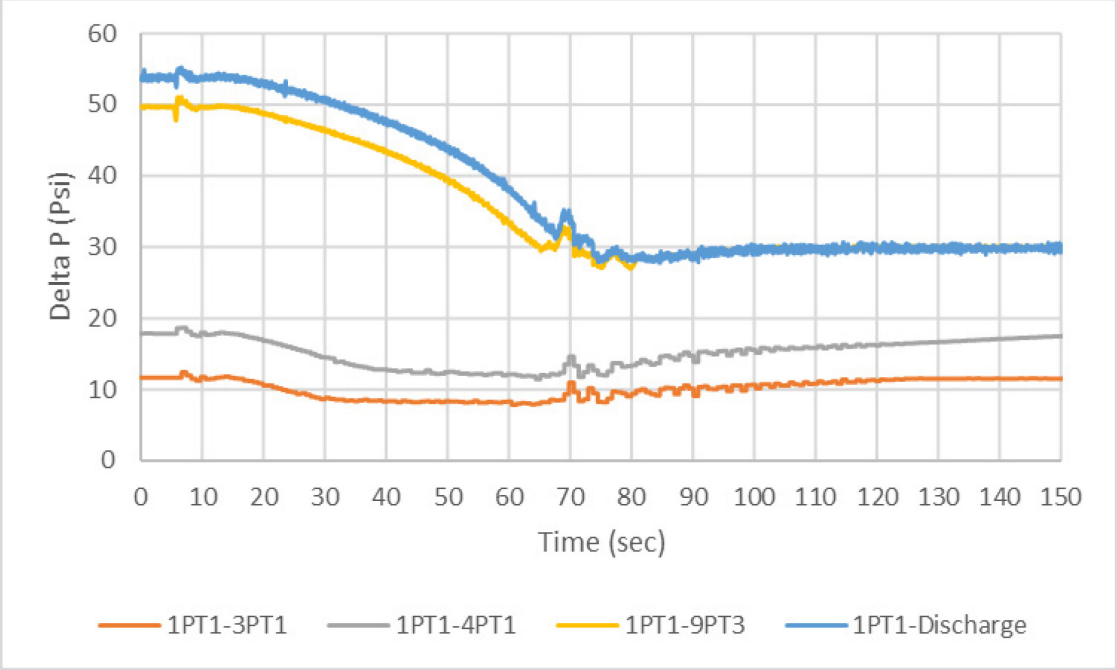

Figure 4-21— Pressure difference between 1st floor and 3rd, 4th, 9th floors, and discharge line

The pressure data was used to analyze the maximum pressure per transmitter to study the gas front travel time between transmitters. The depth between the transmitter is known and used to calculate the migration rate. **Table 4-5** presents the travel rate of the bubble front between each transmitter

The bubble front average travel rate was 2.2977-ft/sec or 0.4352-sec/ft; however, the maximum travel rate was calculated as 4.7465-ft/sec or 0.2107-sec/ft. These rates were

calculated based on the transmitter locations and the time of peak pressure logged following the start of gas injection. The 4.7465-ft/sec rate is important as this is the travel rate of the bubble front from 9pt3 to the discharge line, indicating the unloading velocity through the test section.

	Migration Rate	
	sec/ft	ft/sec
1PT1 to 4PT1	0.4533	2.2062
1PT1 to 9PT3	0.4554	2.1961
1PT1 to Discharge	0.4352	2.2977
4PT1 to 9PT3	0.4565	2.1905
4PT1 to Discharge	0.4263	2.3455
9PT3 to Discharge	0.2107	4.7465

Table 4-5—Bubble front travel rate based on maximum pressure measurements following the initial injection

4.1.1.2.2. A07430 30-Seconds Air Injection at 74.07-Psi

This test was run under static conditions, with 74.07 psi initial air injection pressure. Air was injected for 30 seconds and allowed to freely migrate through the annular space in the Tower Lab flow loop.

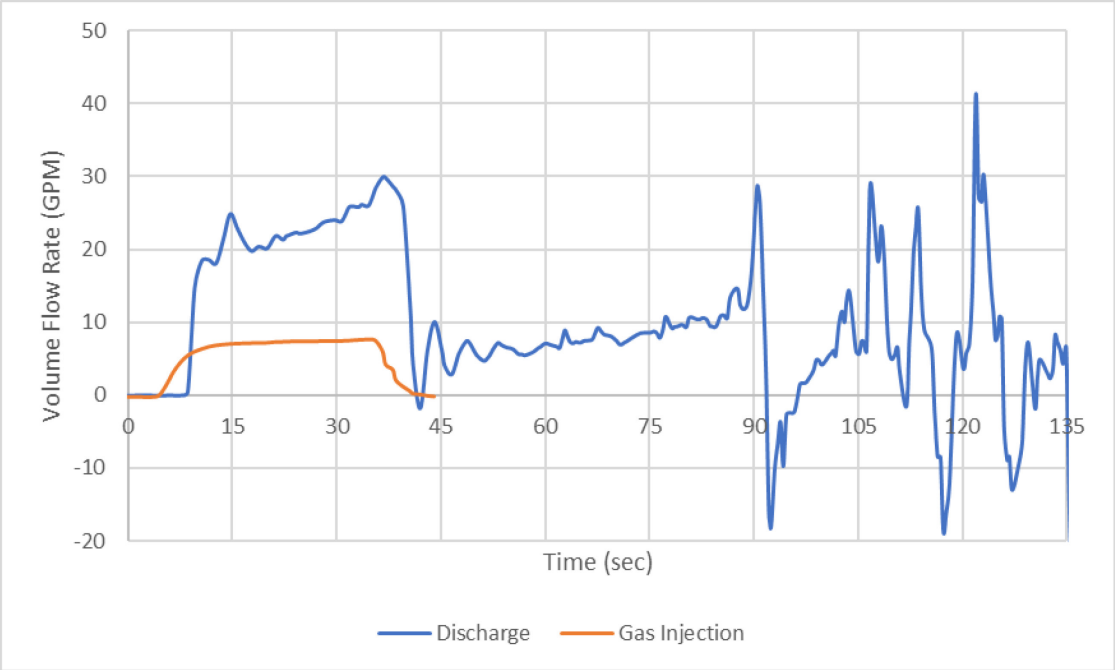

Figure 4-22—Mud Discharge and Gas Injection Rates

Figure 4-22 displays the mud discharge rate and the gas injection rates. Air was injected at an average rate of 5.66-GPM and was terminated at approximately 40.65-seconds. The mud discharge began as soon as gas injection commenced, and the discharge rate increased until the flow loop was unloaded at a rate of 28.69-GPM. The solenoid valve closing caused the discharge rate to drop to zero then begin rising again. Following the gas front reaching the outlet, a higher discharge rate was measured as 41.09-GPM. Figure 4-22 also demonstrates an increasing rate for gas injection with a maximum injection rate of 7.63-GPM right before the solenoid valve closes.

Figure 4-23 displays the cumulative discharge volume and injected gas volume. The total amount of air injected into the flow loop was 3.62-gal. The total mud discharged during unloading was logged as 18.78-gal. The total discharged volume logged by the flow meter was 23.77-gal.

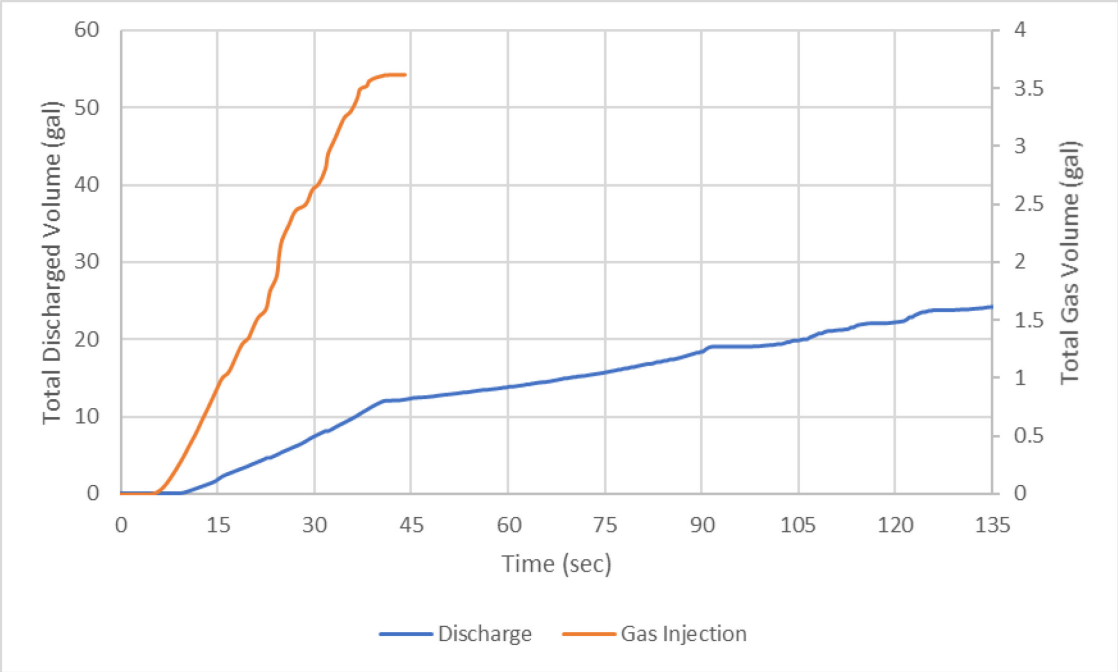

Figure 4-23—Cumulative Discharged Water and Total Gas Volume Injected

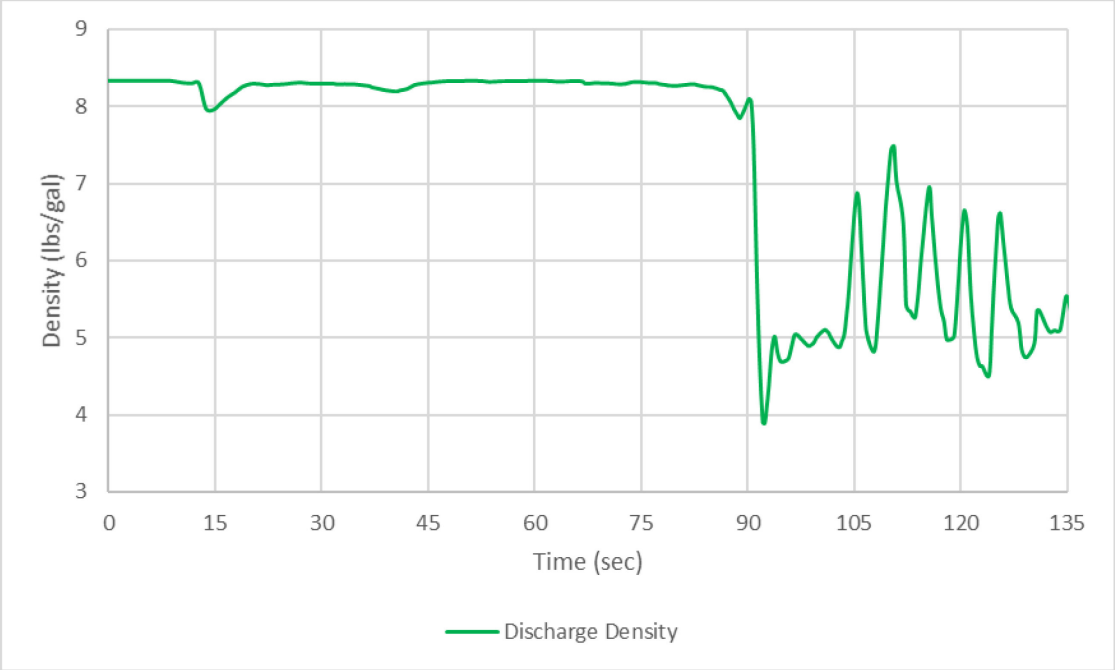

Figure 4-24—Discharge Density

Figure 4-24 displays the density of the fluid logged by the flow meter at discharge. Immediately following the unloading, the density drops and fluctuates between 4- and 7.5-

lbs/gal. **Figure 4-25** displays the temperature logged by the flow meters at the injection port and the discharge line. No significant change in temperature was observed.

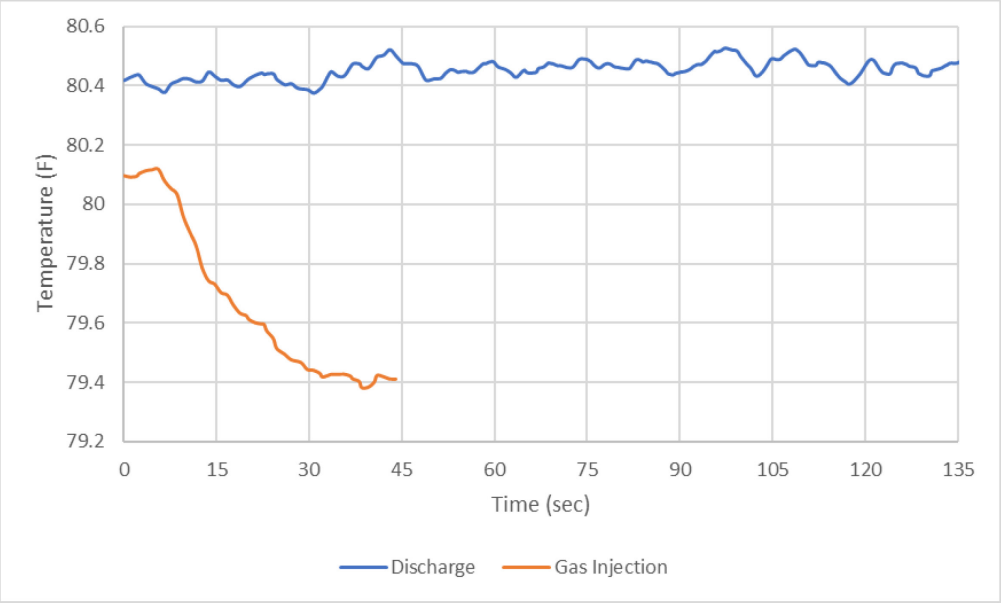

Figure 4-25—Discharge and Gas Injection Temperatures

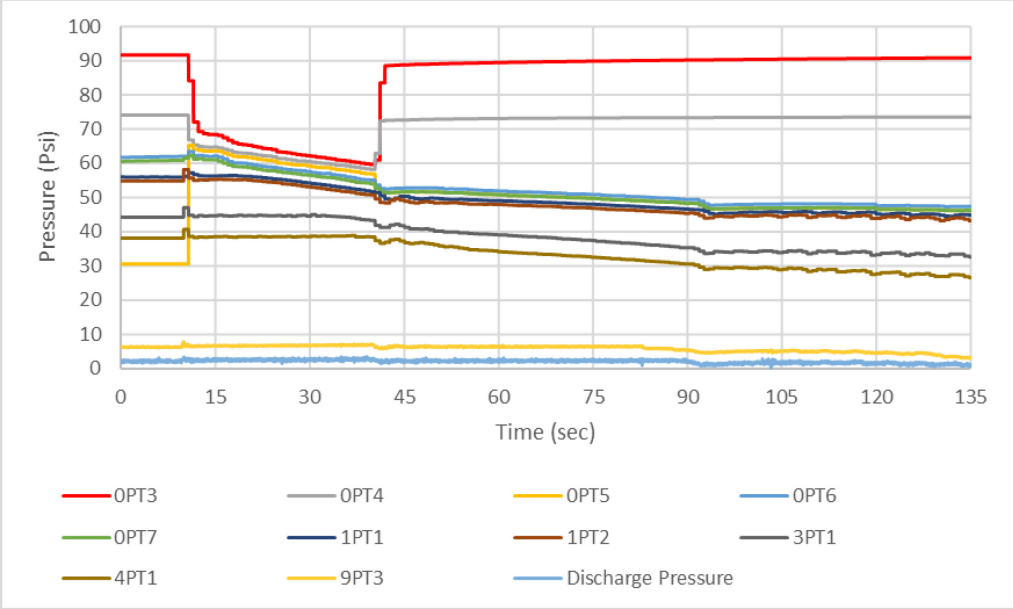

Figure 4-26—All Pressures

Figure 4-26 displays the pressure logged by all the pressure transmitters along the flow loop. All pressure transmitters display a decreasing trend except for 9PT3 and

Discharge Pressure. Gas injection beginning and ending points can be easily observed. However, due to the rate at which unloading occurs, it is difficult to observe exactly when the bubble front reaches the discharge line. At 66-seconds, the solenoid valve closes, and the bubble front reaches discharge at approximately 68-seconds. The opening of the solenoid valve for gas injection can be observed at the earlier part, as the pressure transmitters (1PT1, 1PT2, 3PT1, 4PT1, 9PT3, and Discharge Pressure) on the test section display a sudden small upward spike, then a sudden slight decrease with the solenoid valve closing. 9PT3 and Discharge pressure reach peak pressure when the gas bubble front arrives at these pressure ports.

Figure 4-27 displays 9PT3 and Discharge Pressure along with discharge rate. The initial spike in pressure at approximately 6-seconds is due to the solenoid valve opening and air injection beginning. The two pressure transmitters display a slight increase until the solenoid valve closes and stops injection at 66-seconds. The point where the gas injection stops also overlaps with the slight decrease in discharge rate. The pressure data in 9PT3 and Discharge Pressure continue increasing until the gas bubble arrives at these pressure ports and discharges from the system. At this point, the pressure logged by these two pressure transmitters drop to 0 psi with the water level on the 7^{th} floor.

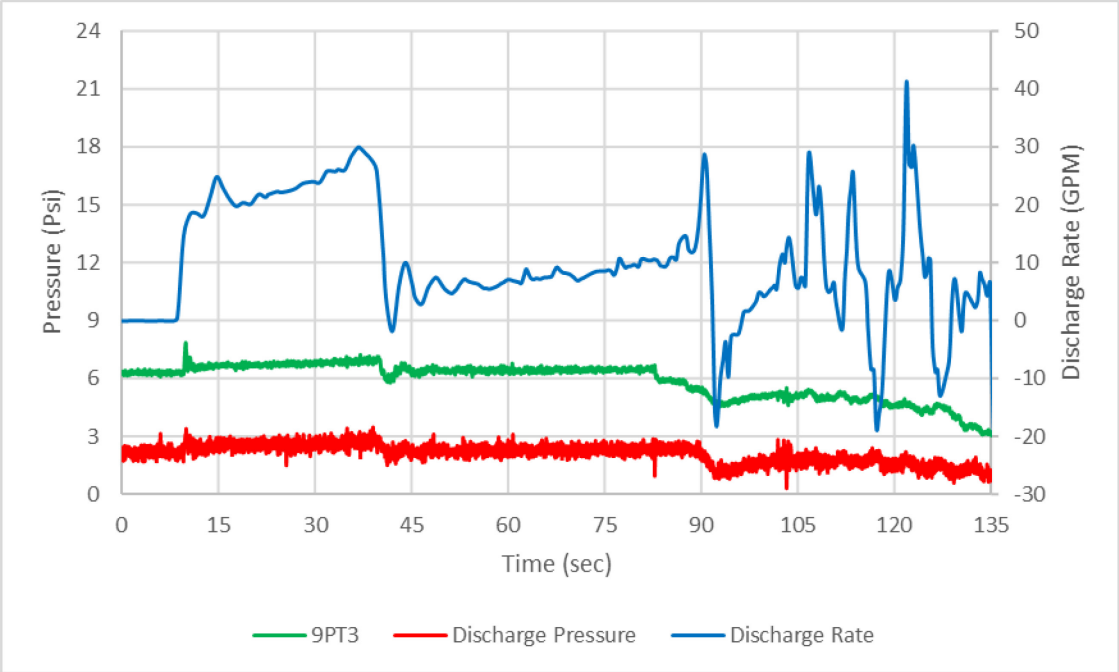

Figure 4-27— Discharge and 9PT3 (15 ft below outlet) pressure and discharge rate

The points where gas injection begins, ends, and the pipe unloads, can be easily observed with the differential pressure method by taking the difference between two pressure transmitters or using a differential pressure transmitter. This method is demonstrated in **Figure 4-28** by subtracting the pressures logged by the 3rd, 4th, 9th, and discharge pressure from the 1st floor pressure transmitter. The lines "1PT1-3PT1 and 1PT1-4PT1" demonstrate a slight decrease until the solenoid valve closes, at which point the lines begin rising, indicating the gas leaving the section between 1PT1-3PT1 and 1PT1-4PT1. The later section also includes the effect of rising friction pressure due to increasing discharge rate. Since the pressure transmitters, 9PT3 and Discharge Pressure read 0-Psi following unloading, "1PT1-9PT3 and 1PT1-Discharge Pressure" lines overlap.

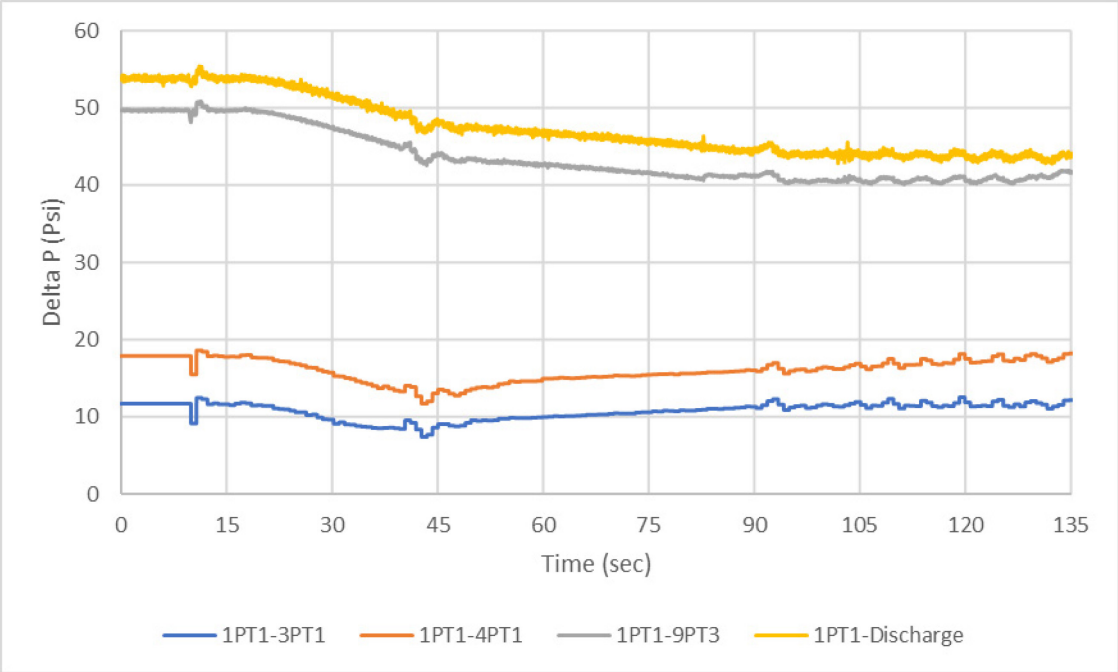

Figure 4-28— Pressure difference between 1st floor and 3rd, 4th, 9th floors, and discharge line

The pressure data was used to analyze the maximum pressure per transmitter to study the gas front travel time between transmitters. The depth between the transmitter is known and used to calculate the migration rate. **Table 4-6** presents the travel rate of the bubble front between each transmitter

The bubble front average travel rate was 1.7290-ft/sec or 0.5784-sec/ft; however, the maximum travel rate was calculated as 2.1179-ft/sec or 0.4722-sec/ft. These were calculated based on the transmitter locations and the time of peak pressure logged following the start of gas injection. The 1.5606-ft/sec rate is important as this is the travel rate of the bubble front from 9pt3 to the discharge line, indicating the unloading velocity through the test section.

	Migration Rate	
	sec/ft	ft/sec
1PT1 to 4PT1	0.4722	2.1179
1PT1 to 9PT3	0.5728	1.7459
1PT1 to Discharge	0.5784	1.7290
4PT1 to 9PT3	0.6292	1.5893
4PT1 to Discharge	0.6306	1.5857
9PT3 to Discharge	0.6408	1.5606

Table 4-6—Bubble front travel rate based on maximum pressure measurements following initial injection

4.1.2. Circulation Rate: 15 GPM

All tests presented under this subsection were run with 15-GPM continuous pump rate. During the test all flow rate and pressure data were logged. The tests conducted under this subsection were performed at approximately 90-91 Psi initial injection pressures and 60-, 30- and 15-seconds injection duration.

Pump Rate (GPM)	15.00		
Initial Injection Pressure (PSI)	91.07	90.65	90.84
Gas Injection Duration (seconds)	60.00	30.00	15.00
Kick Intensity (lbs./gal)	3.85	3.79	3.82
Maximum Injection Rate (GPM)	8.36	7.37	7.15
Average Injection Rate (GPM)	6.67	5.73	4.94
Total Gas Injected (gal)	7.74	3.70	1.91
Maximum Discharge Rate (GPM)	104.88	52.83	38.25
Max Rate at Unloading (GPM)	104.88	52.83	33.07
Total Discharge Volume (gal)	92.81	81.57	63.15
Total Discharge During Unloading (gal)	56.58	41.88	46.63

Table 4-7— Summary of results for 15-gpm circulation rate Tests using Air as the gaseous phase

Table 4-7 summarizes the tests run with a 15-GPM pump rate using air as the injection phase. 60-, 30- and 15-seconds were selected as injection duration with initial injection pressure between 90-91 psi. The table displays the maximum and average injection rates, the total volume of gas injected, maximum discharge rate, maximum discharge rate at unloading, total discharged volume, and total discharge and total discharge during unloading. As seen in the data, a longer duration allowed for a greater maximum and average injection rate. These rates are due to pressure drop created overall in the flow loop with gas entering. The maximum discharge rates also display the same behavior as larger gas enters the flow loop.

The following sections present the data collected from these experiments.

4.1.2.1. 90 Psi Initial Injection Pressure

4.1.2.1.1. A159060 60 Seconds Air Injection at 91.07 Psi

This test was run while pumping water at 15 GPM continuously. Air was injected at 90 psi initial air injection pressure for 60 seconds while pressure and flow rate were logged.

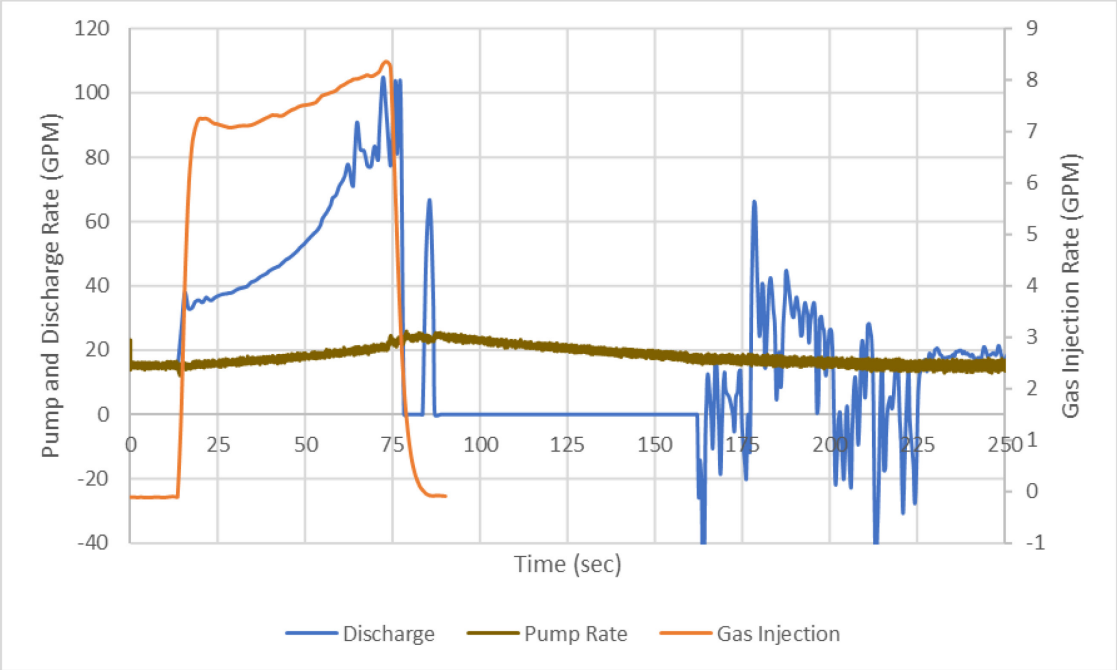

Figure 4-29—Pump, Mud Discharge, and Gas Injection Rates

Figure 4-29 displays the mud discharge rate and the gas injection rates. Air was injected at an average rate of 6.67-GPM and was terminated at approximately 74.52-seconds. The mud discharge rate began increasing as soon as gas injection commenced, and the discharge rate increased until the flow loop was unloaded at a rate of 104.88-GPM. The solenoid valve closing caused the discharge rate to drop slightly. After the gas front reached the outlet, the discharge rate dropped to zero. The 0-GPM measurement was due to the water level dropping to between the 7th and 8th floors. An exact measurement was

difficult as the gas influx continuously moved through the system. This difficulty was also observed during the test and can be seen in video footage. Figure 4-29 also demonstrates an increasing rate for gas injection with a maximum injection rate of 8.36-GPM right before the solenoid valve closes. The fluid level was raised to the flow meter, which allowed the flow meter to begin logging data again. However, the erratic data indicates slugs passing through the flow meter.

Figure 4-30 displays the cumulative pumped and discharged mud and injected gas volumes. The total amount of air injected into the flow loop was 7.74-gal. The increase in discharge rate with gas injection leads to a higher cumulative volume at discharge than the water pumped in at the inlet, indicating an influx.

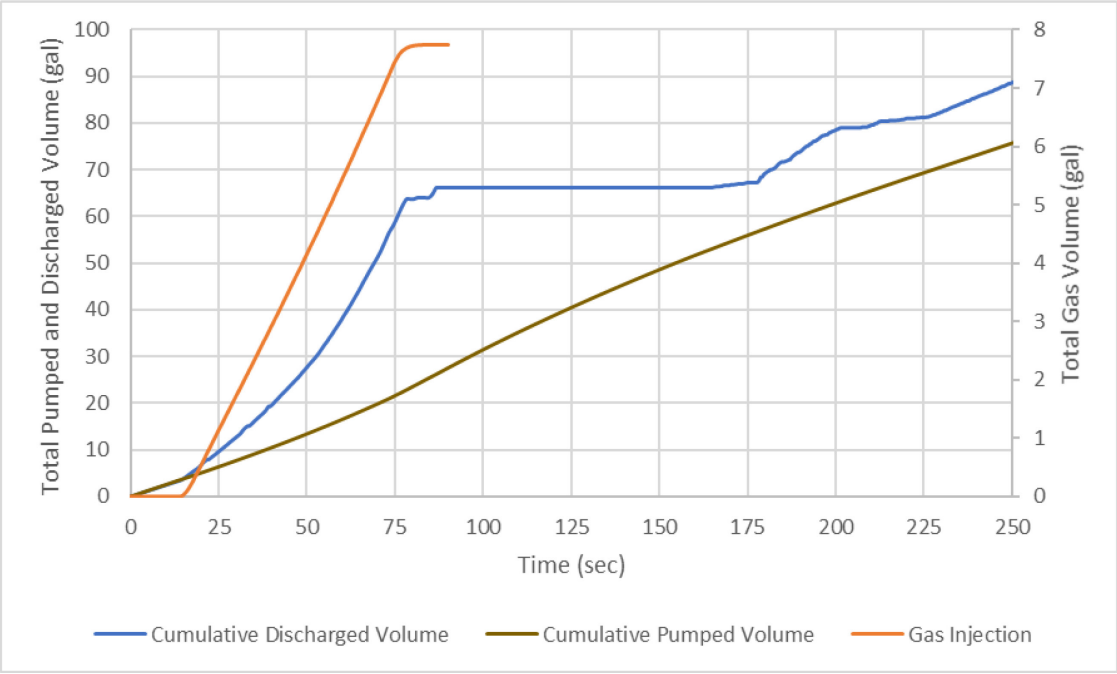

Figure 4-30—Cumulative Pumped, Discharged Water and Injected Gas Volume

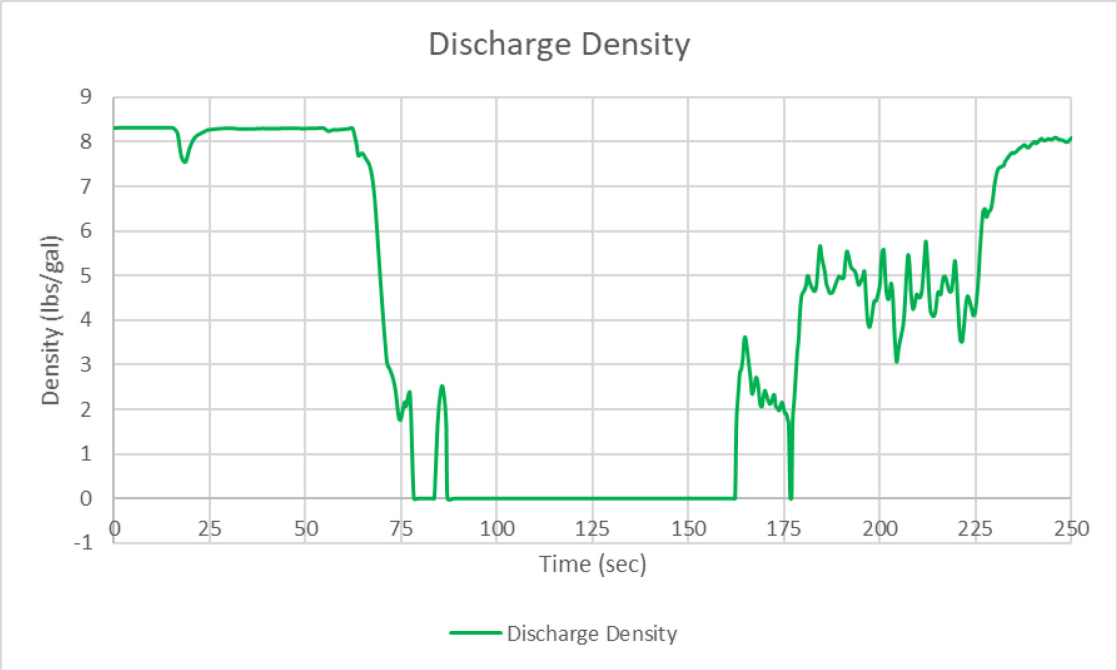

Figure 4-31—Discharge Density

Figure 4-31 displays the density of the fluid logged by the flow meter at discharge. Immediately following the unloading, the density drops to zero as the flow meter stopped logging data. The 0-lbs/gal measurement confirms the behavior observed in the discharge rate. When the fluid level rises with the pumped water, the flow meter begins logging data again. When measurement resumes indicating fluid level reached discharge line, the density fluctuates between 3 and 6-lbs/gal due to the air-water mixture until the density reached 8-lbs/gal when most of the air was removed. **Figure 4-32** contains the temperature logged by the flow meters at the injection port and the discharge line. Again, no significant change in temperature was observed.

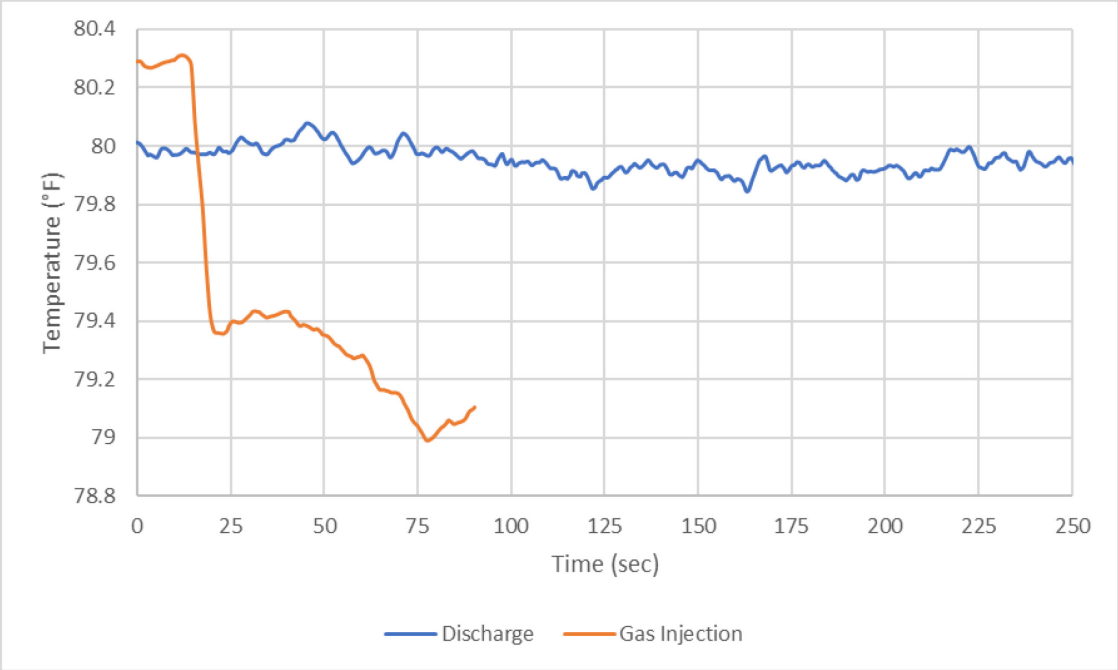

Figure 4-32—Discharge and Gas Injection Temperatures

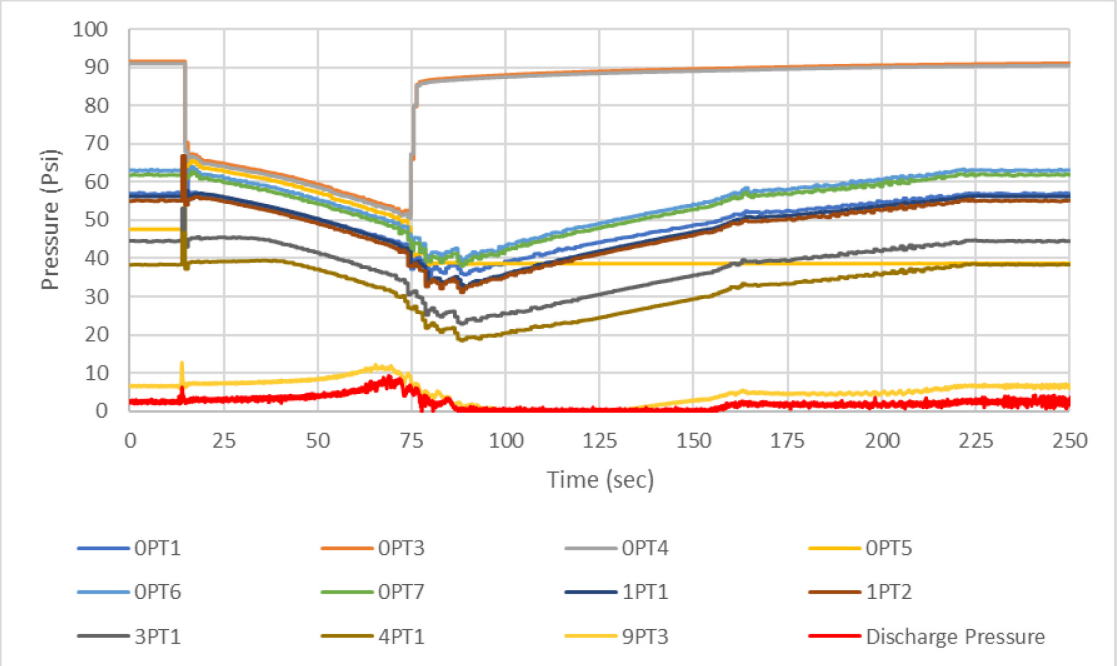

Figure 4-33—All Pressures

Figure 4-33 displays the pressure logged by all the pressure transmitters along the flow loop. All pressure transmitters display a decreasing trend except for 9PT3 and Discharge Pressure. Gas injection beginning point can be easily observed. At 74.79-seconds, the solenoid valve closes, and the bubble front reaches the discharge pressure port at approximately 68.94-seconds. This short time frame leads to difficulty separating the effects of closing the solenoid valve and unloading. Following unloading, all pressures begin rising as water is continuously pumped into the flow loop. Once the water level reaches the discharge line and the water-air mixture is circulated out, the pressure begins to stabilize at all pressure ports.

Figure 4-34 displays 9PT3 and Discharge Pressure along with pump and discharge rate. The initial spike in pressure at approximately 14.74-seconds is due to the solenoid valve opening and air injection beginning. The two pressure transmitters display a slight increase until the gas front arrives at these ports. The peak points of the pressure transmitters are slightly delayed due to the distance between them. However, the timing for peak discharge rate overlaps with peak pressure measured at the discharge line. With the bottom hole pressure drop, the pump rate rises and peaks at 25.8-GPM, then slowly drops back to 15-GPM until the fluid level reaches the top of the flow loop and the gas is circulated out.

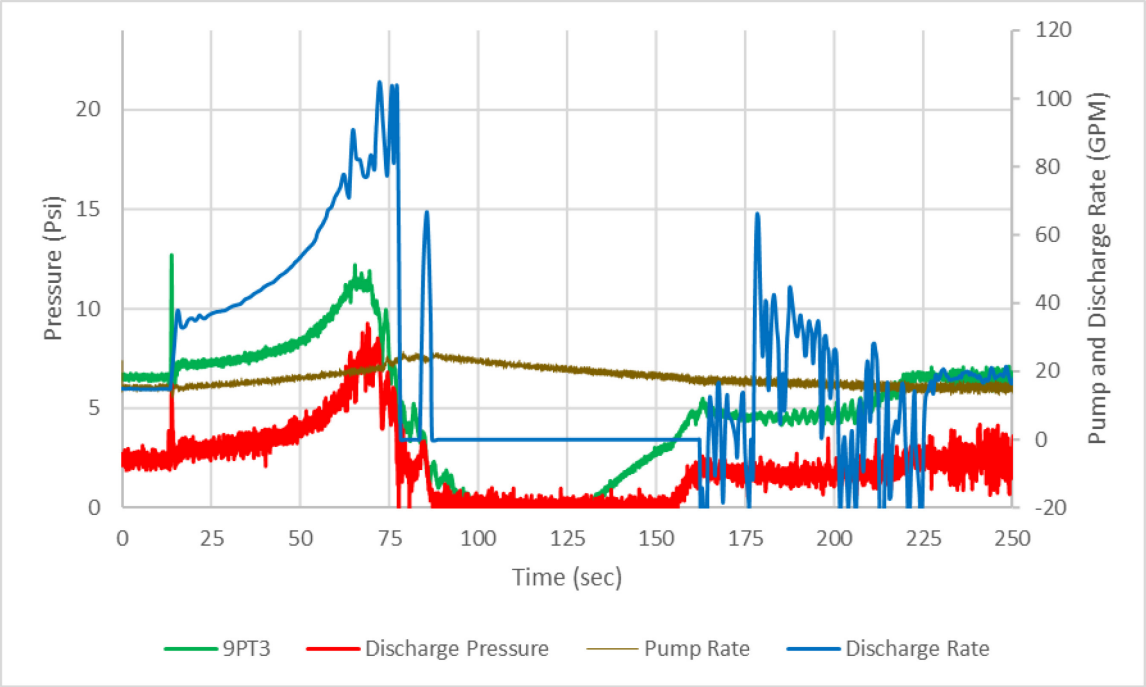

Figure 4-34—Pressure at the outlet and 15 ft below outlet and Pump and Discharge Rate

Figure 4-35 displays the difference in pressure between 1PT1 and 3PT1, 4PT1, 9PT3, and Discharge Pressure. Once the gas reaches the discharge line, measurement drops to zero for the discharge pressure and 9PT3, resulting in the two lines moving up again. The rapid and significant decrease in the difference for the 1PT1-9PT3 and 1PT1-Discharge Pressure lines can be used to detect a change in density or a gas influx in the section between these two pressure ports.

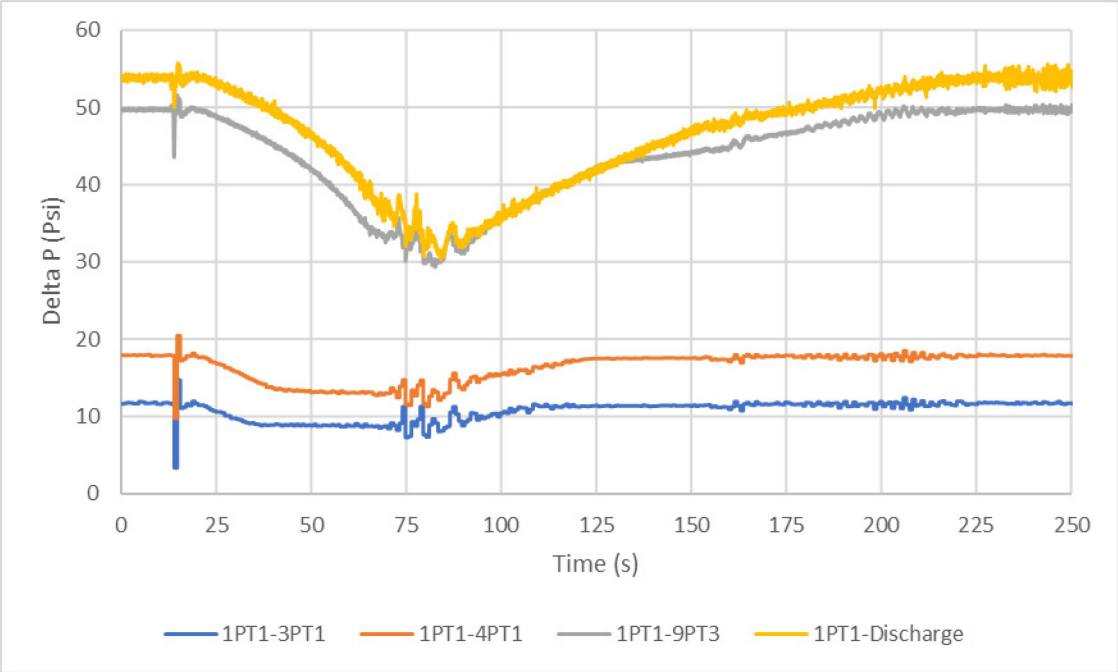

Figure 4-35— Pressure difference between 1st floor and 3rd, 4th, 9th floors, and discharge line

The pressure data was used to analyze the maximum pressure per transmitter to study the gas front travel time between transmitters. The depth between the transmitter is known and used to calculate the migration rate. **Table 4-8** presents the travel rate of the bubble front between each transmitter

The bubble front average travel rate was 2.4901-ft/sec or 0.4016-sec/ft; however, the maximum travel rate was calculated as 2.9345-ft/sec or 0.3408-sec/ft. These were calculated based on the transmitter locations and the time of peak pressure logged following the start of gas injection. The 2.9345-ft/sec rate is important as this is the travel rate of the bubble front from 9PT3 to the discharge line, indicating the unloading velocity through the test section.

	Migration Rate	
	sec/ft	ft/sec
1PT1 to 4PT1	0.4722	2.1179
1PT1 to 9PT3	0.4070	2.4567
1PT1 to Discharge	0.4016	2.4901
4PT1 to 9PT3	0.3705	2.6989
4PT1 to Discharge	0.3669	2.7258
9PT3 to Discharge	0.3408	2.9345

Table 4-8—Bubble front travel rate based on maximum pressure measurements following the initial injection

4.1.2.1.2. A159030 30 Seconds Air Injection at 90.65 Psi

This test was run while pumping water at 15-GPM continuously. Air was injected at 90.65-psi initial air injection pressure for 30-seconds while pressure and flow rate were logged.

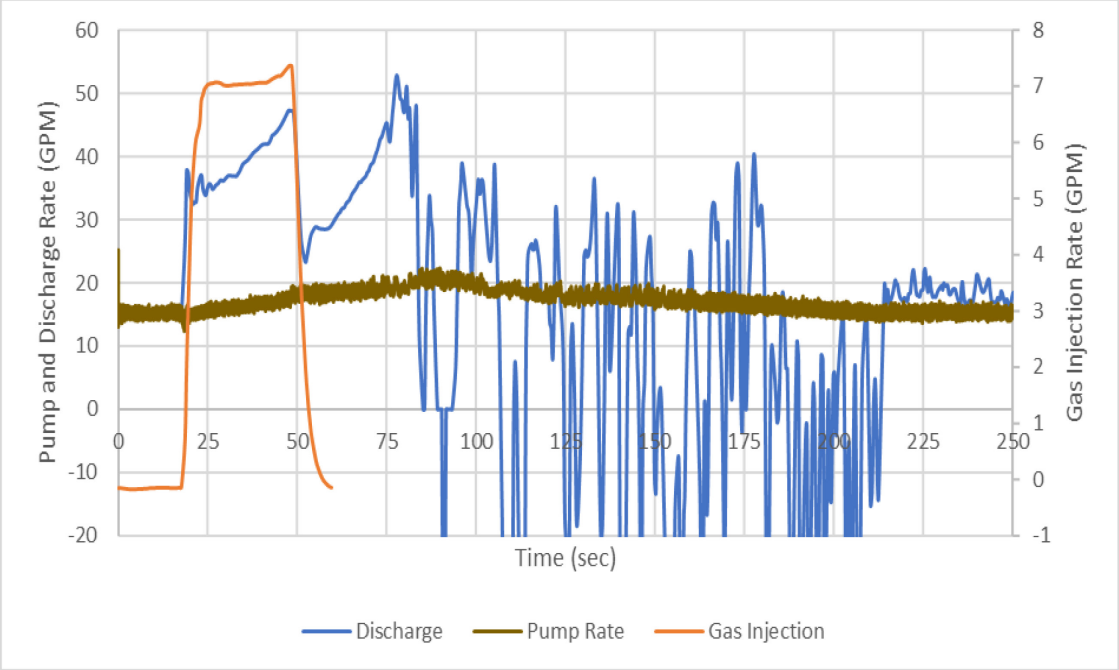

Figure 4-36—Pump, Mud Discharge, and Gas Injection Rates

Figure 4-36 displays the mud discharge rate and the gas injection rates. Air was injected at an average rate of 5.73-GPM and was terminated at approximately 49.38-

seconds. The mud discharge rate began increasing as soon as gas injection commenced, and the discharge rate increased until it peaked at 47.26-GPM when gas injection stopped. Next, the discharge rate dropped to 23.35-GPM then began increasing again until it peaked at 52.83-GPM, where the gas front reached the discharge line. Once gas reached the discharge line, the flow meter logged erratic data until the gas was circulated out of the flow loop. This was also observed during the test and can be seen in video footage. Figure 4-36 also demonstrates an increasing rate for gas injection with a maximum injection rate of 7.37-GPM right before the solenoid valve closes.

Figure 4-37 displays the cumulative pumped and discharged mud and injected gas volume. The total amount of air injected into the flow loop was 3.70-gal. The increase in discharge rate with gas injection leads to a higher cumulative volume at discharge than the water pumped in at the inlet, indicating an influx.

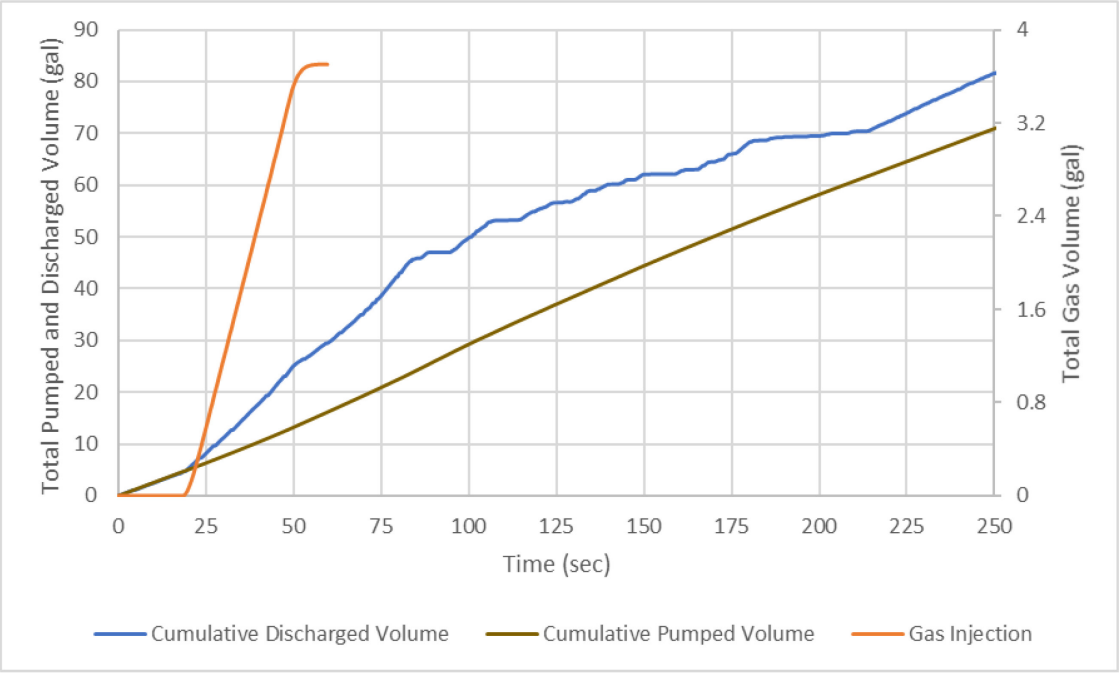

Figure 4-37— Cumulative Pumped, Discharged Water and Injected Gas Volume

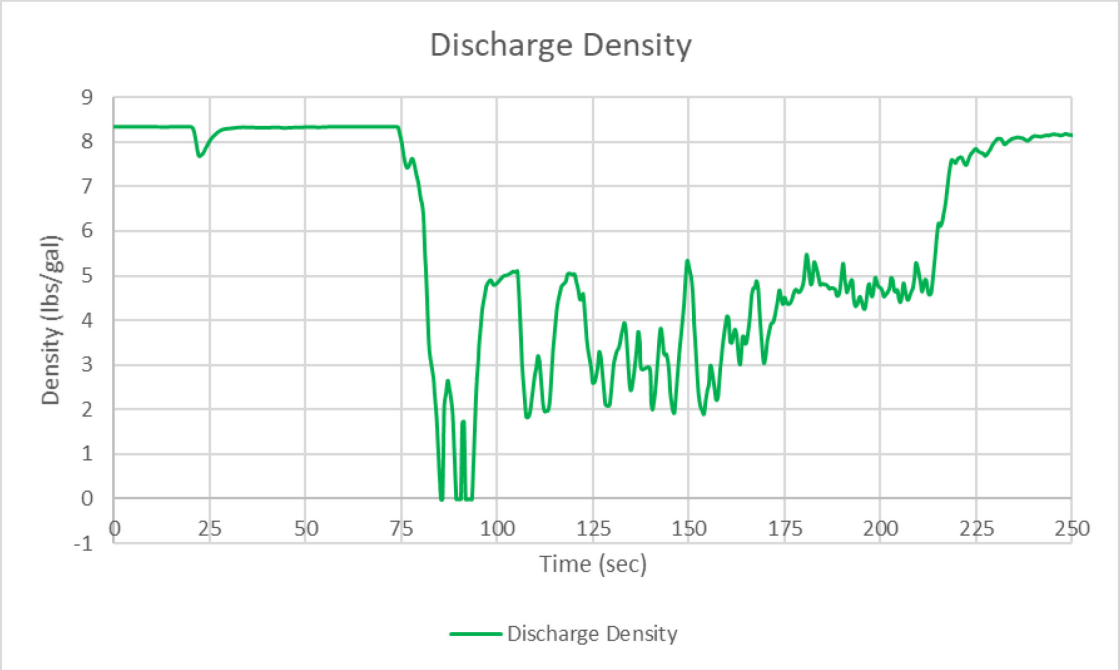

Figure 4-38—Discharge Density

Figure 4-38 displays the density of the fluid logged by the flow meter at discharge. Immediately following the unloading, the density drops to zero then provides data varying between 0-to-5.5-lbs/gal density. Once the gas was circulated out, the density measurement returned to a stable density at 8.1-lbs/gal. This density value indicates smaller air bubbles mixed into the water.

Figure 4-39 contains the temperature logged by the flow meters at the injection port and the discharge line. Again, no significant change in temperature was observed.

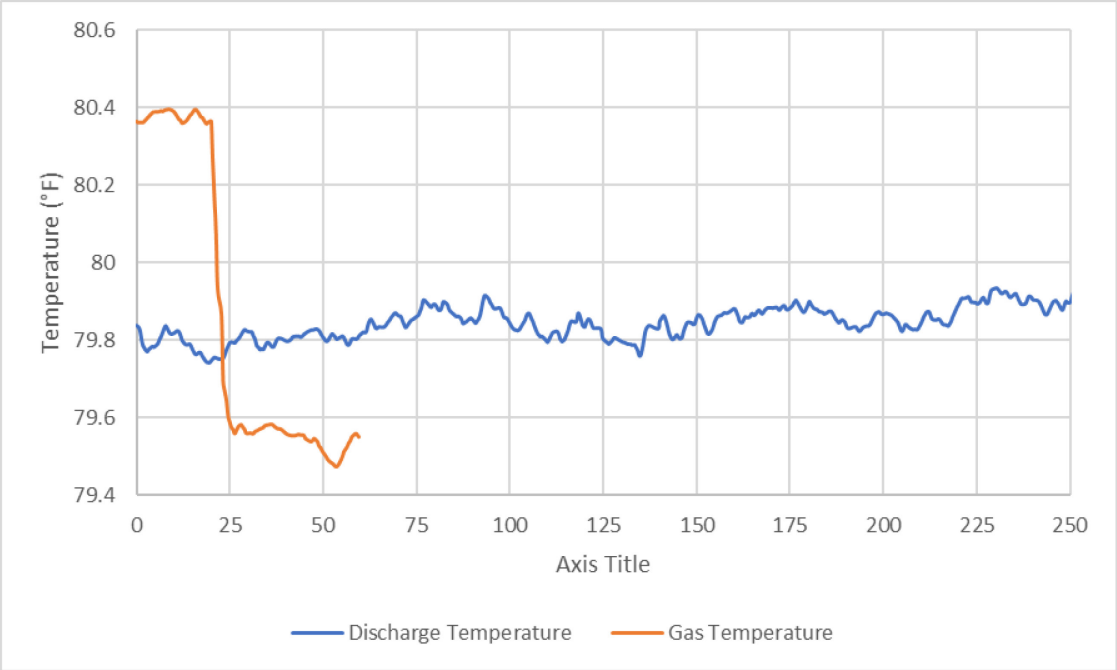

Figure 4-39—Discharge and Gas Injection Temperatures

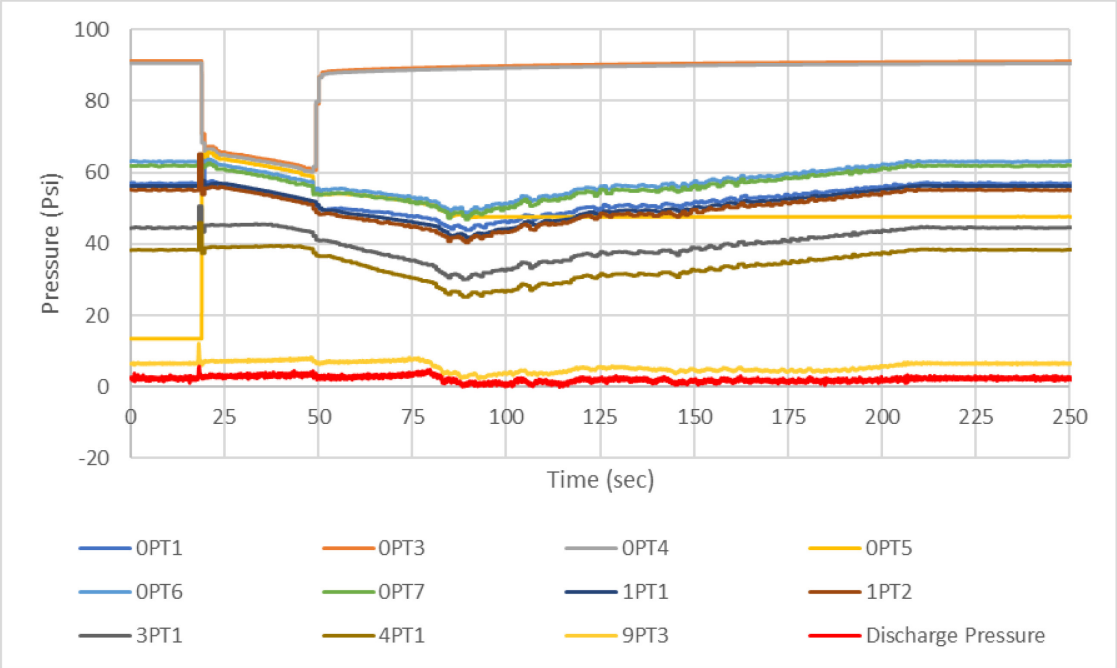

Figure 4-40—All Pressures

Figure 4-40 displays the pressure logged by all the pressure transmitters along the flow loop. All pressure transmitters display a slight instantaneous increase when the

solenoid valve opens, slightly decreasing as gas is injected. Between 48- and 50-seconds, another drop occurs, indicating the solenoid valve closed. Then the pressures continue decreasing until the gas front reaches the discharge line, and the flow loop is unloaded between 75- and 85- seconds. The data from 9PT3 and Discharge Pressure demonstrate increasing pressure during gas injection until the solenoid valve closed and the slight drop occurred. Following the drop, these two lines begin increasing again until the gas bubble arrives at these pressure ports, at which point the pressures drop. After the gas front reaches the outlet, all pressures drop to the lowest point and increase until they stabilize when the gas is completely circulated out of the flow loop.

Figure 4-41 displays 9PT3 and Discharge Pressure along with pump and discharge rate. The initial spike in pressure at approximately 18.96-seconds is due to the solenoid valve opening and air injection beginning. The two pressure transmitters display a slight increase until the solenoid valve closes, at which point the pressures drop. After the drop, the pressures begin rising again until the gas bubble reaches these ports. The peak points of the pressure transmitters are slightly delayed due to the distance between them. However, the timing for peak discharge rate overlaps with peak pressure measured at the discharge line. With the bottom hole pressure drop, the pump rate rises and peaks at 25.19-GPM, then slowly drops back to 15-GPM until the gas is circulated out, and the bottom hole pressure rises and stabilizes.

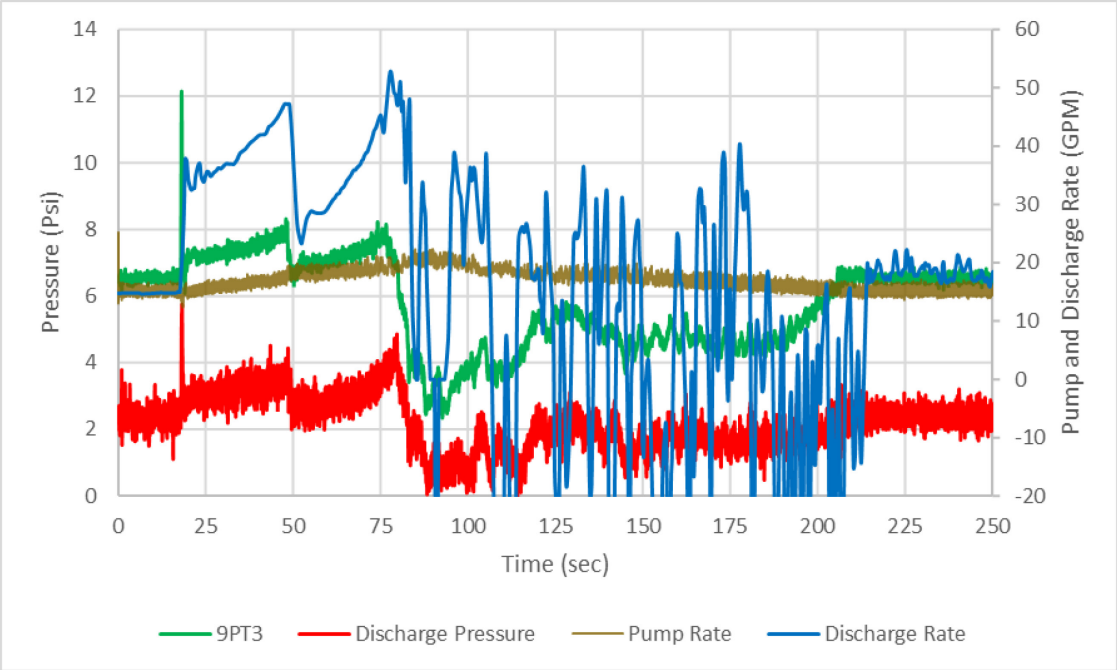

Figure 4-41—Pressure at the outlet and 15 ft below outlet and Pump and Discharge Rate

Figure 4-42 displays the difference in pressure between 1PT1 and 3PT1, 4PT1, 9PT3, and Discharge Pressure. 1PT1-3PT1 and 1PT1-4PT1 lines demonstrate decline until gas injection stops. Once the gas injection is terminated, these lines start increasing, indicating the fluid section between 1PT1 and 3PT1 and 4PT1 is changing from water-air mixture to only water as the pump continuously pumps fresh water from the water tank. The rapid and significant decrease in the difference for the 1PT1-9PT3 and 1PT1-Discharge Pressure lines can be used to detect a change in density or a gas influx location in the section between these two pressure ports. Once these lines start rising, this indicates the gas is being removed from the flow loop.

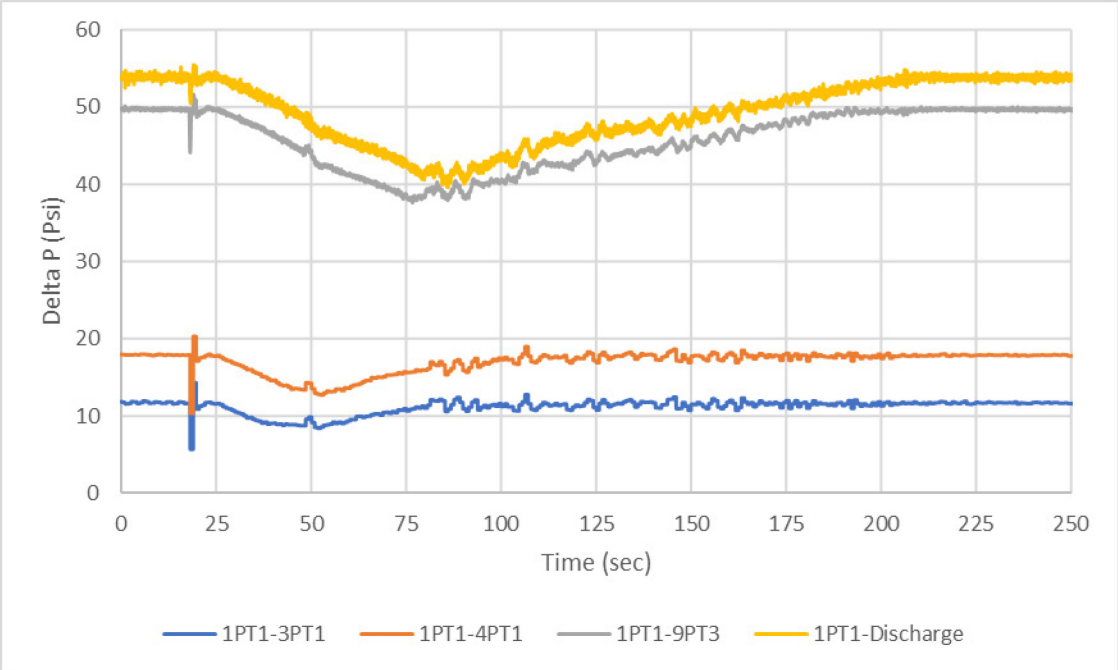

Figure 4-42— Pressure difference between 1st floor and 3rd, 4th, 9th floors, and discharge line

The pressure data was used to analyze the maximum pressure per transmitter to study the gas front travel time between transmitters. The depth between the transmitter is known and used to calculate the migration rate. **Table 4-9** presents the travel rate of the bubble front between each transmitter.

The bubble front average travel rate was 2.2019-ft/sec or 0.4542-sec/ft; however, the maximum travel rate was calculated as 3.333-ft/sec or 0.3000-sec/ft. These were calculated based on the transmitter locations and the time of peak pressure logged following the start of gas injection. The 3.333-ft/sec rate is important as this is the travel rate of the bubble front from 9PT3 to the discharge line, indicating the unloading velocity through the test section.

	Migration Rate	
	sec/ft	ft/sec
1PT1 to 4PT1	0.3400	2.9416
1PT1 to 9PT3	0.4680	2.1369
1PT1 to Discharge	0.4542	2.2019
4PT1 to 9PT3	0.5398	1.8525
4PT1 to Discharge	0.5104	1.9594
9PT3 to Discharge	0.3000	3.3333

Table 4-9— Bubble front travel rate based on maximum pressure measurements following the initial injection

4.1.2.1.3. A159015 15 Seconds Air Injection at 90.84 Psi

This test was run while pumping water at 15-GPM continuously. Air was injected at 90.84-psi initial air injection pressure for 15-seconds while pressure and flow rate were logged.

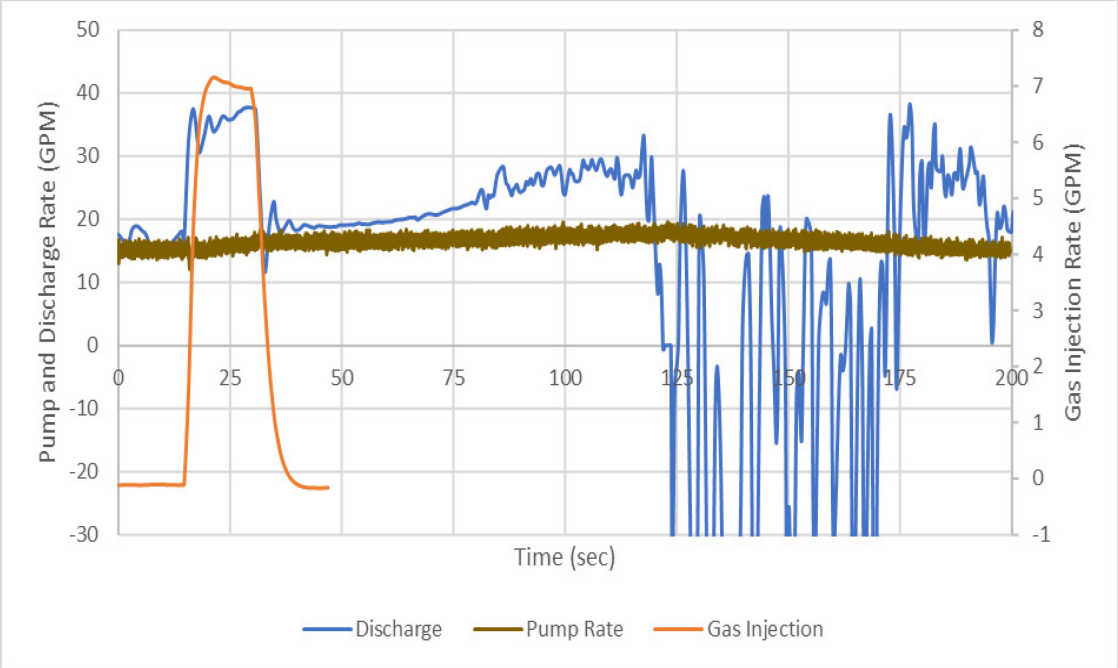

Figure 4-43— Pump, Mud Discharge, and Gas Injection Rates

Figure 4-43 displays the mud discharge rate and the gas injection rates. Air was injected at an average rate of 4.94-GPM and was terminated at approximately 31.89-seconds. The mud discharge rate began increasing as soon as gas injection commenced,

and the discharge rate increased until it peaked at 37.73-GPM when gas injection stopped. Next, the discharge rate dropped to 11.7-GPM then increased again until it peaked at 33.07-GPM when the gas front reached the discharge line. Once gas reached the discharge line, the flow meter began logging erratic data until the gas was circulated out of the flow loop. This was also observed during the test and can be seen in video footage. **Figure 4-43** also demonstrates an increasing rate for gas injection with a maximum injection rate of 7.15-GPM right before the solenoid valve closes.

Figure 4-44 displays the cumulative pumped and discharged mud and injected gas volume. The total amount of air injected into the flow loop was 1.91-gal. The increase in discharge rate with gas injection leads to a higher cumulative volume at discharge than the water pumped in at the inlet, indicating an influx.

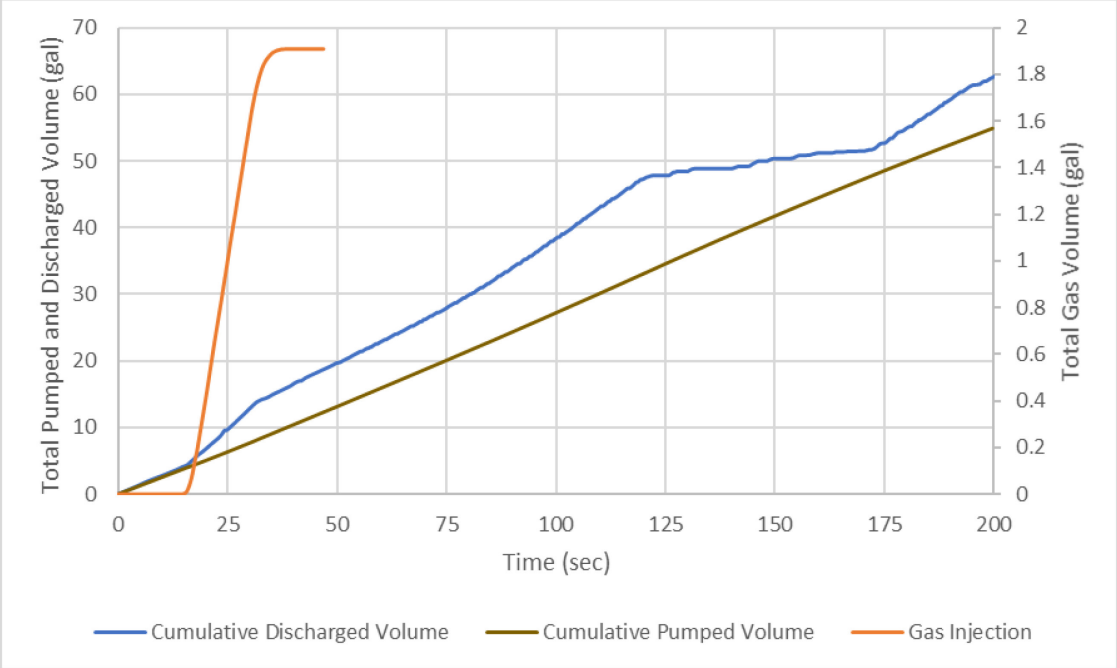

Figure 4-44— Cumulative Pumped, Discharged Water and Injected Gas Volume

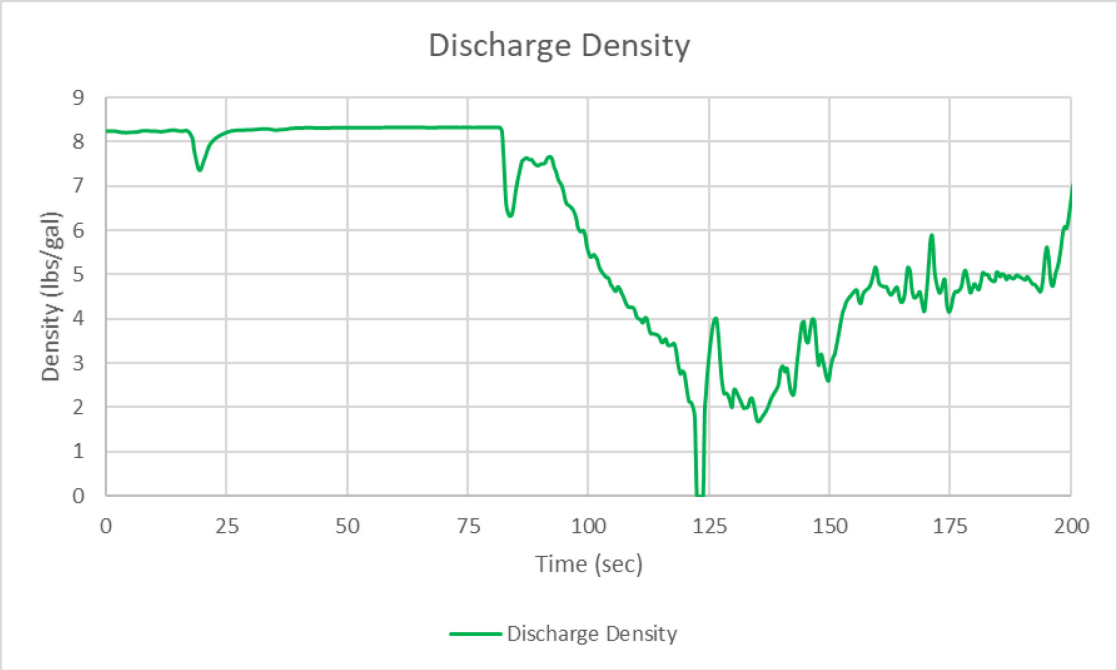

Figure 4-45—Discharge Density

Figure 4-45 displays the density of the fluid logged by the flow meter at discharge. Immediately following the gas front reaching the discharge line begins reducing until a large slug reaches the flow meter causing the flowmeter to read 0-lbs/gal density. Then, the flow meter begins reading flow data with a density between 2.5-to-6-lbs/gal.

Figure 4-46 contains the temperature logged by the flow meters at the injection port and the discharge line. Again, no significant change in temperature was observed.

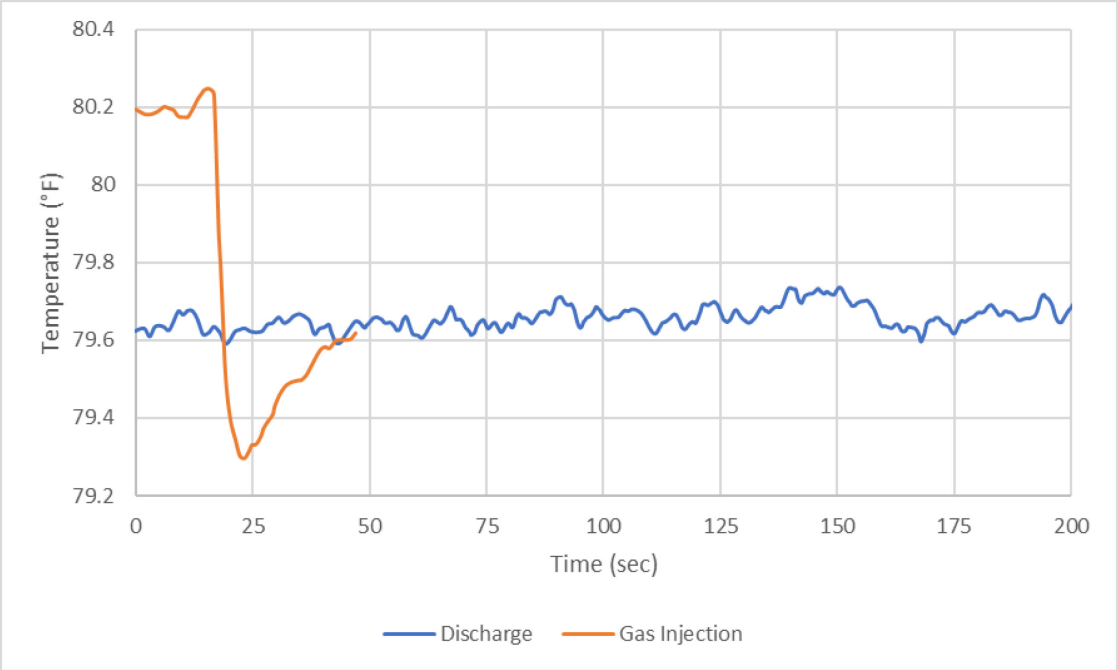

Figure 4-46—Discharge and Gas Injection Temperatures

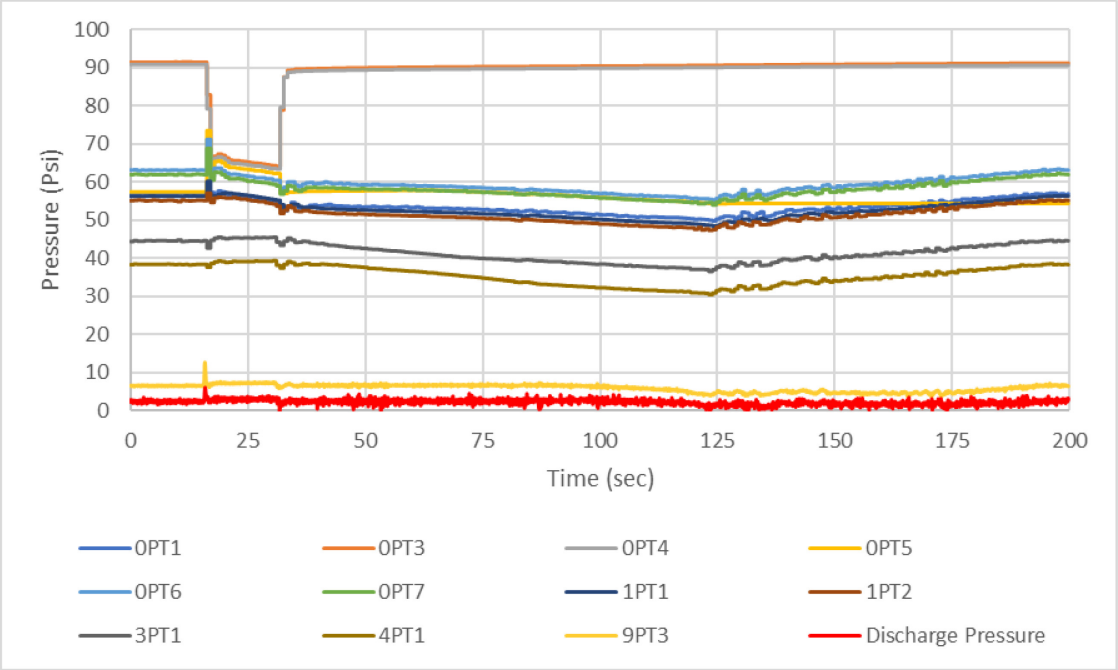

Figure 4-47—All Pressures

Figure 4-47 displays the pressure logged by all the pressure transmitters along the flow loop. In the test section, the pressure transmitters 1PT1 and 1PT2 decline while gas

is being injected, while the transmitters 3PT1, 4PT1, 9PT3, and Discharge Pressure display a slightly increasing trend. When the solenoid valve closes, all pressure transmitters display the sudden decline and recovery in pressure between 31- and 34-seconds. The pressure transmitters 1PT1, 1PT2, 3PT1, and 4PT1 logged decreasing pressure after the solenoid valves until the gas front reached the outlet between 82.6- and 86-seconds. With the gas being circulated out and freshwater entering the flow loop, the pressures start rising

Figure 4-48 displays 9PT3 and Discharge Pressure along with pump and discharge rate. The initial spike in pressure at approximately 16.3-seconds is due to the solenoid valve opening and air injection beginning. The two pressure transmitters display a slight increase until the solenoid valve closes, at which point the pressures drop. After the drop, the pressures rise again slightly and remain stable until after gas is discharged from the test section. The readings from these two pressure transmitters provide limited information for this test. This is due to the wide range (0-300 psi) and the minor fluctuations that these pressure transmitters cannot capture, which led to inconclusive results for this test.

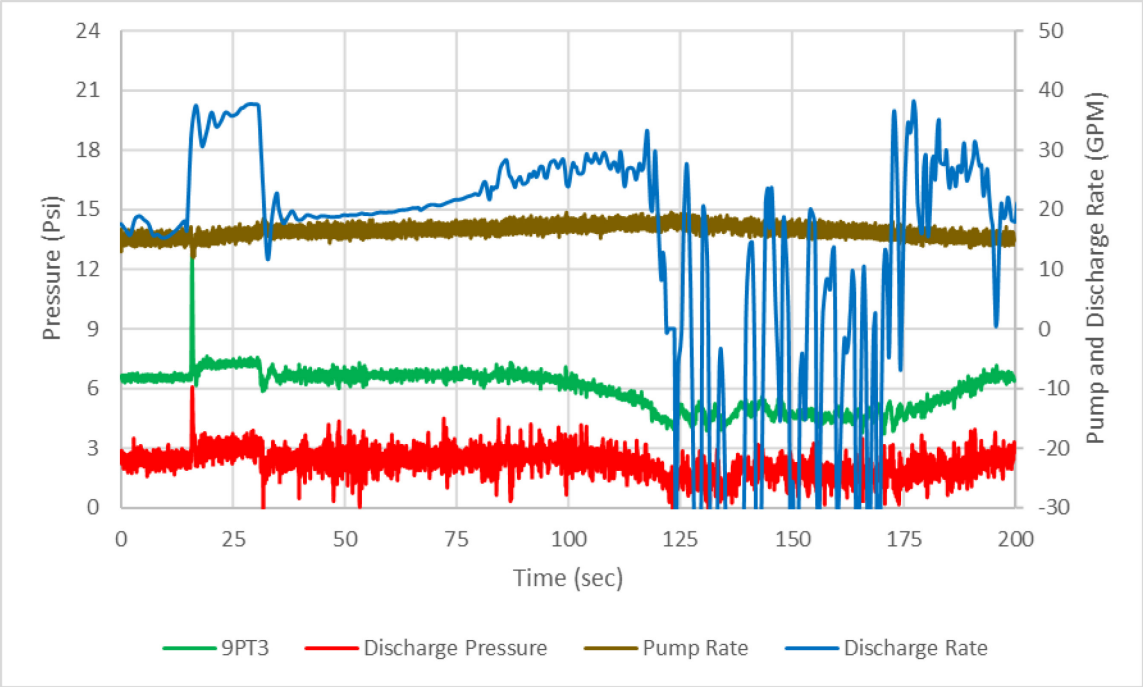

Figure 4-48—Pressure at the outlet and 15 ft below outlet and Pump and Discharge Rate

Figure 4-49 displays the difference in pressure between 1PT1 and 3PT1, 4PT1, 9PT3, and Discharge Pressure. 1PT1-3PT1 and 1PT1-4PT1 lines demonstrate decline until gas injection stops. Once the gas injection is terminated, these lines start increasing, indicating the fluid section between 1PT1 and 3PT1 and 4PT1 is changing from water-air mixture to only water as the pump continuously pumps fresh water from the water tank. The slight fluctuations in these lines between 75- and 90-seconds confirm the start of gas discharge from the flow loop. The 1PT1-9PT3 and 1PT1-Discharge Pressure lines continuously decline until 105 seconds, then begin rising. The small fluctuations from this experiment are not apparent and difficult to analyze.

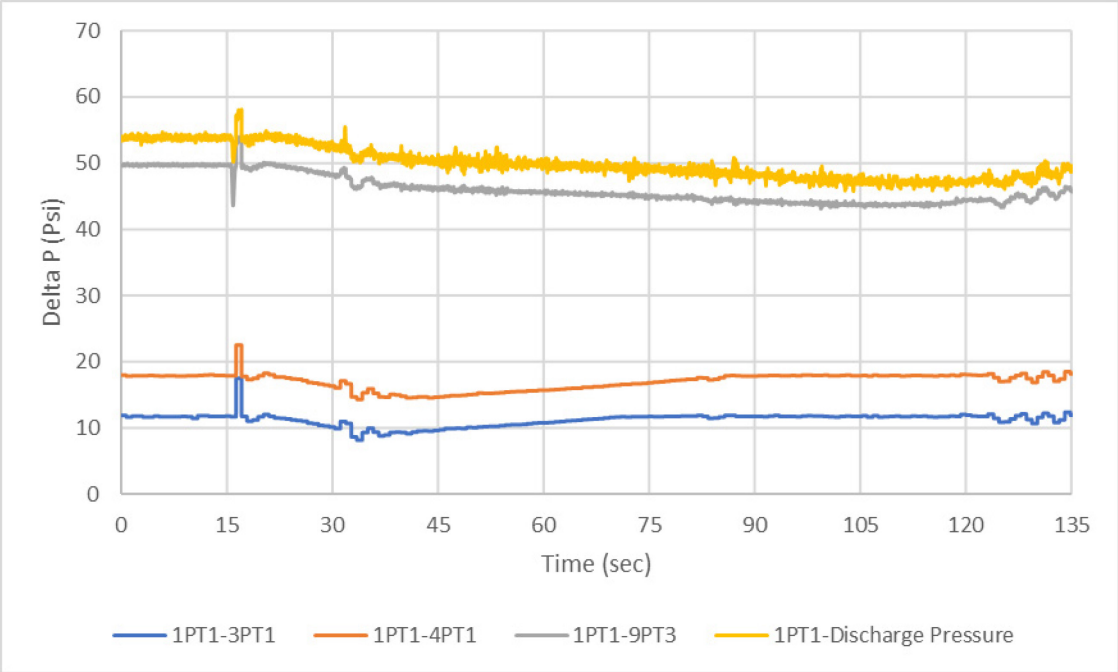

Figure 4-49— Pressure difference between 1st floor and 3rd, 4th, 9th floors, and discharge line

4.1.3. Circulation Rate: 30 GPM

All tests presented under this subsection were run with a 30-GPM continuous pump rate. During the test, all flow rate and pressure data were logged. The tests conducted under this subsection were performed using approximately 90- and 80-Psi initial injection pressures and 60-, 30- and 15-seconds injection duration.

Pump Rate (GPM)	30			30		
Initial Injection Pressure (PSI)	90.92	91	90.67	82.3	82.3	82.4
Gas Injection Duration (seconds)	60	30	15	60	30	15
Kick Intensity (lbs./gal)	3.685	3.684	3.643	2.49	2.5	2.514
Maximum Injection Rate (GPM)	7.74	6.89	6.77	8.02	6.71	6.72
Average Injection Rate (GPM)	6.36	5.61	4.70	6.21	5.55	4.76
Total Gas Injected (gal)	7.23	3.53	1.81	6.97	3.36	1.75
Maximum Discharge Rate (GPM)	111.15	68.71	51.70	108.52	66.82	50.34
Max Rate at Unloading (GPM)	111.15	68.71	44.32	108.52	66.82	44.48
Total Discharge Volume (gal)	120.83	102.76	106.60	125.46	91.50	89.53
Total Discharge During Unloading (gal)	69.53	58.11	59.36	70.68	57.96	45.94

Table 4-10— Summary of results for 30-GPM circulation rate Tests using Air as the gaseous phase

Table 4-10 summarizes the tests run with a 30-GPM pump rate using air as the injection phase. Again, 60-, 30- and 15-seconds were selected as injection duration with 90- and 80-Psi as the initial injection pressure. The table displays the maximum and average injection rates, the total volume of gas injected, maximum discharge rate, maximum discharge rate at unloading, total discharged volume, and total discharge and total discharge during unloading. As seen in the data, a longer duration allowed for a greater maximum and average injection rate. These rates are due to pressure drop created overall in the flow loop with gas entering. The maximum discharge rates also display the same behavior as larger gas enters the flow loop.

The following sections provide data collected during these tests.

4.1.3.1. 90 Psi Initial Injection Pressure

The following section provides results from dynamic tests conducted with a 30-GPM flow rate with an approximate initial injection rate of 90-psi. **Table 4-11** summarizes these tests providing the test parameters and results.

Pump Rate (GPM)	30		
Initial Injection Pressure (PSI)	90.92	91	90.67
Gas Injection Duration (seconds)	60	30	15
Kick Intensity (lbs./gal)	3.685	3.684	3.643
Maximum Injection Rate (GPM)	7.74	6.89	6.77
Average Injection Rate (GPM)	6.36	5.61	4.70
Total Gas Injected (gal)	7.23	3.53	1.81
Maximum Discharge Rate (GPM)	111.15	68.71	51.70
Max Rate at Unloading (GPM)	111.15	68.71	44.32
Total Discharge Volume (gal)	120.83	102.76	106.60
Total Discharge During Unloading (gal)	69.53	58.11	59.36

Table 4-11—Summary of results for 30-GPM circulation rate tests with air injection at approximately 90-Psi

4.1.3.1.1. A309060 60-Seconds Air Injection at 90.92-Psi

This test was run while pumping water at 30-GPM continuously. Air was injected at 90.92-psi initial air injection pressure for 60-seconds while pressures and flow rates were logged.

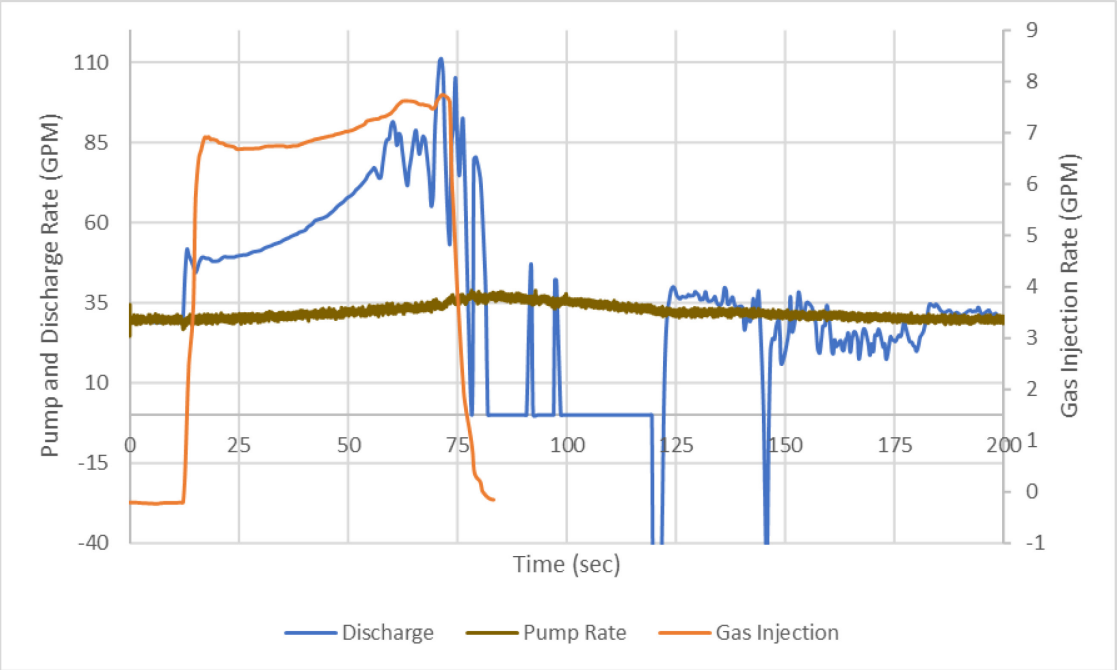

Figure 4-50— Pump, Mud Discharge, and Gas Injection Rates

Figure 4-50 displays the mud discharge rate and the gas injection rates. Air was injected at an average rate of 6.36-GPM and was terminated at approximately 73.25-seconds. The mud discharge rate began increasing as soon as gas injection commenced, and the discharge rate increased until the gas front arrived at the outlet at a rate of 77.08-GPM at 56.01-seconds. The discharge rate continued fluctuating as other small bubbles reached the outlet. The maximum discharge rate was recorded as 111.15-GPM. Following the solenoid valve closing at 73.25-seconds, the discharge rate slightly drops, then rises, and then drops to 0-GPM. Although the video footage shows that the flow regime started as a bubbly flow with no Taylor bubble, a larger discharge rate was logged after the flow regime transitioned to churn flow. Figure 4-50 also demonstrates an increasing rate for gas injection with a maximum injection rate of 7.74-GPM right before the solenoid valve closes. At approximately 82 seconds, the flow meter began reading the 0-GPM rate except

for two instantaneous rates of 47-GPM and 42-GPM. The footage demonstrates large bubbles traveling with water. However, while the flow meter was reading 0-GPM, the video footage on the 8th floor shows the flow regime was still churn flow with the return line full of water. No footage was recorded from the 9th and 10th floor due to the transition to steel pipe for these sections. The pressure data was necessary to confirm the 0-GPM discharge flow. However, the video footage shows that the return line turned to a slow flow at approximately 123-seconds while the logged discharge rate shows a positive increasing discharge rate of 32-GPM. The video footage shows water returning at 136-seconds with the bubbly flow in the test section. The flow meter logged the rate as 37-GPM with a density of 3.45-lbs/gal at 136-seconds, indicating lighter density fluid. The rate and density at the discharge stabilized to initial conditions at approximately 192-seconds.

Figure 4-51 displays the cumulative pumped and discharged mud and injected gas volumes. The total amount of air injected into the flow loop was 7.23-gal. The cumulative discharged and pumped mud volumes are also plotted. The increase in discharge rate with gas injection leads to a higher cumulative volume at discharge than the water pumped in at the inlet, indicating an influx. The increasing discharge rate is mainly observed during gas injection.

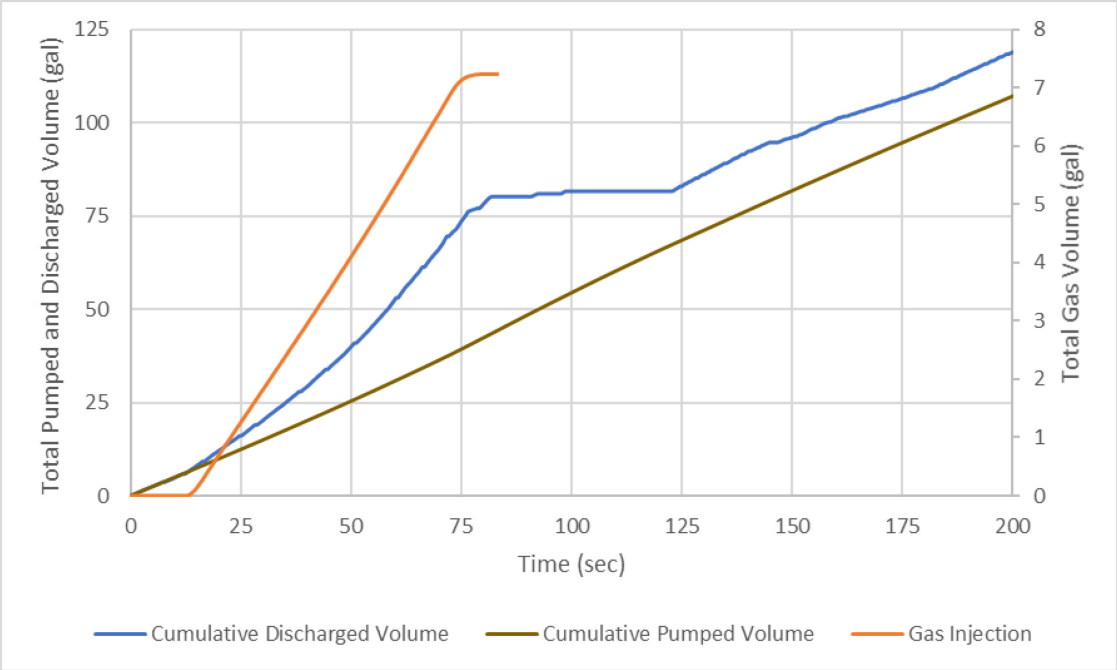

Figure 4-51— Cumulative Pumped, Discharged Water and Injected Gas Volume

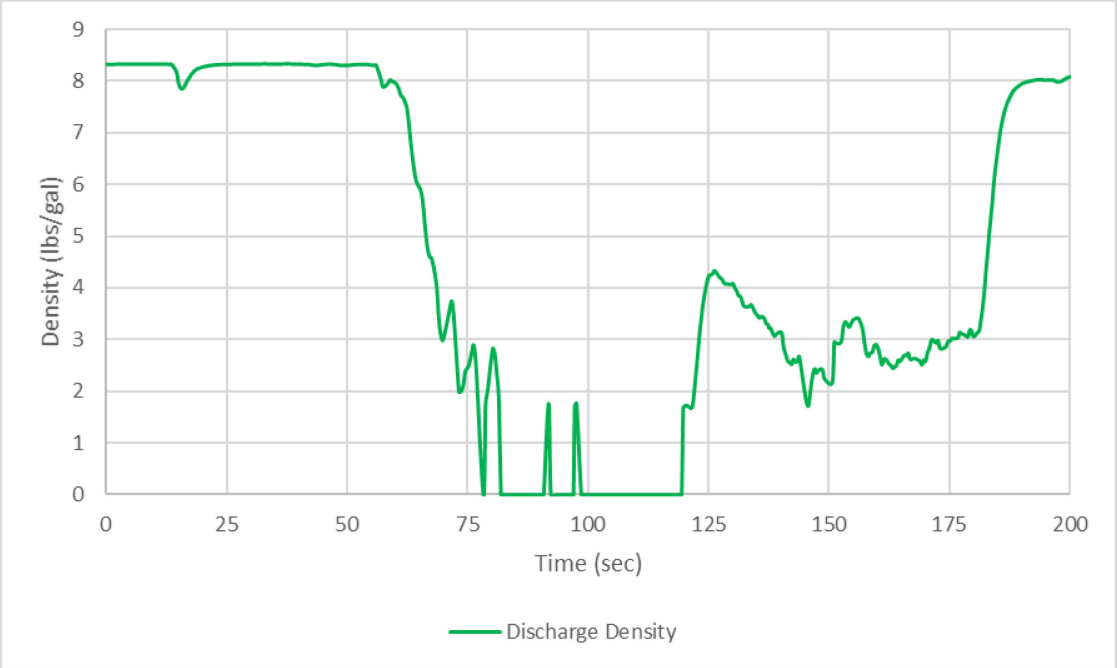

Figure 4-52—Discharge Density

Figure 4-52 displays the density of the fluid logged by the flow meter at discharge. Immediately following gas arrival at discharge, the density rapidly drops to 0-lbs/gal. The

video footage demonstrates a mixture of water and air flowing through the flowmeter and a logged rate of 0-GPM values. The flow meter begins logging data again when the video footage shows no returning mud. The flow and density stabilize again at 192-seconds. **Figure 4-53** contains the temperature logged by the flow meters at the injection port and the discharge line. No significant change in temperature was observed.

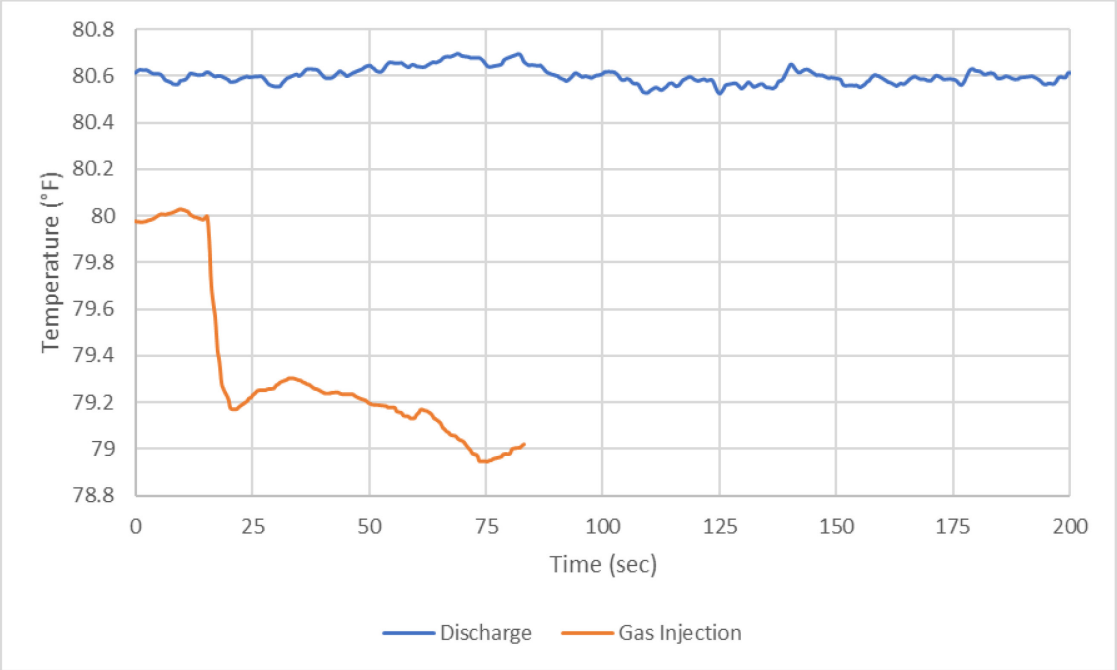

Figure 4-53—Discharge and Gas Injection Temperatures

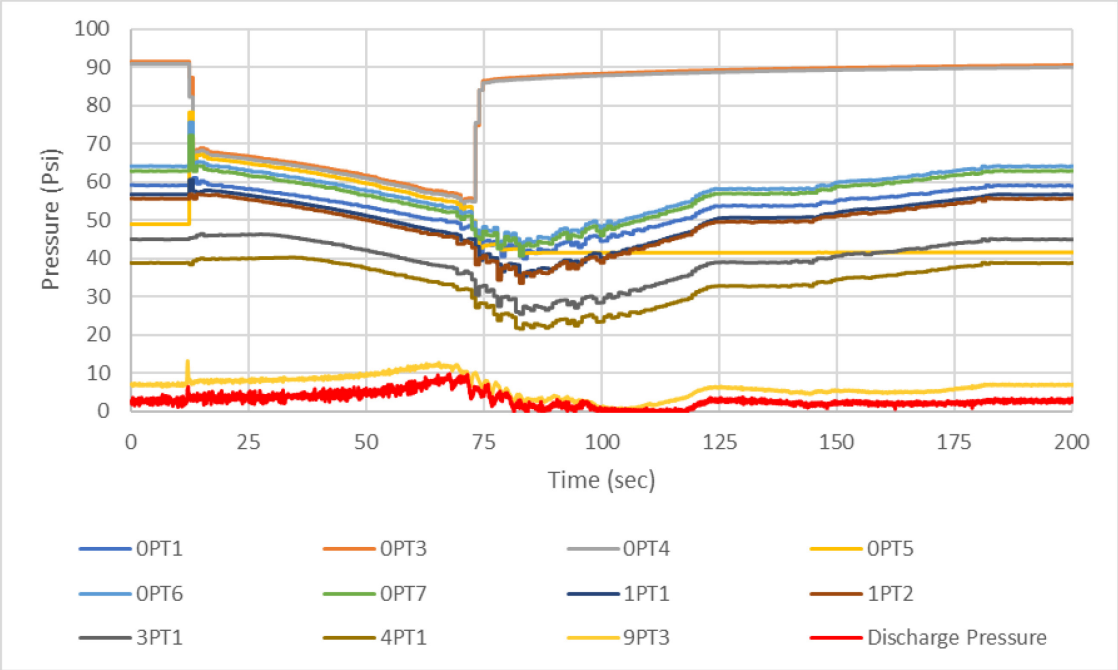

Figure 4-54—All Pressures

Figure 4-54 displays the pressure logged by all the pressure transmitters along the flow loop. All pressure transmitters display a decreasing trend except for 9PT3 and Discharge Pressure. Gas injection beginning point can be easily observed as a slight increase in pressure. The bubble front reaches the discharge pressure port at approximately 56.01-seconds. At 73.25-seconds, the solenoid valve closes. Following unloading, all pressures begin rising as water is continuously pumped into the flow loop. The pressure transmitter Discharge Pressure logged approximately 0 Psi between 98.35- and 118.93-seconds. This provides a better indication of when the fluid level dropped below the discharge line.

Figure 4-55 displays 9PT3 and Discharge Pressure along with pump and discharge rate. The initial spike in pressure at approximately 12.41-seconds is due to the solenoid valve opening and air injection beginning. The two pressure transmitters display a slight

increase until after the gas front arrives at these ports. The peaks of the pressure transmitters are slightly delayed due to the distance between them. The timing for the first gas bubble arriving at the discharge line does not overlap with the timing of peak pressure measured at the discharge line. The first gas arrives at the discharge line earlier than the drop off of pressure at 9PT3 and Discharge Pressure.

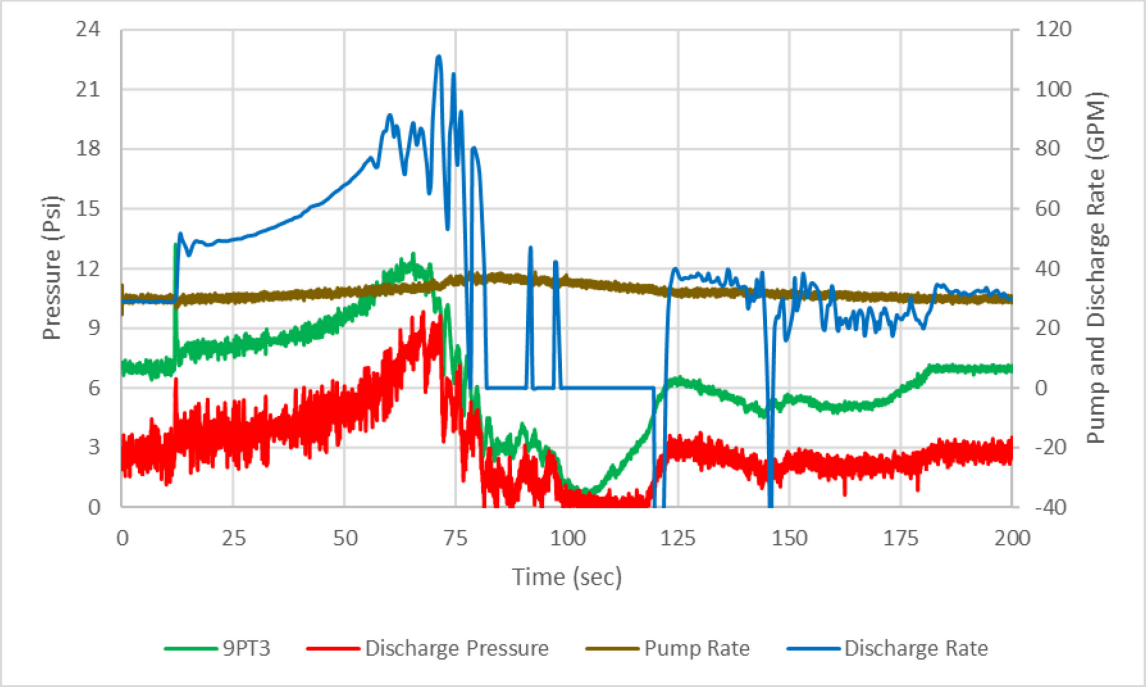

Figure 4-55—Pressure at the outlet and 15 ft below outlet and Pump Rate

Figure 4-56 displays the difference in pressure between 1PT1 and 3PT1, 4PT1, 9PT3, and Discharge Pressure. 1PT1-3PT1 and 1PT1-4PT1 demonstrate a slight decrease with gas arriving first at 1PT1, then 3PT1, and then 4PT1. However, the 1PT1-9PT3 and 1PT1-Discharge Pressure lines demonstrate a more significant reduction with the longer distance between these pressure transmitters.

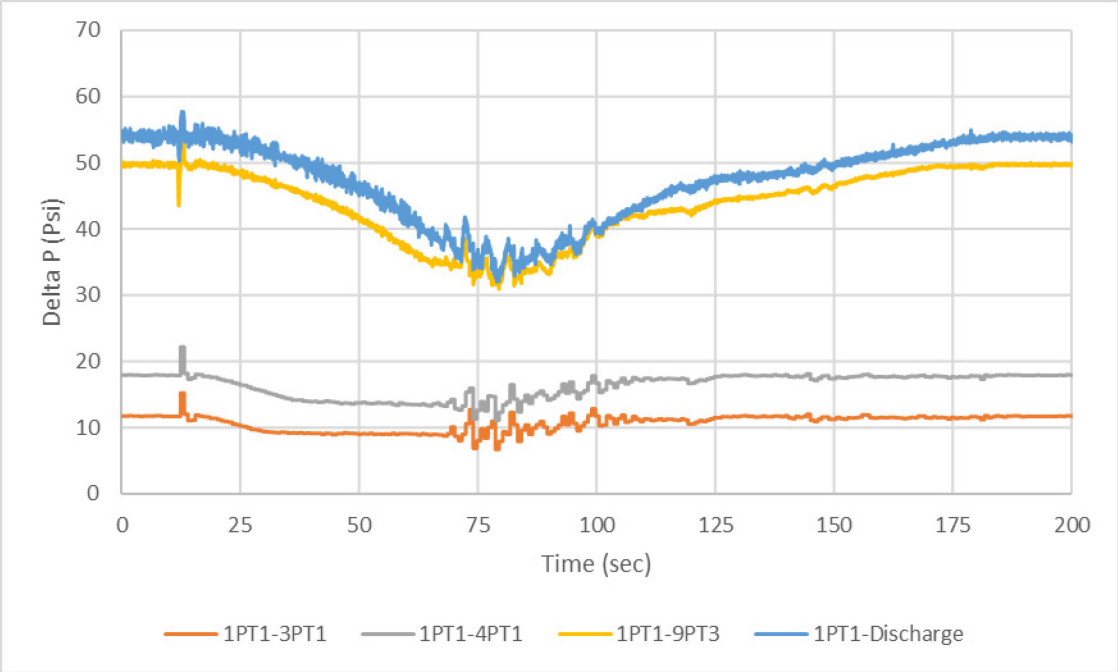

Figure 4-56— Pressure difference between 1st floor and 3rd, 4th, 9th floors, and discharge line

4.1.3.1.2. A309130 30 Seconds Air Injection at 91 Psi

This test was run while pumping water at 30-GPM continuously. Air was injected at 91-psi initial air injection pressure for 30-seconds while pressures and flow rates were logged.

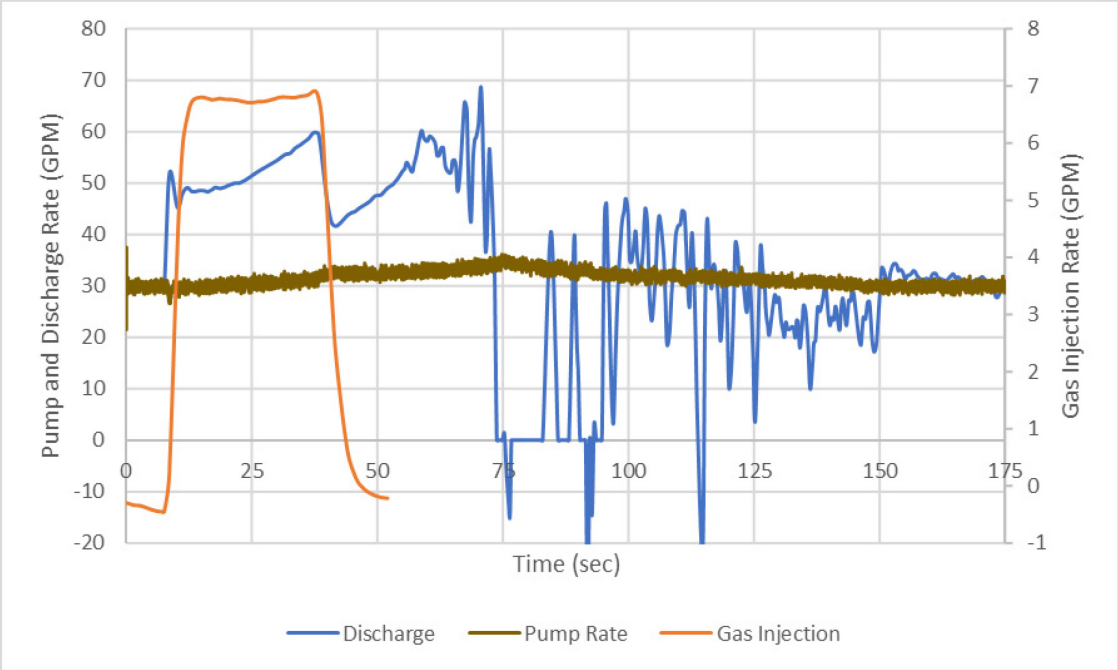

Figure 4-57— Pump, Mud Discharge, and Gas Injection Rates

Figure 4-57 displays the pump and discharge rates and the gas injection rate. Air was injected at an average rate of 5.61-GPM and was terminated at approximately 39.65-seconds. The mud discharge rate began increasing as soon as gas injection began, and the discharge rate increased to 59.48-GPM until the solenoid valve closed and gas injection stopped. The discharge rate suddenly dropped to 41.66-GPM, then began increasing to 54-GPM at 55.88-seconds when the gas front reached the outlet, then slightly dropped and began fluctuating. The maximum discharge rate recorded by the flow meter was 68.71-GPM at 70.58-seconds, then suddenly dropped to 0-GPM. The discharge rate begins fluctuating until it stabilizes 161.57-seconds. The video footage shows that the flow regime started as a bubbly flow with no Taylor bubble; a larger discharge rate was logged after the flow regime transitioned to churn flow. Figure 4-57 also demonstrates an increasing rate for gas injection with a maximum injection rate of 6.89-GPM right before

the solenoid valve closes. At approximately 82.06 seconds, the flow meter began reading 0-GPM discharge rate. The footage from the 8th floor did not demonstrate any interruption of returning mud.

Figure 4-58 displays the cumulative pumped and discharged mud and injected gas volumes. The total amount of air injected into the flow loop was 3.53-gal. The cumulative discharged and pumped mud volumes are also plotted. The increase in discharge rate with gas injection leads to a higher cumulative volume at discharge than the water pumped in at the inlet, indicating an influx. The increasing discharge rate is mainly observed during gas injection.

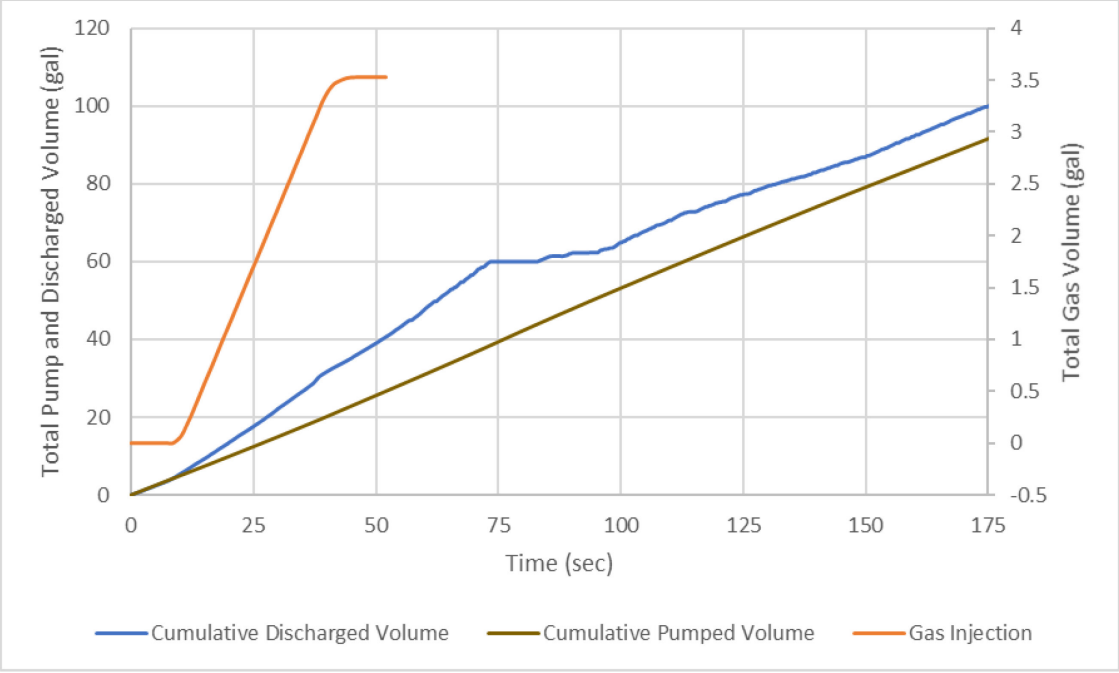

Figure 4-58— Cumulative Pumped, Discharged Water and Injected Gas Volume

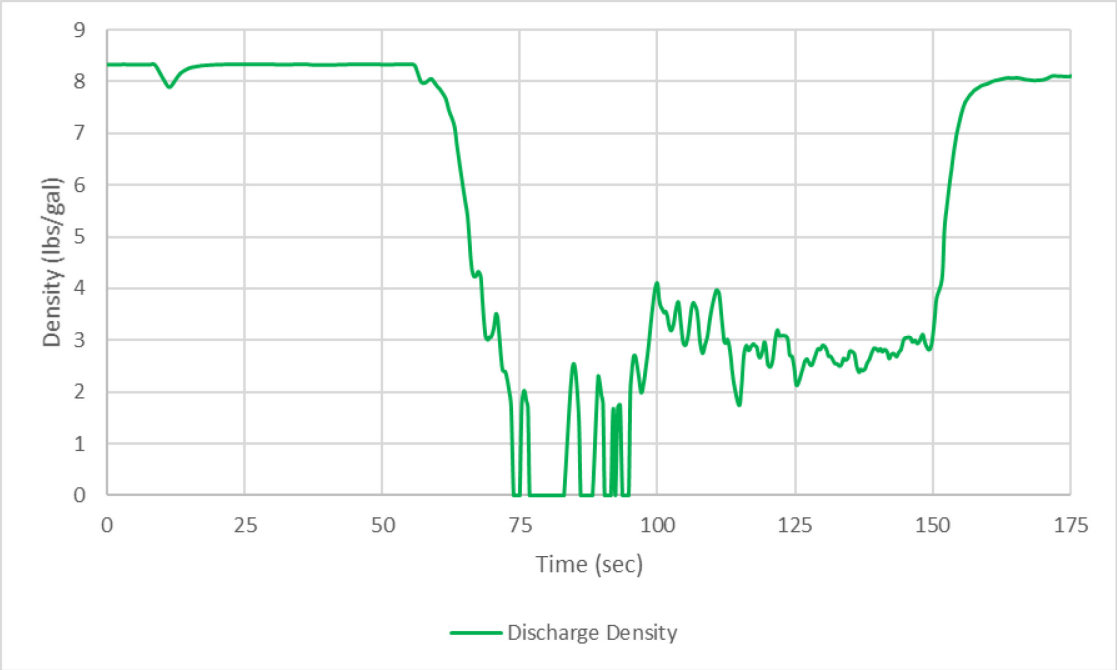

Figure 4-59—Discharge Density

Figure 4-59 displays the density of the fluid logged by the flow meter at discharge. Immediately following gas arrival at discharge, the density rapidly drops to 0-lbs/gal. The density fluctuates between 0- and 3-lbs/gal until 95.55-seconds, then fluctuates between 2- and 4-lbs/gal. Then the density stabilizes at 171.43-seconds. **Figure 4-60** contains the temperature logged by the flow meters at the injection port and the discharge line. No significant change in temperature was observed.

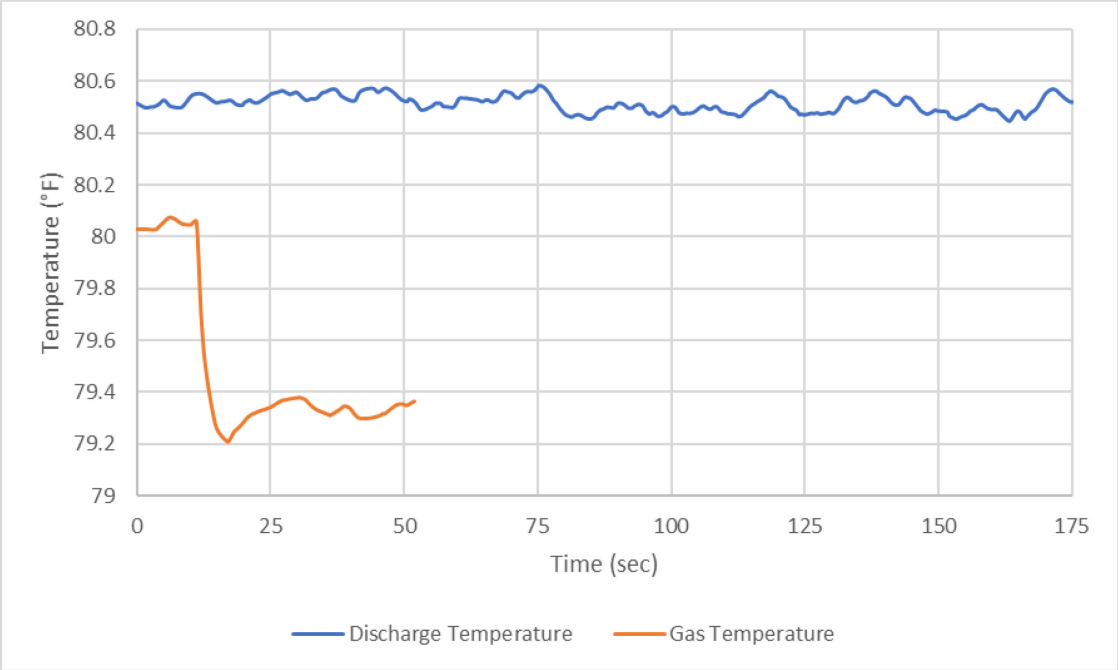

Figure 4-60—Discharge and Gas Injection Temperatures

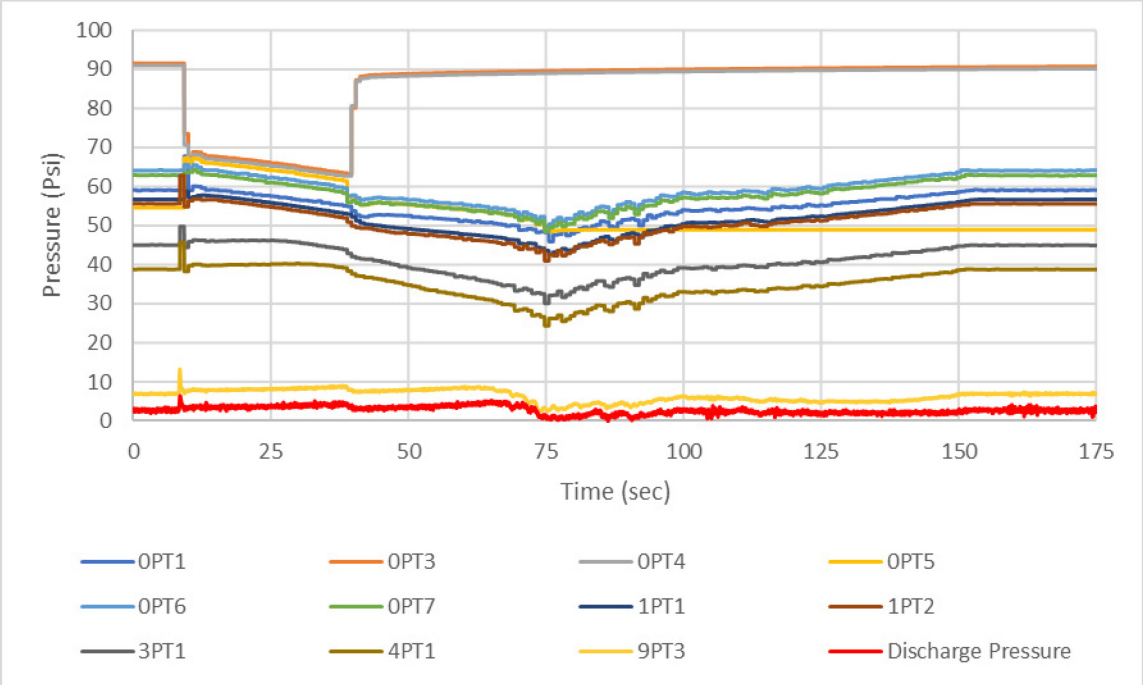

Figure 4-61—All Pressures

Figure 4-61 displays the pressure logged by all the pressure transmitters along the flow loop. All pressure transmitters display a decreasing trend except for 9PT3 and Discharge Pressure after gas injection begins. Gas injection beginning point can be easily observed as a slight increase in pressure for all pressure transmitters on the test section. Gas injection stops at 39.65-seconds, and the gas front reaches the discharge line at 55.88-seconds. The pressures drop when the solenoid valve closes, and gas injection stops. After unloading, the pressures along the test section begin rising.

Figure 4-62 displays 9PT3 and Discharge Pressure along with pump and discharge rate. The initial spike in pressure at approximately 9.23-seconds is due to the solenoid valve opening and air injection beginning. The two pressure transmitters, 9PT3 and Discharge Pressure increase until the solenoid valve closes, where a slight decrease occurs. The pressure then begins increasing again until after the gas front arrives at these ports. The peaks of the pressure transmitters are slightly delayed due to the distance between them. The timing for the first gas bubble arriving at the discharge line does not overlap with peak pressure measured at the discharge line. The first gas arrives at the discharge line earlier than the pressure drop-off at 9PT3 and Discharge Pressure.

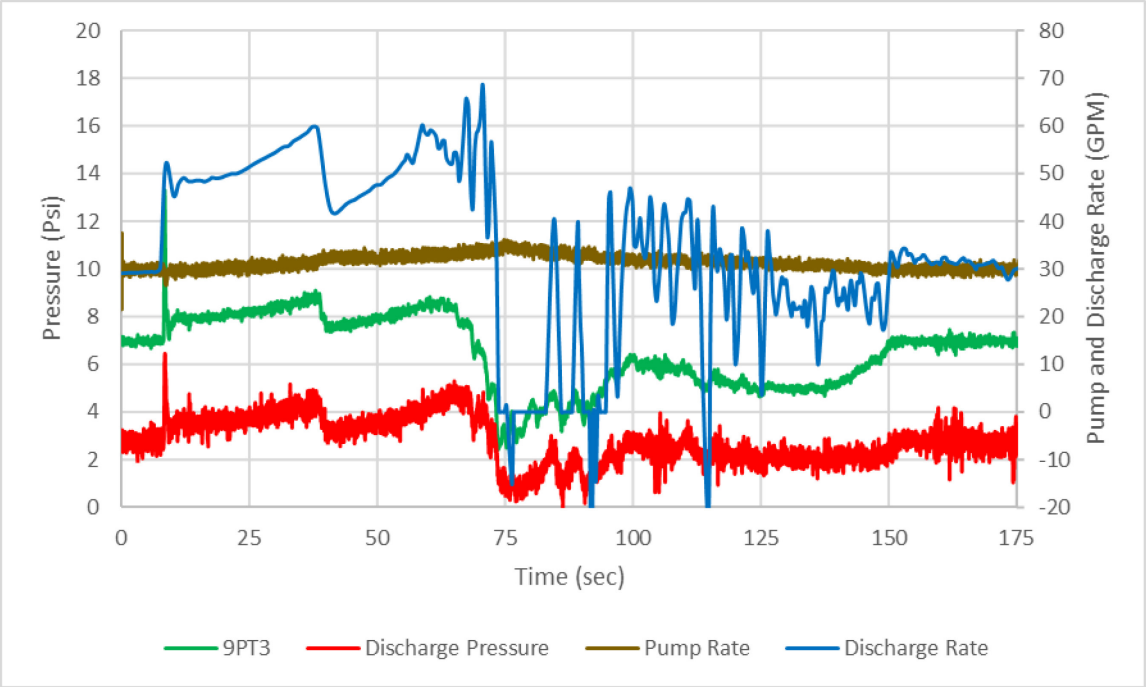

Figure 4-62—Pressure at the outlet and 15 ft below outlet and Pump Rate

Figure 4-63 displays the difference in pressure between 1PT1 and 3PT1, 4PT1, 9PT3, and Discharge Pressure. 1PT1-3PT1 and 1PT1-4PT1 demonstrate a slight decrease with gas arriving first at 1PT1, then 3PT1, and then 4PT1. However, the 1PT1-9PT3 and 1PT1-Discharge Pressure lines demonstrate a more significant reduction with the longer distance between these pressure transmitters.

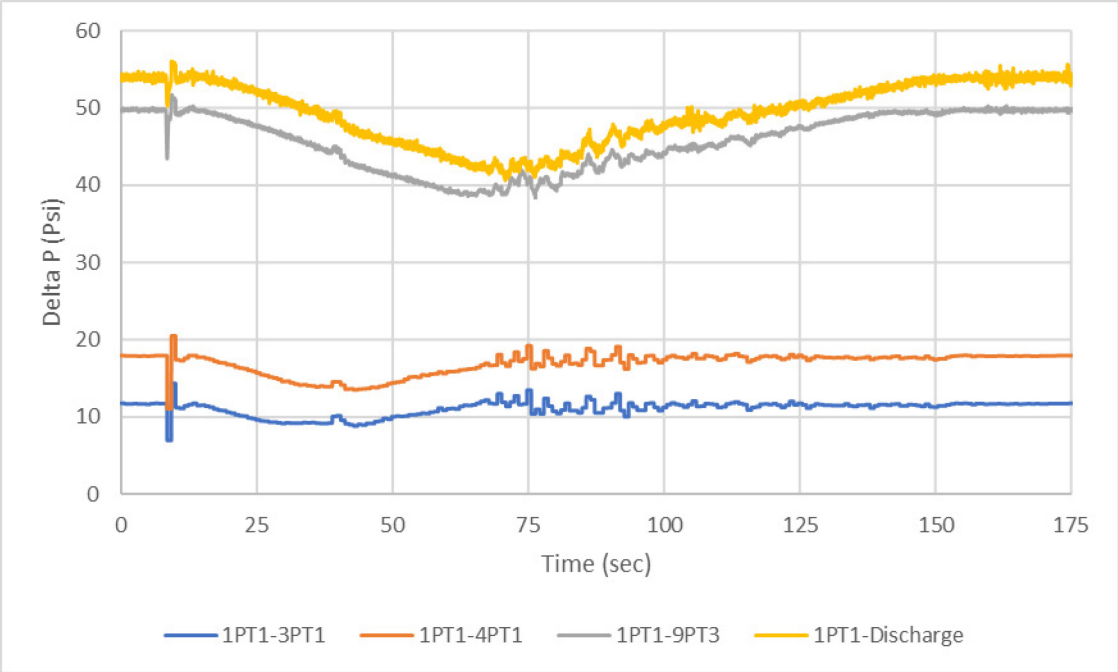

Figure 4-63— Pressure difference between 1st floor and 3rd, 4th, 9th floors, and discharge line

4.1.3.1.3. A309015 15 Seconds Air Injection at 90.67 Psi

This test was run while pumping water at 30-GPM continuously. Air was injected at 90.67-psi initial air injection pressure for 15-seconds while pressures and flow rates were logged.

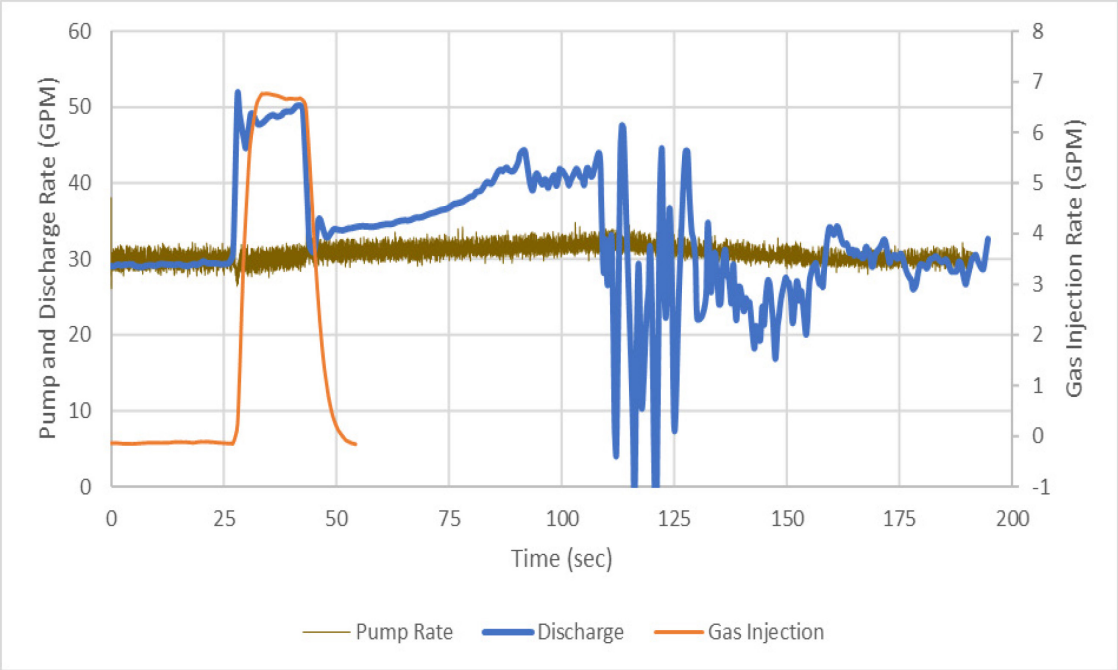

Figure 4-64— Pump, Mud Discharge, and Gas Injection Rates

Figure 4-64 displays the pump and discharge rates and the gas injection rate. Air was injected at an average rate of 4.70-GPM and was terminated at approximately 43.88-seconds. The mud discharge rate began increasing as soon as gas injection began, and the discharge rate increased to 50.18-GPM until the solenoid valve closed and gas injection stopped. The discharge rate suddenly dropped to 30.95-GPM, then began increasing to 40.15-GPM at 83.61-seconds when the gas front reached the outlet, then slightly dropped and surged to 44.32-GPM. The discharge rate then begins fluctuating with a large amount of gas exiting the flow loop. The maximum discharge rate recorded by the flow meter was 51.7-GPM at 28.1-seconds when gas injection began. The video footage shows that the flow regime started as a bubbly flow with no Taylor bubble. Figure 4-64 also displays the gas injection rate with a maximum injection rate of 6.77-GPM when the solenoid valve opens. At approximately 116.2-seconds and 120.96-seconds, the flow meter logged

negative values at the discharge. The footage from the 8th floor did not demonstrate any interruption of returning mud.

Figure 4-65 displays the cumulative pumped and discharged mud and injected gas volumes. The total amount of air injected into the flow loop was 1.81-gal. The cumulative discharged and pumped mud volumes are also plotted. The increase in discharge rate with gas injection leads to a higher cumulative volume at discharge than the water pumped in at the inlet, indicating an influx. The increasing discharge rate is mainly observed during gas injection.

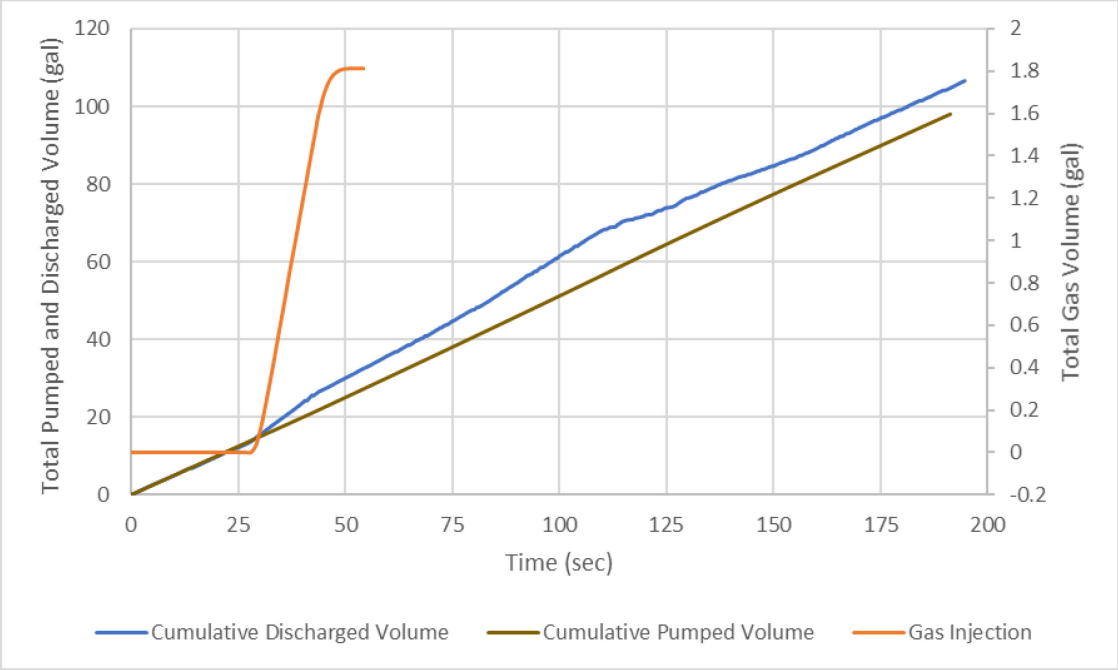

Figure 4-65— Cumulative Pumped, Discharged Water and Injected Gas Volume

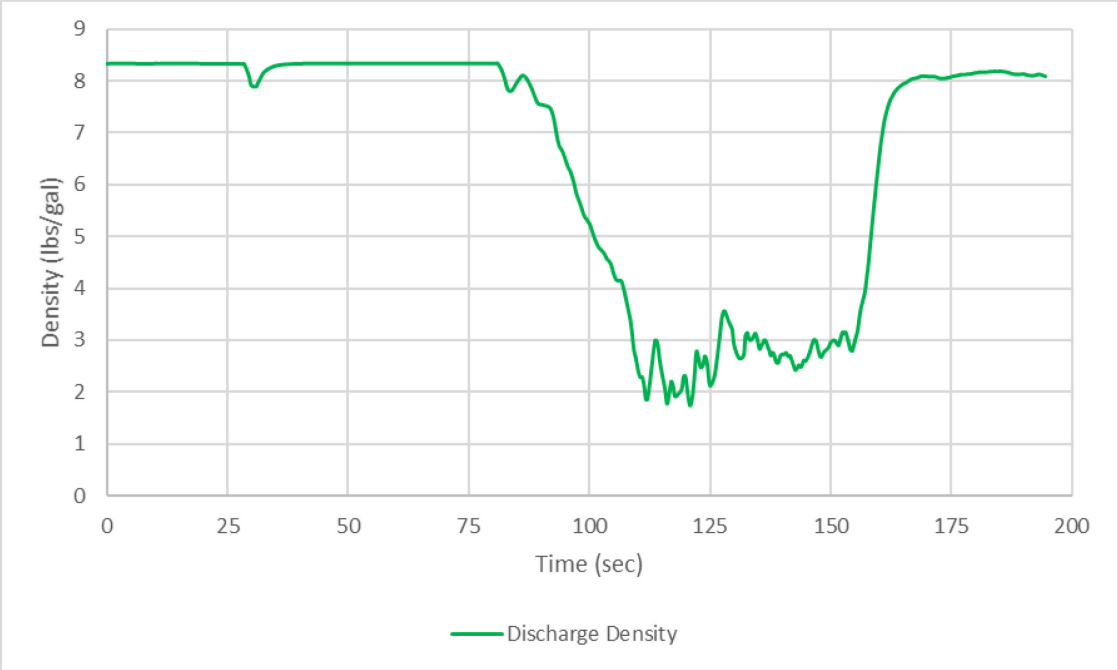

Figure 4-66—Discharge Density

Figure 4-66 displays the density of the fluid logged by the flow meter at discharge. Immediately following gas arrival at discharge 83.61-seconds, the density began decreasing with a minimum density measured as 1.734-lbs/gal. After that, the density fluctuates between 2- and 4-lbs/gal until 157-seconds then stabilizes after 176-seconds. **Figure 4-67** contains the temperature logged by the flow meters at the injection port and the discharge line. Again, no significant change in temperature was observed.

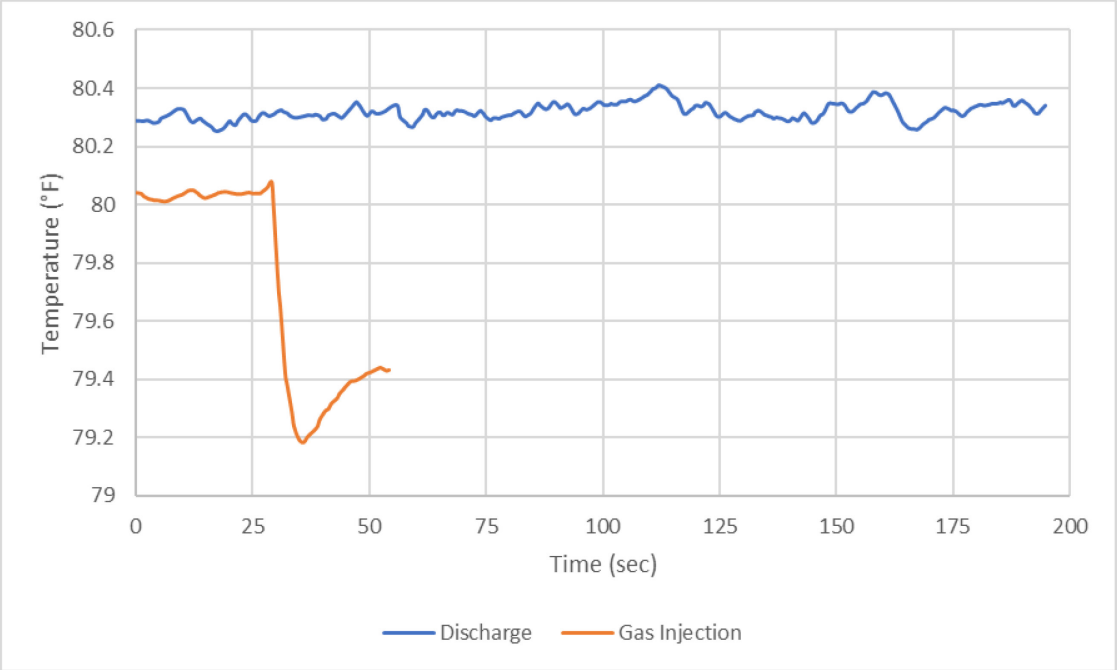

Figure 4-67—Discharge and Gas Injection Temperatures

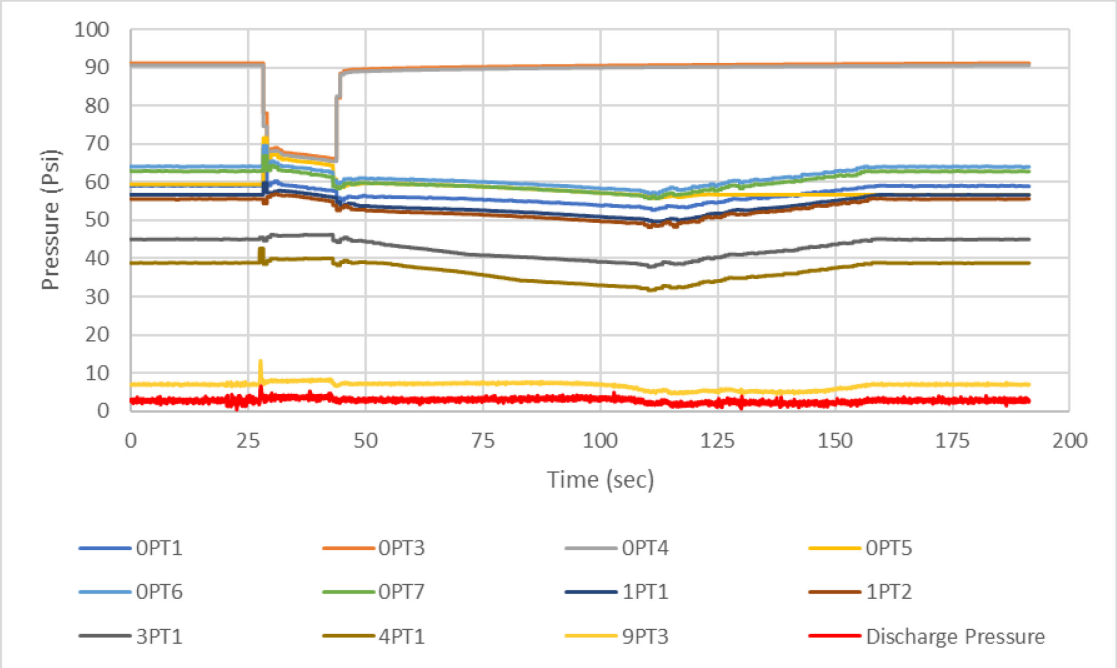

Figure 4-68—All Pressures

Figure 4-68 displays the pressure logged by all the pressure transmitters along the flow loop. All pressure transmitters display a decreasing trend except for 3PT1, 4PT1,

9PT3, and Discharge Pressure during gas injection. Gas injection beginning and ending point can be easily observed as a slight increase and slight decrease in pressure for all pressure transmitters on the test section. Gas injection stops at 43.88-seconds, and the gas front reaches the discharge line at 83.61-seconds. After the gas injection is halted, 3PT1 and 4PT1 also begin decreasing, and when the gas front reaches the outlet, the pressures along the test section begin rising.

Figure 4-69 displays 9PT3 and Discharge Pressure along with pump and discharge rate. The initial spike in pressure at approximately 28.27-seconds is due to the solenoid valve opening and air injection beginning. The two pressure transmitters, 9PT3 and Discharge Pressure, increase until the solenoid valve closes, leading to a slight decrease. The pressure then begins increasing again until after the gas front arrives at the outlet. The timing for the first gas bubble arriving at the discharge line does not overlap with peak pressure measured at the discharge line. The first gas arrives at the discharge line earlier than the pressure drop-off at 9PT3 and Discharge Pressure.

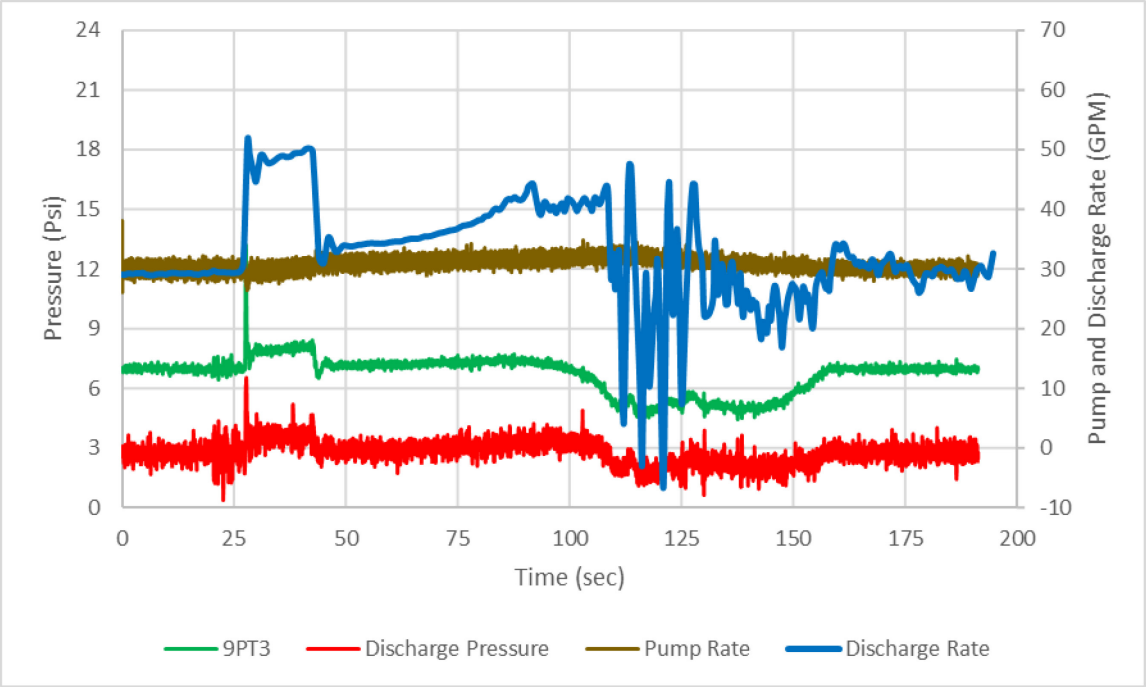

Figure 4-69—Pressure at the outlet and 15 ft below outlet and Pump Rate

Figure 4-70 displays the difference in pressure between 1PT1 and 3PT1, 4PT1, 9PT3, and Discharge Pressure. 1PT1-3PT1 and 1PT1-4PT1 demonstrate a slight decrease with gas arriving first at 1PT1, then 3PT1, and then 4PT1. However, the 1PT1-9PT3 and 1PT1-Discharge Pressure lines demonstrate a more significant reduction with the longer distance between these pressure transmitters.

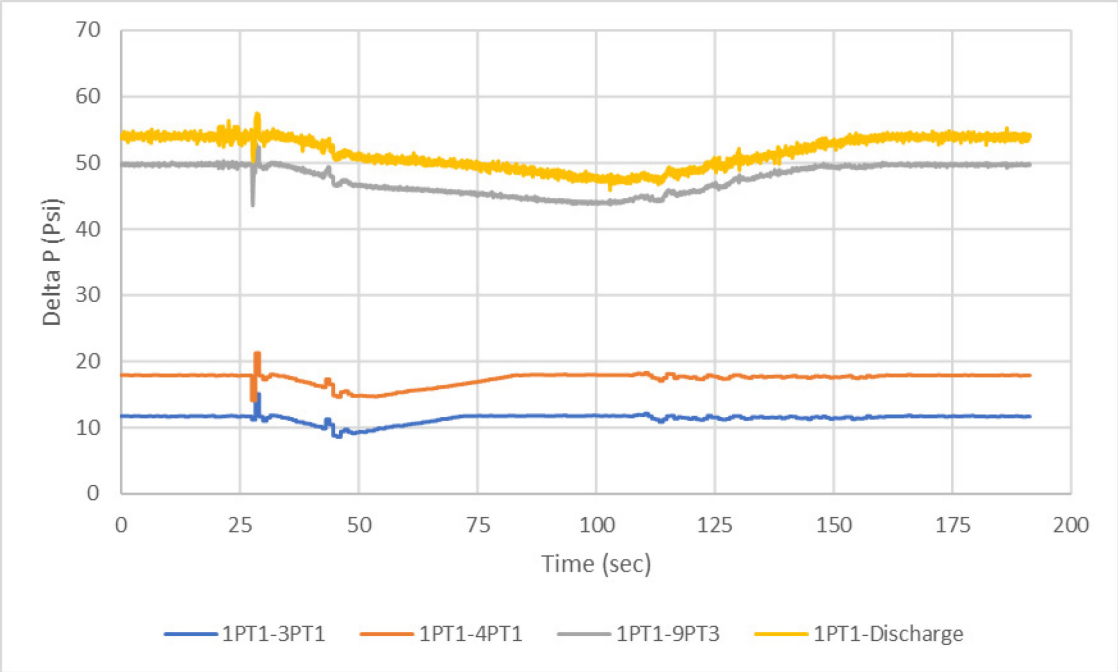

Figure 4-70— Pressure difference between 1st floor and 3rd, 4th, 9th floors, and discharge line

4.1.3.2. 80 Psi Initial Injection Pressure

The following section provides results from dynamic tests conducted with a 30-GPM flow rate with an approximate initial injection rate of 80-psi. **Table 4-12** summarizes these tests providing the test parameters and results.

Pump Rate (GPM)	30		
Initial Injection Pressure (PSI)	82.3	82.3	82.4
Gas Injection Duration (seconds)	60	30	15
Kick Intensity (lbs./gal)	2.49	2.5	2.514
Maximum Injection Rate (GPM)	8.02	6.71	6.72
Average Injection Rate (GPM)	6.21	5.55	4.76
Total Gas Injected (gal)	6.97	3.36	1.75
Maximum Discharge Rate (GPM)	108.52	66.82	50.34
Max Rate at Unloading (GPM)	108.52	66.82	44.48
Total Discharge Volume (gal)	125.46	91.50	89.53
Total Discharge During Unloading (gal)	70.68	57.96	45.94

Table 4-12— Summary of results for 30-GPM circulation rate tests with air injection at approximately 82-Psi

4.1.3.2.1. A308060 60 Seconds Air Injection at 82.3 Psi

This test was run while pumping water at 30-GPM continuously. Air was injected at 82.3-psi for 60-seconds while pressure and flow rate were logged.

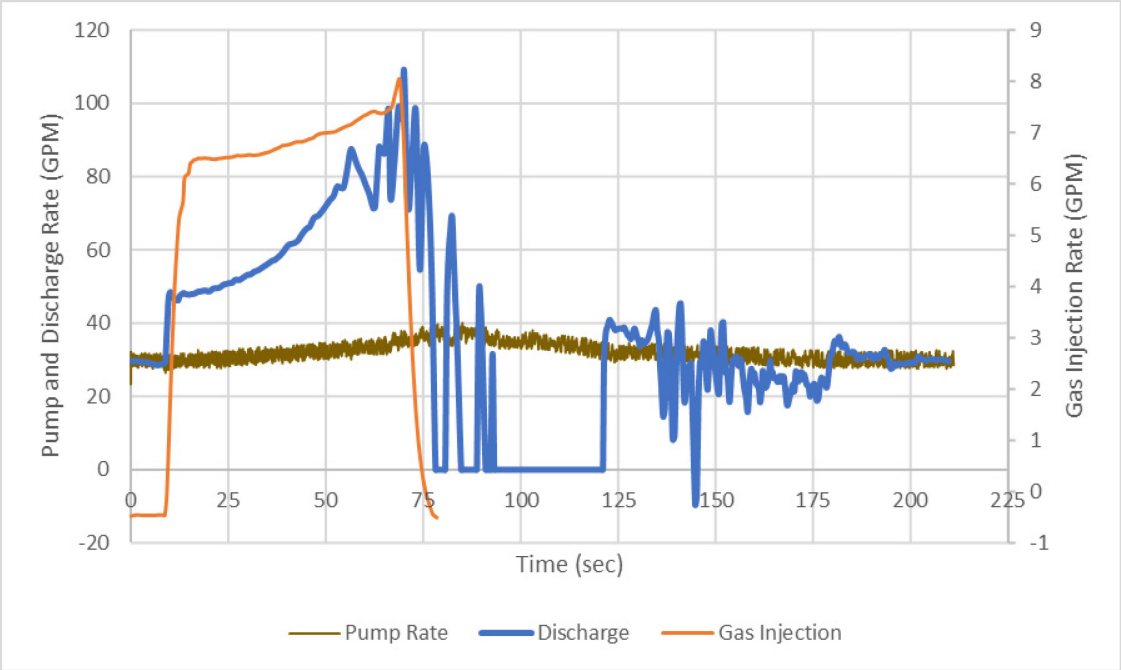

Figure 4-71— Pump, Mud Discharge, and Gas Injection Rates

Figure 4-71 displays the pump and discharge rates and the gas injection rate. Air was injected at an average rate of 6.21-GPM and was terminated at approximately 69.64-seconds. The mud discharge rate began increasing as soon as gas injection began, and the discharge rate increased to 87.54-GPM when the gas front reached the outlet at 56.15-seconds. Following the gas arrival at the outlet, the discharge rate suddenly dropped to 71.13-GPM, then began surging until it reached a maximum discharge rate of 108.52-GPM at 70.1-seconds. Then the discharge rate dropped to zero until 121.38-seconds. The video also confirmed the 0-GPM discharge rate as the fluid level dropped with air bubbles pushing water. The video footage shows that the flow regime started as a bubbly flow with no Taylor bubble; a larger discharge rate was logged after the flow regime transitioned to churn flow. Figure 4-71 also demonstrates an increasing rate for gas injection with a maximum injection rate of 8.02-GPM right before the solenoid valve closes.

Figure 4-72 displays the cumulative pumped and discharged mud, and injected gas volumes. The total amount of air injected into the flow loop was 6.97-gal. The cumulative discharged and pumped mud are also plotted. The increase in discharge rate with gas injection leads to a higher cumulative volume at discharge than the water pumped in at the inlet, indicating an influx. The increasing discharge rate is mainly observed during gas injection.

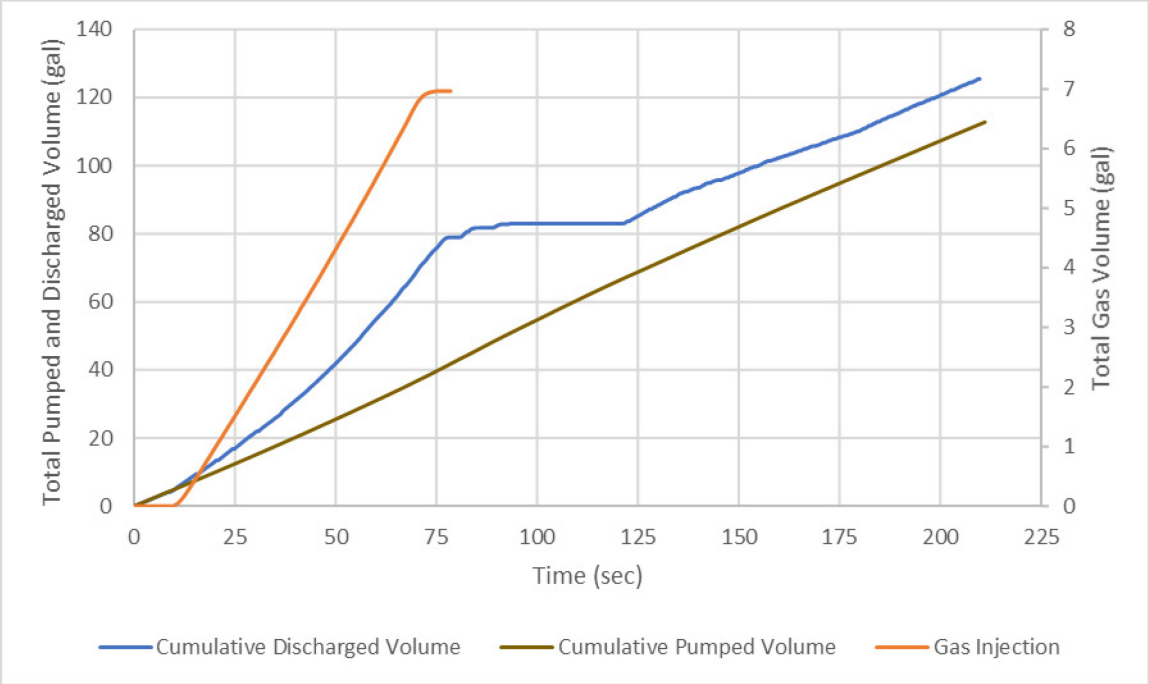

Figure 4-72— Cumulative Pumped, Discharged Water and Injected Gas Volume

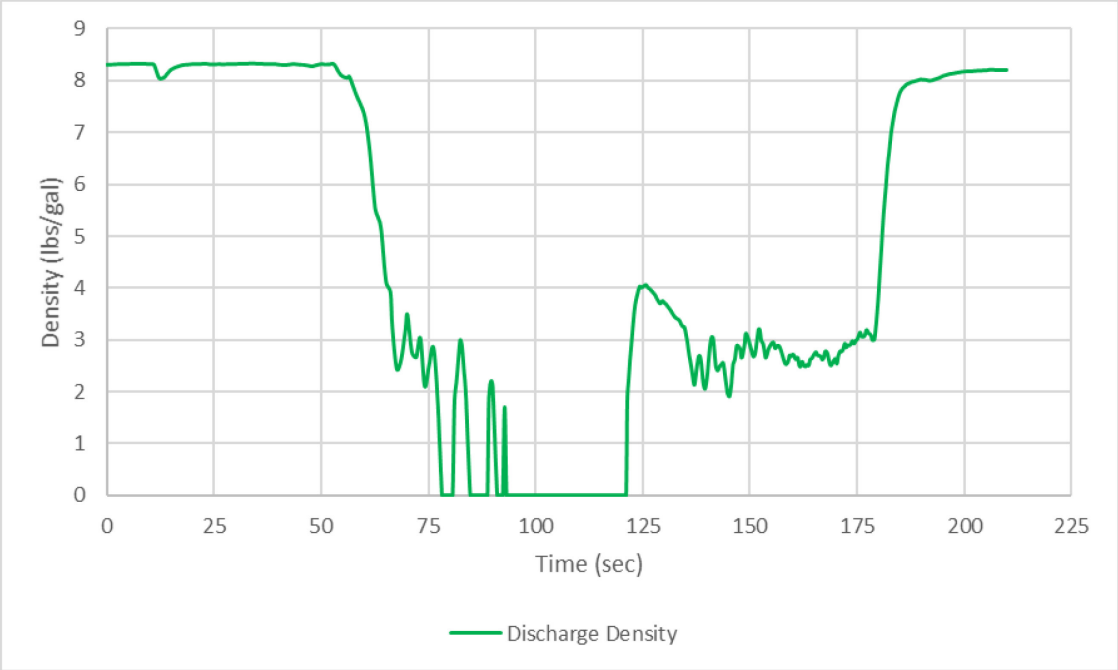

Figure 4-73—Discharge Density

Figure 4-73 displays the density of the fluid logged by the flow meter at discharge. Immediately following gas arrival at discharge, the density rapidly drops to 0-lbs/gal. When the flowmeter started logging again, the density fluctuated between 2- and 4-lbs/gal between 125- and 177-seconds then began to stabilize after 200-seconds. **Figure 4-74** contains the temperature logged by the flow meters at the injection port and the discharge line. Again, no significant change in temperature was observed.

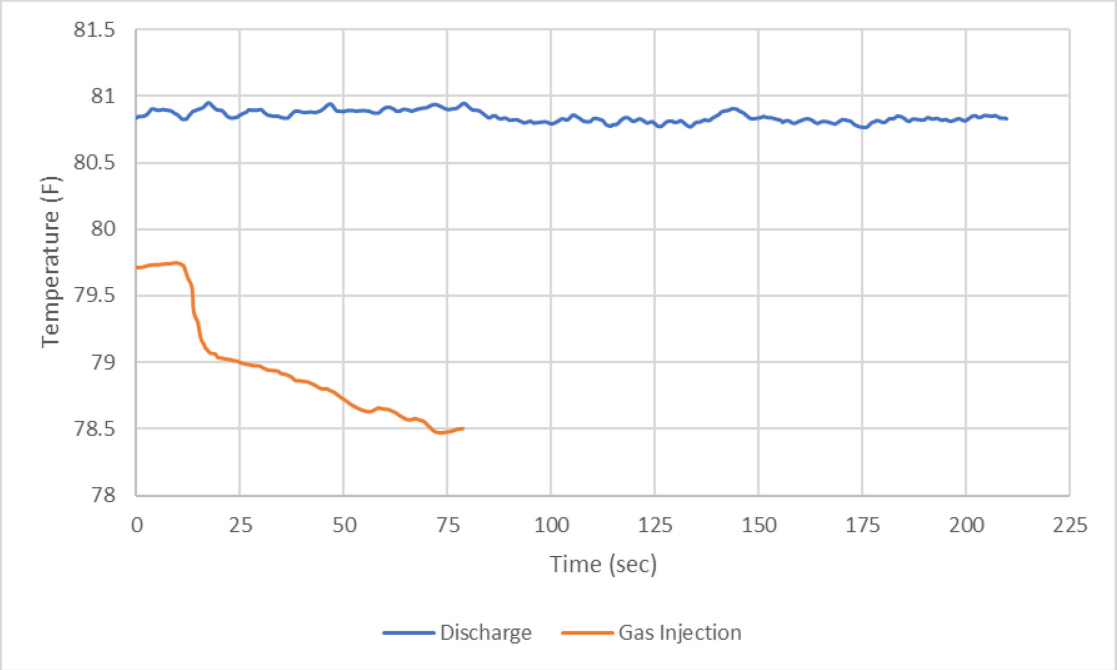

Figure 4-74—Discharge and Gas Injection Temperatures

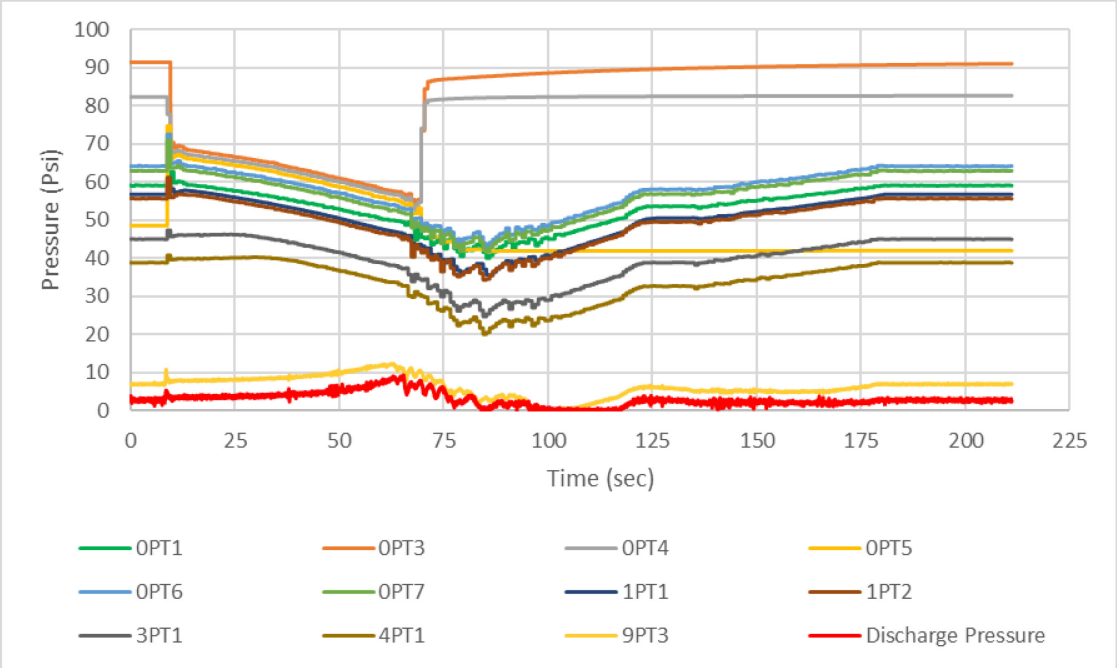

Figure 4-75—All Pressures

Figure 4-75 displays the pressure logged by all the pressure transmitters along the flow loop. All pressure transmitters display a decreasing trend except for 9PT3 and

Discharge Pressure after gas injection begins. Gas injection beginning point can be easily observed as a slight increase in pressure for all pressure transmitters on the test section. Gas injection stops at 69.64-seconds, and the gas front reaches the discharge line at 56.15-seconds. The pressures drop when the solenoid valve closes, and gas injection stops. After unloading, the pressures along the test section begin rising.

Figure 4-76 displays 9PT3 and Discharge Pressure along with pump and discharge rate. The initial spike in pressure at approximately 8.8-seconds is due to the solenoid valve opening and air injection beginning. The data from the two pressure transmitters, 9PT3 and Discharge Pressure, increase until the solenoid valve closes, where a slight decrease occurs. The pressure then begins increasing again until after the gas front arrives at these ports. The peaks of the pressure transmitters are slightly delayed due to the distance between them. The timing for the first gas bubble arriving at the discharge line does not overlap with peak pressure measured at the discharge line. The first gas arrives at the discharge line earlier than the pressure drop-off at 9PT3 and Discharge Pressure.

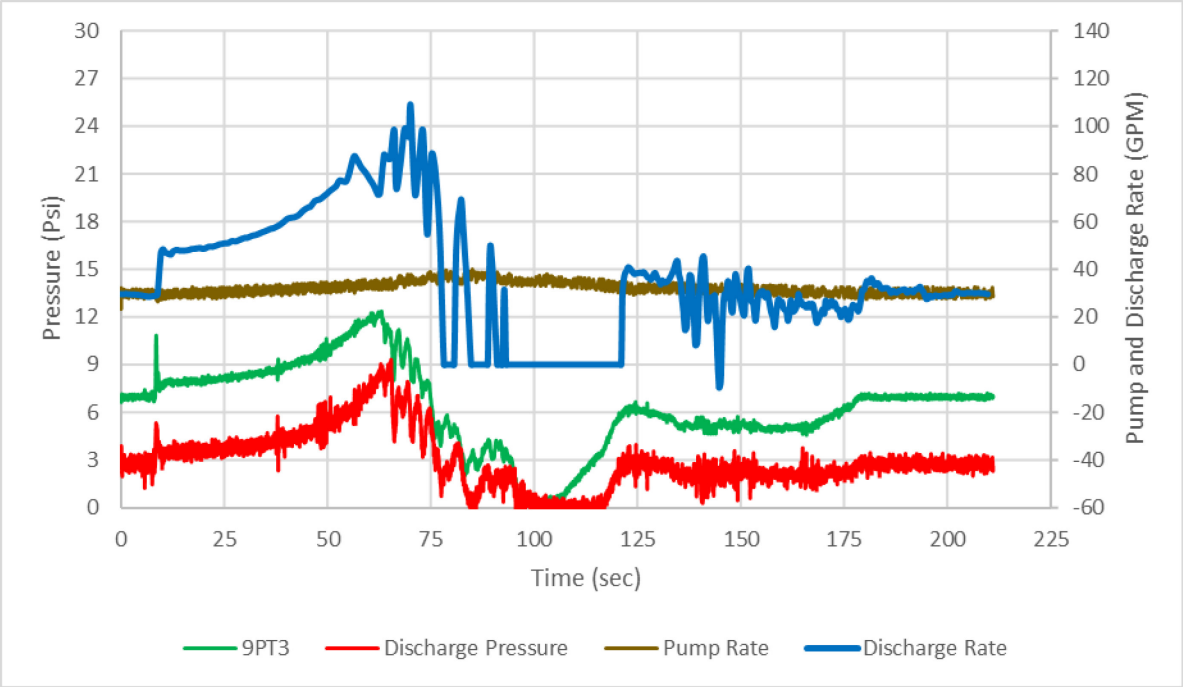

Figure 4-76—Pressure at the outlet and 15 ft below outlet and Pump Rate

Figure 4-77 displays the difference in pressure between 1PT1 and 3PT1, 4PT1, 9PT3, and Discharge Pressure. 1PT1-3PT1 and 1PT1-4PT1 demonstrate a slight decrease with gas arriving first at 1PT1, then 3PT1, and then 4PT1. The 1PT1-9PT3 and 1PT1-Discharge Pressure lines demonstrate a more significant reduction with the longer distance between these pressure transmitters

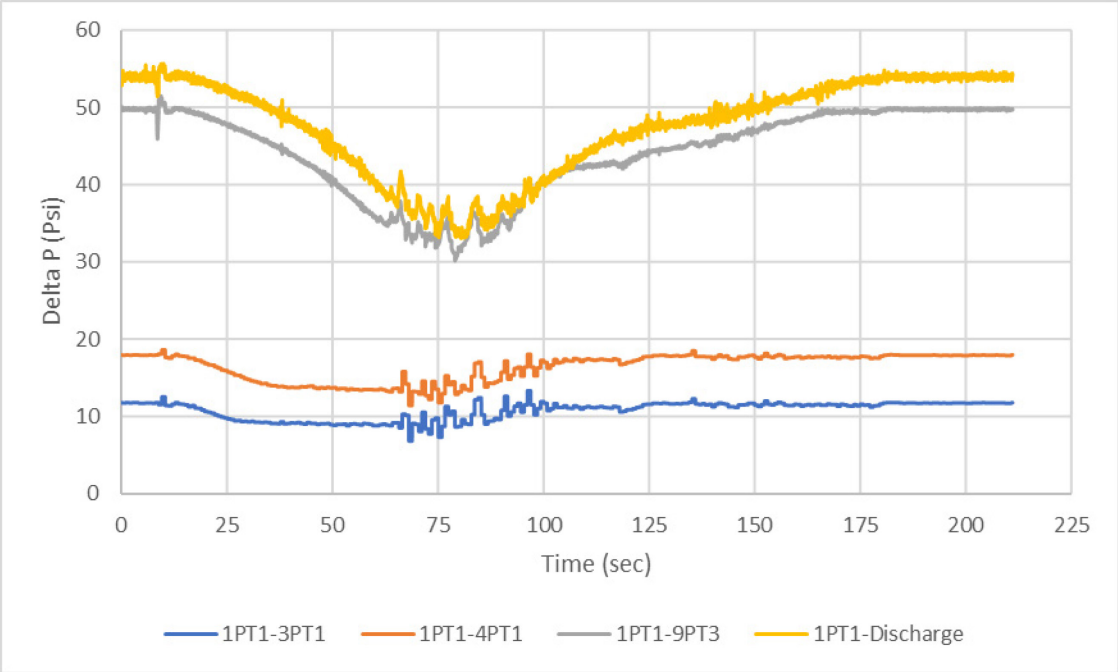

Figure 4-77— Pressure difference between 1st floor and 3rd, 4th, 9th floors, and discharge line

4.1.3.2.2. A308030 30 Seconds Air Injection at 82.3 Psi

This test was run while pumping water at 30-GPM continuously. Air was injected at 82.3-psi for 30-seconds while pressure and flow rate were logged.

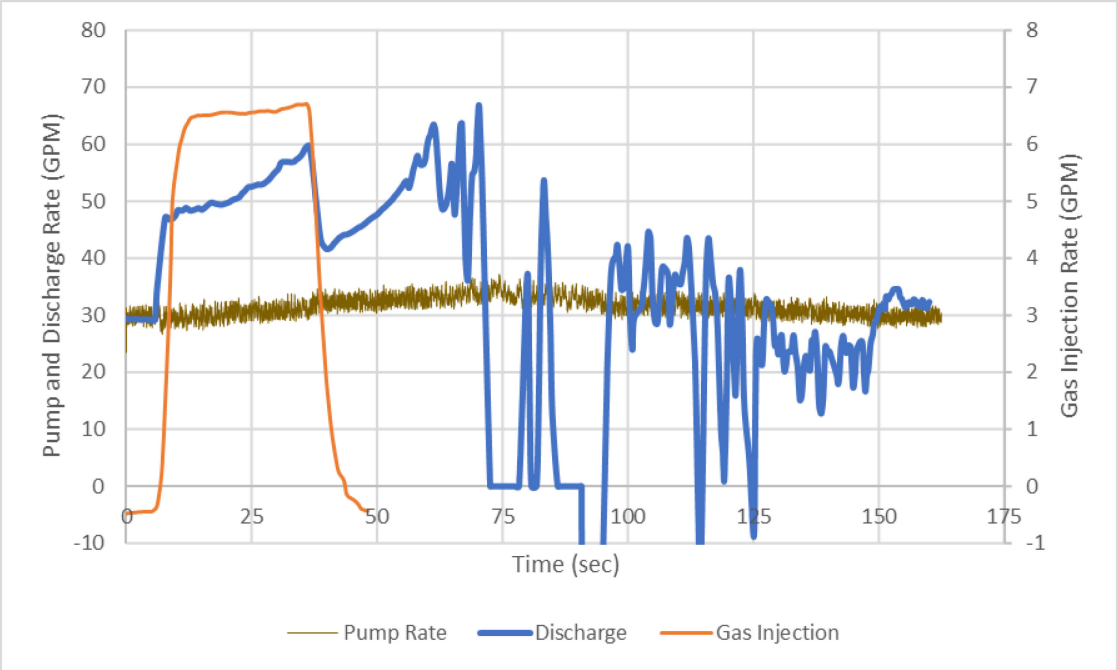

Figure 4-78— Pump, Mud Discharge, and Gas Injection Rates

Figure 4-78 displays the pump and discharge rates and the gas injection rate. Air was injected at an average rate of 5.55-GPM and was terminated at approximately 37.82-seconds. The mud discharge rate began increasing as soon as gas injection began, and the discharge rate increased to 59.76-GPM until the solenoid valve closed and gas injection stopped. The discharge rate suddenly dropped to 41.61-GPM, then began increasing to 53.58-GPM at 63-seconds when the gas front reached the outlet, then slightly dropped and began fluctuating. The maximum discharge rate recorded by the flow meter was 66.81-GPM at 77.47-seconds, then suddenly dropped to 0-GPM. Then the discharge rate begins fluctuating until it stabilizes 158.34-seconds. The video footage shows that the flow regime started as a bubbly flow with no Taylor bubble; a larger discharge rate was logged after the flow regime transitioned to churn flow. Figure 4-78 also demonstrates an increasing rate for gas injection with a maximum injection rate of 6.71-GPM right before

the solenoid valve closes. At approximately 72.55-seconds, the flow meter began reading 0-GPM discharge rate. The footage from the 8th floor did not demonstrate any interruption of returning mud. However, fluid level was not maintained at the discharge.

Figure 4-79 displays the cumulative pumped and discharged mud and injected gas volumes. The total amount of air injected into the flow loop was 3.36-gal. The increase in discharge rate with gas injection leads to a higher cumulative volume at discharge than the water pumped in at the inlet, indicating an influx. The increasing discharge rate is mainly observed during gas injection resulting in a wide separation between the cumulative mud volume lines in Figure 4-79.

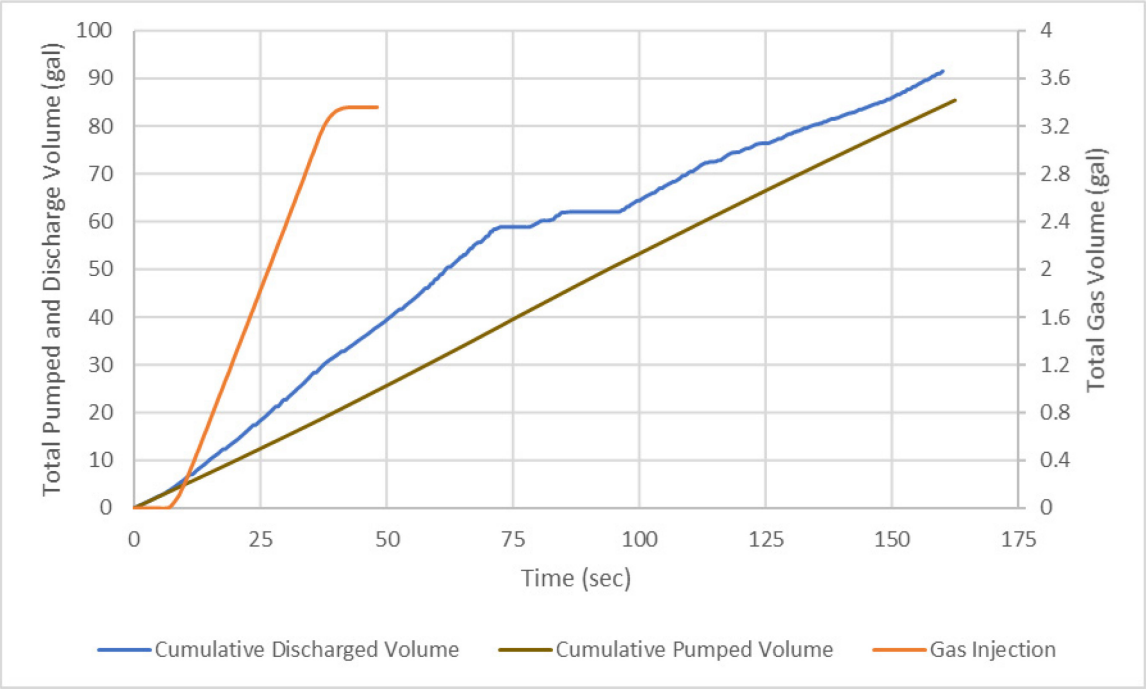

Figure 4-79—Cumulative Pumped, Discharged Water and Injected Gas Volume

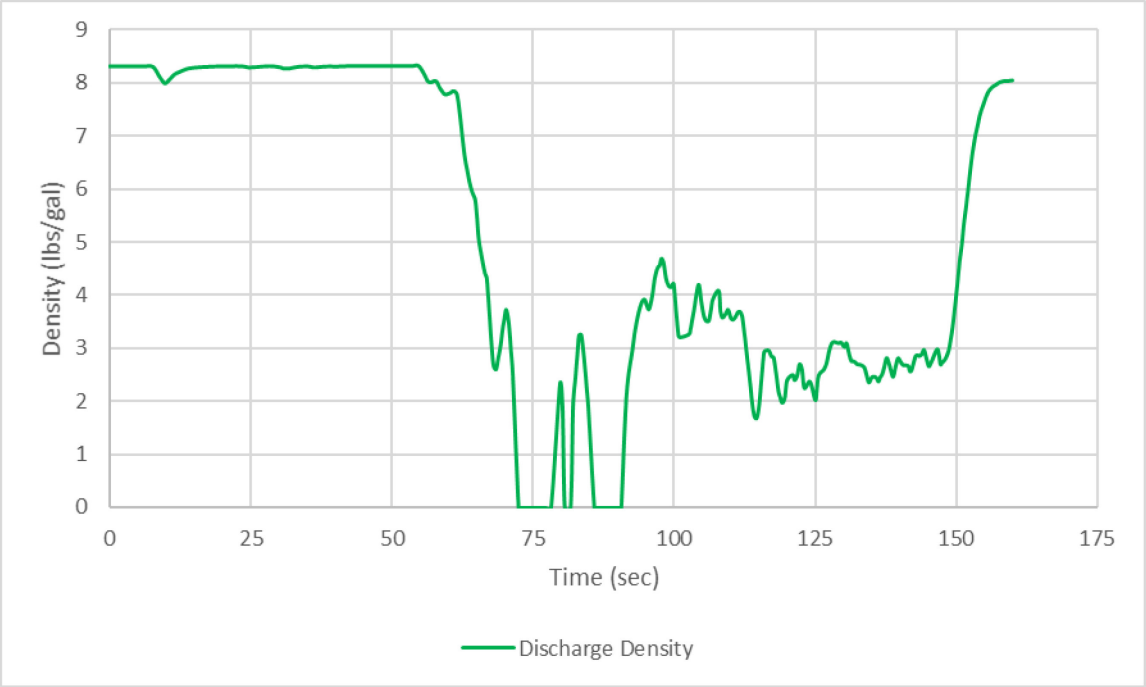

Figure 4-80—Discharge Density

Figure 4-80 displays the density of the fluid logged by the flow meter at discharge. Immediately following gas arrival at discharge, the density rapidly drops to 0-lbs/gal. The density fluctuates between 0- and 3-lbs/gal until 96.3-seconds, then fluctuates between 2- and 4-lbs/gal. **Figure 4-81** contains the temperature logged by the flow meters at the injection port and the discharge line. No significant change in temperature was observed.

.

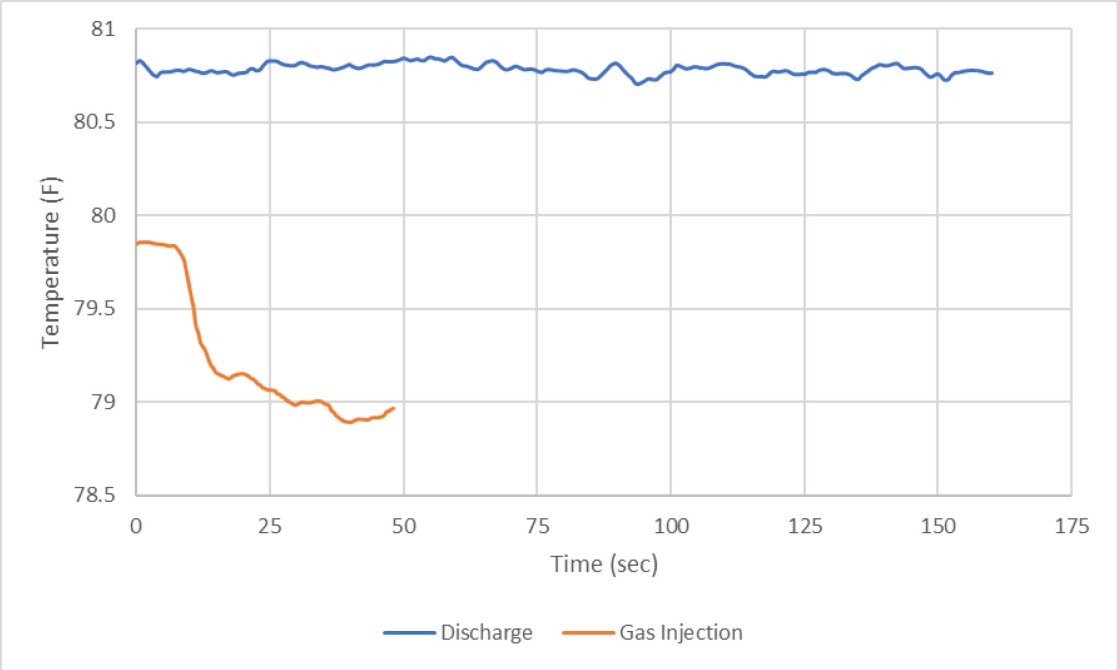

Figure 4-81—Discharge and Gas Injection Temperatures

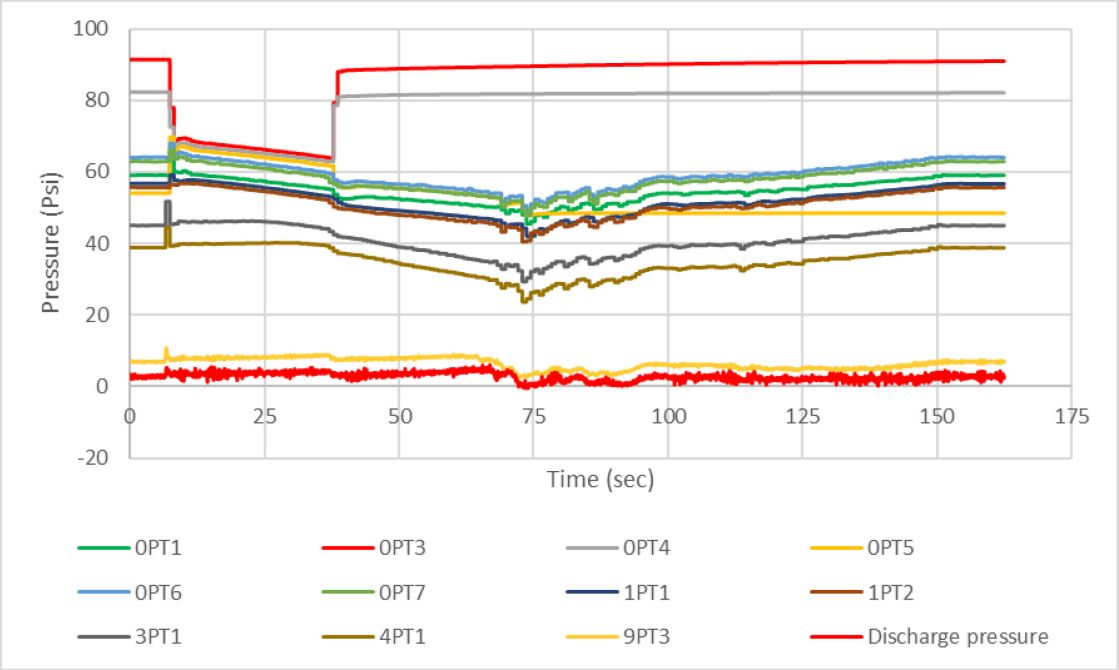

Figure 4-82—All Pressures

Figure 4-82 displays the pressure logged by all the pressure transmitters along the flow loop. All pressure transmitters on the flow loop display decreasing trends except for

9PT3 and Discharge Pressure after gas injection begins. Gas injection beginning point can be easily observed as a slight increase in pressure for all pressure transmitters on the test section. Gas injection stops at 37.82-seconds, and the gas front reaches the discharge line at 63-seconds. The pressures drop when the solenoid valve closes, and gas injection stops. After unloading, the pressures along the test section begin rising.

Figure 4-83 displays 9PT3 and Discharge Pressure along with pump and discharge rate. The initial spike in pressure at approximately 7.4-seconds is due to the solenoid valve opening and air injection beginning. The data logged by two pressure transmitters 9PT3 and Discharge Pressure, increase until the solenoid valve closes, leading to a slight decrease. The pressure then begins increasing again until after the gas front reaches the outlet. The peaks of the pressure transmitters are slightly delayed due to the distance between them. The timing for the first gas bubble arriving at the discharge line does not overlap with peak pressure measured at the discharge line. Therefore, the first gas arrives at the discharge line earlier than the pressure drop-off at 9PT3 and Discharge Pressure.

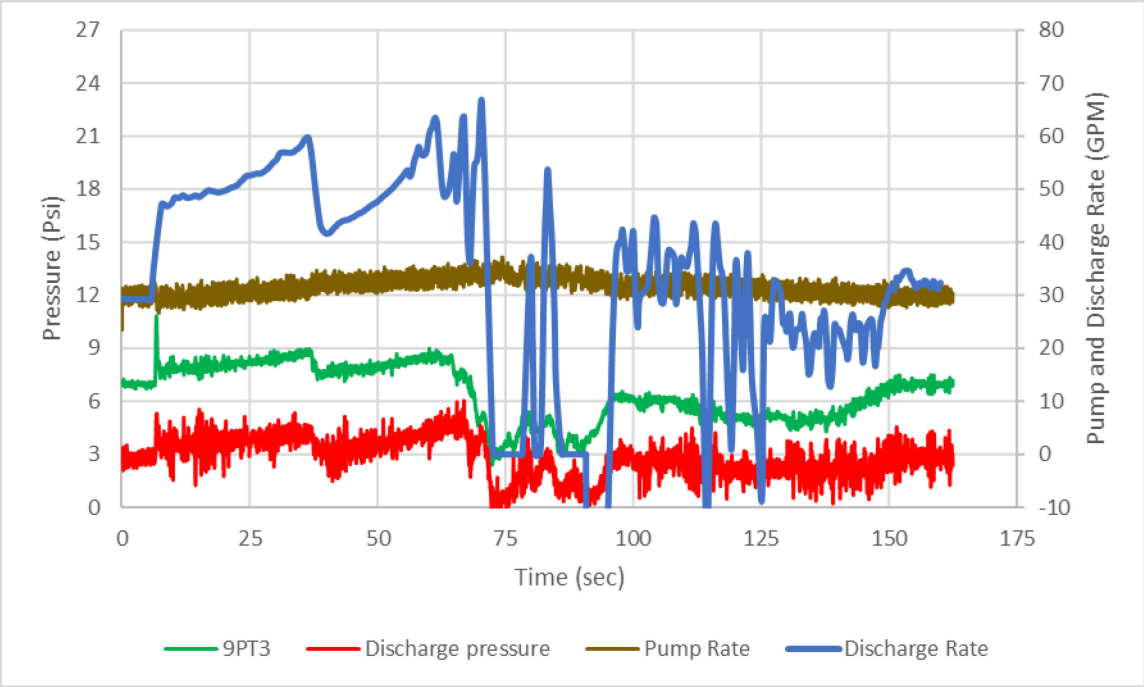

Figure 4-83—Pressure at the outlet and 15-ft below the outlet and Pump Rate

Figure 4-84 displays the difference in pressure between 1PT1 and 3PT1, 4PT1, 9PT3, and Discharge Pressure. 1PT1-3PT1 and 1PT1-4PT1 demonstrate a slight decrease with gas arriving first at 1PT1, then 3PT1, and then 4PT1. The 1PT1-9PT3 and 1PT1-Discharge Pressure lines demonstrate a more significant reduction with the longer distance between these pressure transmitters

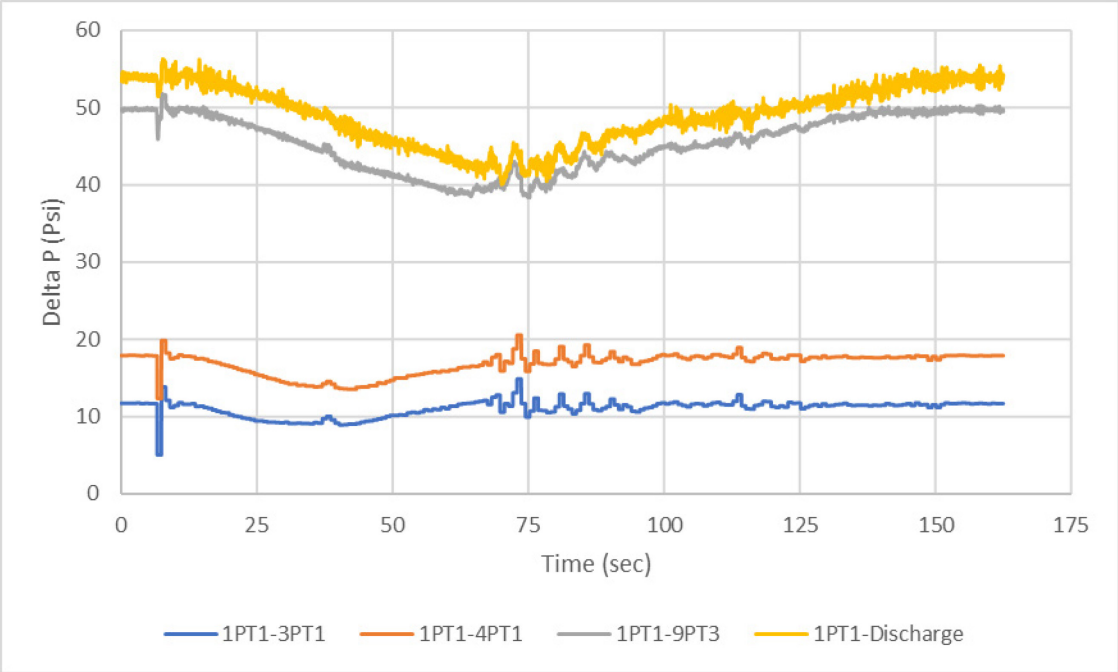

Figure 4-84— Pressure difference between 1st floor and 3rd, 4th, 9th floors, and discharge line

4.1.3.2.3. A308015 15 Seconds Air Injection at 82.4 Psi

This test was run while pumping water at 30-GPM continuously. Air was injected at 82.4-psi for 15-seconds while pressure and flow rate were logged.

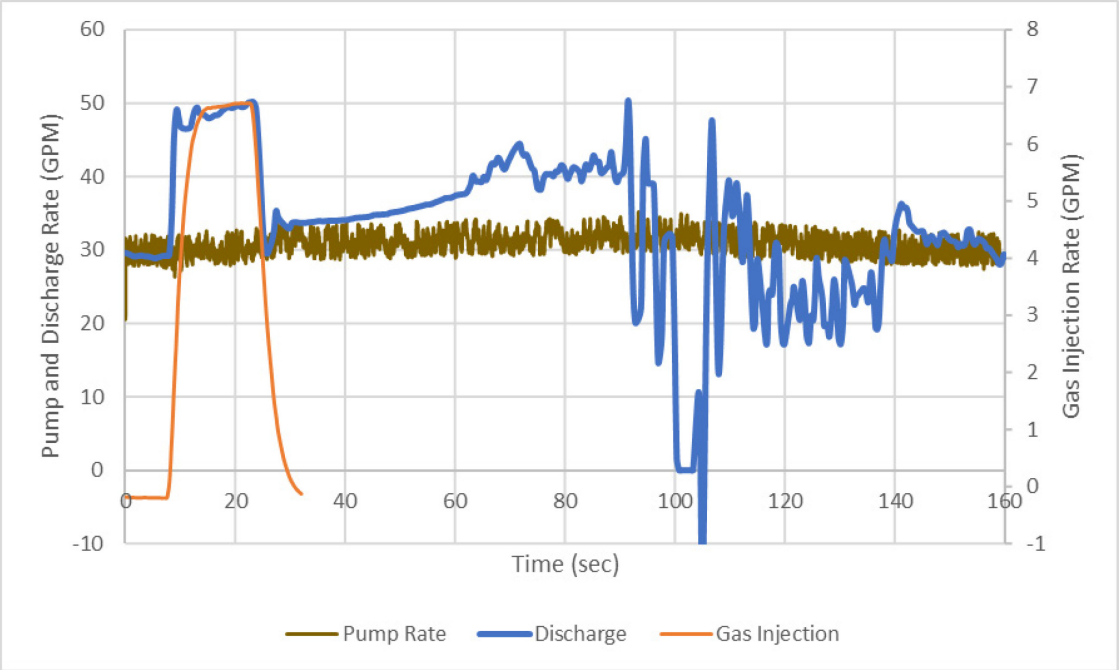

Figure 4-85— Pump, Mud Discharge, and Gas Injection Rates

Figure 4-85 displays the mud pump and discharge rates and the gas injection rate. Air was injected at an average rate of 4.76-GPM and was terminated at approximately 24.13-seconds. The mud discharge rate began increasing as soon as gas injection began, and the discharge rate increased to 50.15-GPM until the solenoid valve closed and gas injection stopped. After that, the discharge rate suddenly dropped to 29.57-GPM, then began increasing to 40.13-GPM at 63.23-seconds when the gas front reached the outlet, then slightly dropped and began fluctuating. The maximum discharge rate recorded by the flow meter was 50.34-GPM at 91.48-seconds. The discharge rate then began decreasing and logged 0 GPM between 100.77- and 104.29-seconds. The video footage shows that the flow regime started as a bubbly flow with no Taylor bubble, then transitioned to churn flow. Figure 4-85 also demonstrates an increasing rate for gas injection with a maximum injection rate of 6.72-GPM right before the solenoid valve closes.

Figure 4-86 displays the cumulative pumped and discharged mud and injected gas volumes. The total amount of air injected into the flow loop was 1.75-gal. The increase in discharge rate with gas injection leads to a higher cumulative volume at discharge than the water pumped in at the inlet, indicating an influx entering the test section. The increasing discharge rate is mainly observed during gas injection. The cumulative mud discharge and pump volume line separate, and the gap widens as the discharge rate increases with gas entering and unloading the pipe.

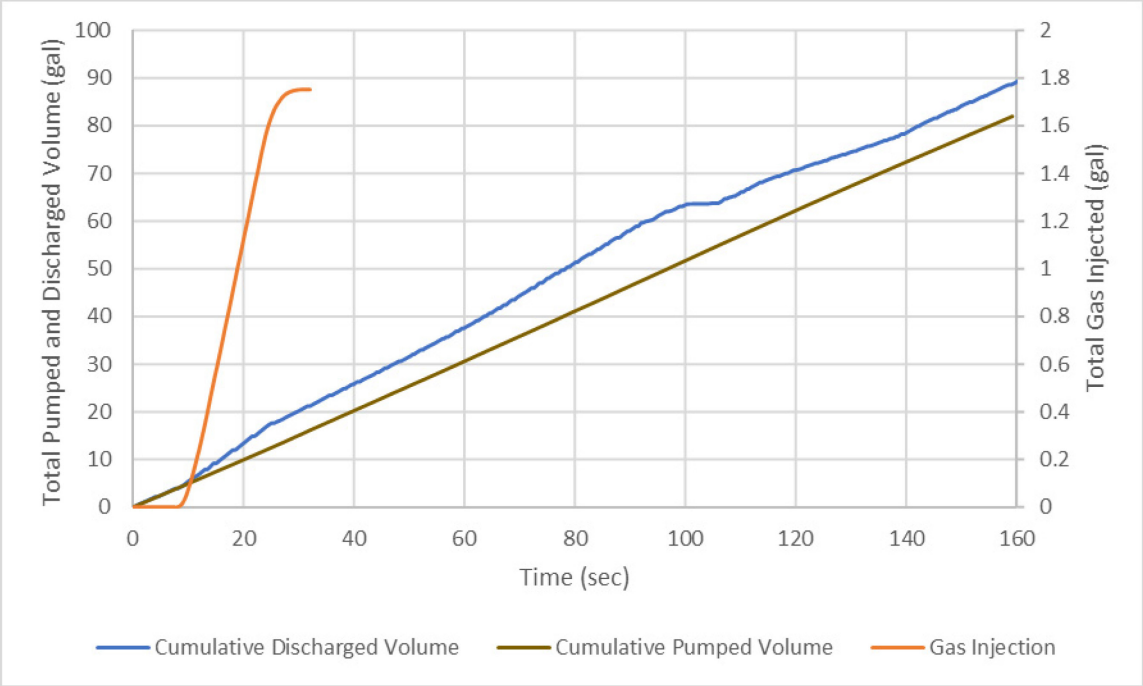

Figure 4-86—Cumulative Pumped, Discharged Water and Injected Gas Volume

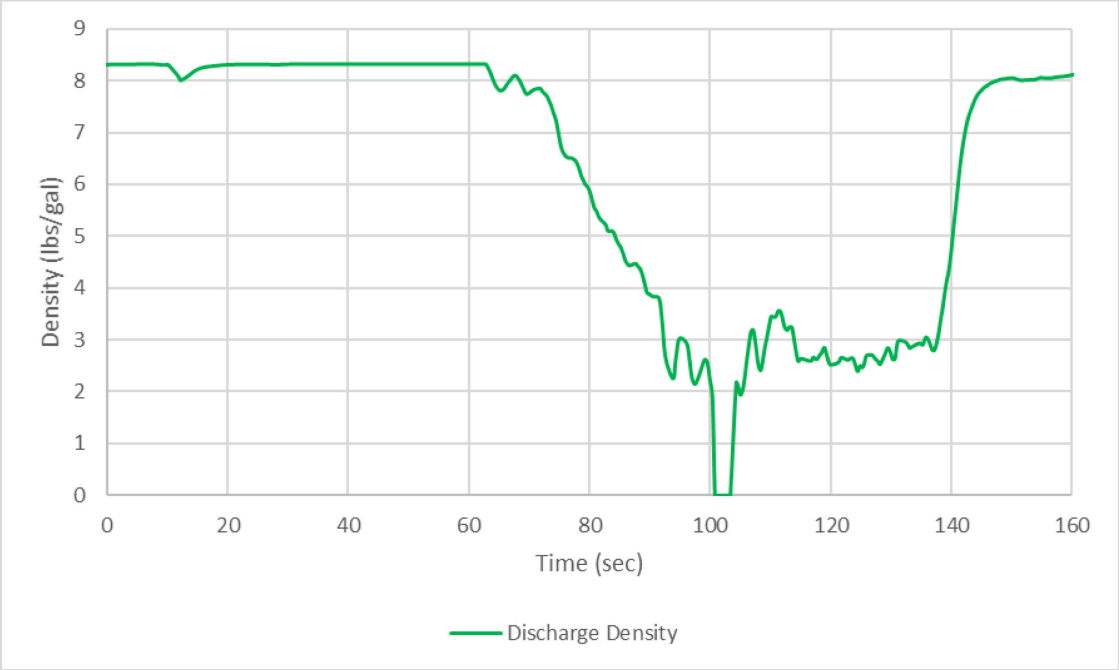

Figure 4-87—Discharge Density

Figure 4-87 displays the density of the fluid logged by the flow meter at discharge. Gas arrives at discharge at 63.23-seconds, then the density rapidly gradually decreases to 0-lbs/gal. Then between 104.29- and 139.1-seconds, the density at discharge fluctuates between 2 and 4-lbs/gal. **Figure 4-88** displays the temperature logged by the flow meters at the injection port and the discharge line. No significant change in temperature was observed.

.

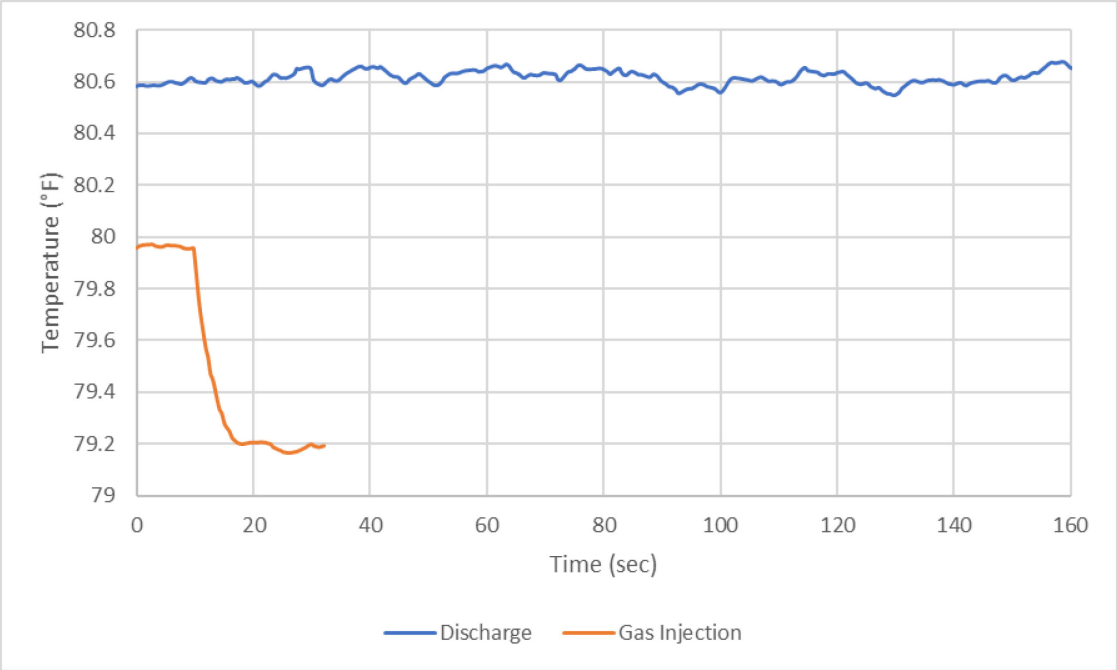

Figure 4-88—Discharge and Gas Injection Temperatures

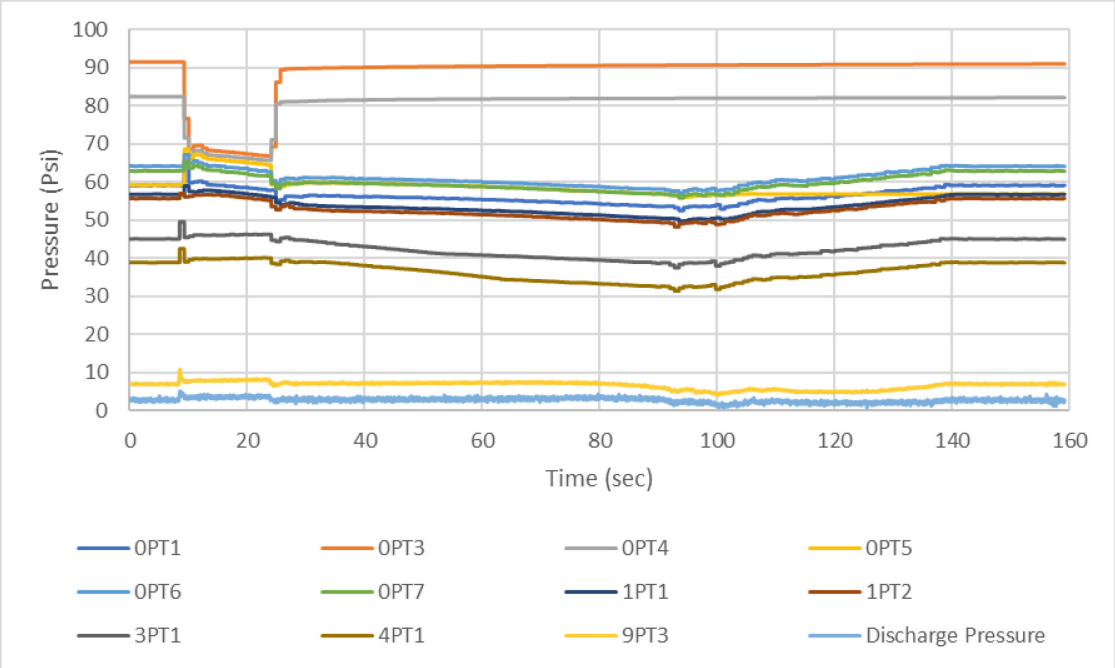

Figure 4-89—All Pressures

Figure 4-89 displays the pressure logged by all the pressure transmitters along the flow loop. All pressure transmitters display a decreasing trend except for 3PT1, 4PT1,

9PT3, and Discharge Pressure after gas injection begins. The point at which the gas injection began can be easily observed as a slight increase in pressure for all pressure transmitters on the test section. Gas injection stops at 24.13-seconds, and the gas front reaches the discharge line at 63.23-seconds. The pressures logged by the pressure transmitters drop when the solenoid valve closes, and gas injection stops. The pressures start increasing at 100-seconds with the water level rising again and the air being circulated out. The pressures stabilize after 140-seconds

Figure 4-90 displays 9PT3 and Discharge Pressure along with pump and discharge rate. The initial spike in pressure at approximately 9.31-seconds is due to the solenoid valve opening and air injection beginning. The data from the two pressure transmitters, 9PT3 and Discharge Pressure, increase until the solenoid valve closes, where a slight decrease occurs. The pressure at these two transmitters remains constant until the gas front arrives at the discharge line.

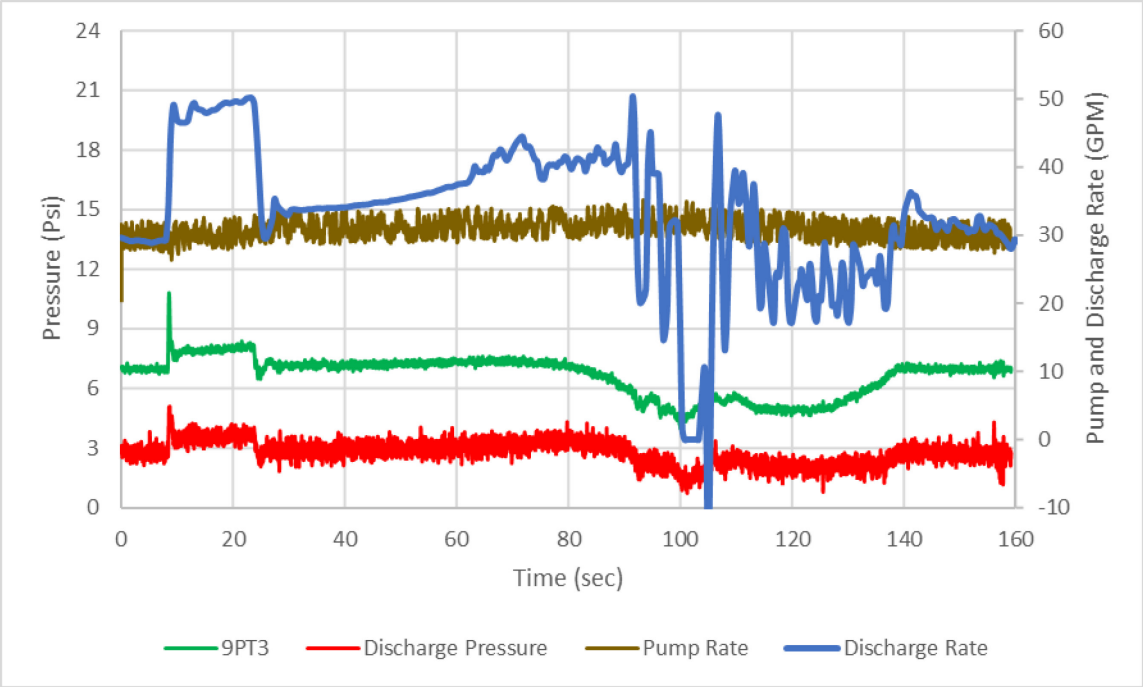

Figure 4-90—Pressure at the outlet and 15 ft below outlet and Pump Rate

Figure 4-91 displays the difference in pressure between 1PT1 and 3PT1, 4PT1, 9PT3, and Discharge Pressure. 1PT1-3PT1 and 1PT1-4PT1 demonstrate a slight decrease with gas arriving first at 1PT1, then 3PT1, and then 4PT1. However, the 1PT1-9PT3 and 1PT1-Discharge Pressure lines demonstrate a more significant reduction with the longer distance between these pressure transmitters. 1PT1-3PT1 and 1PT1-4PT1 recover earlier than 1PT1-9PT3 and 1PT1-Discharge line due to the clean mud pumped into the test section, cleaning out the gas between 1PT1 and 4PT1. The 1PT1-9PT3 and 1PT1-Discharge stabilize once the gas is completely removed from the system.

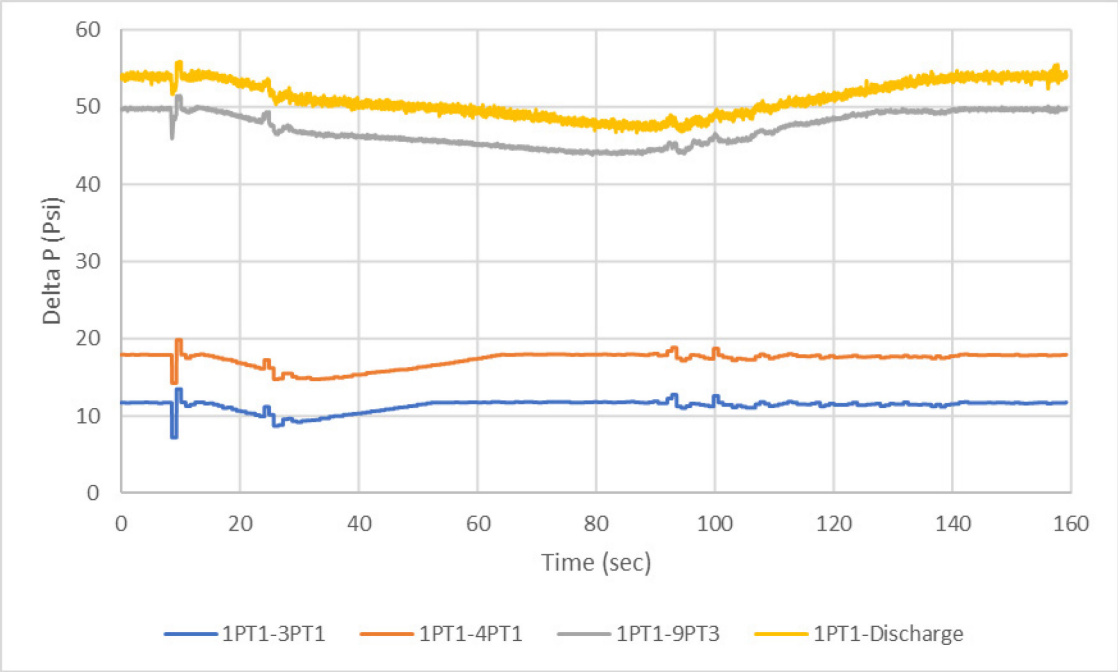

Figure 4-91— Pressure difference between 1st floor and 3rd, 4th, 9th floors, and discharge line

4.2. Carbon Dioxide (CO_2) Injection

Tests run in this section were all run using CO_2 as the gaseous phase. The objectives of this phase were to understand:

1- Effects of solubility on unloading.

2- Effects of Initial Injection Pressure.

3- Effects of unloading on pressure and flow rate.

4.2.1. 89 Psi Initial Injection Pressure

All tests presented under this section were run with CO_2 as the gaseous phase, where 3 tests were conducted with the pump circulating water at 15-GPM, and one case where the pump was off, and the gas could freely migrate through the flow loop. During the test, all flow rate and pressure data were logged. The tests conducted under this subsection were performed at 89-Psi initial injection pressures and 300-, 60-, 30-, and 600-seconds injection duration.

Pump Rate (GPM)	15	15	15	0
Initial Injection Pressure (PSI)	89.6	89.81	88.33	88.83
Gas Injection Duration (seconds)	300	60	30	600
Kick Intensity (lbs./gal)	3.635	3.664	3.436	3.622
Maximum Injection Rate (GPM)	2.36	2.39	1.60	3.15
Average Injection Rate (GPM)	2.00	1.99	1.40	2.25
Total Gas Injected (gal)	10.14	2.07	0.80	24.47
Maximum Discharge Rate (GPM)	38.74	26.59	23.17	47.24
Max Rate at Unloading (GPM)	19.53	19.53	16.15	9.22
Total Discharge Volume (gal)	140.95	78.88	77.23	59.43
Total Discharge During Unloading (gal)	49.20	41.15	38.57	7.03

Table 4-13— Summary of results for tests using CO_2 as the gaseous phase

Table 4-13 summarizes the results for tests run using CO_2 as the injection phase. The table displays the kick intensity, maximum and average injection rates, the total volume of gas injected, maximum discharge rate, maximum discharge rate at unloading,

total discharged volume, and total discharge during unloading. As seen in the data, a longer duration allowed for a greater maximum and average injection rate. The maximum discharge rates also display the same behavior as larger gas enters the flow loop.

The following sections present the data collected during these tests.

4.2.1.1. CO_2 Injection at 89.6 Psi for 5 Minutes

This test was run while pumping water at 15-GPM continuously. CO_2 was injected at 89.6-psi for 5-minutes while pressure and flow rate were logged.

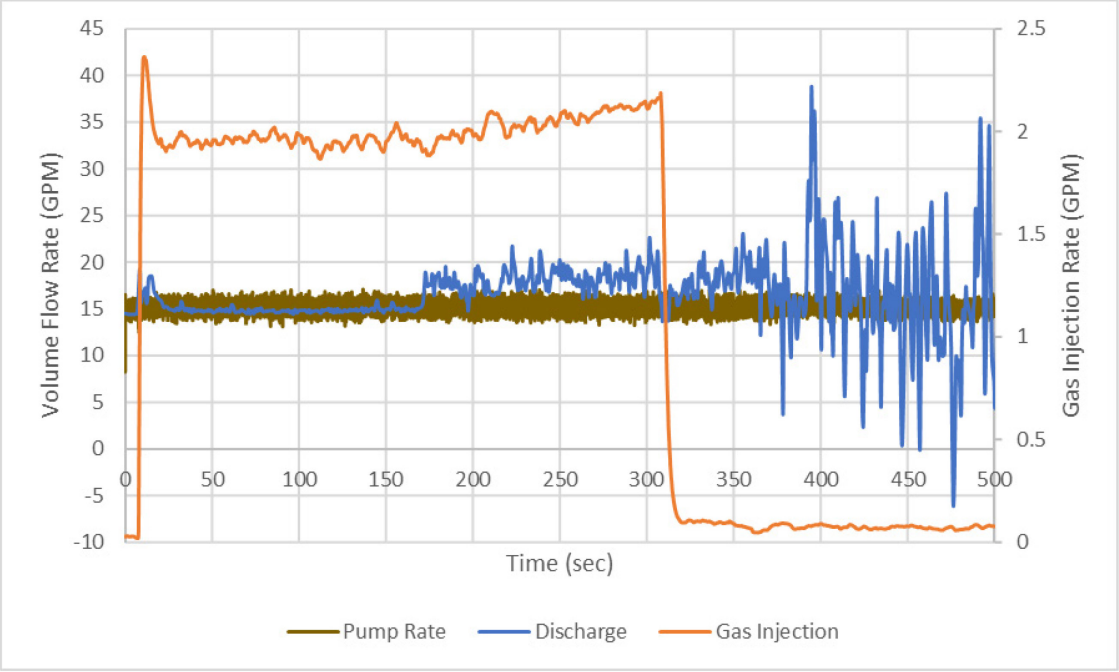

Figure 4-92— Pump, Mud Discharge, and Gas Injection Rates

Figure 4-92 displays the mud pump and discharge rates and the gas injection rate. CO_2 was injected at an average rate of 2.00-GPM and was terminated at approximately 309.31-seconds. The mud discharge rate spiked when the solenoid valve was opened, and gas injection began, then stabilized at the initial rate. The discharge rate rapidly increased to 19.53-GPM when the gas front reached the outlet at 176.65-seconds. The flow meter

continued logging a higher discharge rate until the solenoid valve was closed, which caused the discharge rate to drop to 13.64-GPM. The discharge rate then recovered and began fluctuating, logging a higher rate than the pump rate. At 394.73-seconds, the flow meter on the discharge line logged a 38.74-GPM rate and 3.199-lbs/gal density. During the experiment, no Taylor bubble was observed, and the return line was continuously flowing, indicating this measurement was correct and not a faulty measurement by the flow meter.

Figure 4-93 displays the cumulative pumped and discharged mud and injected gas volumes. The total amount of CO_2 injected into the flow loop was 10.14-gal. During the first half of the CO_2 injection, the discharge rate was stable, and this is also displayed as overlapping cumulative volume. However, the cumulative pumped and discharged volume data begin diverging from each other during the second half of the gas injection. The separation of the data lines continues to expand after gas injection is halted as the water-CO_2 mixture is circulated out of the flow loop.

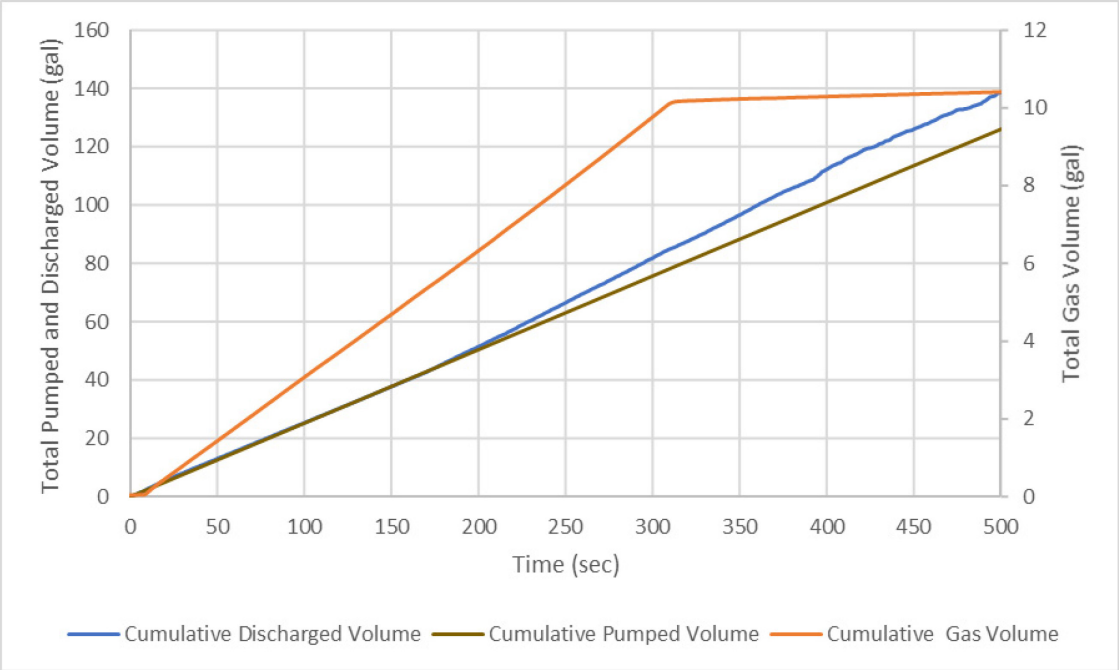

Figure 4-93— Cumulative Pumped, Discharged Water and Injected Gas Volume

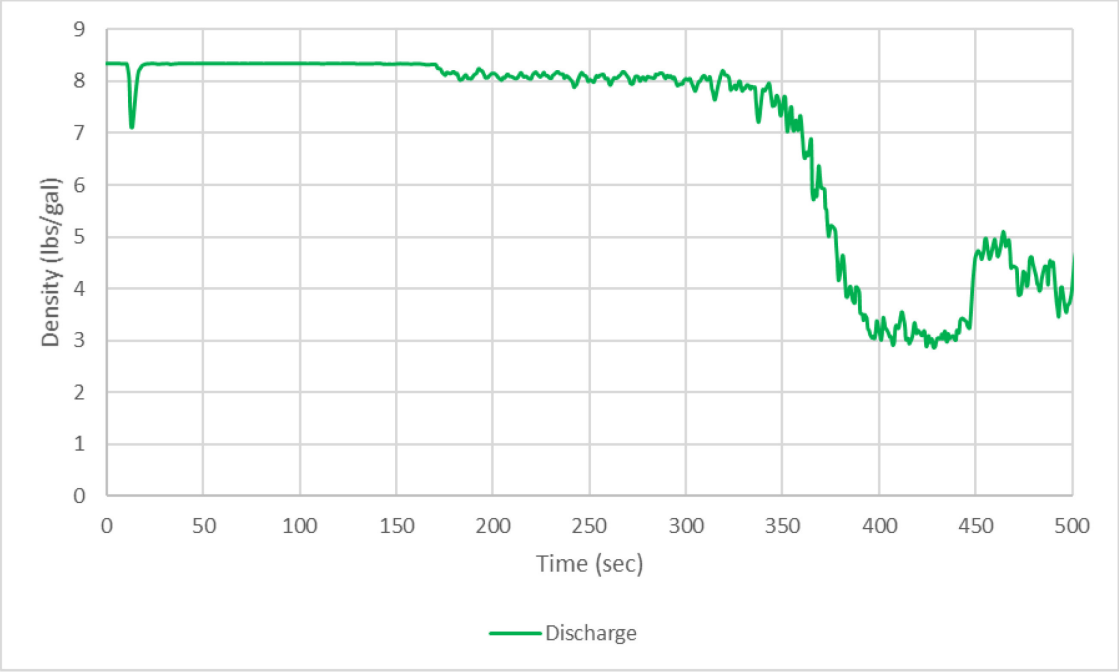

Figure 4-94—Discharge Density

Figure 4-94 displays the density of the fluid logged by the flow meter at discharge. The density logged by the flow meter is stable until the water-CO_2 mixture arrives at the discharge line at 176.65-seconds. After that, the density begins slightly fluctuating until it drops to 2.9- and 3.6-lbs/gal. **Figure 4-95** contains the temperature logged by the flow meters at the injection port and the discharge line. Again, no significant change in temperature was observed.

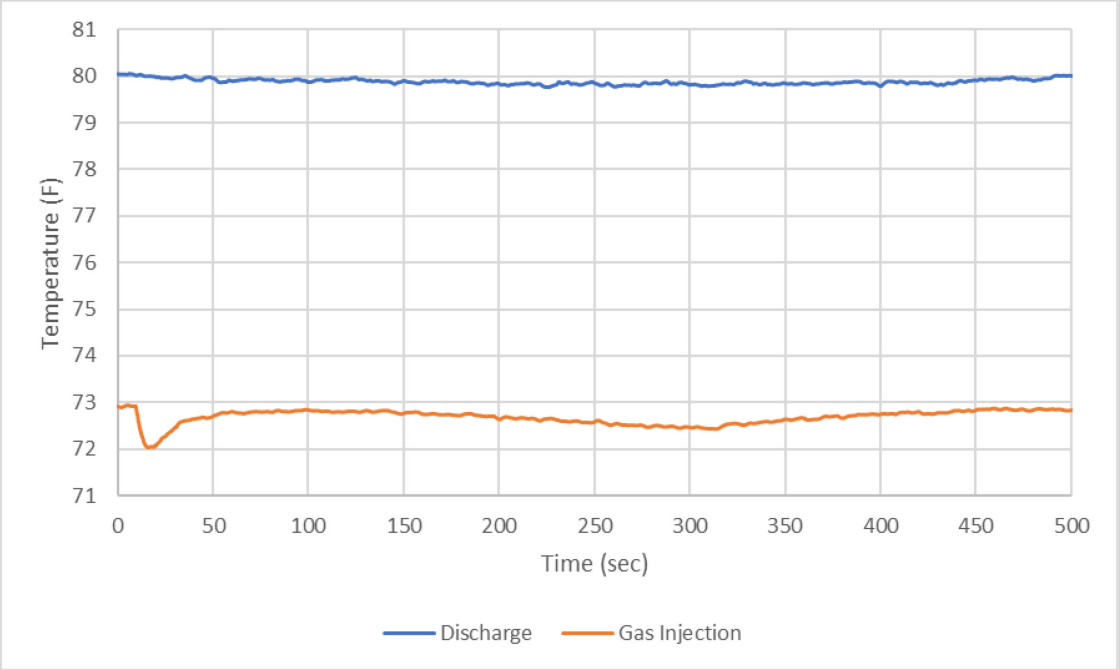

Figure 4-95—Discharge and Gas Injection Temperatures

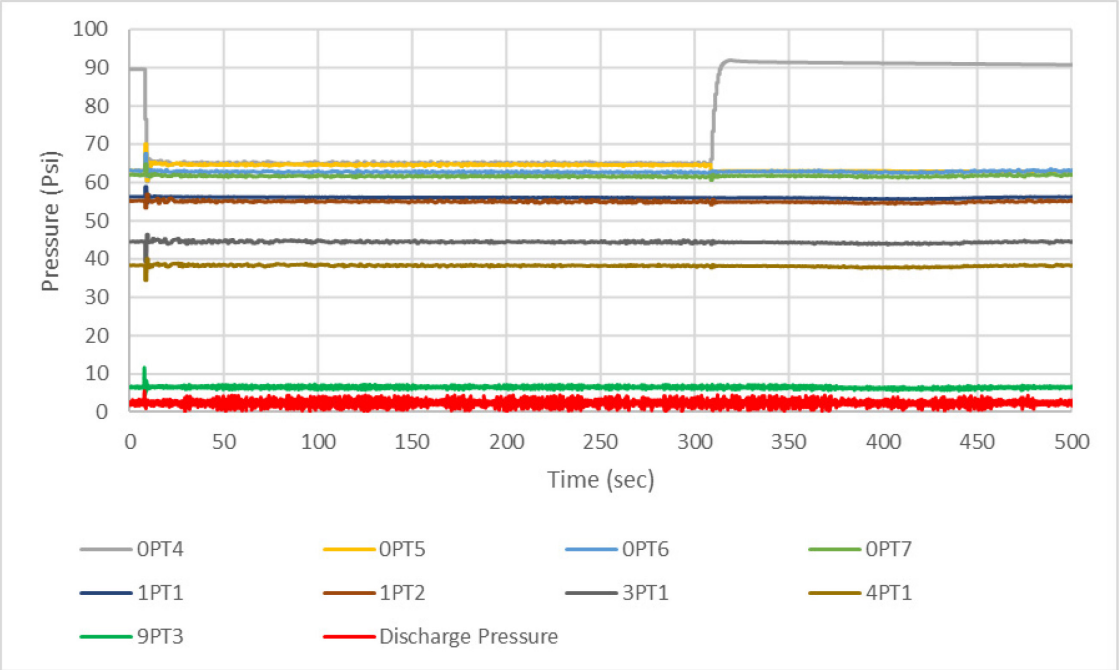

Figure 4-96—All Pressures

Figure 4-96 displays the pressure logged by all the pressure transmitters along the flow loop. The only visual indicator logged by the pressure transmitters was at the point when the solenoid valve was opened and gas injection began. Due to the solubility of CO_2 in water, the pressure transmitters did not log any variation or indicator in pressure.

Figure 4-97 displays 9PT3 and Discharge Pressure along with pump and discharge rate. The initial spike in pressure at approximately 9.23-seconds is due to the solenoid valve opening and air injection beginning. 9PT3 and Discharge Pressure are plotted and demonstrate no indication of gas entering the test section, migrating or expanding. This effect can also be seen with the constant pump rate and stable bottom hole pressure. With experiments where the air was injected, the pump rate automatically increased with decreasing bottom hole pressure. However, the data shows that both the bottom hole pressure and pump rate are constant for this case. Furthermore, the discharge rate

fluctuates; but the maximum discharge rate is not as high as was measured in the air injection tests.

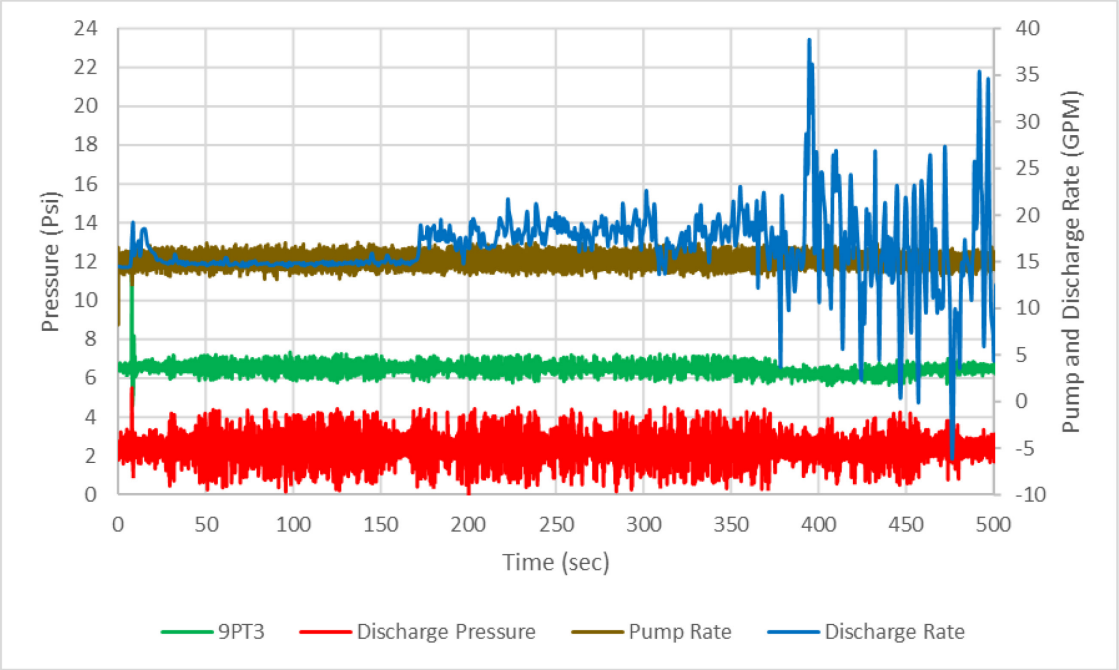

Figure 4-97—Pressure at the outlet and 15 ft below outlet and Pump Rate

Figure 4-98 displays the difference in pressure between 1PT1 and 3PT1, 4PT1, 9PT3 and Discharge Pressure. This graph also demonstrates stable and constant data.

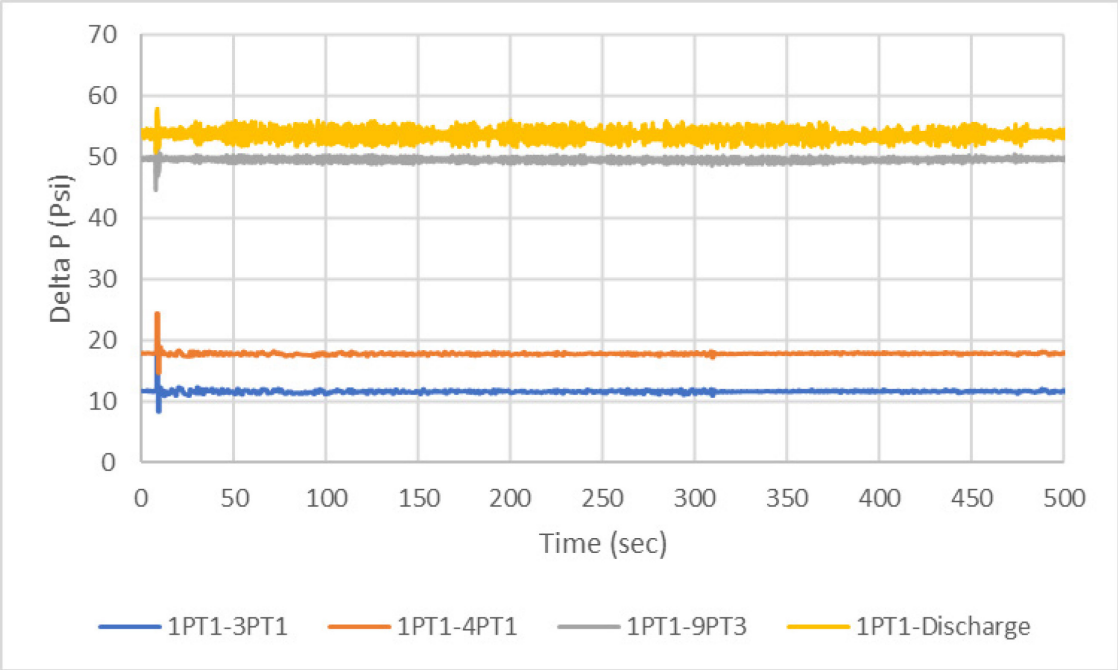

Figure 4-98— Pressure difference between 1st floor and 3rd, 4th, 9th floors, and discharge line

4.2.1.2. CO_2 Injection at 89.81-Psi for 60-Seconds

This test was run while pumping water at 15-GPM continuously. CO_2 was injected at 89.81-psi for 60-seconds while pressure and flow rate were logged.

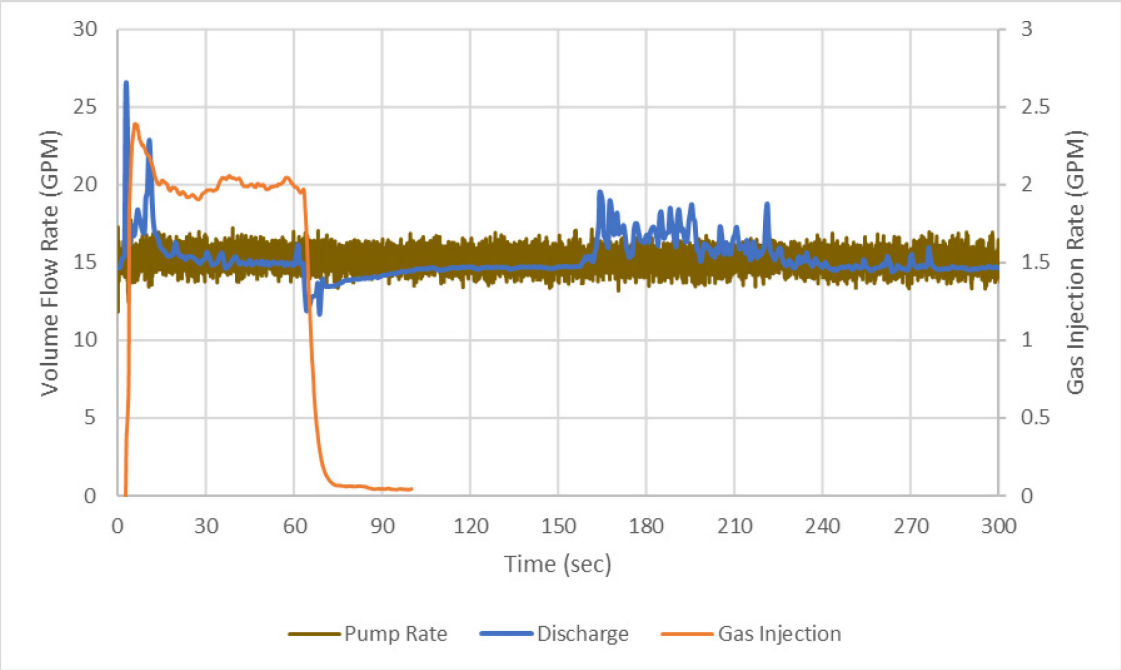

Figure 4-99— Pump, Mud Discharge, and Gas Injection Rates

Figure 4-99 displays the pump and discharge rates and the gas injection rate. CO_2 was injected at an average rate of 1.99-GPM and was terminated at approximately 64.91-seconds. The mud discharge rate spiked to 26.59-GPM when the solenoid valve was opened and gas injection began. The discharge rate stabilized at the initial rate until the solenoid valve was closed when the rate suddenly dropped to 11.94-GPM. The discharge rate gradually began increasing, and when the gas front reached the outlet at 163.84-seconds, the mud discharge rate reached 19.53-GPM. The discharge rate then began fluctuating as CO_2 was being circulated out of the flow loop. Finally, the discharge rate stabilized again at 243.65-seconds. During the test, it was observed that not all of the gas went into solution; however, no Taylor bubble was observed. The flow regime was dispersed bubbly flow.

Figure 4-100 displays the cumulative pumped and discharged mud and injected gas volumes. The total amount of CO_2 injected into the flow loop was 2.07-gal. The figure demonstrates almost no separation between the cumulative discharged and the cumulative pumped volumes. The injected gas volume was much lower than the test with air at 90-psi with a 15-GPM circulation rate.

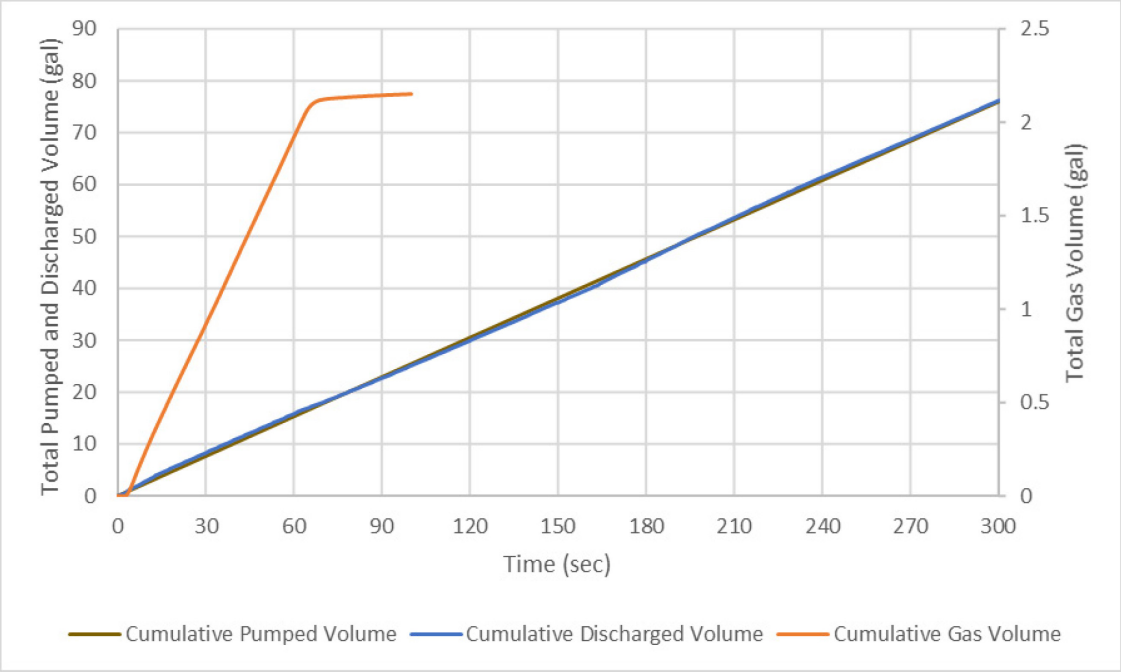

Figure 4-100— Cumulative Pumped, Discharged Water and Injected Gas Volume

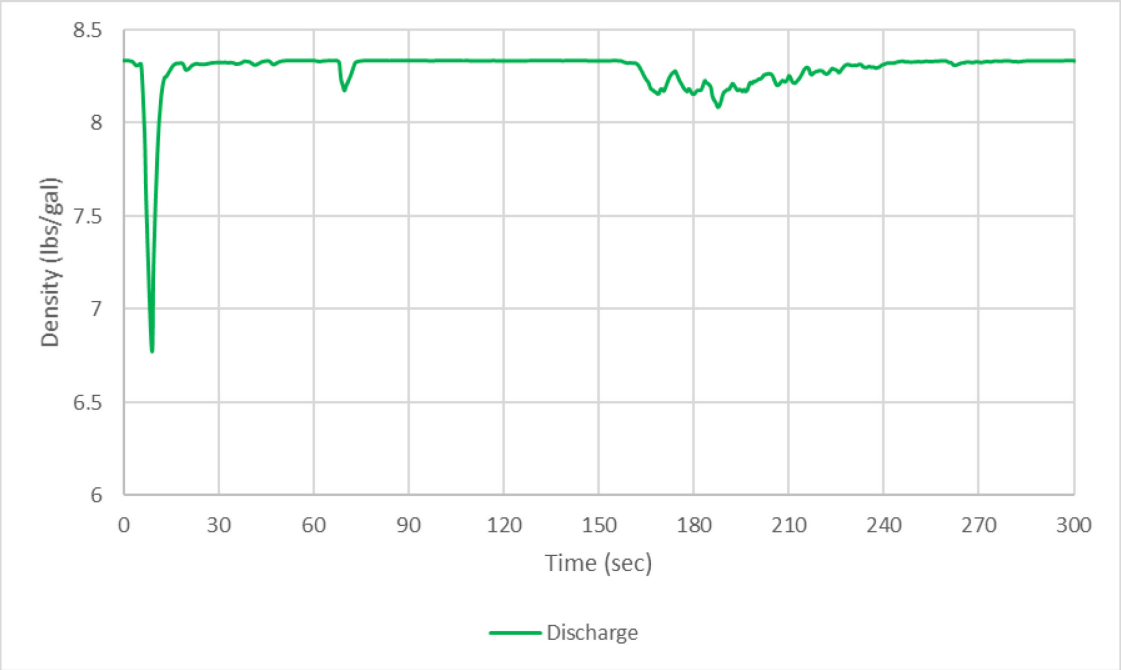

Figure 4-101—Discharge Density

Figure 4-101 displays the density of the fluid logged by the flowmeter at discharge. The density logged by the flowmeter demonstrates minimal fluctuation. When injection starts, the push from the CO_2 injection causes the trapped CO_2 inside the flowmeter to flow out, which is logged as a lower density. The closing of the solenoid valve also causes a slight drop at 64.91-seconds. The density slightly fluctuates when the water-CO_2 mixture reaches the outlet. **Figure 4-102** contains the temperature logged by the flow meters at the injection port and the discharge line. No significant change in temperature was observed.

.

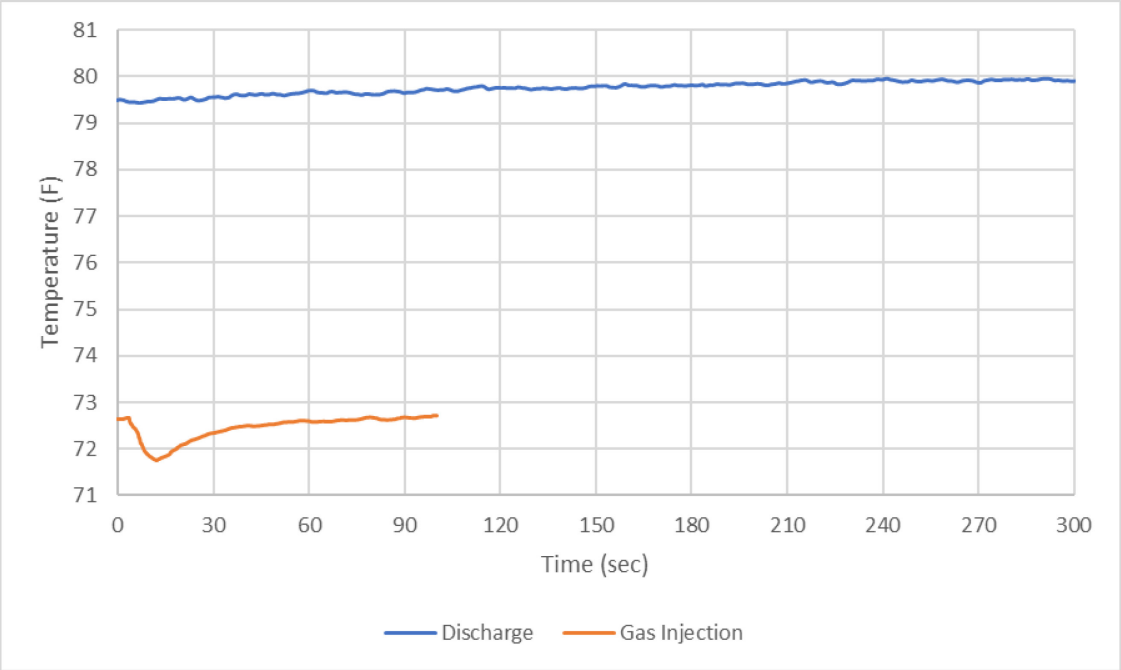

Figure 4-102—Discharge and Gas Injection Temperatures

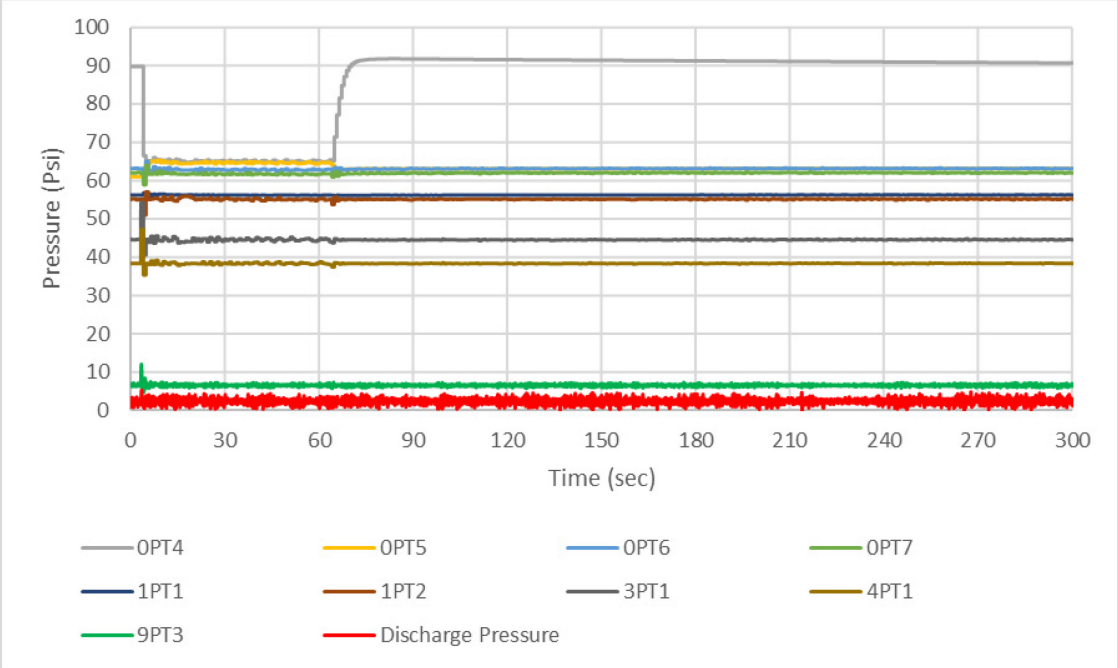

Figure 4-103—All Pressures

Figure 4-103 displays the pressure logged by all pressure transmitters along the flow loop. The only visual indicator logged by the pressure transmitters was at the point when the solenoid valve was opened and gas injection began. Due to the solubility of CO_2 in water, the pressure transmitters do not log any variation or indicator in pressure.

Figure 4-104 displays 9PT3 and Discharge Pressure along with pump and discharge rate. The initial spike in pressure at approximately 4.07-seconds is due to the solenoid valve opening and air injection beginning. 9PT3 and Discharge Pressure were plotted to demonstrate no indication in the pressure data of CO_2 entering and migrating or unloading the flow loop. The pressure transmitters 0PT6, 0PT7, 1PT1, 1PT2, 3PT1, and 4PT1 display slight fluctuation during injection, which smooth out when the gas injection is terminated.

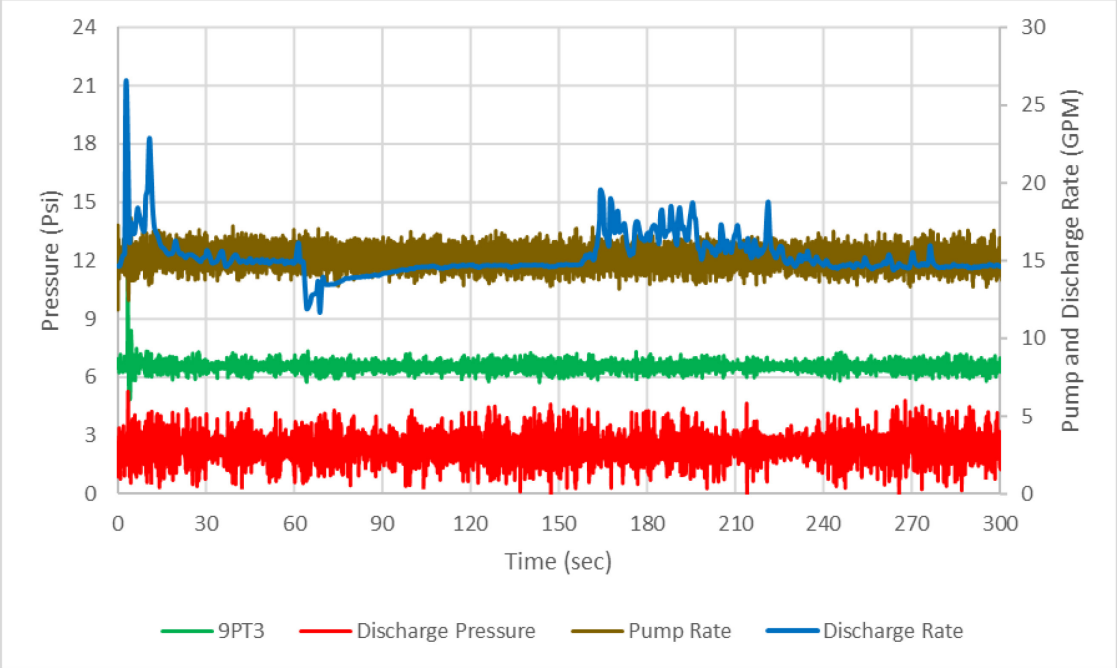

Figure 4-104—Pressure at the outlet and 15 ft below outlet and Pump Rate

Figure 4-105 displays the difference in pressure between 1PT1 and 3PT1, 4PT1, 9PT3, and Discharge Pressure. This graph also demonstrates no variation in pressure.

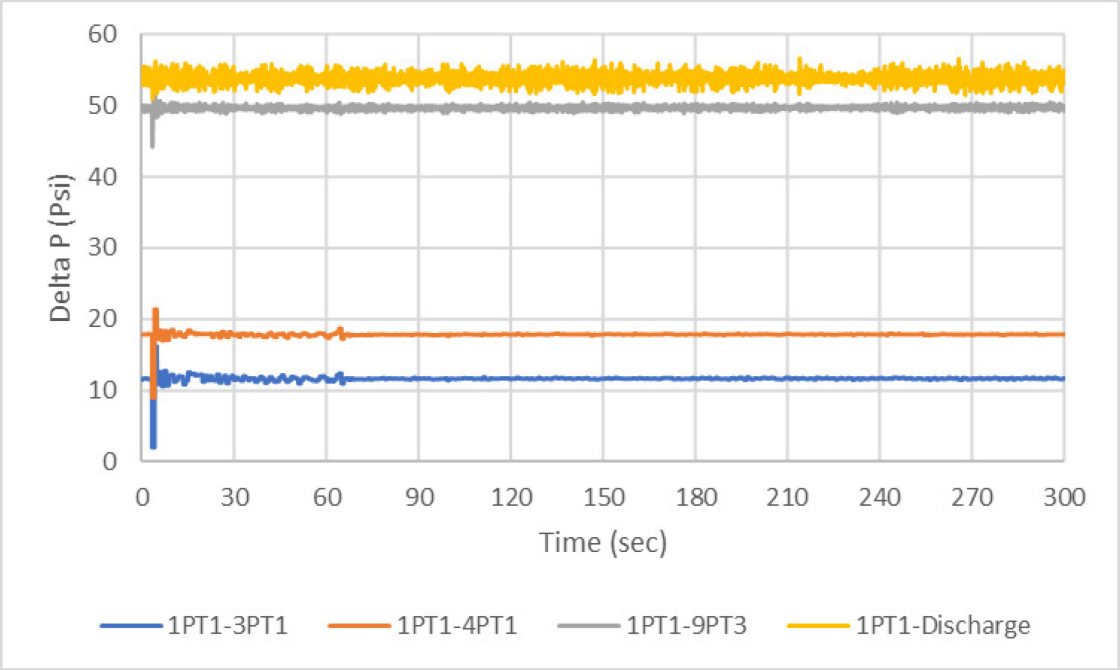

Figure 4-105— Pressure difference between 1st floor and 3rd, 4th, 9th floors, and discharge line

4.2.1.3. CO_2 Injection at 88.33-Psi for 30-Seconds

This test was run while pumping water at 15-GPM continuously. CO_2 was injected at 88.33-psi for 30-seconds while pressure and flow rate were logged.

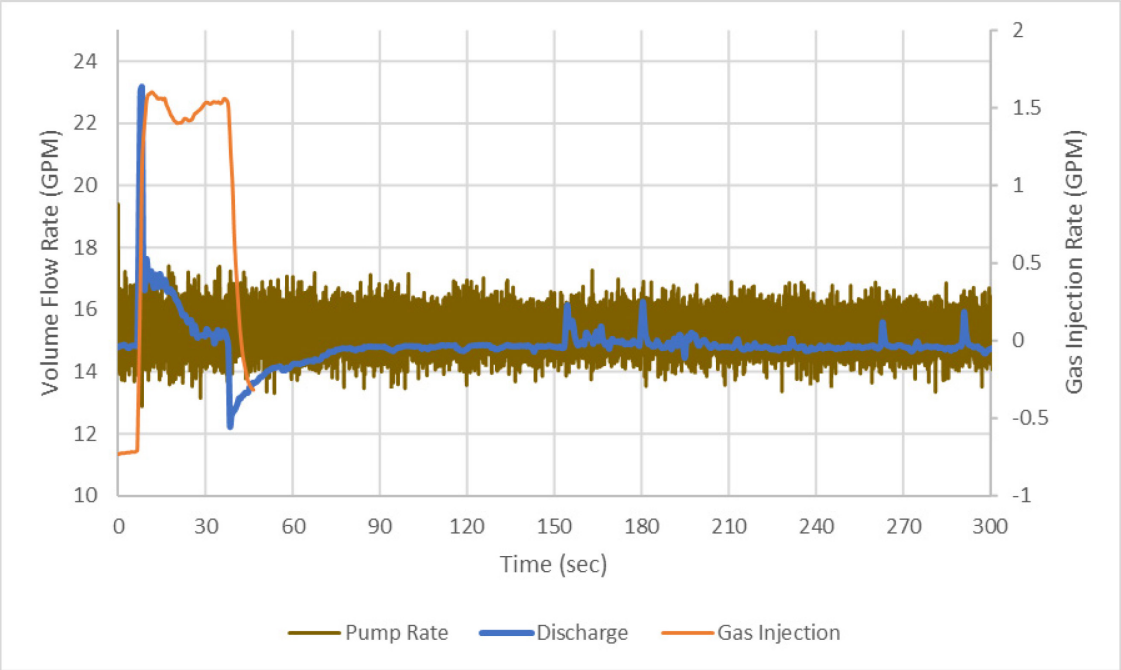

Figure 4-106— Pump, Mud Discharge, and Gas Injection Rates

Figure 4-106 displays the pump and discharge rates and the gas injection rate. CO_2 was injected at an average rate of 1.40-GPM and was terminated at approximately 39.15-seconds. The mud discharge rate spiked to 23.17-GPM when the solenoid valve was opened and gas injection began. The discharge rate then began decreasing until it stabilized. When the solenoid valve closed, the discharge rate suddenly dropped to 12.25-GPM. The discharge rate slowly began increasing and stabilized at the initial rate. The gas front reached the outlet at 155.65-seconds, and the mud discharge rate was logged as 16.15-GPM. The discharge rate fluctuated as CO_2 was circulated out of the flow loop. The discharge rate and density stabilized again at 223.39-seconds. Not all of the injected gas went into solution; however, again, no Taylor bubble was observed. The flow regime was dispersed bubbly flow.

Figure 4-107 displays the cumulative pumped and discharged mud and injected gas volumes. The total amount of CO_2 injected into the flow loop was 0.80-gal. The figure demonstrates almost no separation between the cumulative discharged and the cumulative pumped volumes. The injected gas volume was much lower than the test with air at 90-psi with a 15-GPM circulation rate.

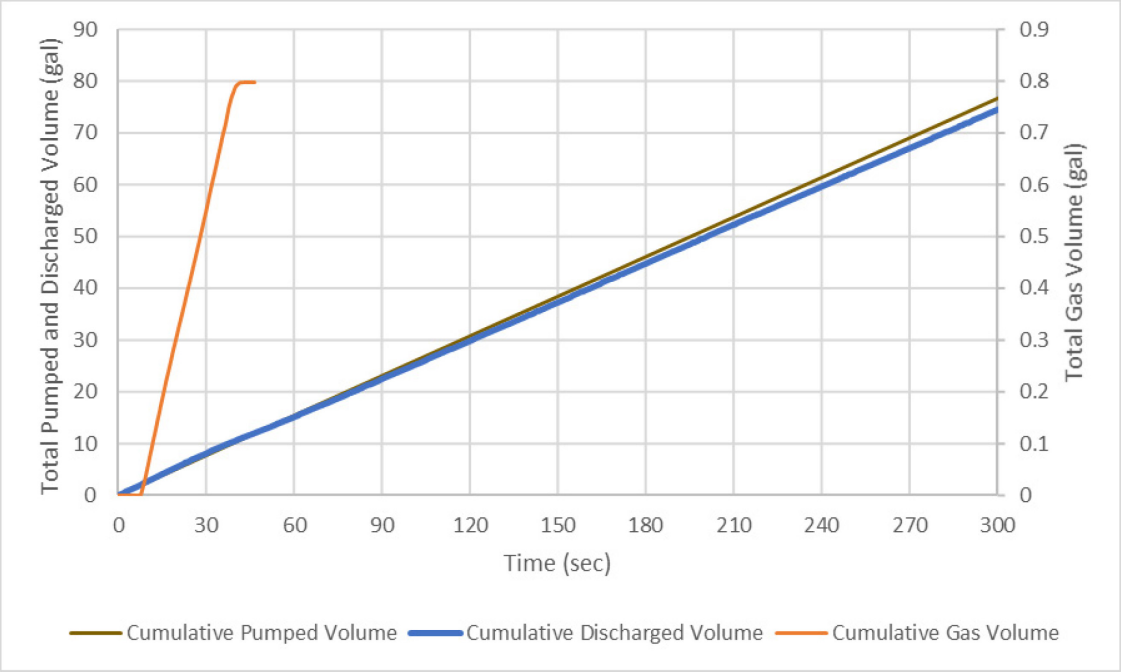

Figure 4-107— Cumulative Pumped, Discharged Water and Injected Gas Volume

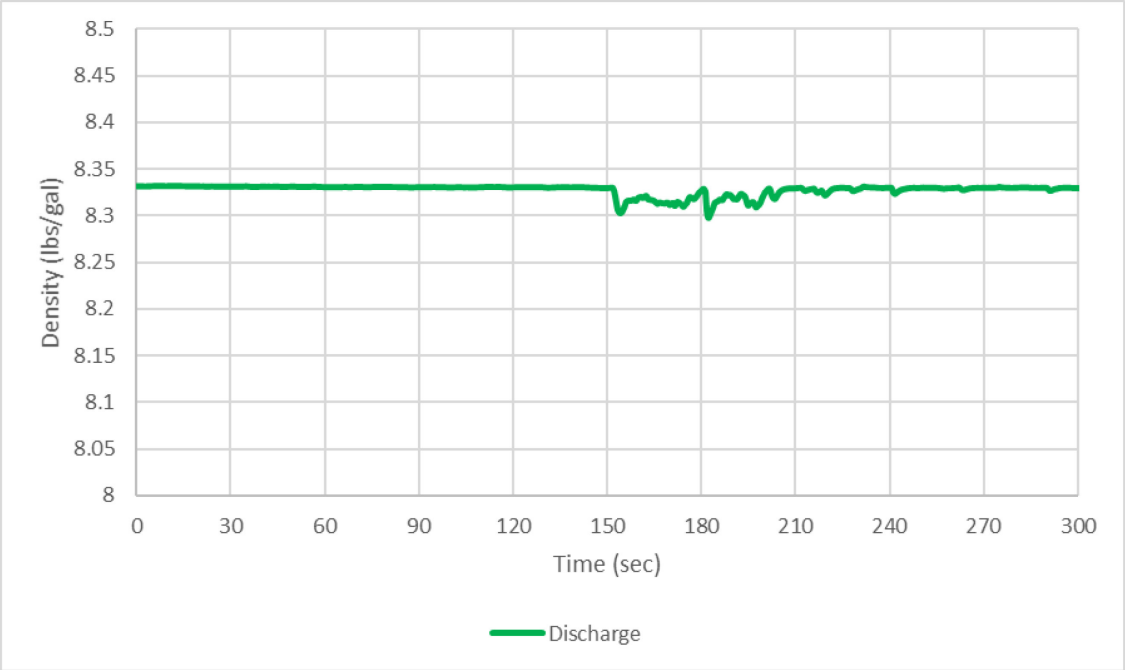

Figure 4-108—Discharge Density

Figure 4-108 displays the density of the fluid logged by the flow meter at discharge. The density logged by the flowmeter only shows minimal fluctuation when the gas begins exiting the flow loop. Opening or closing the solenoid valve caused any fluctuation in the density.

Figure 4-109 contains the temperature logged by the flow meters at the injection port and the discharge line. Again, no significant change in temperature was observed.

.

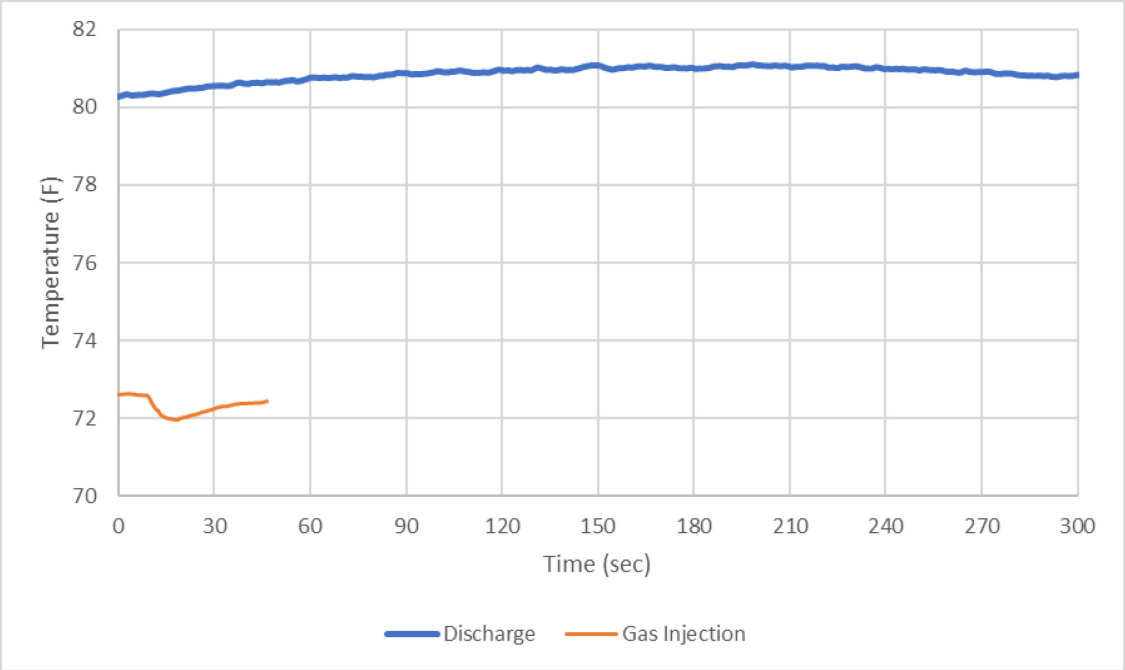

Figure 4-109—Discharge and Gas Injection Temperatures

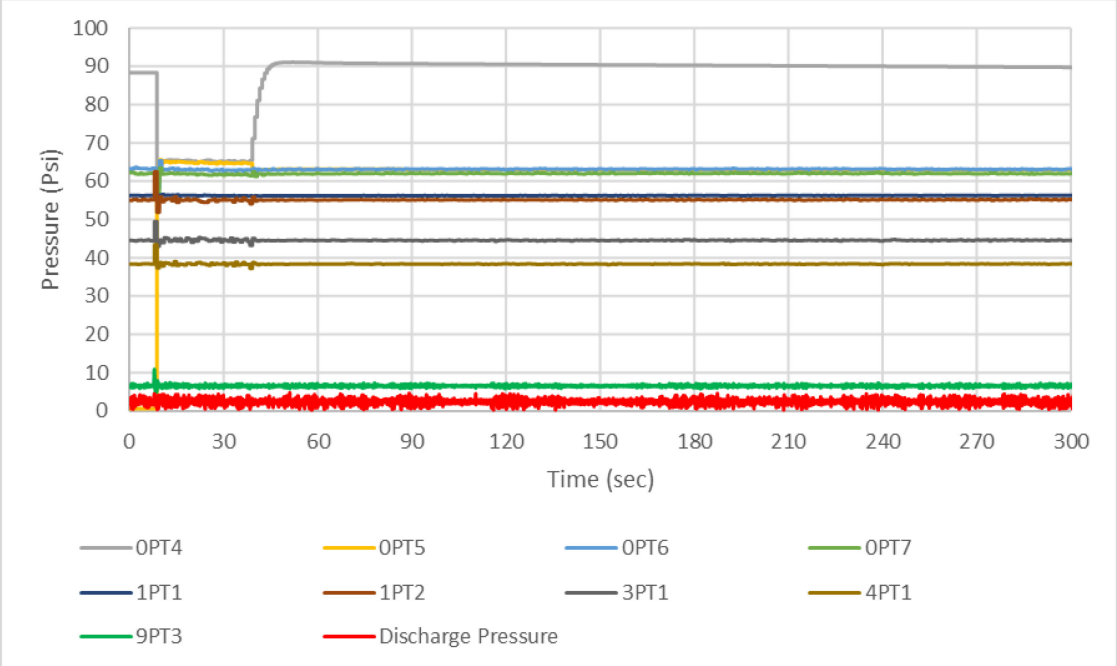

Figure 4-110—All Pressures

Figure 4-110 displays the pressure logged by all the pressure transmitters along the flow loop. The only visual indicator logged by the pressure transmitters was at the point when the solenoid valve was opened and gas injection began. Due to the solubility of CO_2 in water, the pressure transmitters do not demonstrate any variation or indicator in pressure.

Figure 4-111 displays 9PT3 and Discharge Pressure along with pump and discharge rate. The initial spike in pressure at approximately 8.73-seconds is due to the solenoid valve opening and air injection beginning. 9PT3 and Discharge Pressure were plotted to demonstrate no indication in the pressure data of CO_2 entering and migrating or unloading the flow loop. The pressure transmitters 0PT6, 0PT7, 1PT1, 1PT2, 3PT1, and 4PT1 display slight fluctuation during injection, which flattens out when the gas injection is terminated. However, the fluctuations were very small to be noticed or provide any use to detect gas.

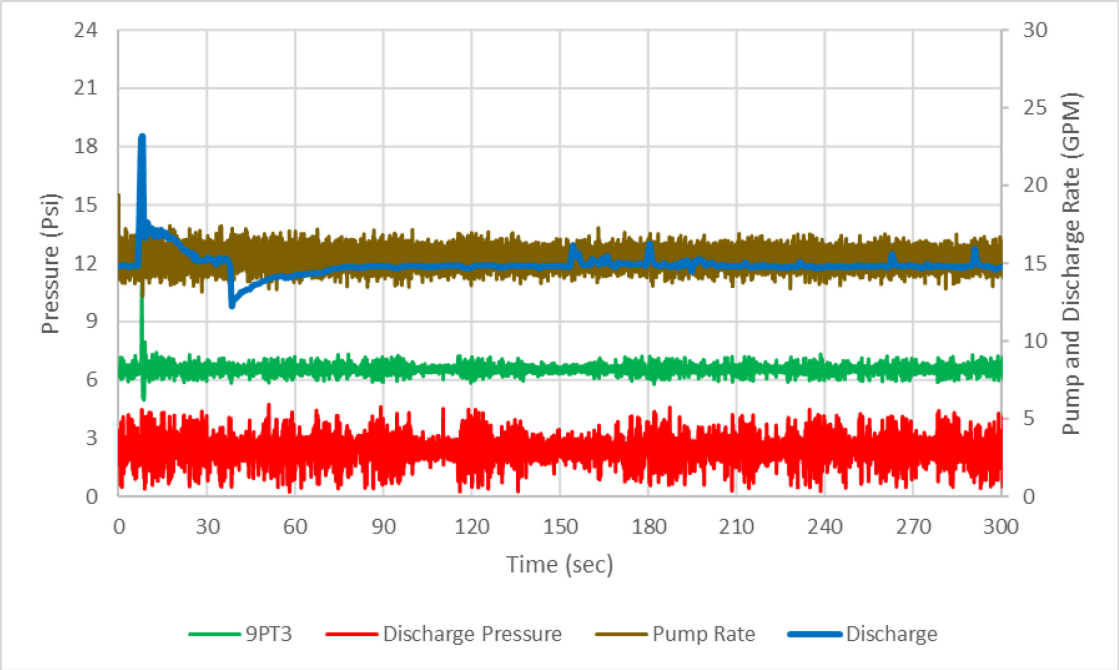

Figure 4-111— Discharge and 9PT3 (15 ft below outlet) pressure, pump, and discharge rate

Figure 4-112 displays the difference in pressure between 1PT1 and 3PT1, 4PT1, 9PT3, and Discharge Pressure. This graph also demonstrates no variation in pressure.

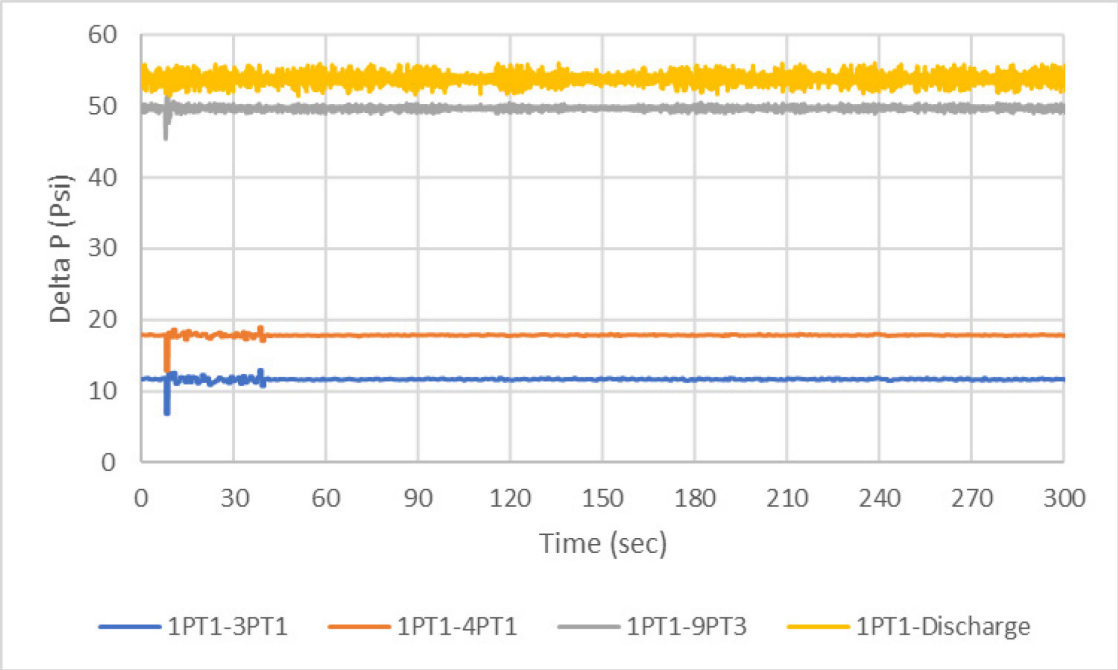

Figure 4-112— Pressure difference between 1st floor and 3rd, 4th, 9th floors, and discharge line

4.2.1.4. CO_2 Injection at 88.83-Psi for 10-Minutes – Static Conditions

This test was run in static conditions with the pump off. CO_2 was injected at 88.83-psi for 10-minutes while pressure and flow rate were logged.

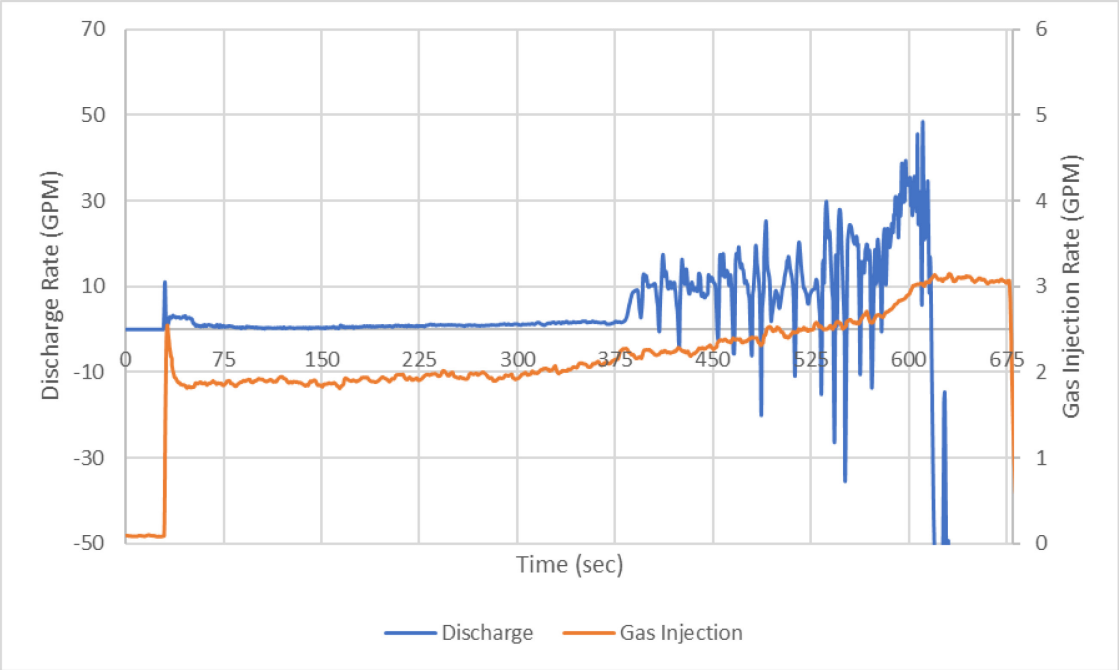

Figure 4-113—Mud Discharge and Gas Injection Rates

Figure 4-113 displays the discharge rate and the gas injection rate. CO_2 was injected at an average rate of 2.25-GPM. The discharge rate spiked to 11.05-GPM when the solenoid valve was opened, and gas injection began, then decreased and stabilized at under 1-GPM. The discharge rate very gradually increased to 1.79-GPM right before the gas front reached the discharge line. The density logged by the flow meter showed the first drop at 383.45-seconds, indicating contaminated water passing through the discharge line. The discharge rate then rapidly increases to 9.74-GPM. After that, the discharge rate began fluctuating, and the maximum discharge rate was logged as 45.57-GPM at 610.13-seconds. The density logged by the flow meter at this point was 1.703-lbs/gal. This measurement indicates a high concentration of CO_2 in the mud or only gas flow traveling through the flowmeter. However, during the test, the liquid level had dropped to the 7th floor.

Figure 4-114 displays the cumulative discharged mud and injected gas volumes. The total amount of CO_2 injected into the flow loop was 24.47-gal. The cumulative discharged and pumped mud volumes are also plotted. The total mud discharged until the gas front arrived at the discharge line was logged as 7.03-gal. The total amount of mud discharged throughout this test was 59.43-gal. The significant difference between total discharged until gas front arrival and the total discharged mud can be seen in the graph, with the slope increasing after the gas front arrived at the discharge line. After the gas front arrived at the outlet, the discharged mud volume rapidly increased until 623.04-seconds when the liquid level finally dropped to the 7th floor.

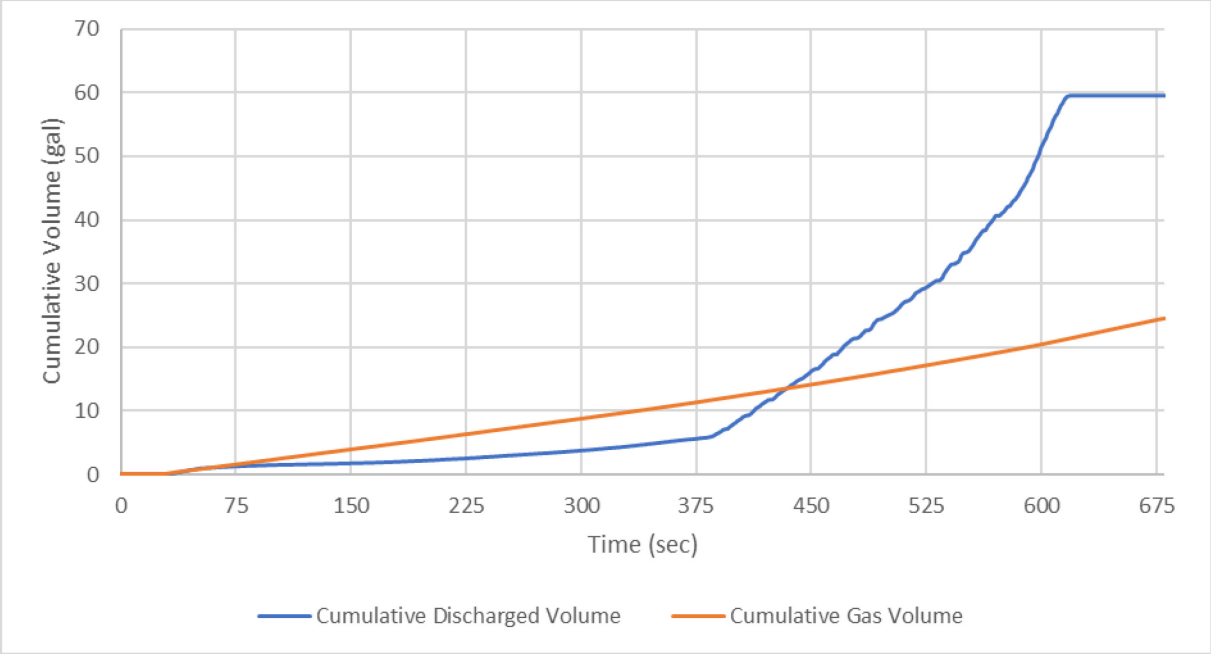

Figure 4-114— Cumulative Discharged Water and Injected Gas Volume

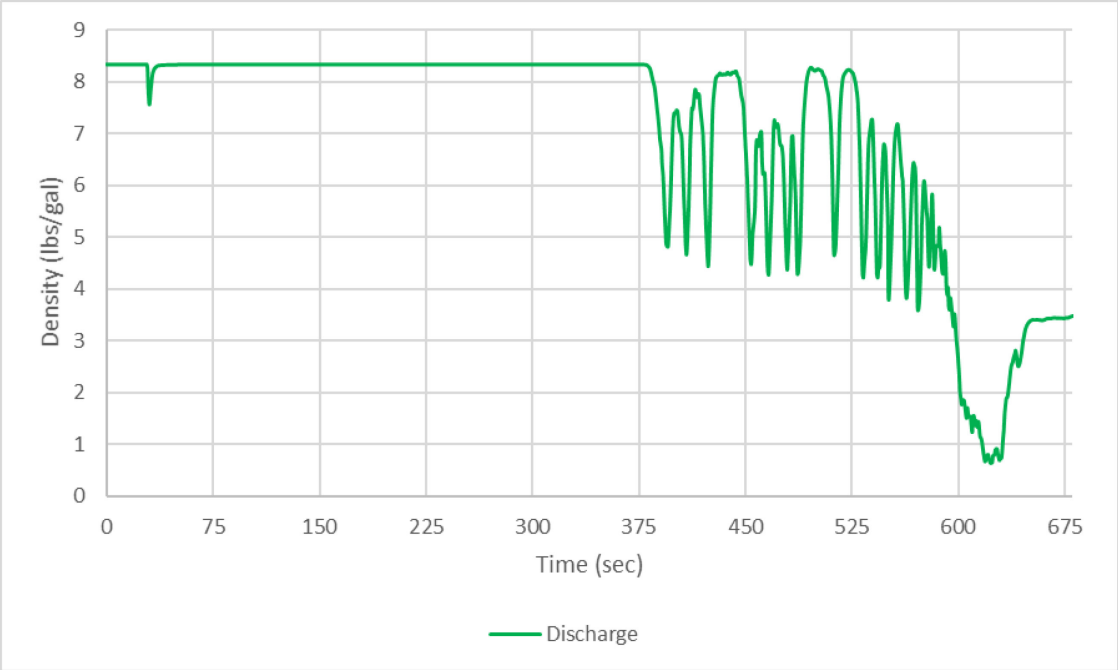

Figure 4-115—Discharge Density

Figure 4-115 displays the density of the fluid logged by the flow meter at discharge. Immediately following gas arrival at discharge, the density rapidly drops to 4.81-lbs/gal then fluctuates as free gas and solubilized CO_2 and water mixture arrive at the discharge line. The density finally drops to 0.64-lbs/gal at 622.92-seconds. **Figure 4-116** contains the temperature logged by the flow meters at the injection port and the discharge line. No significant change in temperature was observed.

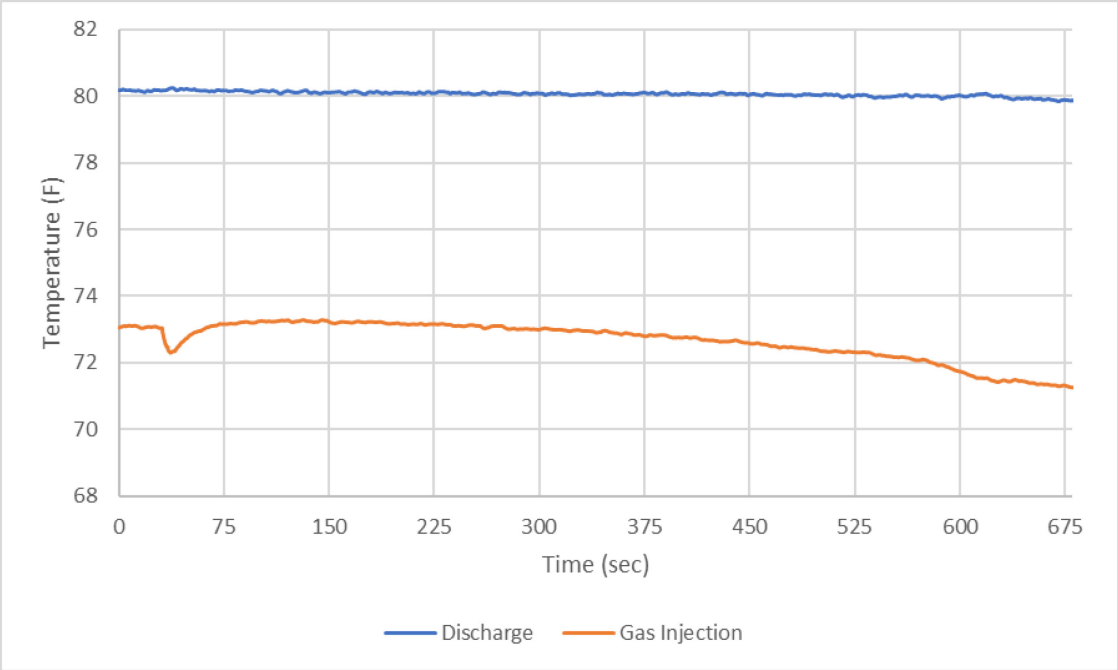

Figure 4-116—Discharge and Gas Injection Temperatures

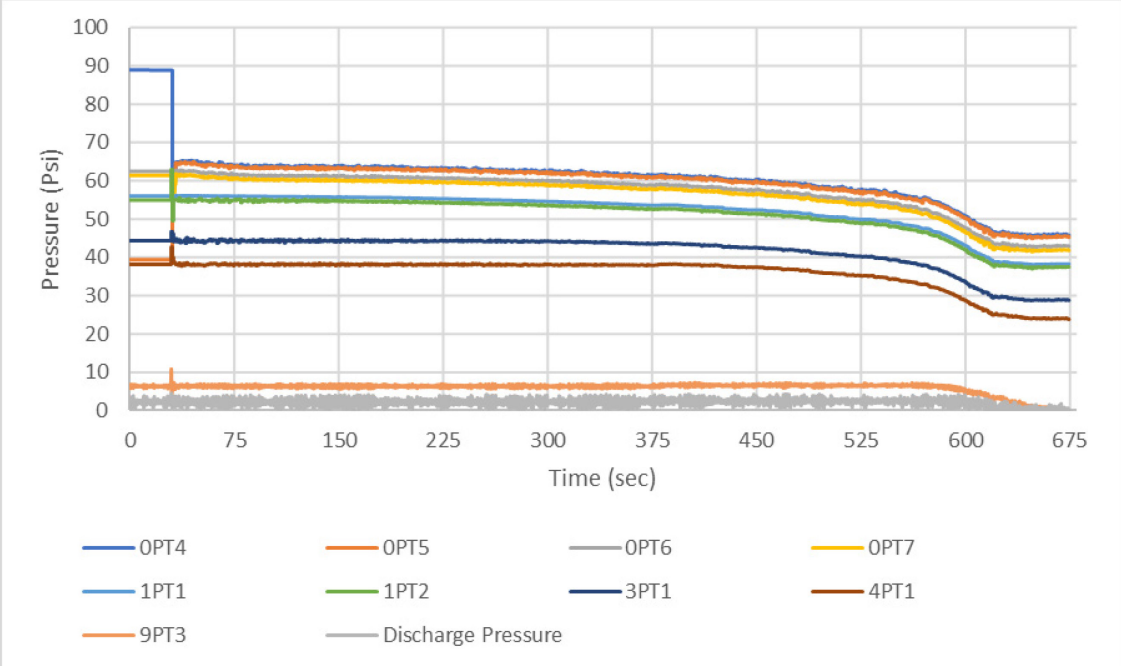

Figure 4-117—All Pressures

Figure 4-117 displays the pressure logged by all the pressure transmitters along the flow loop. All pressure transmitters display a decreasing trend except for 9PT3 and Discharge Pressure after gas injection begins. Gas injection beginning point can be easily observed as a slight increase in pressure for all pressure transmitters on the test section. Gas front reaches the discharge line at 383.45-seconds. With no mud circulation, the bottom hole pressure decreased (0PT6) and allowed the gas injection rate to increase.

Figure 4-118 displays 9PT3 and Discharge Pressure along with discharge rate. The point when the gas front reached the flow meter can be observed in the discharge rate line; however, the pressure transmitters demonstrate no indication of CO_2 entering the flow loop. The two pressures drop off near the end when the liquid level finally drops and settles at the 7th floor.

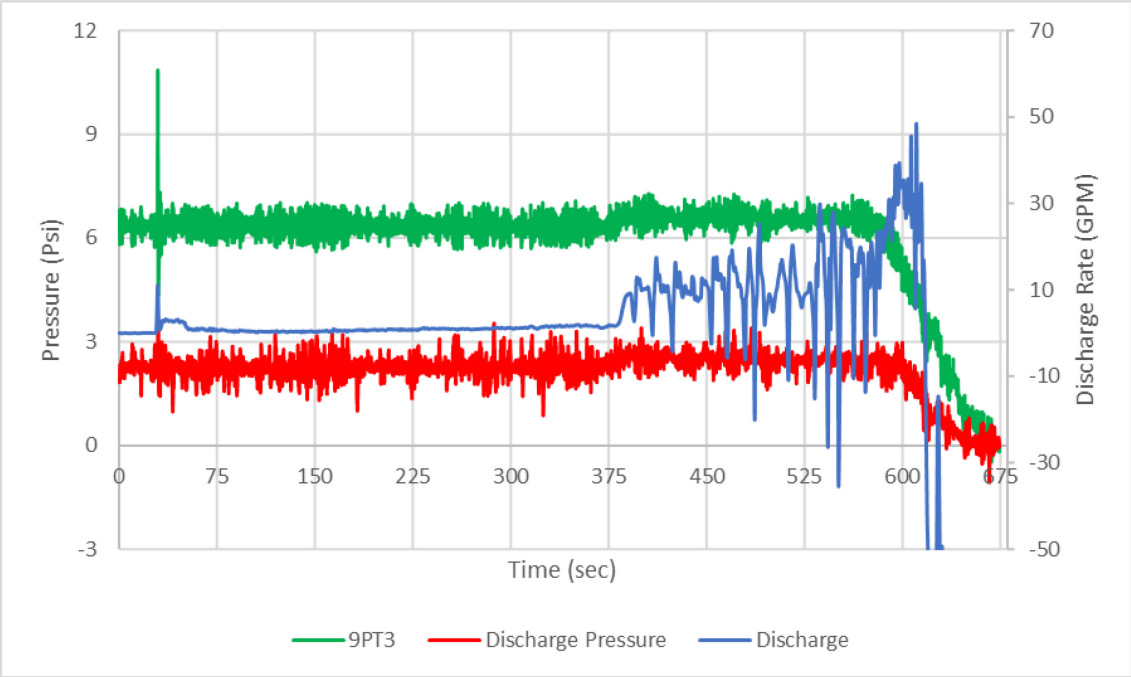

Figure 4-118— Discharge and 9PT3 (15 ft below outlet) pressure and discharge rate

Figure 4-119 displays the difference in pressure between 1PT1 and 3PT1, 4PT1, 9PT3, and Discharge Pressure. 1PT1-3PT1 and 1PT1-4PT1 demonstrate a slight decrease with gas arriving first at 1PT1, then 3PT1, and then 4PT1. The 1PT1-9PT3 and 1PT1-Discharge Pressure lines demonstrate a more significant reduction with the longer distance between these pressure transmitters. In the final stage, when the liquid level drops to the 7th floor, the lines in the figure display a slight increase. This indicates the 0-psi reading in the "9PT3 and Discharge Pressure" ports.

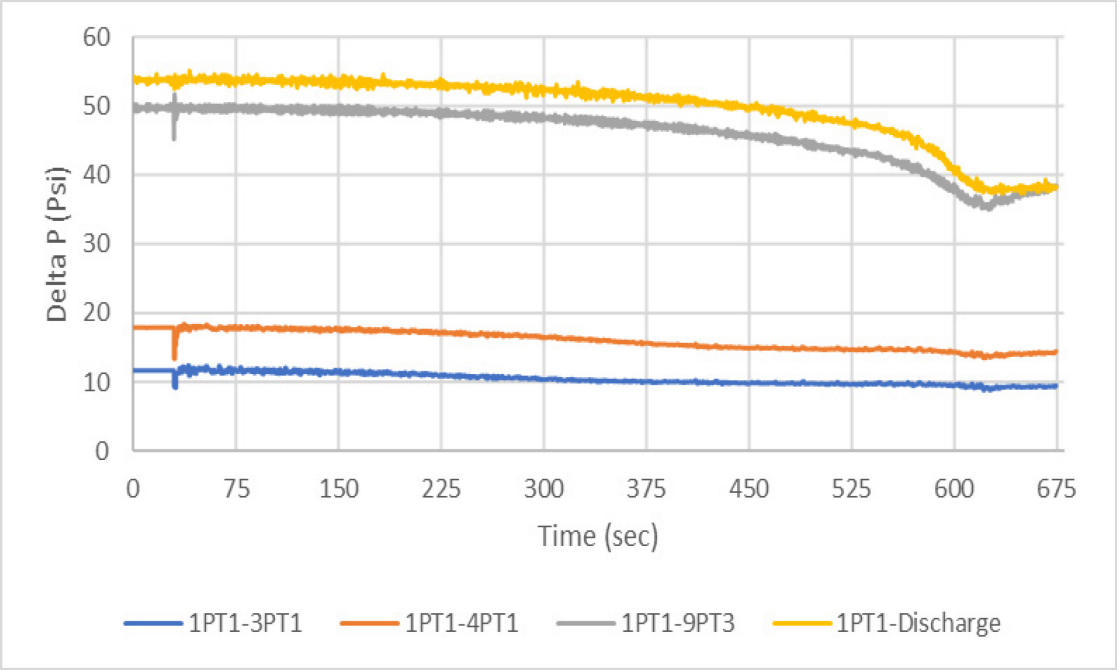

Figure 4-119— Pressure difference between 1st floor and 3rd, 4th, 9th floors, and discharge line

5. SIMULATIONS

Computational Fluid Dynamics (CFD) provides a numerical approximation to the equations that govern fluid flow. The steps to run a CFD analysis are as follows:

1- to choose the correct mathematical equations that describe the fluid flow problem that is being investigated (continuity, momentum, energy, turbulence, heat transfer, etc.),
2- discretize the mathematical equations to perform the numerical analysis,
3- define the flow geometry,
4- divide into small mesh or grid,
5- set initial conditions and boundary conditions,
6- choose the correct solution method and convergence, stability, and accuracy methods.

CFD is a method used by various engineering and sciences to study fluid flow in various systems and conditions. For example, the oil and gas industry uses CFD to study the effects of currents around a riser in offshore drilling and production systems. CFD is also used in modeling blowouts and blowout capping, as it is a powerful tool that provides accurate calculations for temperature, flow, velocity, and pressure effects.

In this research, Ansys Fluent Software was used for the CFD study. Fluent is a CFD software capable of simulating single-phase, multi-phase, compressible, incompressible, laminar, and turbulent flows. Fluent simultaneously solves a series of equations such as momentum, continuity, energy equations for a broad range of geometries. The conservation equations are solved in CFD modeling using Fluent are the Mass

Conservation (Continuity) Equation and the Momentum Conservation Equation, Energy Conservation Equation (ANSYS® 2017).

5.1.1. The Mass Conservation Equation

In the most basic form, the mass conservation equation is as follows:

$$\frac{\partial \rho}{\partial t} + \nabla \cdot (\rho \vec{v}) = S_m \ldots\ldots\ldots\ldots\ldots \textbf{Equation 4.1}$$

where S_m is defined as the mass added to the primary phase from the secondary phase.

For a 2D axisymmetric geometry, the mass conservation equation can be written as:

$$\frac{\partial \rho}{\partial t} + \frac{\partial}{\partial x}(\rho v_x) + \frac{\partial}{\partial x}(\rho v_r)\frac{\rho v_r}{r} = S_m \ldots\ldots\ldots\ldots \textbf{Equation 4.2}$$

Where x and r denote the axial and radial coordinate (ANSYS® 2017).

5.1.2. Momentum Conservation Equations

The momentum conservation is defined as follows:

$$\frac{\partial}{\partial t}(\rho \vec{v}) + \nabla \cdot (\rho \vec{v}\vec{v}) = -\nabla p + \nabla \cdot (\bar{\bar{\tau}}) + \rho \vec{g} + \vec{F} \ldots\ldots\ldots \textbf{Equation 4.3}$$

p: Static pressure

$\bar{\bar{\tau}}$: Stress tensor

The $\rho \vec{g}$ *and* $\vec{F}$ define the gravitational and external forces. (ANSYS® 2017)

5.1.3. Energy

The energy equation, in its simplest form for multiple phases, is as follows:

$$\rho \frac{De}{Dt} + P(\nabla . V) = \frac{\partial Q}{\partial t} - (\nabla . \mathrm{q}) + \Phi \ldots\ldots\ldots \textbf{Equation 4.4}$$

Where;

ρ: fluid density,

V: velocity vector,

P: pressure

e: internal energy

Q: heat source term,

∇.q: heat loss by conduction.

After choosing the appropriate equations and setting up the flow geometry and boundary and initial conditions, the solver method and solution control methods must be selected.

5.1.4. Simulation Setup

The CFD Analyses are performed on complex geometries and flow problems that require multiple attempts and significant computing power. The process adopted in this research was, to begin with, a simple single-phase case for a smaller geometry, adding the multi-phase model, scaling up the geometry, and repeating the process. This process was due to the difficulty in determining the reason for the divergence of a complex simulation. For this purpose, the CFD study for this research is split into 2 phases.

5.1.4.1. Phase 1

This phase aimed to test various multi-phase flow modes, turbulence models, solver methods, and solution controls using water as the continuous phase and air as the dispersed phase in a 10-meter pipe under static conditions. Gas was injected from the base of the 6-inch pipe into the static column of water. The models and control methods that were tested are as follows:

1- Pressure-Based Transient Solver.

2- The Eulerian-Eulerian Volume of Fluid (VOF) multi-phase flow method.

3- Energy Equation.

4- Turbulence Models:

- K-epsilon turbulence model.
- K-omega turbulence model.

Solution Methods:

- SIMPLE Pressure-Velocity Coupling
- Spatial Discretization for Scalars
    - Gradient (Least Squares Cell-Based, Green Gauss Node Based)
    - Pressure (PRESTO!)
    - Density (Second Order Upwind)
    - Momentum (Second Order Upwind)
    - Volume Fraction (Geo-Reconstruct)
    - Turbulent Kinetic Energy (Second Order Upwind)
    - Turbulent Dissipation Rate (Second Order Upwind)
    - Energy (Second Order Upwind)
    - First Order Implicit Transient Formulation.

Monitors and animation files were also recorded for this case to test settings. Monitors included Mass and Volume Flow rate, y-velocity, Total, Absolute, Dynamic and Static Pressure, Total and Static Temperature

5.1.4.1.1. Results

The first simulations were run using a 10-meter pipe with a 6” diameter. After running multiple cases, it was observed that a containment tank that extended the exit

boundary condition above the pipe was necessary to allow the software to create the animation of riser unloading above the pipe. These simulations were run using a transient, pressure-based solver, using water as the liquid (continuous) phase and air as the gaseous phase at 70F temperature. Two different simulation types were attempted:

1- Predefined 4-liter gas bubble, with no initial velocity in the water column,

2- Continuous injection of air at 50 ft/min into a static column of water.

5.1.4.1.1.1. Predefined 4-liter gas

In this simulation, 4-lt of air was placed in the bottom of the 10-meter, 6-inch pipe. No initial velocity was defined, and compressibility was allowed. After multiple diverging trials, the simulation converged, and below are the results of this simulation. **Figure 5-1**displays the geometry and the phase diagram. It was also determined that the boundary condition at the outlet needs to be extended beyond the pipe outlet to view pipe unloading (overflow). For this reason, a containment tank was placed in the simulations. **Figure 5-2** displays the outlet mass flow rate of water and air, driven by the air expansion and migration. **Figure 5-3** displays the total and dynamic pressure at the outlet of the pipe. **Figure 5-4** displays the outlet volume flow rate of water and air. In the initial 10-seconds of the simulation, Figure 5-2,Figure 5-3, andFigure 5-4 demonstrate oscillating values. This oscillation was attributed to air compression that was not defined in the initial phase. The oscillating air mass flow rate and volume flow rate at the outlet demonstrate that air was being pulled into the pipe to fill the void created by the water compressing the air at the bottom of the pipe. The dynamic pressure graph in Figure 5-3 demonstrates the change

in pressure as well. The low-pressure values were due to the incorrect selection of mass-weighted average-pressure monitors.

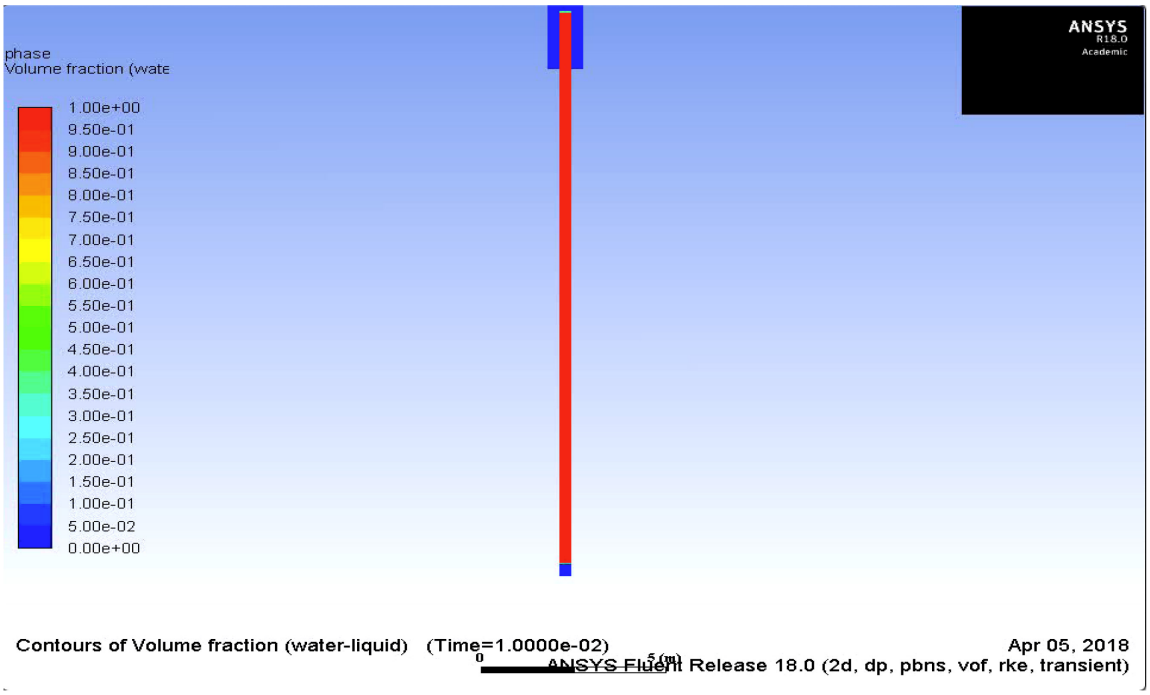

Figure 5-1—Initial Image of Phases (Water: Red, Air: Blue)

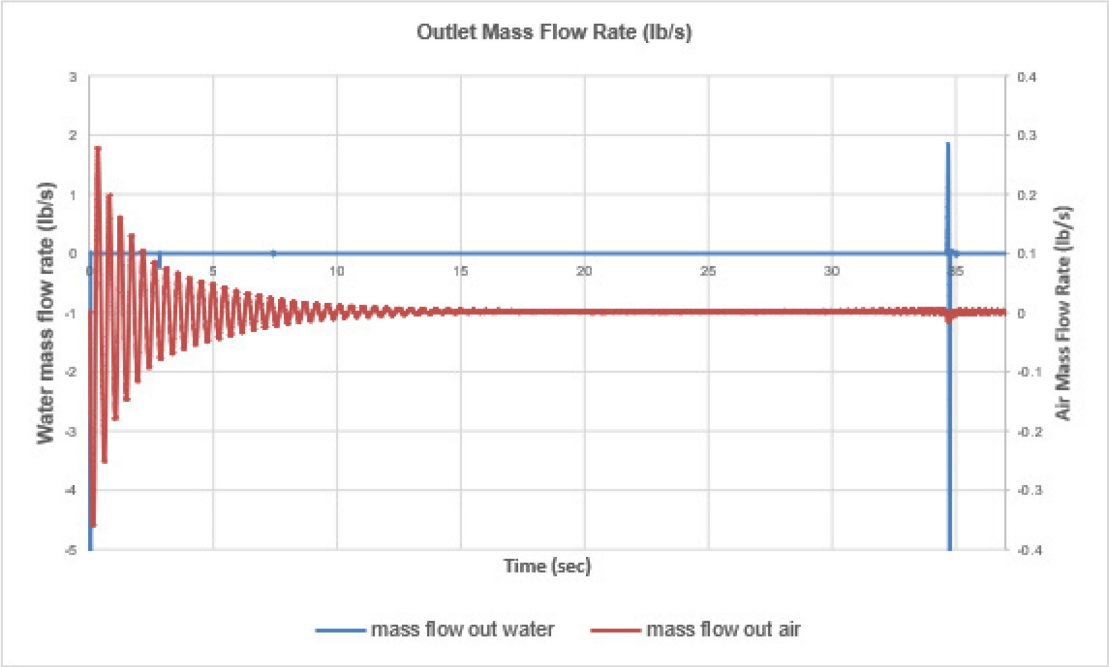

Figure 5-2—Outlet Mass Flow Rate vs. Time

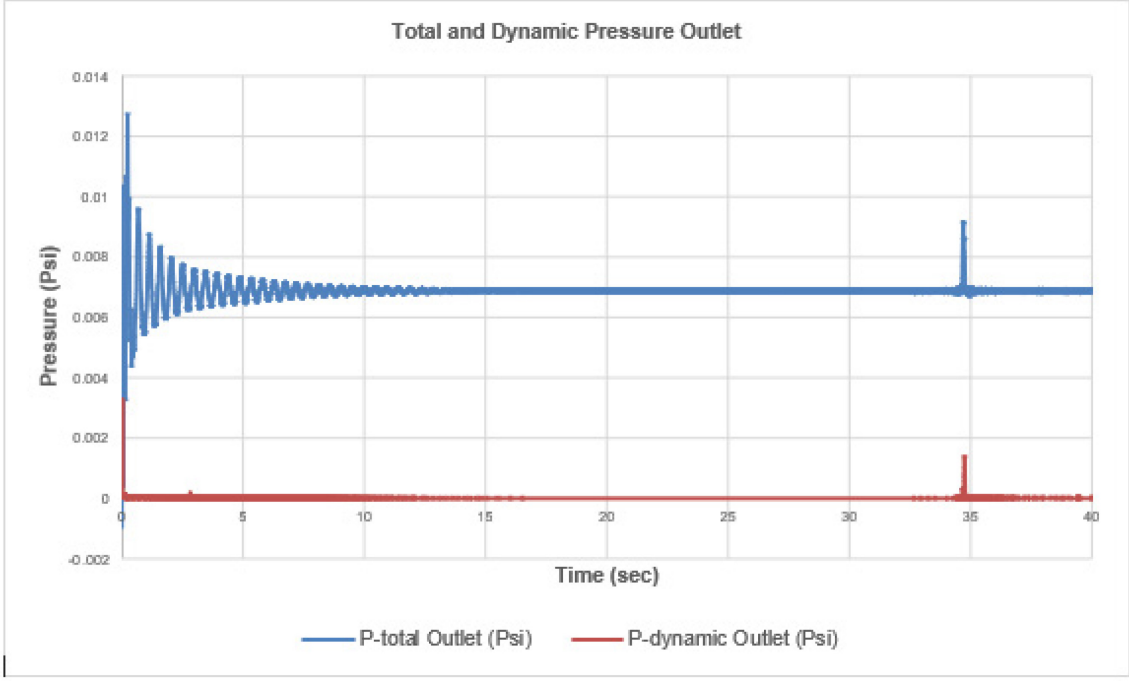

Figure 5-3—Total and Dynamic Pressure vs. Time

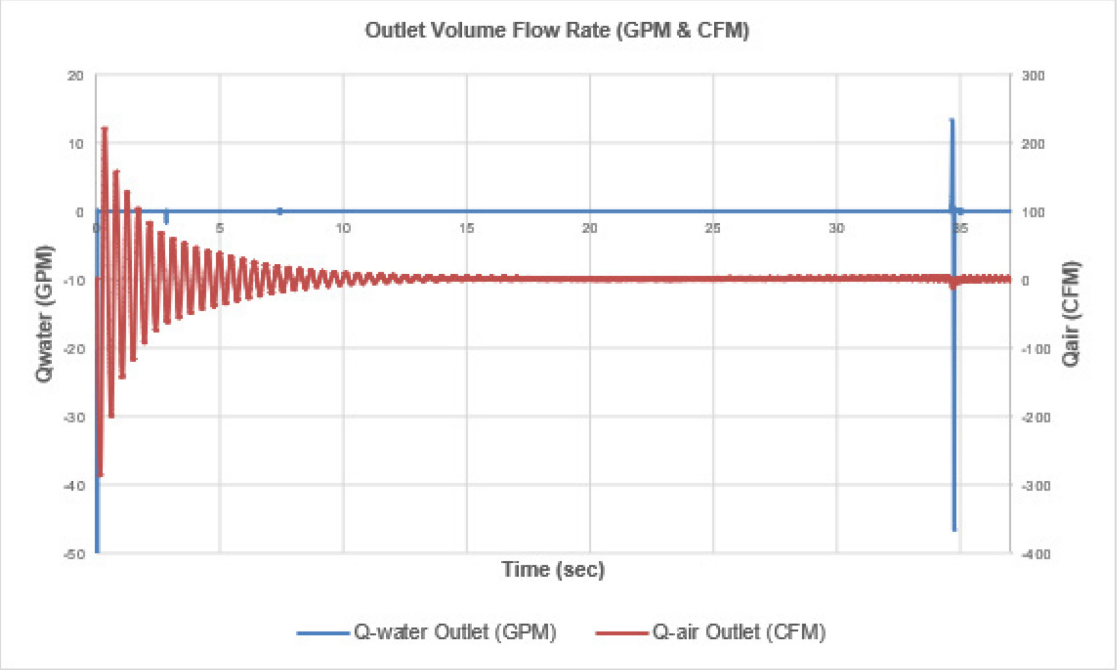

Figure 5-4—Outlet Volume Flow Rate vs. Time during continuous injection

5.1.4.1.1.2. 10 Meter Pipe with Continuous Air Injection at 58-ft/min

After convergence was achieved in the previous subsection, the rate was reduced to 58-ft/min. This trial was set up with the same settings as the previous trial. **Figure 5-5** displays the volume fraction contours of the phases and the geometry.

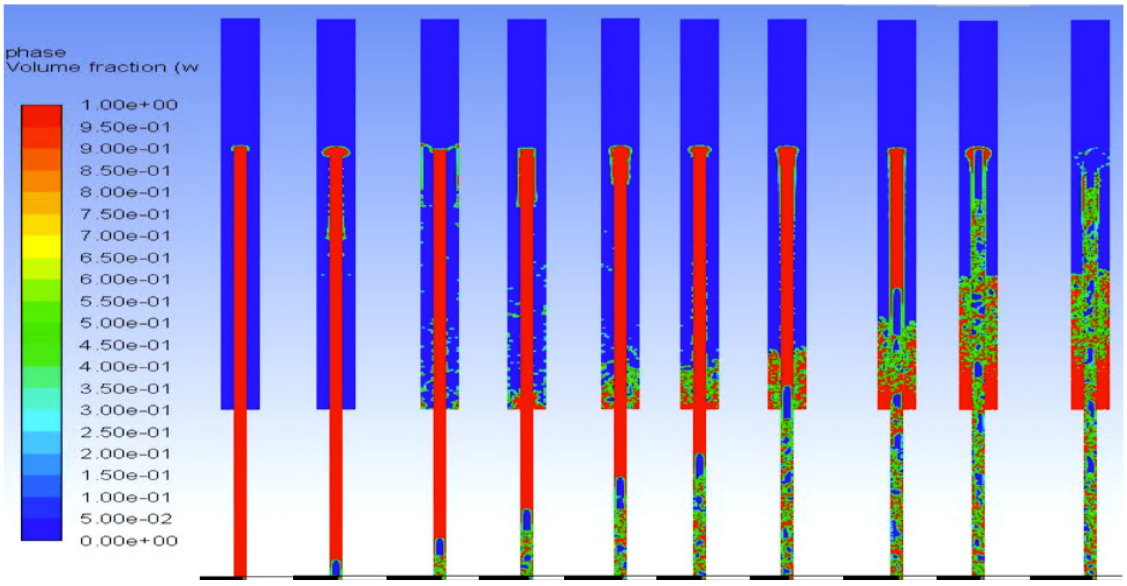

Figure 5-5—Image of Phases (Water: Red, Air: Blue)

Figures 5-6, **5-7**, **5-8**, **5-9**, and **5-10** demonstrate the dynamic pressure, total pressure, y-velocity, mass flow rate, and volume flow rate, respectively.

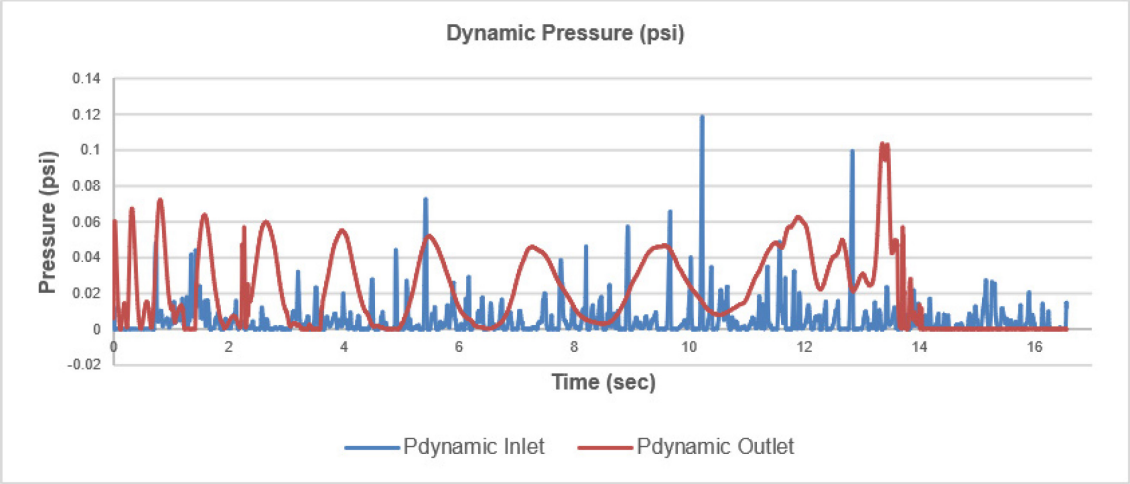

Figure 5-6— Dynamic Pressure (psi) vs. Time (sec)

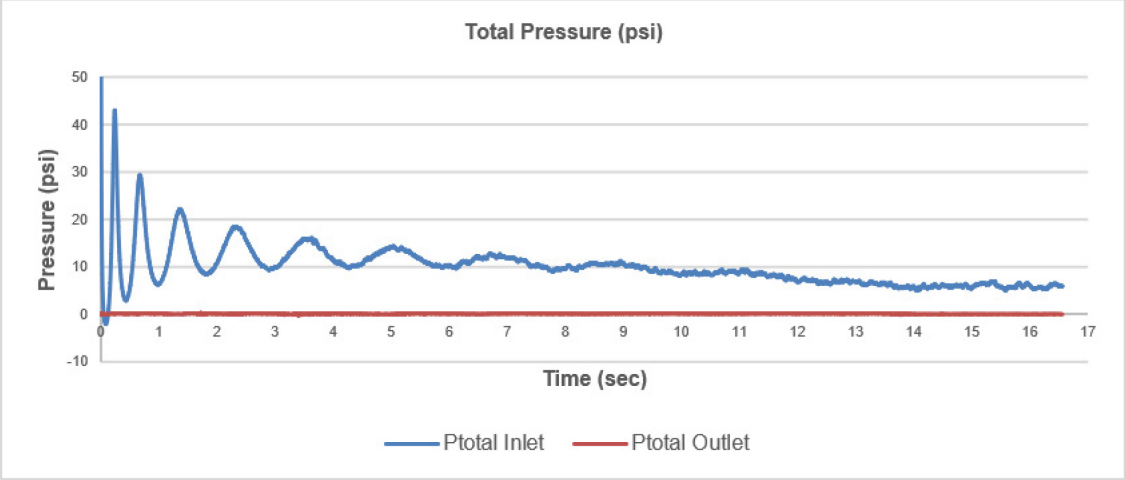

Figure 5-7—Total Pressure (psi) vs. Time (sec)

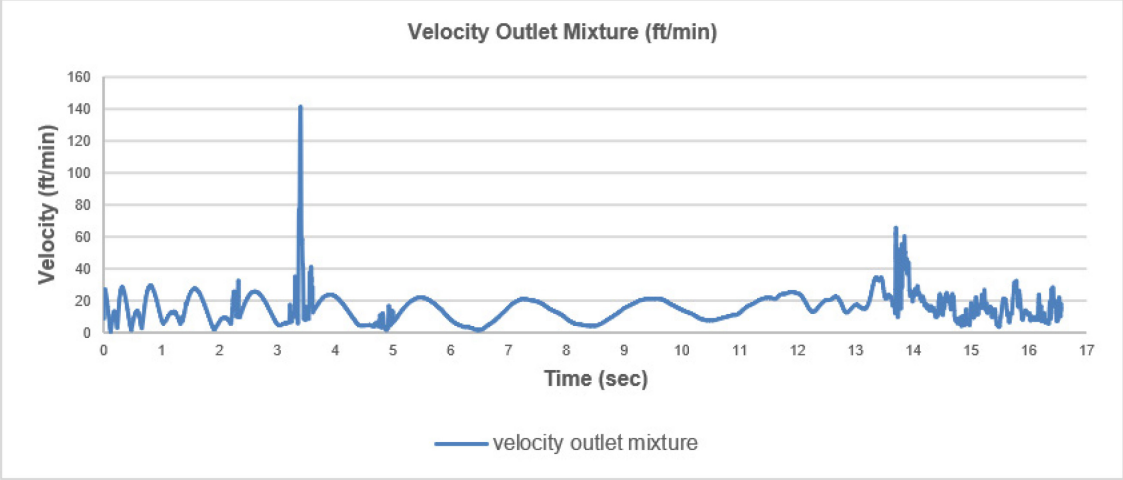

Figure 5-8—Outlet Mixture Velocity in the y-direction (ft/min) vs. Time (sec)

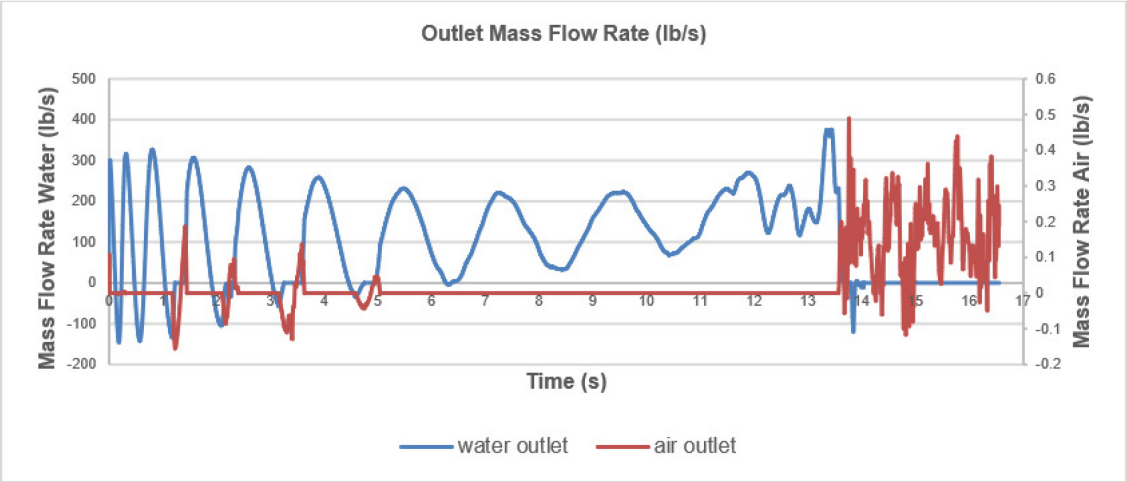

Figure 5-9—Outlet Mass Flow Rate vs. Time

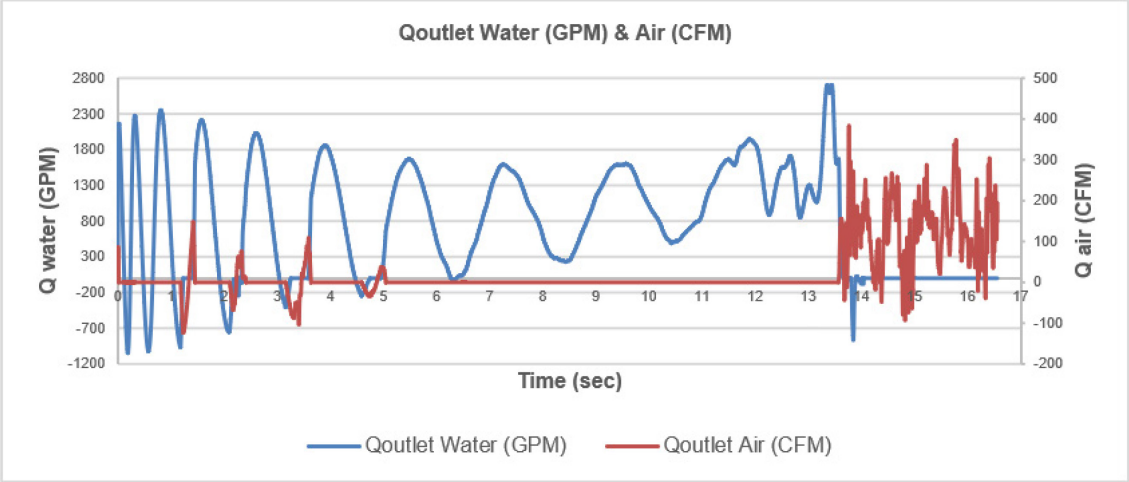

Figure 5-10—Outlet Volume Flow Rate vs. Time

As seen in **Figures 5-6**, **5-8**, **5-9**, and **5-10**, the continuous air injection causes a fluctuation or oscillation of the y-velocity, mass flow rate, and volume flow rate at the outlet.

5.1.4.2. Phase 2:

Phase 2 is presented in detail in chapter 6.

6. LARGER SCALE COMPUTATIONAL FLUID DYNAMICS ANALYSES[2]

6.1. 2-D Computational Fluid Dynamics Modeling of Riser Gas and Unloading in Various Pipe Diameters and Lengths

6.1.1. Abstract

Limited studies are available for modeling gas migration in risers. Outdated and small-scale models provide insufficient reliability, and a thorough mechanistic description of the problem is still not available. A significant part of the problem concerns understanding how pressure, temperature, liquid properties, and gas-liquid dynamics affect gas expansion during migration.

This paper provides information on Computational Fluid Dynamics (CFD) simulations performed on gas injections in three static and dynamic vertical fluid columns, with and without back pressure measuring 27-ft. and 330-ft. tall with 6, 12, 19.5 in. diameter. These CFD simulations analyzed the recorded gas expansion, change in pressure and temperature, and the gas volume fraction throughout the riser. In addition, these simulations also analyzed the change in flow rate, velocity, and the unloading effect at the inlet and outlet.

The 330-ft. pipe simulation demonstrated explosive unloading behavior with maximum discharge velocity and flow rate of over 2.8-ft./sec and 6617.5-GPM. The shorter pipes demonstrated relatively slower overflow. The case with a 330-ft. pipe also

[2] Reprinted with permission from "2-D Computational Fluid Dynamics Modeling of Riser Gas and Unloading in Various Pipe Diameters and Lengths" by Kaldirim, Omer, Kaldirim, Ebubekir, Geresti, Cameron, Manikonda, Kaushik, Schubert, Jerome J., Hasan, A. Rashid, 2020, Society of Petroleum Engineers/International Association of Drilling Contractors – Managed Pressure Drilling and Underbalanced Operations Conference and Exhibition, 1-24, Copyright 2020 SPE.

recorded a rapid change in temperature close to the top. Back pressure application at the surface minimized the effects of unloading and slowed down expansion.

6.1.2. Introduction

Gas migration in pipes is an important process to consider while drilling wells. Whether the well being drilled is on land or offshore, uncontrolled and undetected gas migration can cause serious consequences. Gas inside a well must be detected and controlled to prevent further influxes and a rapid expansion that can lead to a high flow discharge of mud from the well, called pipe/riser unloading. This unloading happened in the past in documented cases such as the 1984 Zapata Lexington (K. W. Blake 1986) and 2010 Macondo (CSB 2016) blow-outs on offshore vessels and on the 2018 Oklahoma Pryor Trust well on land (CSB 2019)

When the gas enters a well during drilling, it migrates up because of buoyancy and circulation. The gas bubble also expands because of pressure loss during this migration process. In an uncontrolled situation, the gas moves up and begins pushing mud out of the well. This process reduces the hydrostatic pressure in the well, leading to additional gas expansion. This interdependence between pressure loss and gas expansion creates a feedback loop where gas expansion is continuous and increases at a rapid rate. This rapid expansion becomes the driving force for the gas to travel up and push mud at even higher rates. This expansion process becomes explosive at a certain depth/pressure, leading to "rapid unloading of the well". Rapid unloading occurs due to the volume necessary in the well or riser for the gas bubble to occupy at the given pressure, is occupied by a mud column which is then suddenly ejected out of the well.

This rapid unloading process is critical to consider while drilling wells. A key driver for this process is that the well is full of mud, the gas is undetected, and the migration and expansion are uncontrolled. Recently this has become an important research subject for deep-water drilling and has resulted in multiple projects involving experimental and simulation modeling efforts.

Riser unloading involves uncontrolled gas migration and gas expansion. The gas migration part of this has been studied in lab-scale experimental apparatus and numerical simulations. For example, Rader et al. (1975) investigated the effects of bubble length, mud density and viscosity, surface tension, liquid velocity, and pipe deviation on gas migration and expansion. Their experiments discovered that applying back pressure slows down a rising gas bubble, and removing the back pressure allows the gas to expand significantly, which results in a greater rise velocity.

Johnson and White (1991) described studies performed in an inclinable 12-meter long, 200-mm pipe. The authors performed gas rise experiments using air with water and water-xanthan gum mixture. The results of the use of viscosifier demonstrated that gas rises faster in the viscosified water-xanthan gum solution than just in water.

Kaldirim and Schubert (2017) presented the results of experiments in a small-scale flow loop while circulating mud and simulating the pumped riser system. They studied the effects of a discharge pump on gas migration and expansion. Kaldirim and Schubert (2018) continued the work from the 2017 paper while using a vacuum pump to enhance the gas expansion ratio in the small-scale flow loop. They concluded that gas expansion

rates could be studied using small-scale clear pipes by applying a hard vacuum (1.9 psia.) at the top of the liquid.

Rommetveit and Olsen (1989) describe Larger scale gas migration experiments performed on the 2020-meter deep Ullrigg Research Well at the Rogaland Research Institute. These experiments involved tests with OBM and WBM. They investigated the effects of mud density and rheology, gas type, mud viscosity, inclination, solubility, surface tension while measuring pump strokes, pit gain, pit level, choke position, pressure, and liquid density. The main conclusion from these studies was that mud return rate was the most sensitive measurement significant for kick detection. In Hovland and Rommetveit (1992), the authors conducted tests on gas solubility. They discovered that gas solubility in OBM depended on the gas concentration, pump rate, pressure, and how long the gas remained in the well. They also concluded that gas migration was independent of density and that void fraction, inclination angle, surface tension, mud rheology, and viscosity had no significant effect on gas migration.

The software and numerical simulations performed on riser gas unloading are also essential to review and understand. Studies on the expansion part of this problem are slightly less ubiquitous but still well documented. For instance, Manikonda et al. (2019) presented comprehensive models for understanding gas kick migration and expansion in both water-based muds (WBM) and oil-based muds (OBM). Their semi-analytical model also included a procedure to account for kick solubility in OBM. They concluded that gas kicks in OBM are more insidious and difficult to detect at early stages, posing a greater

risk than kicks in WBM. However, their models only considered gas kicks in well annuli and not in risers.

Aarsnes et al. (2016) presented their mathematical model of riser gas on a single bubble case for conventional drilling, controlled mud level drilling, and back pressure managed pressure drilling systems. They validated their model using the 250 kg Nitrogen injection case on the Troll Well described in Hauge et al. (2015).

Kiran and Salehi (2018) describe their single bubble analytical model that incorporates real gas law, temperature, mud type, back pressure, solubility. They put significant consideration into the heat transfer, temperature, and solubility effects on riser unloading. They concluded that there is a difference in the unloading behavior for equal density and gas concentration in WBM and OBM.

In Gu et al. (2019), the authors describe their triple-mode constant bottom hole controller that can operate in pressure control, flow control, and solubility control modes. In addition, the authors demonstrated the ability of back pressure application to control gas kicks in OBM and maintain the gas in solution through the riser.

These studies provide important additions to literature and shed light on a very significant subject in deep-water drilling. It is imperative to maintain safe processes through all operations in this industry. We can achieve this only through conducting research and understanding the physics behind the limiting factors that can cause major incidents. In this context, these experimental, numerical, and analytical modeling studies provide a good understanding of riser gas. However, it is important to be cautious while scaling these results to field cases and evaluating the effects of the length, diameters, flow

rates, and temperatures. A simple extrapolation of pressure, temperature, flow rate results based on length and diameter may lead to significant errors. Thus, there is a need to connect these studies with larger diameters and lengths. This paper describes small and large diameter simulations performed at Texas A&M University to develop a riser gas model using commercial computational fluid dynamics (CFD) software.

CFD is a powerful tool used in many engineering fields and sciences to simulate complicated flow problems. Using CFD is beneficial because it combines mathematical methods and numerical methods to solve the Navier Stokes Equations. Navier Stokes equations are the governing equations of fluid flow. Navier stokes equations are supplemented by the conservation of mass and energy equations to solve a fluid flow problem.

Running CFD simulations before manufacturing pumps, aircraft, or any machinery that involves fluid flow eliminates the process of trial and error in experimentation. This improvement allows multiple simulations of a flow problem to be run to achieve maximum efficiency before manufacturing. Another benefit of running CFD simulations is that it can simulate cases that are impractical to recreate in a controlled environment. Riser unloading is one such case, and CFD can be an invaluable tool in further researching this phenomenon. However, running riser unloading experiments in the field is complex, risky, and expensive. So, CFD was used to supplement existing experimental studies and to simulate large-scale cases.

6.1.3. Modeling Approach

CFD is a dynamic fluid flow analysis tool that uses numerical methods to solve the Navier-Stokes equations on a given geometry with pre-defined boundary conditions and parameters.

The process of CFD analysis begins with defining the problem. The problem includes the geometry, the fluid(s), and the boundary conditions. After defining the problem, the proper fluid mechanics and fluid dynamics equations are applied and solved by discretizing the geometry and defining the numerical method to solve the problem using the selected equations. Finally, the solution produces certain data types such as pressure, temperature, energy, flow rate, velocity, etc., by placing monitors to collect data.

The goal of this study is to develop a riser gas model through experimentation and simulation. The simulation aspect of the research was to be validated through small-scale experiments at the Dual Gradient Drilling and Tower Lab at Texas A&M University. The validation process is in progress, and the initial models were scaled up for pipe flow studies and presented in this paper.

Smaller-scale simulations provide rapid results compared to large-scale simulations. However, CFD analysis can be time-consuming for large and complicated geometries and require great memory and computing power. Therefore, the CFD simulations were computed using the Texas A&M University, High-Performance Research Computing (HPRC) Center to reduce computing time and support larger models.

6.1.4. Methodology

The first step in this study was to develop the geometries for each length and diameter. The smaller scale geometries were prepared based on the flow loop in the DGD Lab at Texas A&M University. This paper also presents the results of the larger model 330-ft. loop, with 12-in and 19.5-in. diameters. The primary focus of this paper is surrounding the 330-ft., 12-in., and 19.5-in. cases.

6.1.4.1. Description of the geometries

This paper categorizes the CFD simulations by their length and diameters. All simulations presented are for pipe flow with no drill pipe. Gas was injected at the bottom in the vertical direction. The discharge line was placed at the top horizontally with no vertical exit to simulate a rotating control device (RCD). A single case (330-ft. length, 19.5-in. diameter) was presented with vertical discharge to simulate unloading in a conventional open-top riser system. The following figure provides a simple cad drawing of the geometry used for these simulations.

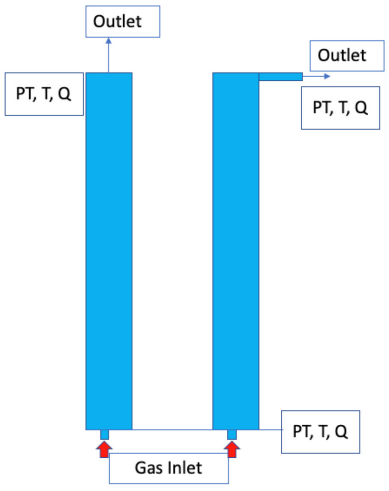

Figure 6-1— Schematic of the 2-D Cad model used for the simulations. Reprinted from (Kaldirim et al. 2020)

Figure 6-1 displays the schematic of the 2-D cad model used for the simulations. The left side of displays the schematic for the open-top riser with upward discharge, and the right side displays the schematic for the closed riser using a rotating control device (RCD) with discharge in the x-axis. The pipe length, diameter, and inlet and outlet diameters were varied based on the dimensions provided in **Table 6-1**.

Simulation	Length (ft.)	Pipe Diameter (in.)	Inlet Diameter (in.)	Discharge Diameter (in.)	Direction
1-a and 1-b	27	6	2	2	x-axis
3-a and 3-b	330	12	2	2	x-axis
3-c and 3-d	330	19.5	4	8	x-axis
3-e and 3-f	330	19.5	4	19.5	y-axis

Table 6-1—Dimensions for geometries used for CFD analysis. Reprinted from (Kaldirim et al. 2020)

The 27-ft. length was selected to mimic the existing Dual Gradient Drilling lab and Tower Labs. The simulation results presented in this paper were limited to adhere to a readable paper length. The 330-ft. section was an attempt at scaling up simulations.

Each simulation ran with atmospheric conditions at the outlet, then again with back pressure. The simulator injected specific quantities of gas into a static mud column through the inlet at 50-ft./min. The mud used in these simulations was an 11-ppg., 22-cp water-based mud, with air as the gaseous phase. The model followed the Peng-Robinson density model to incorporate real gas properties. The simulator ran two cases per simulation, one with atmospheric pressure and another with back pressure at the outlet.

Simulation	Length (ft.)	Pipe Diameter (in.)	Injection Volume (bbl.)	Average Injection Rate ($ft.^3$/min.)	Back Pressure (psig.)
1-a	27	6	0.3	27.3	0
1-b	27	6	0.27	27.4	30
3-a	330	12	5.1	24.9	0
3-b	330	12	5.1	24.8	200
3-c	330	19.5	5.6	51.4	0
3-d	330	19.5	5.6	52	200
3-e	330	19.5	5.1	53.5	0
3-f	330	19.5	28.7	50.6	0

Table 6-2—Injection volume and outlet pressure. Reprinted from (Kaldirim et al. 2020)

Table 6-2 displays the total injected gas volume and back pressure for each simulation. To simulate multiphase flow, the model used the Volume of Fluid multiphase flow model, which allows no void and requires the addition of two-phase fractions in any grid in the geometry to equal 1. The energy equation was utilized to observe temperature changes and heat transfer. The k-omega turbulence model was chosen to model the turbulent behavior of gas migration, sudden gas expansion, and the near-wall condition when a gas bubble occupies near the total diameter. The simulations were run with a pressure-based transient solver, using a simple Pressure-Velocity coupling method.

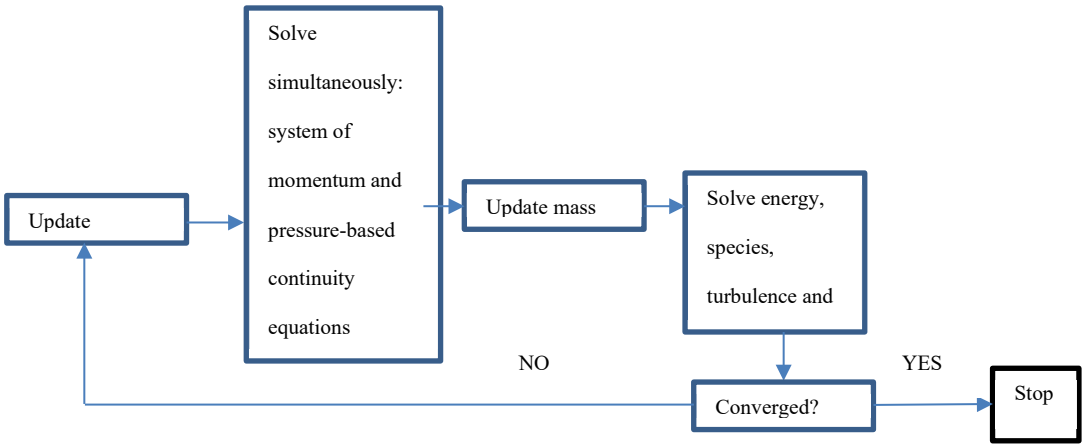

Figure 6-2—Pressure Based Solver Method. Modified from (ANSYS® 2017)

Figure 6-2 displays the iterative pressure-based solver method. For all simulations in this paper, the time-step size selected was 0.1- and 0.01-seconds with 100 iterations per time step.

6.1.5. Results and Analysis

Mud discharge rate, gas flow rate, gas fraction, total pressure, and total temperature data were collected for each simulation. This section presents this data, plotted for flow time. The simulations were run as described in the previous section using Ansys Fluent.

6.1.5.1. Simulation 1-a: 27-ft., 6-in., 0-psig. back pressure (with RCD)

This section presents the results and discussion for the 27-ft. 6-in. diameter case. In this case, 0-psig back pressure was applied, and the mud return was through a side outlet at the very top to simulate an RCD. The total injected gas volume was 0.3 bbl at a rate of 27.3 ft3/min.

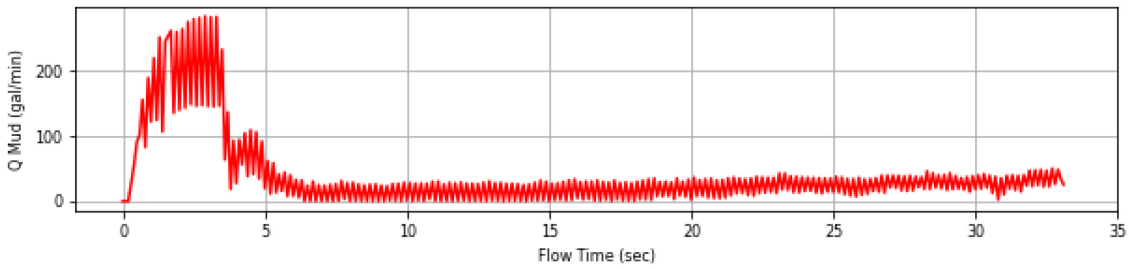

Figure 6-3—Mud discharge rate vs. Flow time (Total Pit Gain=0.51 bbl.). Reprinted from (Kaldirim et al. 2020)

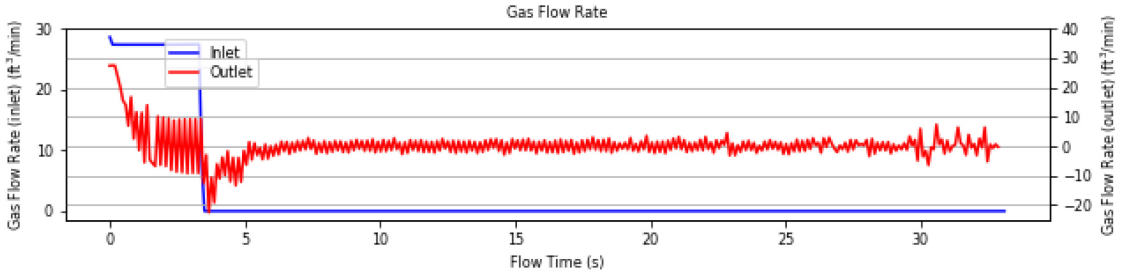

Figure 6-4—Gas Flow Rate vs. Flow Time at inlet and outlet (Total injected gas volume=0.3 bbl.). Reprinted from (Kaldirim et al. 2020)

Figure 6-3 & **Figure** 6-4 display the mud discharge rate and gas flow rates versus flow time. This injection resulted in a total pit gain of 0.51 bbl, indicating a small amount of gas expansion. However, since the liquid was not replaced into the flow loop, this resulted in only a limited pit gain.

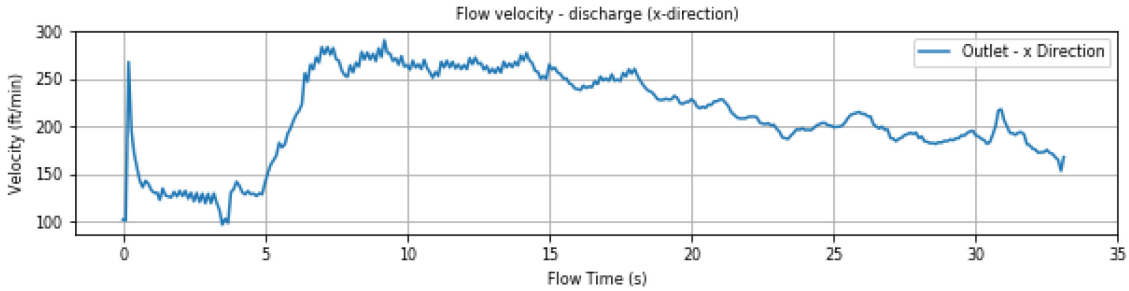

Figure 6-5— Discharge Velocity vs. Flow Time. Reprinted from (Kaldirim et al. 2020)

Figure 6-5 displays the cross-sectional velocity through the 2-in. outlet. The maximum velocity recorded at the discharge was 269.63-ft/min. This high velocity was due to the high discharge flow rate and the outlet's reduced diameter (2-in).

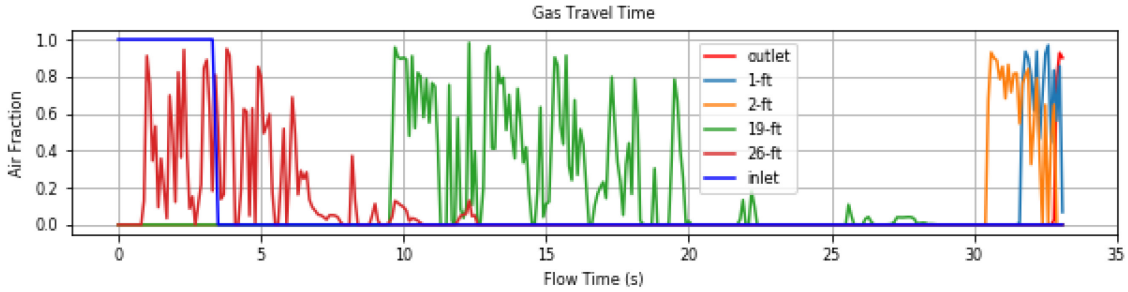

Figure 6-6—Air Volume Fraction vs. flow time. Reprinted from (Kaldirim et al. 2020)

The influx travel time is presented in **Figure 6-6**. Monitors were placed along the geometry to monitor the location of the top of the gas. As the gas reached a sensor a monitor, the phase fraction value for the air increased and fluctuated between 0 and 1. This fluctuation is because the VOF multiphase flow model does not allow for a void. The entire volume of the system must be occupied by at least one fluid. Monitors were placed at the inlet, outlet, and 1-, 2-, 19- and 26-ft depths.

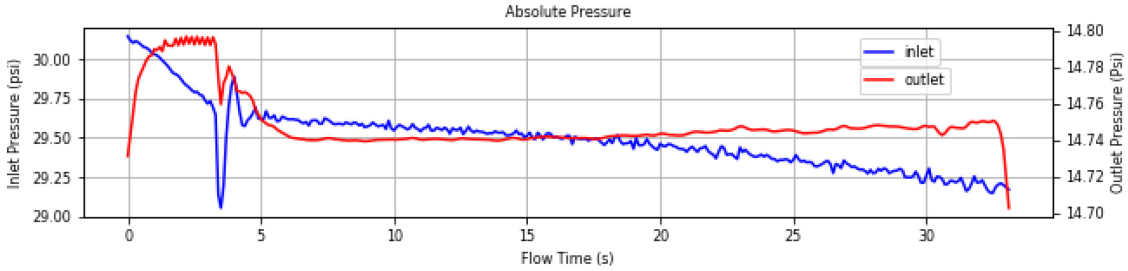

Figure 6-7—Absolute Pressure vs. Flow Time. Reprinted from (Kaldirim et al. 2020)

Figure 6-7 conveys the variation in inlet and outlet pressures as gas moves through the riser. A slight pressure drop is observed at the inlet as the gas influx expands and

pushes mud out of the pipe. However, this simulation does not demonstrate significant changes as the gas expansion was negligible.

6.1.5.2. Simulation 1-b: 27-ft. 6-in. 30-psig. back pressure

The figures below display the results for the 27-ft. 6-in. diameter case. In this case, 30-psig back pressure was applied, and the flow was through a side outlet at the top to simulate an RCD. The total injected gas volume was 0.27-bbl at a rate of 27.4-ft^3/min.

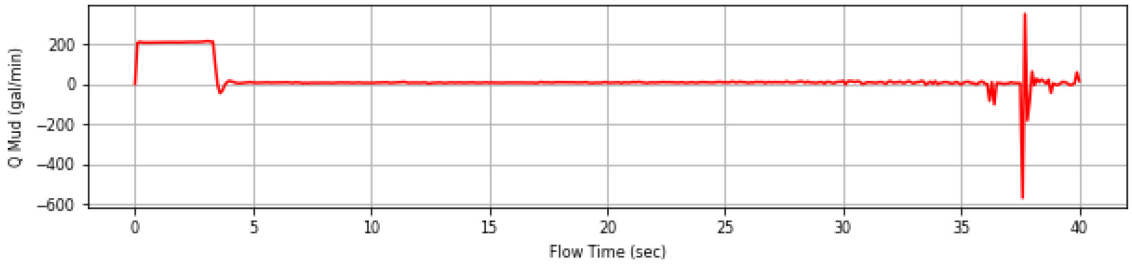

Figure 6-8— Mud discharge rate vs. Flow time (Total Pit Gain=0.34-bbl). Reprinted from (Kaldirim et al. 2020)

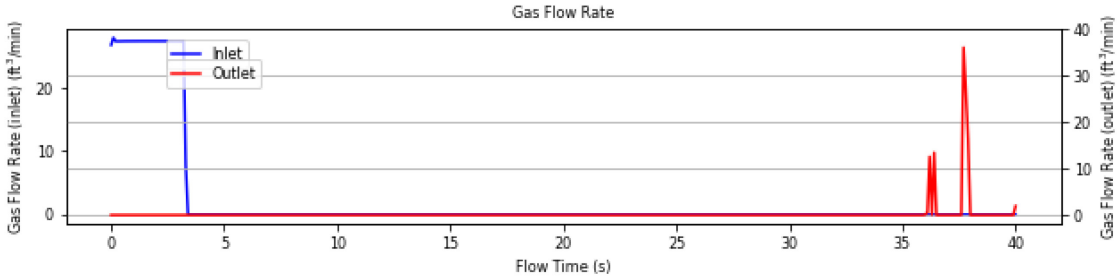

Figure 6-9— Gas Flow Rate vs. Flow Time at inlet and outlet (Total injected gas volume=0.27-bbl). Reprinted from (Kaldirim et al. 2020)

Figure 6-8 & Figure 6-9 display the mud discharge rate and gas flow rates versus flow time. This injection resulted in a total pit gain of 0.3-bbl, indicating a slight expansion due to the applied back pressure.

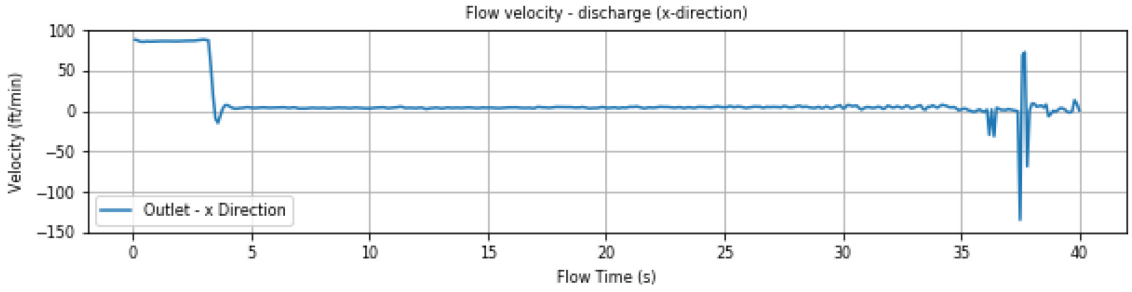

Figure 6-10— Discharge Velocity vs. Flow Time. Reprinted from (Kaldirim et al. 2020)

The cross-sectional velocity through the 2-in. outlet is displayed in **Figure 6-10**. The maximum discharge velocity measured was 88.2-ft/min, much less than the velocity in the previous section (269.6-ft/min). This is due to limiting gas expansion by applying the 30-psig. back pressure.

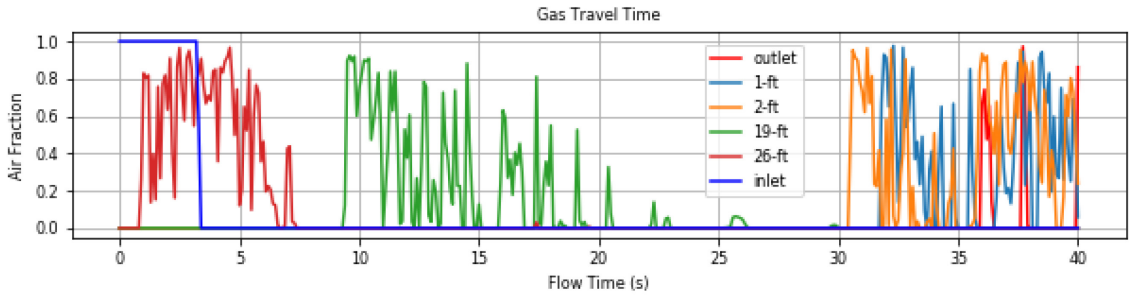

Figure 6-11— Air Volume Fraction vs. flow time. Reprinted from (Kaldirim et al. 2020)

The influx travel time can be observed in **Figure 6-11**. Monitors were placed at the inlet, outlet, and 1-, 2-, 19- and 26-ft depths to measure gas volume fraction. The gas bubble reached the outlet in approximately 33 seconds.

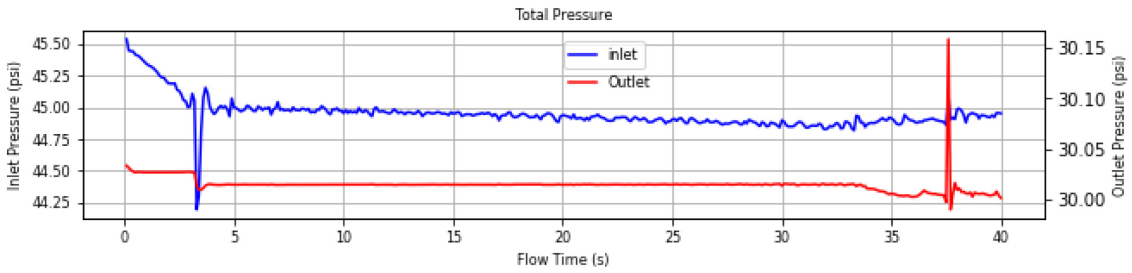

Figure 6-12—Total Pressure vs. flow time. Reprinted from (Kaldirim et al. 2020)

Figure 6-12 displays the total pressure versus flow time for the inlet and outlet. The inlet pressure remains relatively constant after the air injection stops, then decreases slightly after the gas begins leaving the system between 35- and 40-seconds.

6.1.5.3. Simulation 3-a: 330-ft 12-in 0 psig back pressure

The figures below display the results for the 330-ft,12-in diameter case. In this case, 0-psig back pressure was applied, and the flow was through a side outlet at the top to simulate an RCD. The total injected gas volume was 5.1-bbl at a rate of 24.9-ft^3/min.

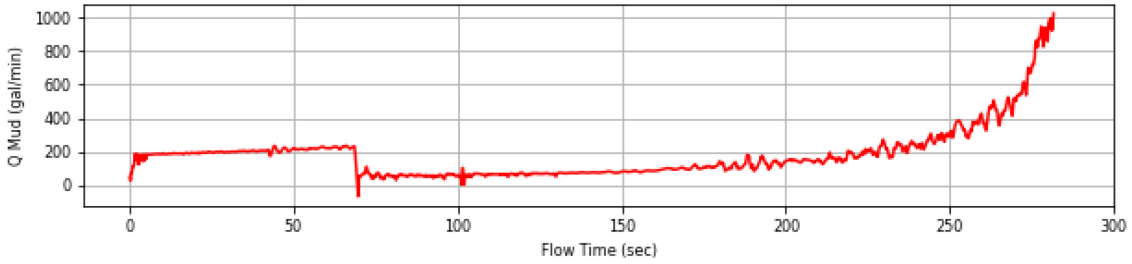

Figure 6-13— Mud discharge rate vs. Flow time (Total Pit Gain=20.25-bbls.). Reprinted from (Kaldirim et al. 2020)

Figure 6-13 presents the mud discharge rate as gas was injected into the flow loop in the first 70 seconds. The sudden drop in flow rate is due to terminating the gas injection, while the increased flow rate after 70-sec is due to the expanding gas pushing mud out of the riser. The total pit gain due to the 5.1 bbl gas influx was 20.25 bbls.

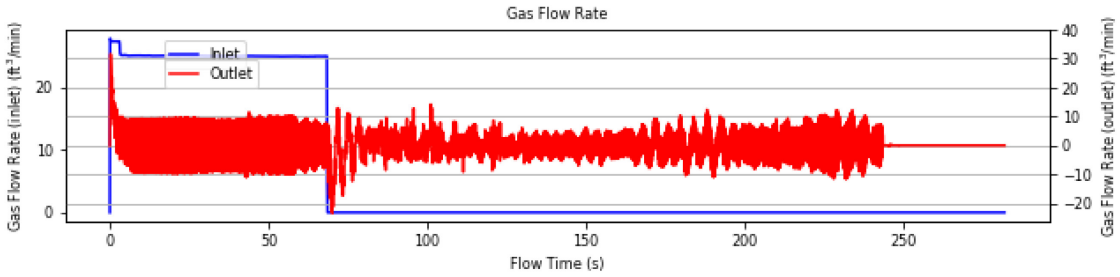

Figure 6-14— Gas Flow Rate vs. Flow Time at inlet and outlet (Total injected gas volume= 5.1-bbl). Reprinted from (Kaldirim et al. 2020)

Figure 6-14 also supports the data plotted in Figure 6-13. Again, the scatter in data on the outlet side is due to the gas leaving the outlet and backflow.

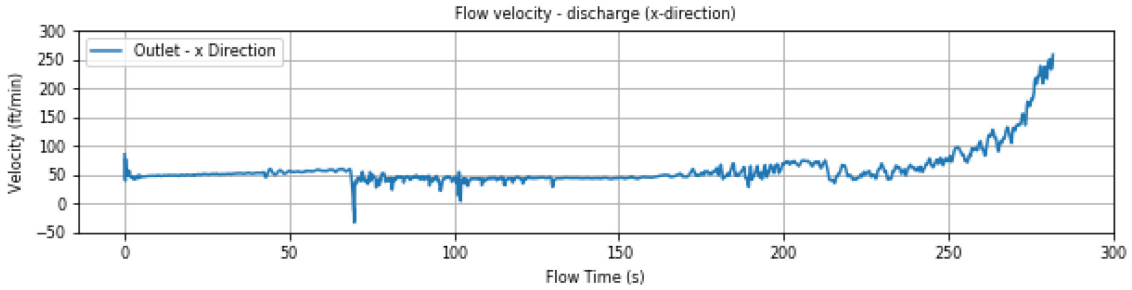

Figure 6-15— Discharge Velocity vs. Flow Time. Reprinted from (Kaldirim et al. 2020)

The maximum discharge velocity at the outlet, as shown in **Figure 6-15**, is approximately 258-ft./min when the gas is exiting the discharge line.

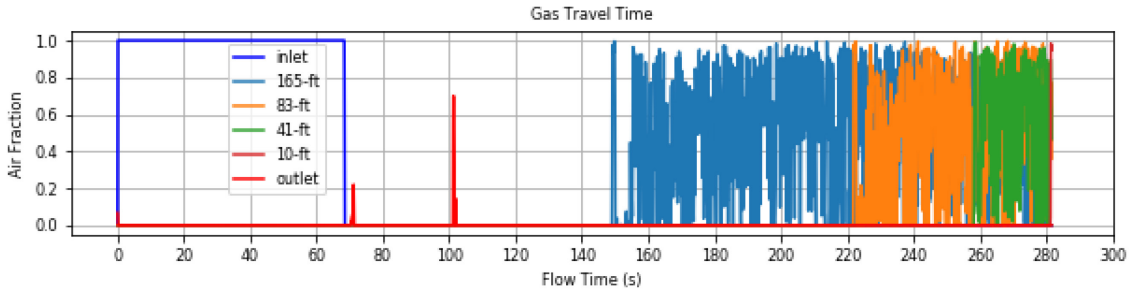

Figure 6-16—Air Volume Fraction vs. flow time. Reprinted from (Kaldirim et al. 2020)

Figure 6-16 displays the time when the gas phase reaches the sensors placed along the riser in the simulation. As seen in Figure 6-16, the gas traveled 150-seconds to reach the riser midpoint, an additional 70 seconds to reach near the top quarter of the riser (82.5-ft.), and an additional 40-seconds to reach 41-ft. from the top of the riser. The remaining two sensors at 10-ft. and outlet took place rapidly, indicating acceleration of the gas migration and expansion. One crucial observation is that the gas bubble became dispersed and extended along half the riser length as it began to exit the riser.

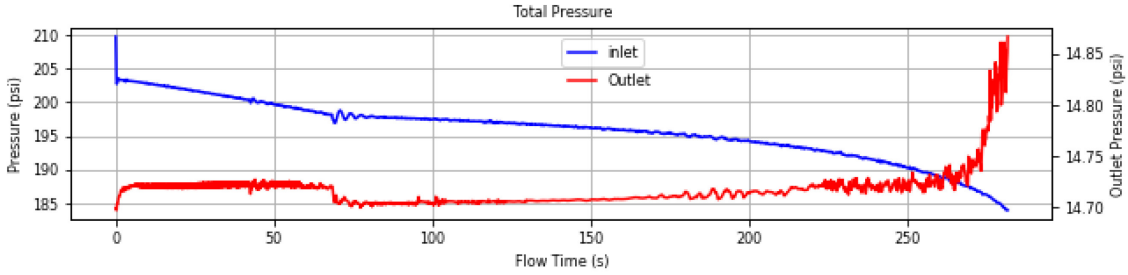

Figure 6-17—Total Pressure vs. Flow Time. Reprinted from (Kaldirim et al. 2020)

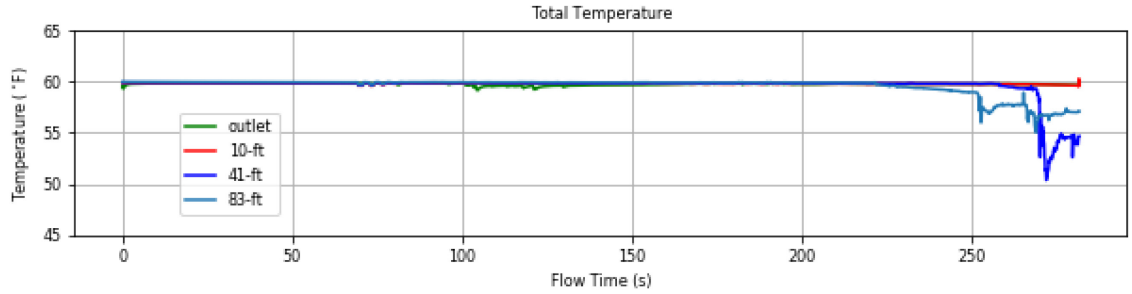

Figure 6-18—Total Temperature vs. Flow Time. Reprinted from (Kaldirim et al. 2020)

Figure 6-17 demonstrates the declining inlet pressure with increasing discharge rate and the gas volume in the riser, while on the outlet, the pressure rises due to the rising friction. Finally, in **Figure 6-18**, a temperature decrease of nearly 10 °F is observed near the top section of the riser. This temperature drop is significant for this simulation due to the size of the riser.

6.1.5.4. Simulation 3-d: 330-ft 12-in 200 psig back pressure

The figures below display the results for the 330-ft. 12-in. diameter case. In this case, 200-psig back pressure was applied, and the flow was through a side outlet at the very top to simulate an RCD. The total injected gas volume was 5.1 bbl at a rate of 24.8 ft^3/min.

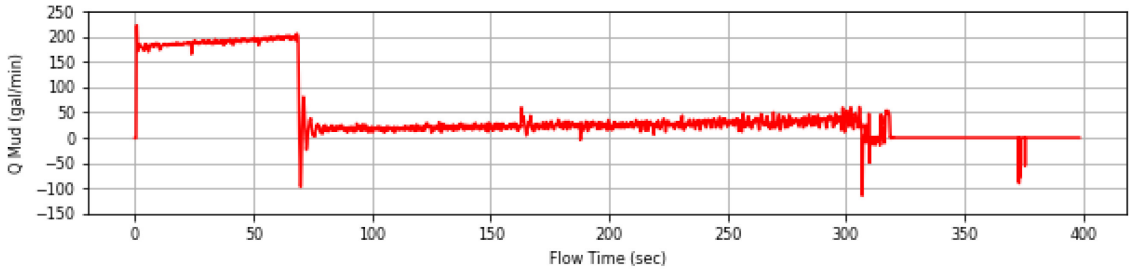

Figure 6-19—Mud discharge rate vs. Flow time (Total Pit Gain=7.5 bbls). Reprinted from (Kaldirim et al. 2020)

In this case, gas injection led to a total pit gain of 7.5-bbls. The mud discharge rate over time is presented in **Figure 6-19**. The negative values in this figure indicate that mud was pumped back into the riser to maintain the 200-psig surface back pressure.

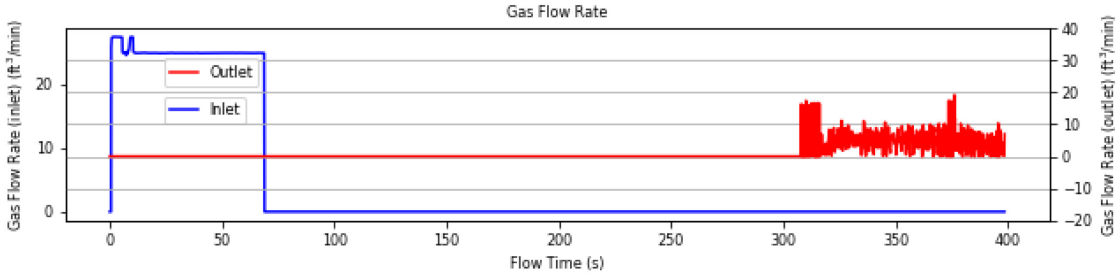

Figure 6-20— Gas Flow Rate vs. Flow Time at inlet and outlet (Total injected gas volume= 5.1 bbl). Reprinted from (Kaldirim et al. 2020)

Figure 6-20 displays the gas flow rate at the inlet and outlet. The outlet data demonstrates 0-ft^3/min until the first gas bubble reaches the outlet at approximately 308 seconds.

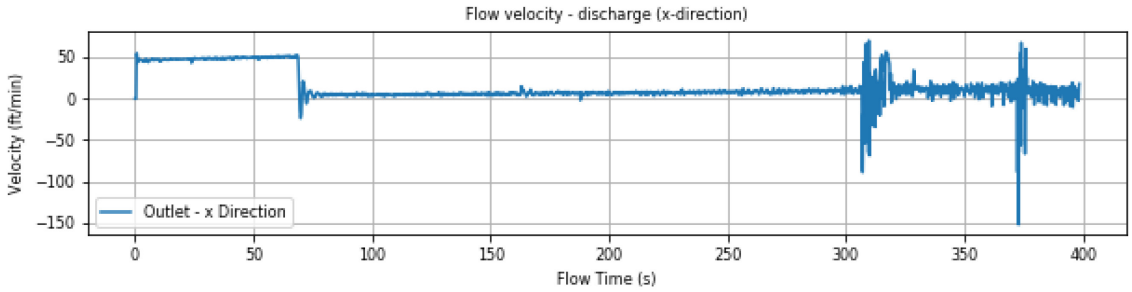

Figure 6-21— Discharge Velocity vs. Flow Time. Reprinted from (Kaldirim et al. 2020)

Figure 6-21 displays the discharge velocity through the 2-in side outlet. The negative values follow the trend in Figure 6-19 and indicate backflow to maintain the 200-psig surface back pressure.

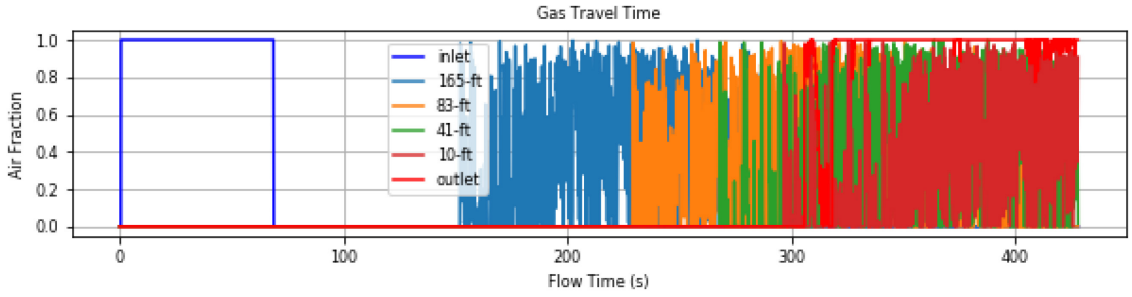

Figure 6-22—Air Volume Fraction vs. flow time. Reprinted from (Kaldirim et al. 2020)

Figure 6-22 presents the air volume fraction, where the gas travel time can be observed. Monitors placed on the riser at the inlet, outlet, and 10-, 41-, 83- and 165-ft help monitor the location of the top of the gas. In this case, the gas bubble reached the midpoint (165-ft) at 150 seconds. The first bubble reached the outlet at approximately 308 seconds.

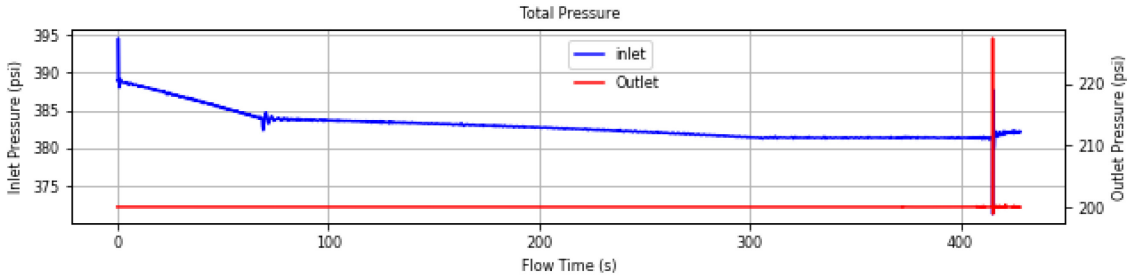

Figure 6-23— Total Pressure vs. Flow Time. Reprinted from (Kaldirim et al. 2020)

The Total Pressure graph presented in **Figure 6-23** presents a slight decrease in pressure at the inlet as the gas bubble enters and expands as it pushes mud out of the well. The total pressure drop observed at the inlet was less than 15-psi. The sudden pressure increase at the outlet after 400-seconds was due to the attempt to maintain a full riser and 200-psi back pressure.

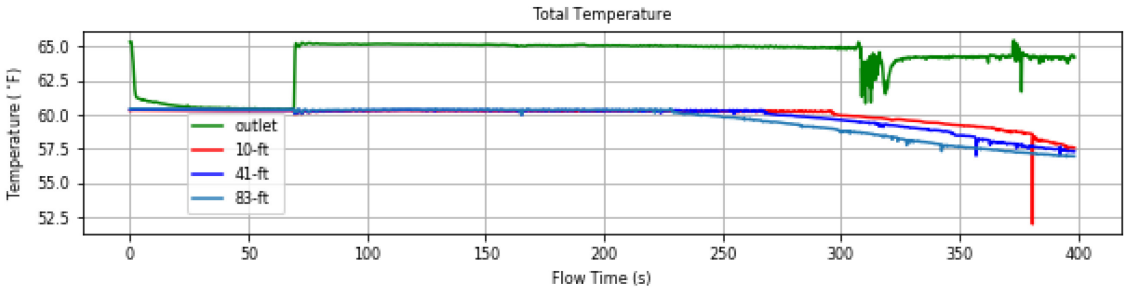

Figure 6-24—Total Temperature vs. Flow Time. Reprinted from (Kaldirim et al. 2020)

Figure 6-24 demonstrates temperature drop as the gas leaves the riser. However, the temperature drop is not as significant as in the previous case.

6.1.5.5. Simulation 3-d: 330-ft., 19.5-in., 0 psig. back pressure

This section presents the results for the 330-ft. 19.5-in. diameter case. In this case, 0-psig back pressure was applied, and the flow was through a side outlet at the very top to simulate an RCD. The total injected gas volume was 5.6 -bbl at a rate of 52 ft^3/min.

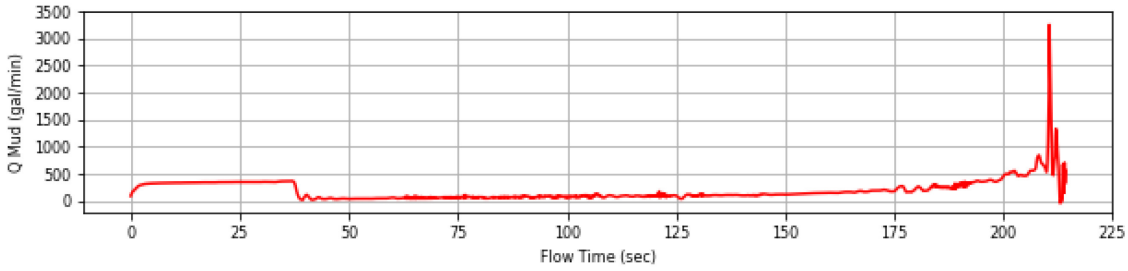

Figure 6-25—Mud discharge rate vs. Flow time (Total Pit Gain=16.7 bbl.). Reprinted from (Kaldirim et al. 2020)

The injection of 5.6-bbl of gas into the risers results in a 16.7-bbl pit gain. The first gas bubble reaches the outlet at 210-seconds. The discharge rate graph is presented in **Figure 6-25**. The maximum discharge rate from the 8-in side outlet at the top of the riser was recorded as 3250.8-GPM.

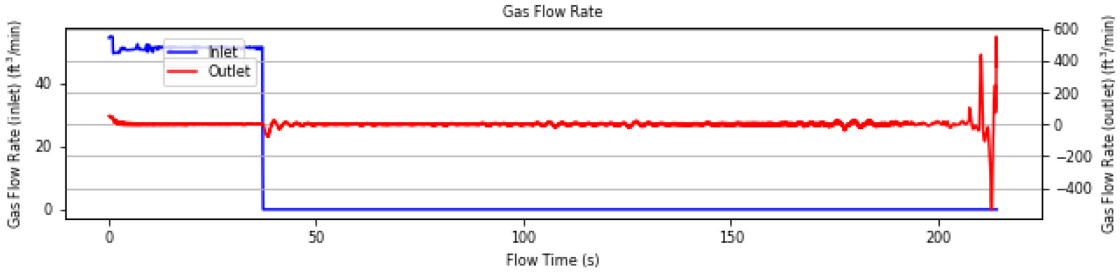

Figure 6-26— Gas Flow Rate vs. Flow Time at inlet and outlet (Total injected gas volume= 5.6 bbl.). Reprinted from (Kaldirim et al. 2020)

Figure 6-26 displays the pit gain and gas flow rates versus flow time. This gas injection was terminated at 37 seconds. The first gas bubble reached the outlet at 210 seconds.

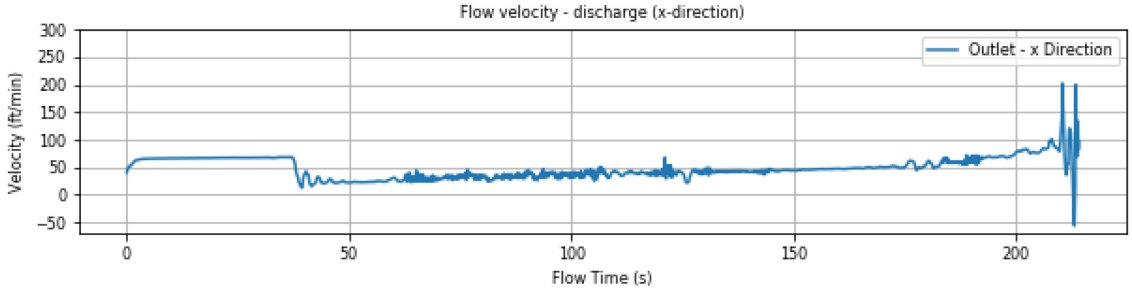

Figure 6-27— Discharge Velocity vs. Flow Time. Reprinted from (Kaldirim et al. 2020)

Figure 6-27 displays the velocity in the x-direction at the outlet. The velocity follows the discharge rate graph in Figure 6-25.

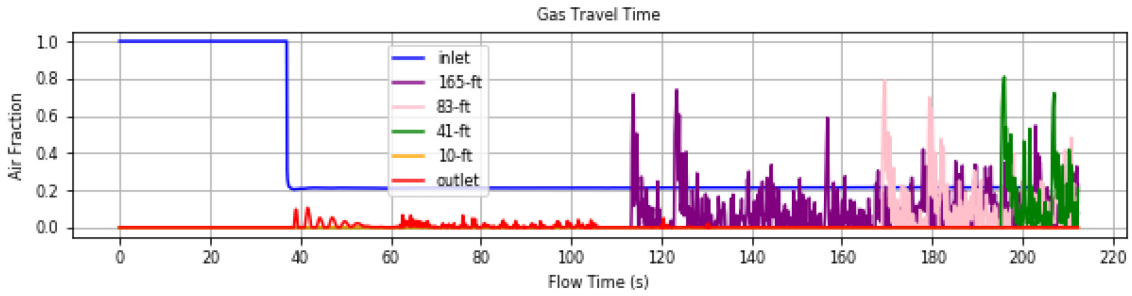

Figure 6-28—Air Volume Fraction vs. flow time. Reprinted from (Kaldirim et al. 2020)

Figure 6-28 displays the air volume fraction where the influx travel time and the length of the dispersed gas-mud column can be calculated using this graph. As seen in the graph, even when the first gas bubble reaches the outlet, the bottom of the gas extends below the midpoint (165-ft) of the riser.

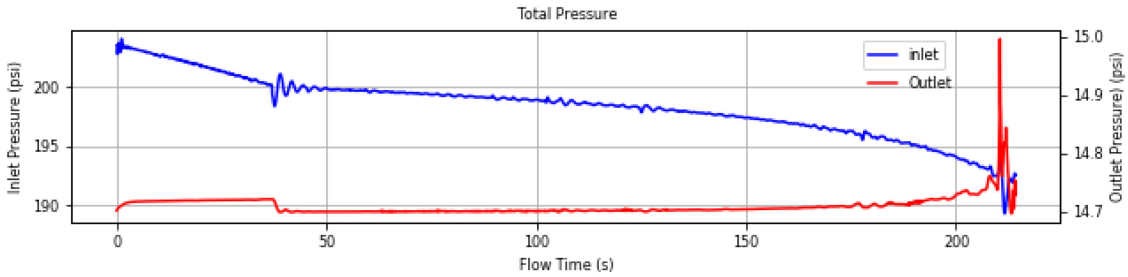

Figure 6-29— Total Pressure vs. Flow Time. Reprinted from (Kaldirim et al. 2020)

Figure 6-29 displays a declining total pressure at the inlet due to discharging mud and increasing gas volume, while the pressure at the outlet begins rising after 175-sec. The pressure at the inlet dropped approximately 15-psi due to mud being removed from the riser.

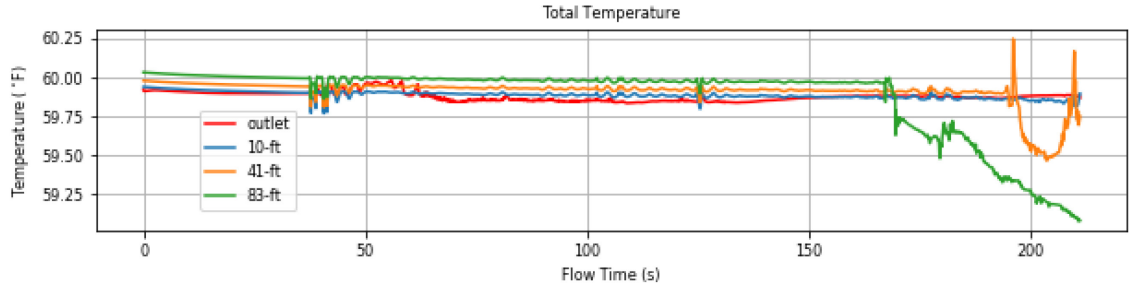

Figure 6-30—Total Temperature vs. Flow Time. Reprinted from (Kaldirim et al. 2020)

Figure 6-30 presents the total temperature versus flow time graph. This simulation did not yield a significant temperature change.

6.1.5.6. Simulation 3-d: 330-ft. 19.5-in. 200 psig. back pressure (with RCD)

This section presents the results for the simulation of a 330-ft 19.5-in riser with 200-psig back pressure applied at the top. The flow at the outlet was rotated to the x-axis into an 8-in outlet. A total of 5.1-bbl. of gas was injected at the bottom of the riser at a rate of 53.5-ft^3/min.

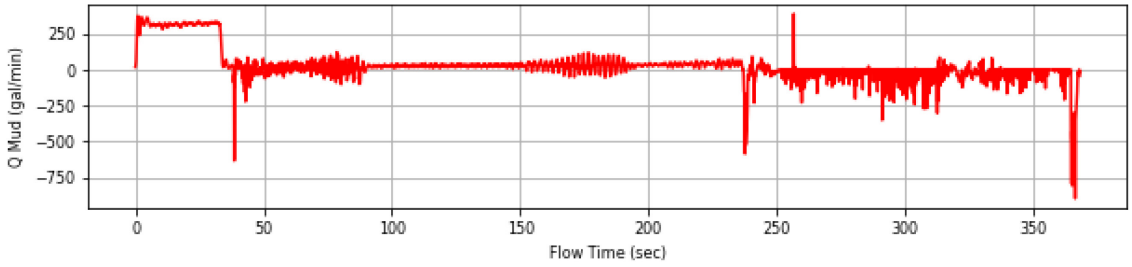

Figure 6-31—Mud discharge rate vs. Flow time (Total Pit Gain= 7.97 bbl.). Reprinted from (Kaldirim et al. 2020)

The mud discharge rate is presented in **Figure 6-31**, where 5.1-bbl of gas influx resulted in a total pit gain of 7.97 bbl. The maximum discharge rate recorded was 224.2-gpm, significantly lower than the same case with no back pressure presented in the previous section.

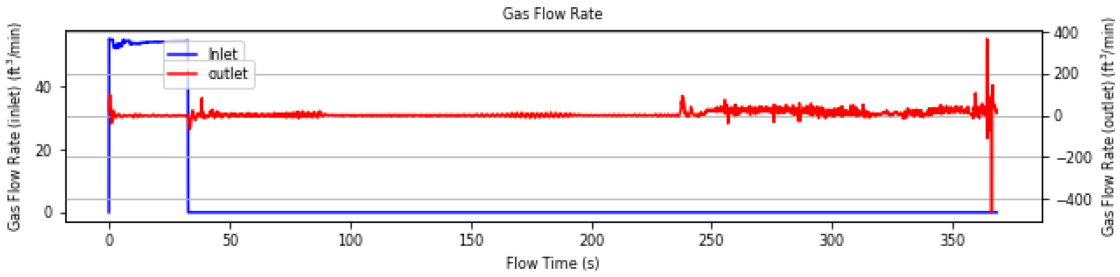

Figure 6-32— Gas Flow Rate vs. Flow Time at inlet and outlet (Total injected gas volume= 5.6 bbl.). Reprinted from (Kaldirim et al. 2020)

Figure 6-32 presents the gas flow rate at the inlet and outlet, with the first gas bubble arriving at the outlet at 235 seconds. The figure demonstrates that the 200-psig surface back pressure provided control over the gas expansion and riser unloading. **Figure**

6-33 displays the velocity through the 8-in. side outlet at the top of the riser, displaying lower values than the previous simulation.

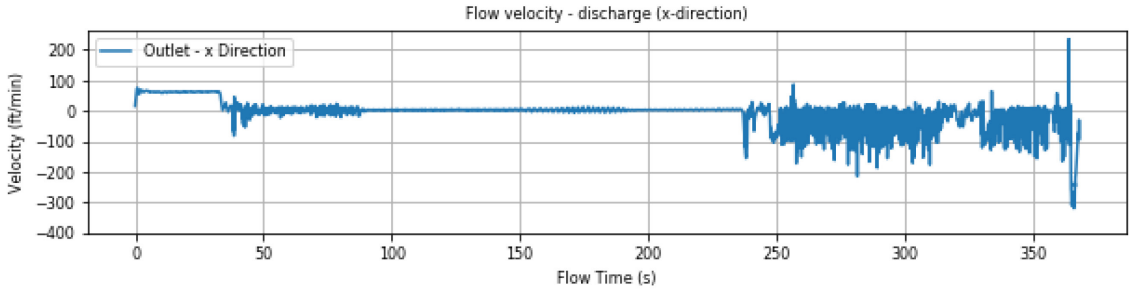

Figure 6-33— Discharge Velocity vs. Flow Time. Reprinted from (Kaldirim et al. 2020)

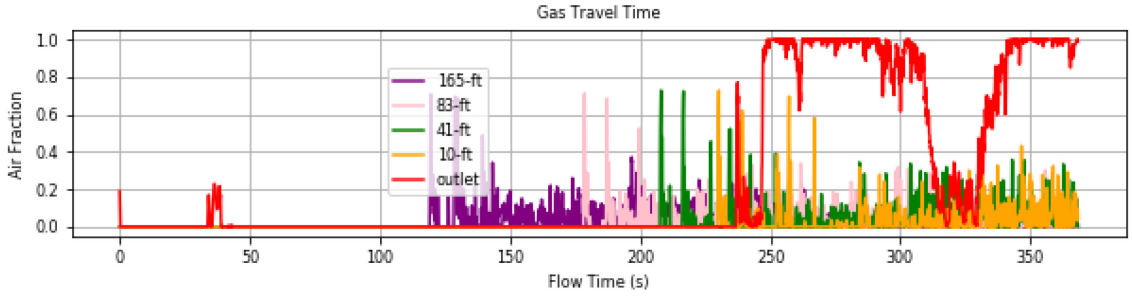

Figure 6-34—Air Volume Fraction vs. flow time. Reprinted from (Kaldirim et al. 2020)

Figure 6-34 displays the air volume fraction with flow time. As with the previous section, the influx travel time can be calculated using this graph. The gas leaving the riser is observed in this graph. This graph also provides an observation of the length of the dispersed gas-mud column through the riser.

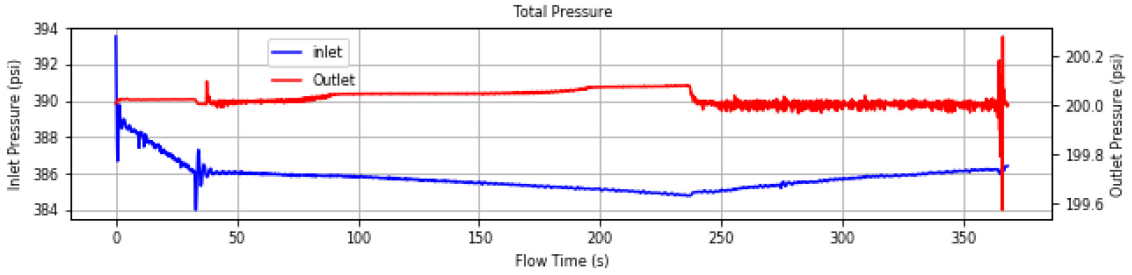

Figure 6-35— Total Pressure vs. Flow Time. Reprinted from (Kaldirim et al. 2020)

Figure 6-35 presents the total pressure data, where the pressure drop observed at the inlet occurs as the gas bubble approaches the outlet of the riser. The surface back pressure system mitigates the pressure drop by filling the riser with mud from the outlet, causing the pressure to go up again. **Figure 6-36** displays the temperature graph, where no significant change occurs.

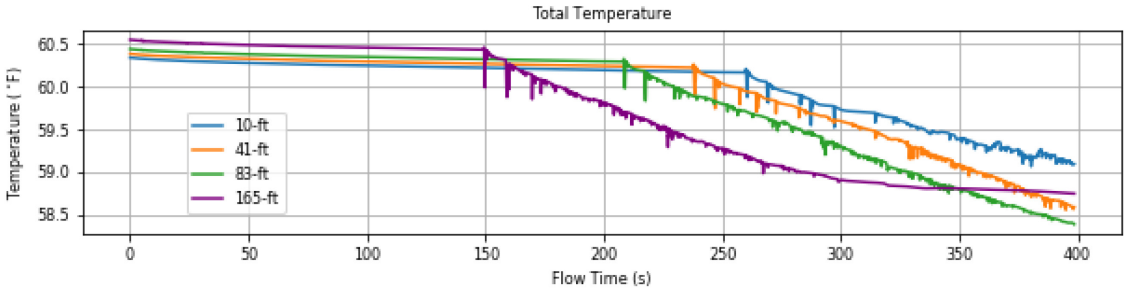

Figure 6-36—Total Temperature vs. Flow Time. Reprinted from (Kaldirim et al. 2020)

6.1.5.7. Simulation 3-e: 330-ft 19.5-in 0 psig back pressure (open top riser)

This section presents the results and discussion for the simulation where a 5-bbl gas influx was injected into an open-top riser at 53.5 ft^3/min. The travel time for the bubble was approximately 211-seconds. The total pit gain recorded due to injection and expansion was 16.1-bbls with a maximum discharge rate of 1433.82-gpm. **Figure 6-37** displays the discharge rate data.

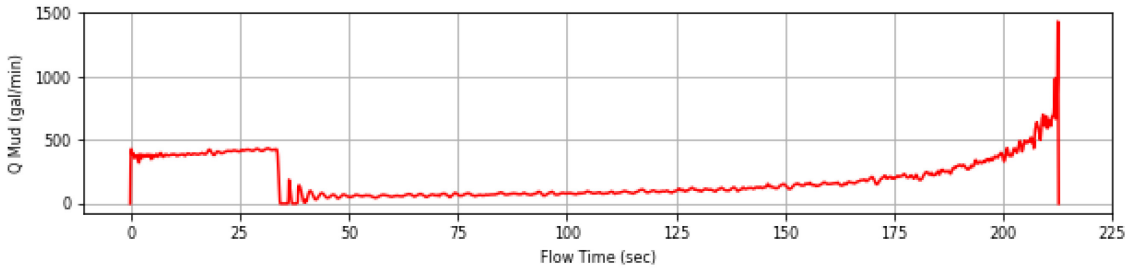

Figure 6-37—Mud discharge rate vs. Flow time (Total Pit Gain= 16.1 bbl.). Reprinted from (Kaldirim et al. 2020)

Figure 6-38 displays the gas flow rate for the inlet and the outlet. As seen in the figure, when the gas injection is terminated at 36-seconds, the outlet fluctuates. Then with the migrating and expanding gas influx, the mud discharge rate begins to rise, as shown in Figure 6-37.

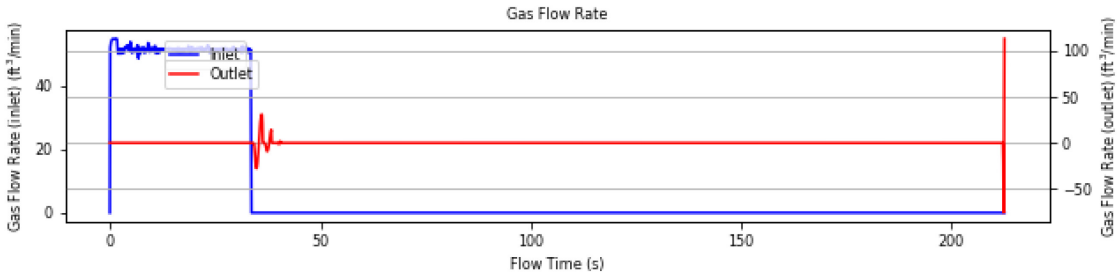

Figure 6-38— Gas Flow Rate vs. Flow Time at inlet and outlet (Total injected gas volume= 5.1 bbl.). Reprinted from (Kaldirim et al. 2020)

Figure 6-39 captures the flow velocity at the outlet, which demonstrates the same trend as Figure 6-37 & Figure 6-38. The maximum discharge velocity, in this case, was 204-ft/min.

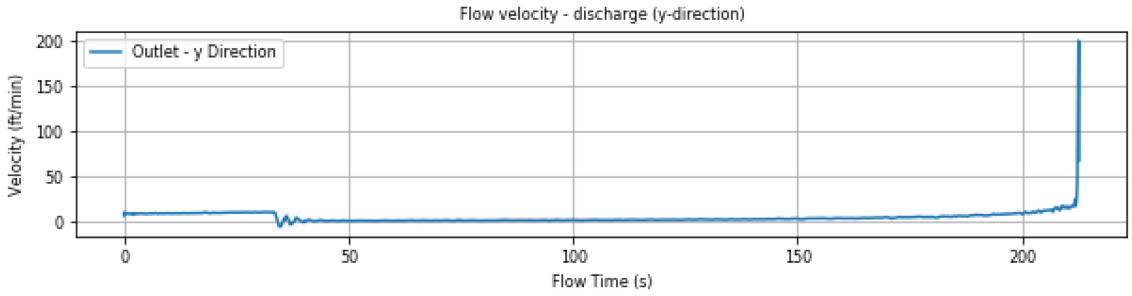

Figure 6-39— Discharge Velocity vs. Flow Time. Reprinted from (Kaldirim et al. 2020)

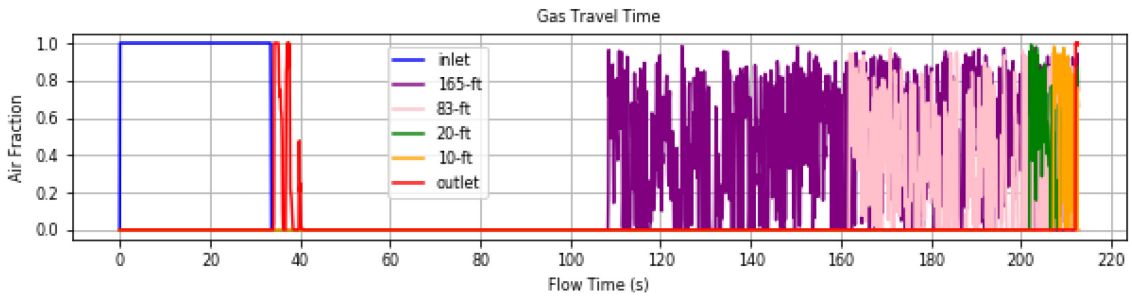

Figure 6-40—Air Volume Fraction vs. flow time. Reprinted from (Kaldirim et al. 2020)

Figure 6-40 & **Figure** 6-41 display the air volume fraction for the monitors placed at the inlet, outlet, and 10-, 20-, 83-, and 165-ft depths. The first gas bubble arrives at the midpoint (165-ft.) at approximately 107 seconds and 83-ft. at 160 seconds. Figure 6-41 displays the last 14 seconds of Figure 6-40 to observe the gas travel time in the top 20-ft of the riser.

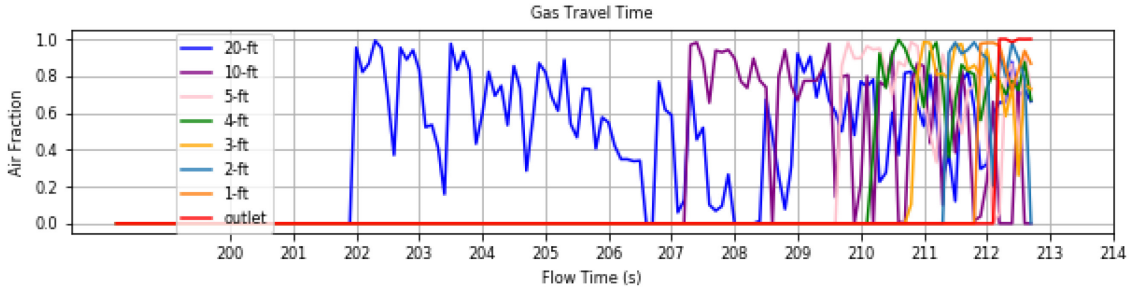

Figure 6-41—Air Volume Fraction vs. flow time. Reprinted from (Kaldirim et al. 2020)

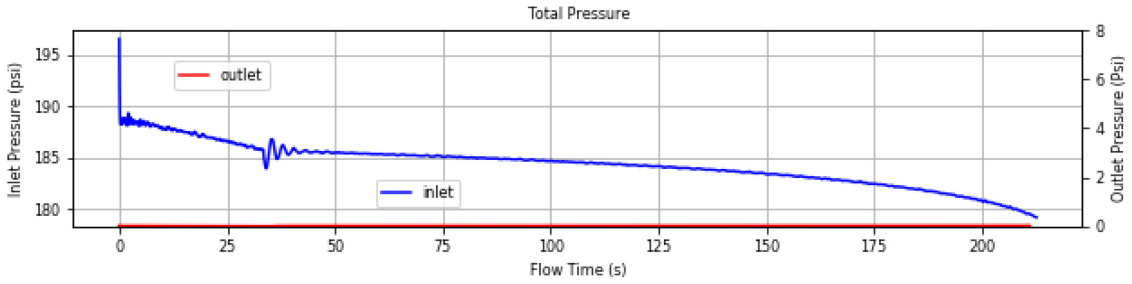

Figure 6-42— Total Pressure vs. Flow Time. Reprinted from (Kaldirim et al. 2020)

Pressure decrease at the outlet is observed in **Figure 6-42** as the 5.1-bbl gas bubble injection and expansion cause mud to be discharged from the riser. In this case, there is a temperature drop, although the temperature at the riser inlet, outlet, and surroundings were maintained at 65-°F. The temperature drop is displayed in **Figure 6-43**

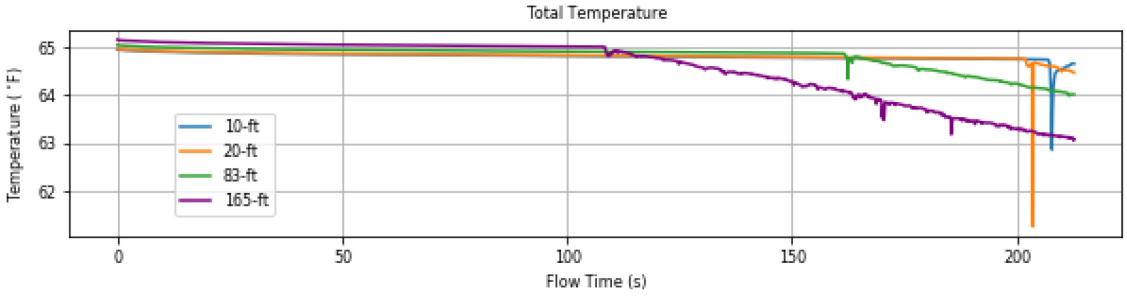

Figure 6-43—Total Temperature vs. Flow Time. Reprinted from (Kaldirim et al. 2020)

6.1.5.8. Simulation 3-f: 330-ft 19.5-in 0 psig back pressure (open top riser)

The section presents the results and discussion for a case where the BOP is open, and gas continuously enters the riser. In this case, 0-psig back pressure was applied at the surface, and the flow was through the top of the riser to demonstrate unloading in conventional open-top risers. Thus, gas was continuously injected at 50.6-ft^3/min until the gas reached the outlet. The total injected gas volume was 28.7 bbl.

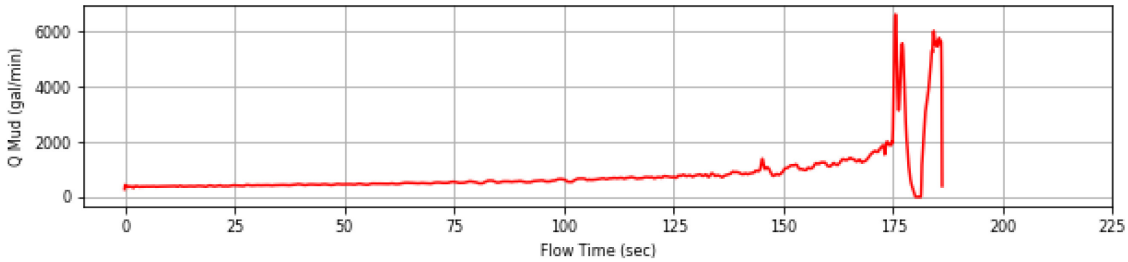

Figure 6-44—Mud discharge rate vs. Flow time (Total Pit Gain=60.7 bbl.). Reprinted from (Kaldirim et al. 2020)

As seen in **Figure 6-44**, the well began discharging mud as soon as the gas injection was initiated. Thus, the well discharged a total mud volume of 60.7 bbl. of mud in 187 seconds. The maximum discharge rate was measured as 6617.5-GPM.

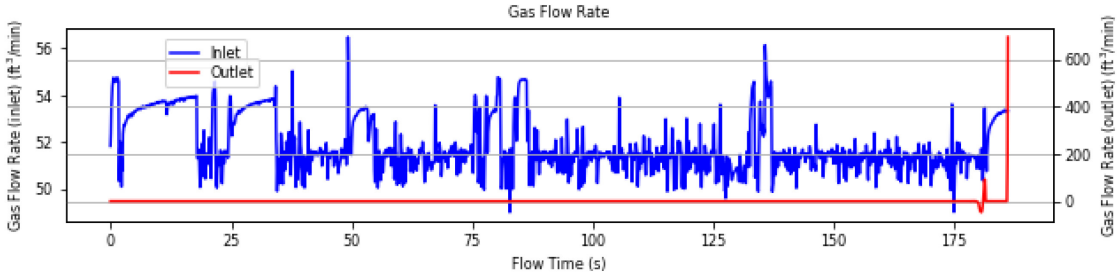

Figure 6-45— Gas Flow Rate vs. Flow Time at inlet and outlet (Total injected gas volume= 28.7 bbl.). Reprinted from (Kaldirim et al. 2020)

Figure 6-45 displays the gas injection and gas discharge rate from the well. This figure also demonstrates that the first gas bubble reached the outlet at approximately 180 seconds.

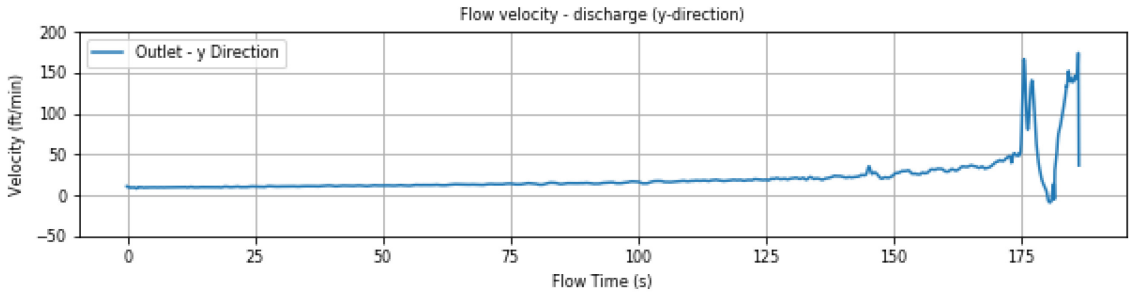

Figure 6-46— Discharge Velocity vs. Flow Time. Reprinted from (Kaldirim et al. 2020)

Figure 6-46 follows the trends of Figure 6-44 with the discharge velocity maximizing as the first gas bubble reached the top of the riser. The maximum velocity recorded at the outlet was 173.94-ft/min.

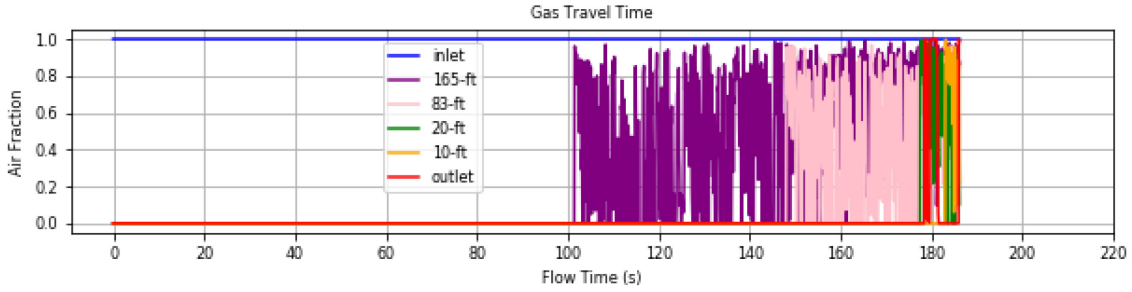

Figure 6-47—Air Volume Fraction vs. flow time. Reprinted from (Kaldirim et al. 2020)

The gas fraction is displayed in **Figure 6-47** for the monitors placed at the outlet and inlet, and 10-, 20-, 83-, 165-ft depths. The first gas bubble reached the midpoint (165-ft.) of the 330-ft. riser in 101 seconds which is fasted for the previous case with the 5-bbl injection. Following that point, the acceleration of the gas bubble and the expansion can be observed. **Figure 6-48** captures the last 10 seconds of Figure 6-47 to zoom into the observe the travel time for the gas bubble in the top 20-ft. of the riser. The first gas bubble arrives at 20-ft from the top at 177.3-seconds. The outlet data demonstrates that gas arrived between 178-179-secs; however, this occurs before gas arrival at other points in the top 20-ft of the riser. This data point indicates air backflow into the riser. The gas bubble arrives at the 10-ft point at 183-seconds, 5-ft at 184.5-seconds, and the gas travels the last 4-ft in less than 1-second.

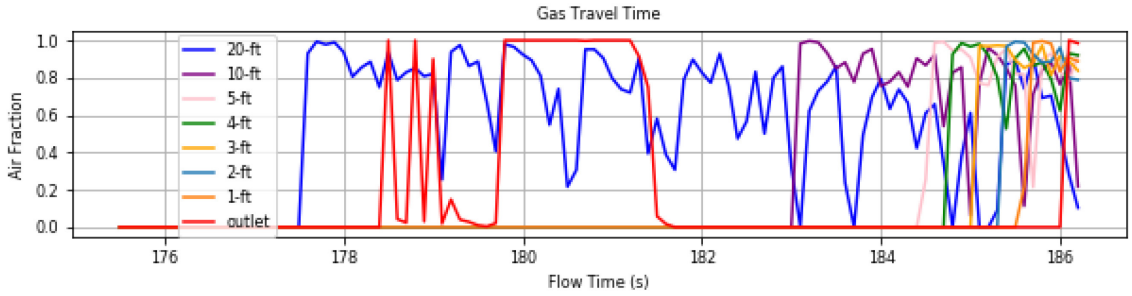

Figure 6-48—Air Volume Fraction vs. flow time. Reprinted from (Kaldirim et al. 2020)

The decrease in total pressure at the inlet can be observed in **Figure 6-49** as the gas injection and expansion causes mud to be removed from the riser. The decrease in pressure is also due to the increased volume of air in the riser. The total pressure drop is approximately 38-psig.

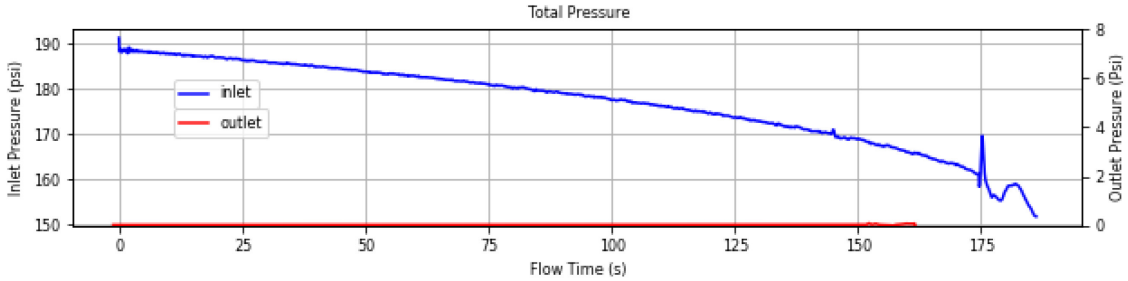

Figure 6-49— Total Pressure vs. Flow Time. Reprinted from (Kaldirim et al. 2020)

The temperature graph in **Figure 6-50** displays some significance as the gas injected into the flow loop was at 120-°F degrees, and the pipe outlet was kept at 65-°F degrees. The pipe wall was maintained at 45-°F, and the initialized temperature for the mud in the riser was 65-F degrees. The goal was to observe heat transfer and temperature change of the mud. However, due to the limited time, the temperature change was not observed until the gas bubble reached the top of the riser. It is important to note that the temperature at the midpoint began rising after 170 seconds while the top quarter-point (83-ft) began cooling since the gas had already extended through these depths.

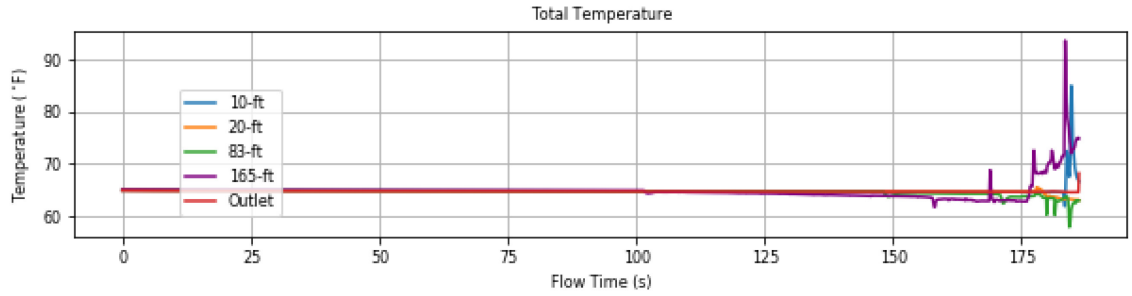

Figure 6-50—Total Temperature vs. Flow Time. Reprinted from (Kaldirim et al. 2020)

6.1.6. Discussions

The CFD analyses presented in this paper simulate well control cases in WBM (11-ppg., 22-cp.), where gas enters the riser and continues to migrate up and expand. The

BOP is closed for all cases except for the last case after gas injection. Thus, there was no outside interference on the gas migration and expansion. MPD back pressure applications were also studied to investigate the benefits of surface back pressure to restrict and control riser gas migration and expansion. The total pressure, discharge rate, gas flow rate, air volume fraction, total temperature, and discharge velocity were recorded for these cases. A summary of the results is presented in the table below.

Simulation	Length (ft.)	Pipe Diameter (in.)	Injection Volume (bbl.)	Average Injection Rate ($ft.^3/min.$)	Back Pressure (psig.)	Total Pit Gain (Bbl.)	Maximum discharge rate (GPM)
1-a	27	6	0.3	27.3	0	0.51	252.4
1-b	27	6	0.27	27.4	30	0.3	235
3-a	330	12	5.1	24.9	0	20.25	1023.4
3-b	330	12	5.1	24.8	200	7.5	222
3-c	330	19.5	5.6	51.4	0	16.7	3250.8
3-d	330	19.5	5.6	52	200	7.97	224.2
3-e	330	19.5	5.1	53.5	0	16.1	1433.82
3-f	330	19.5	28.7	50.6	0	60.7	6617.5

Table 6-3—Summary of Simulation Results. Reprinted from (Kaldirim et al. 2020)

Table 6-3 presents the total pit gain and maximum discharge rate for the simulations presented in this paper. The benefits of surface back pressure MPD can be

observed in handling riser gas. The expansion of gas and riser unloading was restricted by applying back pressure. This feature can be seen in simulation 3-d, where a 5.6 bbl gas influx was injected into the riser, resulting in a total pit gain of 7.97-bbls and a maximum discharge rate of 224.2-GPM. The same system with the RCD but without back pressure (simulation 3-c) resulted in a total pit gain of 16.7-bbl and a maximum discharge rate of 3250.8-GPM.

Simulation 3-f demonstrates a gas influx continuously injected into the riser with no RCD or back pressure. This leads to a total pit gain of 60.7 bbl and a maximum discharge rate of 6617.5 GPM.

Simulations 1-a and 1-b were run to demonstrate the benefits of applying surface back pressure in a small-scale flow loop. There was no unloading observed in that case; however, the injection rate was high enough to cause a high discharge rate. Thus, these simulations need to be refined with finer mesh (0.1-, 0.01-in.) and time step size (smaller than 0.01-sec.).

In the larger models, the temperature results varied when the attempt was made to compare the results. Further attempts at modeling the temperature will improve the accuracy of these models, as the temperature has an important effect on gas expansion for both oil-based mud and water-based mud; however, it might be more significant for an OBM for gas solubility.

6.1.7. Conclusions

Eight CFD simulations were presented, two simulations on a 27-ft. 6-in. riser with an RCD, two simulations on a 330-ft. 12-in riser with an RCD, two simulations on a 330-

ft. 19.5-in riser with an RCD and two simulations on a 330-ft. 19.5-in riser without a riser. The simulations demonstrated gas migration and expansion rate, riser gas unloading, and surface back pressure MPD benefits.

1. In the 27-ft. 6-in. riser case, 30-psig surface back pressure provided more control on gas migration and expansion.
2. In the 330-ft, 12-in riser case, 200-psig surface back pressure restricted gas expansion and limited pit gain.
3. The comparison of the 330-ft. 19.5-in. riser cases with and without an RCD demonstrated that an RCD with low back pressure (200 psig.) could safely remove a kick from the riser and restrict gas expansion, pit gain, bubble migration velocity.
4. CFD analyses can provide necessary guidance on riser unloading and temperature changes during a rapid gas expansion.
5. Surface back pressure applications in MPD can significantly reduce the expansion rate of gas and the maximum expansion the gas influx can achieve. This feature also provides continuous control over the influx and limits pit gain.
6. Applying back pressure using MPD equipment could eliminate riser unloading problems and create opportunities to circulate kicks through the riser safely.

6.1.8. Future Work

- Improve the mud viscosity model.
- Greater riser lengths 3000-ft+.
- Annular flow simulations for riser gas in conventional and back-pressure MPD operations.

- Improved temperature modeling for small- and full-scale riser
- 3D model of the riser with and without drill pipe.
- Investigate the liquid leg integrity during riser unloading through CFD analyses.

7. CONCLUSIONS

The work in this dissertation was conducted through funding provided by the National Academies of Sciences, Engineering, and Medicine, Gulf Research Program. The goal was to provide information on riser gas behavior, gas migration and expansion in marine risers, riser unloading, and to attempt to mitigate riser unloading through surface back pressure applications using managed pressure drilling methods using experimental and simulation. This experimental study was conducted at the Dual Gradient Drilling Lab and the Tower Lab facilities at Texas A&M University. The simulations were conducted using the Computational Fluid Dynamics (CFD) Analyses.

The experimental process for the research was heavily conducted in the Tower Lab as this lab provided access to a vertical 140 ft concentric clear pipe system. The Dual Gradient Drilling lab consists of an inclinable 27-ft clear pipe system. These labs were inoperable at the beginning of this project, and the redesign and modification process required multiple iterations to achieve the desired testing apparatus.

The CFD analyses were performed using Ansys Fluent on multiple workstations and the Texas A&M University High-Performance Research Computing (HPRC) Center Clusters. The size of the geometry used to run the CFD analyses required multiple reruns, refinement of mesh and time-step-size, testing of different models. The simulations were then moved to the supercomputer at the HPRC Center and run using the clusters ADA, TERRA, and GRACE. Even with the aid of the HPRC, the duration for each simulation varied between 5 days to 22 days. The data obtained from these simulations were analyzed

against results from the experiments. The simulations started with small-scale geometries, then scaled up to 140 ft length to simulate the Tower Lab, then 330-ft to attempt to scale up results.

7.1. Tower Lab

The tests present were a small sample of the tests conducted at the Tower Lab following the modifications. These tests demonstrate a striking contrast between solubility and free gas influxes. Air injection has a more significant impact on the maximum discharge rates, the total discharged mud volume, the pressure. The only CO_2 case where a significant discharge rate was captured during unloading was the 10-minute injection into the static water column. In this case, the mud had become highly saturated, and a churn flow regime was observed near the end of the test. However, even in this case, the discharge rate, volume, and pressure drop were impacted less than the static tests in which air was injected.

1- The Tower Lab was rebuilt to a working condition with newer sensor and wiring, increased capacity pump, redesigned and new supply lines, CO_2 line, new data acquisition system, improved safety, and reliability.

2- CO_2 injection occurred at a much lower rate. Therefore, the rate was not controlled; however, the pressure was controlled using a manual two-stage pressure regulator and a second single-stage pressure regulator.

3- The injection pressure and the injection duration impacted the average and maximum injection rate, maximum rate at unloading, and total discharged mud volume with air injection.

4- The maximum discharge rate was not affected by the pump rate. The main variation observed in discharge rate was due to injection time and injection pressure.
5- The pressure data demonstrates that the pressure data could be used as an indicator of an insoluble influx. However, there were no pressure indicators of gas migration or expansion when CO_2 was injected. The only indication of CO_2 in the well was the slight increase in flow rate, which may be difficult to measure.
6- Flow rate data becomes unreliable when a gas slug arrives at the Coriolis meter. Therefore, adding a secondary flow meter in line with the existing flow meter is important to capture the liquid rate.
7- No significant change in temperature was observed during these tests.

7.2. Computational Fluid Dynamics Analyses

Below are the conclusions based on the results from the CFD Analyses performed

1. In the 27-ft. 6-in. riser case, 30-psig. back pressure provided better control on gas migration and expansion.
2. In the 330-ft. 12-in. riser case, 200-psig back pressure restricted gas expansion and limited pit gain.
3. Comparing the 330-ft. 19.5-in. riser cases with and without an RCD demonstrated that an RCD with low back pressure (200 psig.) could safely remove a kick from the riser and restrict gas expansion, pit gain, bubble migration velocity.

4. The CFD software can provide insight into the temperature changes in the riser during a rapid unloading event.
5. Back pressure applications in MPD were demonstrated to reduce the expansion rate of gas and the maximum volume the gas influx could expand to during discharge. These applications provide continuous control over the influx and monitor the behavior of the gas influx. The MPD systems currently available allow the user to react quickly to changing conditions resulting from gas influxes.
6. Refinement of the mesh size and time step improved stability and convergence of the simulations. However, further iterations are necessary before scaling up the simulations to a real-case marine riser.
7. Most divergence occurs either at the start of the simulation when gas is injected or during the first gas bubble exiting the riser.

.

8. FUTURE WORK

This section proposes future work to be conducted to understand and model riser gas unloading and is split into two sections for experimental and CFD analyses.

8.1. Experimental Analyses for Riser Unloading

8.1.1. Tower Lab

1- The tower lab was remodeled without incorporating thermocouples. Reinstalling thermocouples can help understand the temperature behavior throughout the Tower Lab.

2- The Pressure Transmitters used in the tower lab provide measurements in a range of 0-300 psi. Installing narrower range Pressure Transmitters near and on the discharge and the mud-gas separator on the 10^{th} floor can improve the accuracy and resolution of the data collected during unloading.

3- The vertical check valve on the 1^{st} floor needs to be replaced with a 2" pipe nipple as this check valve traps gas in the supply line after the gas injection port.

4- Check valve downstream of the mud pump needs to be replaced with a new check valve to stop return flow.

5- Place a check valve downstream of the water tank on the second floor to prevent backflow and trap pressure downstream from the pump.

6- Install a turbine and vortex flow meter on the discharge line on the 10^{th} floor to obtain additional flow measurements in addition to the flow measurement from the Coriolis meter. The Coriolis meter measurements cut off when a water/gas slug enters the meter causing the measurement to drop off to zero or negative value.

7- Once the above modifications are made, rerun the experiments listed in this dissertation. Additional experiments can then be run, injecting smaller volumes of gas. These changes can improve measurement accuracy for the volume of gas injected into the flow loop.

8- Run experiments by injecting two gas injections with the second injection as the gas bubble top reaches the 5th floor camera to observe the change in the behavior and study the interaction between two gas influxes.

9- Install a control valve at the outlet to restrict the discharge rate. The control valve can provide experimental data on using back pressure at discharge to control gas expansion and unloading rate. However, it is essential to be cautious not to exceed the operating pressure of the Tower Lab Flow Loop.

10- Optionally a remotely controlled pressure regulator can be installed on the gas line to control the gas injection pressure from the 6th floor lab.

11- A pump can be installed on the outlet of the water tank using the existing discharge port to mix viscosified muds. In addition, a centrifugal pump with a variable frequency drive and agitator are available in the 201-lab storage room. Using viscosified mud can help create a more realistic case for riser unloading gas migration. The viscosified mud can also provide a better understanding of the relationship between gas migration and viscosity. Two sets of wires were pulled to the 2nd floor Tower Access room to control the pump.

8.1.2. Dual Gradient Drilling Lab

8.1.2.1. Dual Gradient Drilling Lab Modifications

1- Purchase and install small range pressure transmitters along the flow loop with 2-ft spacing.

2- Install pressure transmitters at the bottom and top of the mud gas separator.

3- Install Coriolis meters at the gas injection port and vent line of the mud gas separator.

4- Install a new Data Acquisition System to collect data from multiple pressure transmitters, flow meters and control the Variable Frequency Drives.

5- Modify the liquid leg of the mud gas separator to simulate a mud gas separator and place a pressure transmitter on this modified section.

8.1.2.2. Experiments

1- Run experiments using various gas volumes both in static fluid column and while circulating.

2- Perform experiments with back pressure using a control valve at the discharge.

3- Inject gas, then shut in the discharge as the gas begins unloading the pipe.

4- Perform continuous gas injection while circulating at high pump rates and collect data from the mud gas separator to study the height of the liquid seal. This study on the mud gas separator can provide information on the flow rate necessary to break the liquid seal and cause gas to go down into the liquid leg.

8.2. CFD Analyses for Riser Unloading

1- The simulations that were presented varied between 33-ft to 330-ft in length, using various diameters. However, the mesh sizing and design need to be improved to obtain more accurate results.

2- The results from the CFD simulations presented here don't provide an exact match. This lack of match was attributed to the check valve on the 1st floor, and the limitations of the Coriolis Meter on the discharge line. However, when the changes are performed, the new experiments can be compared with the results presented in this dissertation.

3- Scale up the simulations in steps to simulate an actual riser.

4- Once scaled-up simulations are performed, the geometry can be modified to simulate an actual offshore riser with hose connections.

5- Simulate the 8-ft mud gas separator in the Dual Gradient Drilling lab. Use the measured rates from the experiments as the inlet rate to simulate the effects of the unloading riser into the mud gas separator.

6- Simulate riser gas unloading with shut-in riser.

7- Simulate riser unloading with two separate gas influxes to study the interactions between two influxes

9. REFERENCES

Aarsnes, Ulf Jakob Flø, Hauge, Espen, and Godhavn, John-Morten. 2016. Mathematical Modeling of Gas in Riser. Presented at the SPE Deepwater Drilling and Completions Conference, Galveston, Texas, USA. 2016/9/14/. https://doi.org/10.2118/180292-MS.

ANSYS®. 2017. *Ansys Fluent Theory Guide-18.2*, Release 18.2 edition. Ansys: Ansys.

API RP 59, Recommended Practice for Well Control Operations; Second Edition; Reaffirmed, December 2016, 2006. API: API.

API RP 13B-2, Recommended Practice for Field Testing Oil-Based Drilling Fluids; Fifth Edition, 2014. API: API.

API Specification 16C, Choke and Kill Equipment; Second Edition, 2015. API: API.

API Standard 64, Diverter Equipment Systems; Third Edition, 2017a. API: API.

API RP 13D, Rheology and Hydraulics of Oil-well Drilling Fluids; Seventh Edition, 2017b. API: API.

API Specification 16F, Specification for Marine Drilling Riser Equipment; Second Edition; Effective Date: May 1, 2018, API Specification 16F. 2017c. API: API.

API Specification 53, Well Control Equipment Systems for Drilling Wells; Fifth Edition, 2018. API: API.

API RP 13B-1, Field Testing Water-based Drilling Fluids; Fifth Edition, 2019.

Bourgoyne, Adam T., Jr. and Holden, William R. 1985. An Experimental Study of Well Control Procedures for Deepwater Drilling Operations. *Journal of Petroleum Technology* **37** (07): 1239-1250. https://doi.org/10.2118/12803-PA.

Bryan, P. L. and Bourgoyne, A. T. 1989. Methods for Handling Drilled Gas in Oil-Based Drilling Fluids. *SPE Drilling Engineering* **4** (03): 237-246. https://doi.org/10.2118/16159-PA.

Bryan, Patrick L. and Bourgoyne, Adam T., Jr. 1990. Swelling of Oil-Based Drilling Fluids Resulting From Dissolved Gas. *SPE Drilling Engineering* **5** (02): 149-155. https://doi.org/10.2118/16676-PA.

Bryan, Patrick L., Bourgoyne, Adam T., Jr., Monger, Teresa G. et al. 1988. An Experimental Study of Gas Solubility in Oil-Based Drilling Fluids. *SPE Drilling Engineering* **3** (01): 33-42. https://doi.org/10.2118/15414-PA.

Casariego, V. and Bourgoyne, A. T., Jr. 1988. Generation, Migration, and Transportation of Gas-Contaminated Regions of Drilling Fluid. Presented at the SPE Annual Technical Conference and Exhibition, Houston, Texas. 1988/1/1/. https://doi.org/10.2118/18020-MS.

Christman, S., Kelly, A., Plaisance, M. et al. 1999. An Overview of the IADC Deepwater Well Control Guidelines. Presented at the SPE/IADC Drilling Conference, Amsterdam, Netherlands. 1999/1/1/. https://doi.org/10.2118/52761-MS.

CSB. 2016. Macondo Blowout and Explosion. Investigation Report, CSB, CSB (4/20/2016).

CSB. 2019. Gas Well Blowout and Fire at Pryor Trust Well 1H-9. Investigation Report, 2018-01-I-OK, CSB, CSB (June 12, 2019).

F. T. Bryan, L. T. Herbst, C. J. Schoennagel. 1994. Investigation of Loss of Well Control, Well No. 24, South Pass Block 60, Lease OCS-G 1608, December 26, 1992. Investigation. Report No. OCS MMS 94-0024, OCS Report MMS 94-0024, MMS, US Department of the interior/Minerals Management Services (March 1994).

Feo, Giuseppe, Sharma, Jyotsna, Kortukov, Dmitry et al. 2020a. Distributed Fiber Optic Sensing for Real-Time Monitoring of Gas in Riser during Offshore Drilling. *Sensors* **20** (1): 267. https://www.mdpi.com/1424-8220/20/1/267.

Feo, Giuseppe, Sharma, Jyotsna, Santos, Otto et al. 2020b. Multiphase Flow Characterization and Modeling Using Distributed Fiber Optic Sensors to Prevent Well Blowout. *Proc.,* Optical Sensors and Sensing Congress, Washington, DC, 2020/06/22, EM3C.5. http://www.osapublishing.org/abstract.cfm?URI=ES-2020-EM3C.5.

Feo, Giuseppe, Sharma, Jyotsna, Williams, Wesley et al. 2019. Application of Distributed Fiber Optics Sensing Technology for Real-Time Gas Kick Detection. Presented at the SPE Annual Technical Conference and Exhibition, Calgary, Alberta, Canada. 2019/9/23/. https://doi.org/10.2118/196113-MS.

Fernandez Alvarez, Juan Jose. 2009. *Design of a high-pressure research flow loop for the experimental investigation of liquid loading in gas wells*.

Gu, Qifan, Fallah, AmirHossein, Ambrus, Adrian et al. 2019. A Switching Controller for Mitigating Riser Gas Unloading Hazards in Offshore Drilling. Presented at the SPE/IADC International Drilling Conference and Exhibition, The Hague, The Netherlands. 2019/3/4/. https://doi.org/10.2118/194163-MS.

Gu, Qifan, Fallah, Amirhossein, Feng, Tianheng et al. 2021. A novel dilution control strategy for gas kick handling and riser gas unloading mitigation in deepwater drilling. *Journal of Petroleum Science and Engineering* **196**: 107973. https://www.sciencedirect.com/science/article/pii/S0920410520310287.

Haegh, Thor and Rossemyr, Leif I. 1980. A Comparison of Weathering Processes of Oil From the Bravo and the Ixtoc Blowouts. Presented at the Offshore Technology Conference, Houston, Texas. 1980/1/1/. https://doi.org/10.4043/3702-MS.

Hall, J. E., Roche, J. R., and Boulet, C. G. 1986. Means for Handling Gas Influx in a Marine Riser. Presented at the SPE/IADC Drilling Conference, Dallas, Texas. 1986/1/1/. https://doi.org/10.2118/14739-MS.

Hauge, E., Godhavn, J. M., Molde, D. O. et al. 2015. Analysis of Field Trial Well Control Results with a Dual Gradient Drilling System. Presented at the Offshore Technology Conference, Houston, Texas, USA. 2015/5/4/. https://doi.org/10.4043/26056-MS.

Holden, William R. and Bourgoyne, Adam T. 1982. An Experimental Study of Well Control Procedures for Deep Water Drilling Operations. Presented at the Offshore Technology Conference, Houston, Texas. 1982/1/1/. https://doi.org/10.4043/4353-MS.

Hovland, Frank and Rommetveit, Rolv. 1992. Analysis of Gas-Rise Velocities From Full-Scale Kick Experiments. Presented at the SPE Annual Technical Conference and Exhibition, Washington, D.C. 1992/1/1/. https://doi.org/10.2118/24580-MS.

IADC Deepwater Well Control Guidelines (2nd Edition), 2015: International Association of Drilling Contractors (IADC). https://app.knovel.com/hotlink/toc/id:kpIADCDWC1/iadc-deepwater-well-control/iadc-deepwater-well-control.

J. L. Guidry, D. Lueck, C. J. Schoennagel. 1986. Investigation of the December 1985 Blowout and Fire, Lease OCS-G 4268, West Cameron Block 648, Gulf of Mexico, Off the Louisiana Coast. Investigation. Report No. OCS MMS 86-0100, OCS REPORT MMS 86-0100, MMS, US DEPARTMENT OF THE INTERIOR/MINERALS MANAGEMENT SERVICES (October 1986).

Johnson, A. B. and Cooper, Steven. 1993. Gas Migration Velocities During Gas Kicks in Deviated Wells. Presented at the SPE Annual Technical Conference and Exhibition, Houston, Texas. 1993/1/1/. https://doi.org/10.2118/26331-MS.

Johnson, A. B. and White, D. B. 1991. Gas-Rise Velocities During Kicks. *SPE Drilling Engineering* **6** (04): 257-263. https://doi.org/10.2118/20431-PA.

K. W. Blake, D. J. Bourgeois, D. C. Howard, C. J. Schoennagel. 1986. Investigation of September 1984 Blowout and Fire Lease OCS-G 5893, Green Canyon Block 69 Gulf Of Mexico, Off the Louisiana Coast+-. Investigation. Report No. OCS 86-0101, OCS 86-0202, MMS, US Departmnet of The Interior/Minerals Management Services (October 1986).

Kaldirim, Omer. 2015. *Riser Gas Migration in EC-Drill™ Operations*. Master of Science Master's Thesis, Texas A&M University, Texas A&M University (December 2015).

Kaldirim, Omer, Kaldirim, Ebubekir, Geresti, Cameron et al. 2020. 2-D Computational Fluid Dynamics Modeling of Riser Gas and Unloading in Various Pipe Diameters and Lengths. *Proc.,* SPE/IADC Managed Pressure Drilling and Underbalanced Operations Conference and Exhibition. https://doi.org/10.2118/200523-MS.

Kaldirim, Omer and Schubert, Jerome J. 2017. An Experimental Study on Riser Gas Behavior for Dual Gradient Drilling. Presented at the IADC/SPE Managed Pressure Drilling & Underbalanced Operations Conference & Exhibition, Rio de Janeiro, Brazil. 2017/3/28/. https://doi.org/10.2118/185297-MS.

Kaldirim, Omer and Schubert, Jerome J. 2018. Experimental Study on Riser Gas Expansion and Unloading. Presented at the SPE/IADC Managed Pressure Drilling and Underbalanced Operations Conference and Exhibition, New Orleans, Louisiana, USA. 2018/4/17/. https://doi.org/10.2118/190004-MS.

Kiran, Raj, Ahmed, Ramadan, and Salehi, Saeed. 2020a. Experiments and CFD modelling for two phase flow in a vertical annulus. *Chemical Engineering Research and Design* **153**: 201-211. https://www.sciencedirect.com/science/article/pii/S0263876219304824.

Kiran, Raj, Elgaddafi, Rida, Ahmed, Ramadan et al. 2020b. Wellbore fluid sonic conditions during blowouts. *Journal of Petroleum Science and Engineering* **195**: 107822. https://www.sciencedirect.com/science/article/pii/S0920410520308834.

Kiran, Raj and Salehi, Saeed. 2018. Mathematical Modeling and Analysis of Riser Gas Unloading Problem. (51296): V008T11A063. http://dx.doi.org/10.1115/OMAE2018-77719.

Langlinais, J. P., Bourgoyne, A. T., Jr., and Holden, W. R. 1983. Frictional Pressure Losses for the Flow of Drilling Mud and Mud/Gas Mixtures. Presented at the SPE Annual Technical Conference and Exhibition, San Francisco, California. 1983/1/1/. https://doi.org/10.2118/11993-MS.

Madsen, Henrik Overgaard, Bennett, Graham, and Eriksen, Remi. 2014. Enhancing Offshore Safety and Environmental Performance – Key Learnings from Major Offshore Accidents. Presented at the 21st World Petroleum Congress, Moscow, Russia. 2014/1/1/. https://doi.org/.

Manikonda, Kaushik. 2020. *Modeling Gas Kick Behavior in Water and Oil-Based Drilling Fluids*. Master of Science, Texas A&M University, Texas A&M University.

Manikonda, Kaushik, Hasan, Abu Rashid, Barooah, Abinash et al. 2020a. A Mechanistic Gas Kick Model to Simulate Gas in A Riser with Water and Synthetic-Based Drilling Fluid. *Proc.,* Abu Dhabi International Petroleum Exhibition & Conference. https://doi.org/10.2118/203159-MS.

Manikonda, Kaushik, Hasan, Abu Rashid, Kaldirim, Omer et al. 2020b. Estimating Swelling in Oil-Based Mud due to Gas Kick Dissolution. *Proc.,* ASME 2020 39th International Conference on Ocean, Offshore and Arctic Engineering. https://doi.org/10.1115/OMAE2020-18115.

Manikonda, Kaushik, Hasan, Abu Rashid, Kaldirim, Omer et al. 2019. Understanding Gas Kick Behavior in Water and Oil-Based Drilling Fluids. Presented at the SPE Kuwait Oil & Gas Show and Conference, Mishref, Kuwait. 2019/10/13/. https://doi.org/10.2118/198069-MS.

Manikonda, Kaushik, Hasan, Abu Rashid, Rahmani, Nazmul H. et al. 2021. A Gas Kick Model that Uses the Thermodynamic Approach to Account for Gas Solubility in Synthetic-based Mud. *Proc.,* SPE/IADC Middle East Drilling Technology Conference and Exhibition. https://doi.org/10.2118/202152-MS.

Matthews, J. L. and Bourgoyne, A. T., Jr. 1983. Techniques for Handling Upward Migration of Gas Kicks in a Shut-In Well. Presented at the IADC/SPE Drilling Conference, New Orleans, Louisiana. 1983/1/1/. https://doi.org/10.2118/11376-MS.

Maurice Stewart, Jack Hendricks, Robert Whitaker, Robert Meurer, Ronald Prehoda. 1985. Investigation of October 20-27, 1983 Blowout, Eugene Island Block 10, Lease OCS-G 2892 Gulf of Mexico. Investigation. Report No. OCS MMS 85-0050, OCS Report MMS 85-0050, MMS, US Departmnet of The Interior/Minerals Management Services (1985).

Nahri, Syed Y., Chen, Yuanhang, Williams, Wesley et al. 2019a. Buoyancy Induced Convection of Riser Gas in Deepwater Drilling Operations. *Proc.,* ASME 2019 38th International Conference on Ocean, Offshore and Arctic Engineering. https://doi.org/10.1115/OMAE2019-96649.

Nahri, Syed Y., Chen, Yuanhang, Williams, Wesley et al. 2019b. Understanding the Phenomenon of Dissolved Gas Migration of Gas in Riser During Drilling Operations. *Proc.,* ASME 2019 38th International Conference on Ocean, Offshore and Arctic Engineering. https://doi.org/10.1115/OMAE2019-96683.

Nwaka, Nnamdi, Wei, Chen, Ambrus, Adrian et al. 2020. Gas in riser: On modeling gas influxes in non-aqueous drilling fluids with time-dependent desorption considerations. *Journal of Petroleum Science and Engineering* **195**: 107785. https://www.sciencedirect.com/science/article/pii/S0920410520308469.

Rader, D. W., Bourgoyne, A. T., Jr., and Ward, R. H. 1975. Factors Affecting Bubble-Rise Velocity Of Gas Kicks. *Journal of Petroleum Technology* **27** (05): 571-584. https://doi.org/10.2118/4647-PA.

Rommetveit, R. and Olsen, T. L. 1989. Gas Kick Experiments in Oil-Based Drilling Muds in a Full-Scale, Inclined Research Well. Presented at the SPE Annual Technical Conference and Exhibition, San Antonio, Texas. 1989/1/1/. https://doi.org/10.2118/SPE-19561-MS.

Santos, O. L. A., Lima, H. R. de Paula, and Bourgoyne, A. T., Jr. 1991. An Analysis of Gas Kick Removal From the Marine Riser. Presented at the SPE/IADC Drilling

Conference, Amsterdam, Netherlands. 1991/1/1/. https://doi.org/10.2118/21968-MS.

Santos, Otto L., Williams, Wesley C., Sharma, Jyotsna et al. 2021. Use of Fiber Optic Information to Detect and Investigate the Gas-in-Riser Phenomenon. *Proc.,* SPE/IADC International Drilling Conference and Exhibition. https://doi.org/10.2118/204115-MS.

Sharma, Jyotsna, Santos, Otto L. A., Feo, Giuseppe et al. 2020. Well-scale multiphase flow characterization and validation using distributed fiber-optic sensors for gas kick monitoring. *Optics Express* **28** (26): 38773-38787. http://www.opticsexpress.org/abstract.cfm?URI=oe-28-26-38773.

Stracke, K.J. 1970. Clean-Up at Santa Barbara. *Proc.,* SPE Evangeline Section Regional Meeting. https://doi.org/10.2118/3197-MS.

Velmurugan, Naveen, Godhavn, John-Morten, and Hauge, Espen. 2016. Dynamic Simulation of Gas Migration in Marine Risers. Presented at the SPE Bergen One Day Seminar, Grieghallen, Bergen, Norway. 2016/4/20/. https://doi.org/10.2118/180022-MS.

Visser, Robert C. 2011. Offshore Accidents, Regulations and Industry Standards. Presented at the SPE Western North American Region Meeting, Anchorage, Alaska, USA. 2011/1/1/. https://doi.org/10.2118/144011-MS.

Waltrich, Paulo J., Capovilla, Matheus S., Lee, Woochan et al. 2019. Experimental Evaluation of Wellbore Flow Models Applied to Worst-Case-Discharge

Calculations for Oil Wells. *SPE Drilling & Completion* **34** (03): 315-333. https://doi.org/10.2118/184444-PA.

Waltrich, Paulo J., Falcone, Gioia, and Barbosa, Jader R. 2011. Performance of Vertical Transient Two-Phase Flow Models Applied to Liquid Loading in Gas Wells. *Proc.,* SPE Annual Technical Conference and Exhibition. https://doi.org/10.2118/147128-MS.

Wang, Xiaohui, Guan, Zhichuan, Xu, Yuqiang et al. 2018. Signal analysis of acoustic gas influx detection method at the bottom of marine riser in deepwater drilling. *Journal of Process Control* **66**: 23-38. https://www.sciencedirect.com/science/article/pii/S0959152417302305.

William Martin, Jack Sandridge, Robert Goodman, Kenneth Blake, Ulysses Cotton, Lt. Cmdr. Max Miller. 1984. Investigation of July 20, 1983, Blowout Matagorda Island Block 657, Lease OCS-G-4139, Gulf of Mexico. Investigation. Report No. OCS MMS 84-0040, OCS REPORT MMS 84-0040, MMS, US Departmnet of The Interior/Minerals Management Services (1984).

Williams, W. C., Taylor, C. E., Almeida, M. A. et al. 2020. Distributed Sensing and Real Time Visualization of Gas Kick Dynamics in a Full-Scale Wellbore. *Proc.,* SPE Annual Technical Conference and Exhibition. https://doi.org/10.2118/201539-MS.

Yin, Bangtang, Lin, Yingsong, Wang, Zhiyuan et al. 2020. A gas kick early detection method outside riser based on Doppler ultrasonic wave during deepwater drilling.

Petroleum Exploration and Development **47** (4): 846-854. https://www.sciencedirect.com/science/article/pii/S1876380420601008.

Yuan, Zhaoguang, Morrell, Dan, Sonnemann, Paul et al. 2017. Mitigating Gas-in-Riser Rapid Unloading for Deepwater-Well Control. *SPE Drilling & Completion* **32** (02): 105-111. https://doi.org/10.2118/185179-PA.

Zhou, Guangzhao, Leach, Colin, Denduluri, Veerabhadra S. et al. 2021. Pressure-Difference Method for Gas-Kick Detection in Risers. *SPE Journal*: 1-19. https://doi.org/10.2118/205362-PA.